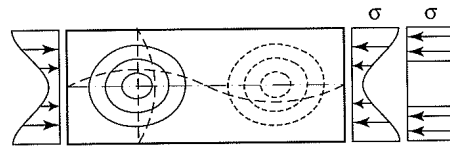
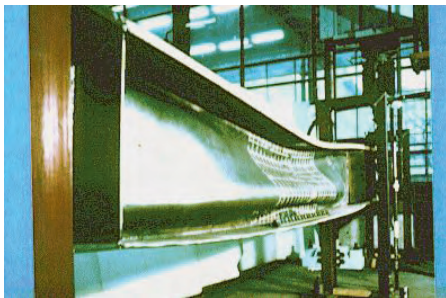
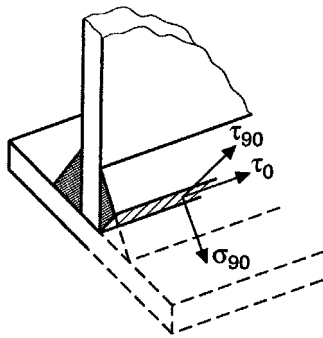




Thomas Hansen

# Theory of Plasticity for Steel Structures

- Solutions for Fillet Welds, Plate Girders and Thin Plates



# **Theory of Plasticity for Steel Structures**

**- Solutions for Fillet Welds, Plate Girders and Thin Plates**

**Thomas Hansen**

Ph.D. Thesis

BYG•DTU – Department of Civil Engineering  
Technical University of Denmark

Birch & Krogboe A/S  
Consultants and Planners

2006

Theory of Plasticity for Steel Structures  
- Solutions for Fillet Welds, Plate Girders and Thin Plates

Copyright ©, Thomas Hansen, 2006  
Printed by DTU-Tryk  
BYG•DTU – Department of Civil Engineering  
Technical University of Denmark  
Report No.: R-146  
ISSN: 1601-2717  
ISBN: 87-7877-218-4

## PREFACE

This thesis marks the conclusion of the industrial Ph.D. project entitled *Theory of Plasticity for Steel Structures*. The thesis is prepared as partial fulfilment of the requirements for the Industrial Ph.D. degree in accordance with *The Industrial PhD Initiative* under the Danish Ministry of Science Technology and Innovation, VTU.

The work has been carried out at the Department of Civil Engineering, BYG•DTU, the Technical University of Denmark and at Birch & Krogboe A/S, Consultants and Planners during the period October 2003 to September 2006. It has been conducted under the supervision of Professor Dr. techn. M. P. Nielsen, BYG•DTU, Associate Professor Henning Agerskov, BYG•DTU and Head of Structural Department Jesper Gath, Birch & Krogboe A/S.

All my supervisors are gratefully acknowledged for their valuable support and guidance during the study. I would especially like to thank M. P. Nielsen for his valuable advice on theoretical terms, as well as in practice for his inspiration and for many fruitful discussions and criticism during the daily meetings, the “coffee breaks”. Furthermore, I would like to thank his former group of Ph.D. students, João Luís Domingues Costa, Lars Zenke Hansen, Tim Gudmand-Høyer and Karsten Findsen, with whom I have had many invaluable discussions.

I would also like to thank the Knud Højgaard Foundation and DS Stålkonstruktion A/S for the financial support that made it possible to realise the project. Furthermore, DS Stålkonstruktion A/S is acknowledged for supplying the plate girder specimens for the experimental program, which was carried out by Alan Øskan and Christian Bak during their M.Sc. thesis work. I very much appreciate the hard work they did in the laboratory.

Furthermore, I would like to thank the support group for their engagement and criticism during the study. Besides the three supervisors, the support group consists of Niels J. Gimsing (BYG•DTU), Niels Kjeldgaard (MT Højgaard A/S), Niels Pedersen (DS Stålkonstruktion A/S), Lars G. Hagsten (Engineering College of Aarhus) and Aage P. Jensen (BYG•DTU). Particular thanks are due to Aage P. Jensen for supplying important information and test results regarding welds.

Finally, I would like to thank Arun Sharma, who did a great job of proofreading and editing the English. Of course, I am the one to be blamed for any errors that may still be present.

Kgs. Lyngby, 2006

Thomas Hansen



## ABSTRACT

Research within civil engineering structures has changed considerably along with the development of computer programs. Consequently, at universities it has caused the development of simple hand-calculation methods to cease more or less completely. This is not so convenient for the consulting companies, as the computer programs are often too heavy to work with in normal design projects. Only for very large and important structures can the use of heavy computer programs be justified. Therefore, the aim of the present research project is to derive simple hand-calculation methods within the chosen topics, and thereby create a coherent basis corresponding to what exists for reinforced concrete structures.

The theory of plasticity for steel structures deviates little from the theory of plasticity for concrete structures in the form developed in Denmark. Thus, the present project is a natural extension of the now century old development of concrete structures in Denmark.

The thesis is subdivided into four individual parts concerning the chosen topics. The four parts are: *Plasticity Theory of Fillet Welds*, *The Plastic Tension Field Method*, *Post-Buckling Strength of Plates in Compression* and *Patch Loading on Plate Girders*.

Initially, simple methods for calculation of fillet welds based on the theory of plasticity are derived.

Currently, static calculations of fillet welds are based on a semi-empirical failure condition, where the effective weld stresses are determined as the mean values of the stresses on the throat section without knowledge of the entire stress field. In the thesis it is shown that fortunately, only small corrections are needed according to a consistent treatment.

The plasticity solutions are compared with yield load tests carried out at the Engineering Academy of Denmark in the early nineties as well as older failure load tests. The new failure conditions are in very good agreement with the yield load tests, while in less good agreement with the older failure load tests.

Furthermore, a calculation method for steel plate girders with transverse web stiffeners subjected to shear is described. It may be used for predicting the failure load, or as a design method, to determine the optimal number of internal web stiffeners.

The new method is called *the plastic tension field method*. It is based on the theory of plasticity and is analogous to the so-called *diagonal compression field method* developed for reinforced concrete beams with transverse stirrups. Many other theories have been developed, but the method presented here differs from these by incorporating the strength of the transverse stiffeners and by the assumption that the tensile bands may pass the transverse stiffeners, something that is often observed in tests. Other methods have only dealt with a single web field between two stiffeners.

The load-carrying capacity may be predicted by applying both the lower-bound theorem and the upper-bound theorem. The upper-bound solutions show very good correlation with both old and new tests.

Currently, calculations of plates in compression are based on the semi-empirical effective width method, which was developed by Winter et al. It is a well known fact that plates in compression may carry loads much larger than the load for which elastic

## ABSTRACT

buckling will occur. The effective width method takes the post-buckling capacity into account. A new effective width method is established, derived on the basis of a consistent theory. The new method rests on the theory of plasticity, particularly the yield line theory. The emphasis is placed on buckling problems related to plate girders. Two general cases are studied: Plates in uniaxial compression supported along all edges, e.g. the compressed flange in a box girder, and plates with one free edge, e.g. the compressed flange and the internal web stiffeners in an I-shaped girder. The resulting equations are compared with the semi-empirical method developed by Winter et al. The plastic solutions give approximately the same results as Winter's solutions without any empirical modifications.

Finally, a simplified theory for calculation of steel plate girders subjected to concentrated loads, denoted *patch loading*, is presented.

The theory is simplified due mainly to the assumption that the whole web panel under the patch load will always be active. The post-buckling strength of the web panel is determined by the effective width approach. The stresses in these effective widths will be uniformly distributed under the flange and utilised in a flange mechanism, which is calculated separately.

The solutions are derived separately for girders with a square web panel and for those with a rectangular web panel.

Both solutions are compared with experimental results, and the theories correlate well with the tests, especially for girders with rectangular web panels.

Additionally, it is shown that the theory is also able to deal with the phenomenon of *flange induced buckling*.

## RESUMÉ

Forskningen inden for bærende konstruktioner har ændret sig markant sideløbende med udviklingen af computerprogrammer. Denne drejning af forskningen har medført, at udviklingen af simple håndregningsmetoder stort set er ophørt på universiteterne. Dette er uheldigt for de rådgivende ingeniørfirmaer, da de udviklede computerprogrammer ofte er for tunge at arbejde med ved den daglige projektering. Kun for meget store og betydningsfulde bærende konstruktioner kan brugen af dem forsvares. Det er derfor formålet med dette projekt at forsøge at udvikle simple håndregningsmetoder inden for de udvalgte områder og dermed skabe et sammenhængende grundlag for praktisk dimensionering, der svarer til, hvad der findes for armerede betonkonstruktioner.

Plasticitetsteori for stålkonstruktioner adskiller sig ikke nævneværdigt fra plasticitetsteori for betonkonstruktioner således, som den er udviklet i Danmark. Projektet kan derfor ses som en naturlig forlængelse af den hundredårige udvikling af teorier for betonkonstruktioner i Danmark.

Afhandlingen er opdelt i fire individuelle dele, omhandlende de valgte emner. De fire dele er: *Plasticitetsteori for kantsømme*, *diagonaltrækmetoden*, *overkritisk bæreevne for plader i tryk* og *koncentreret last på pladedragere*.

Indledningsvist er der udviklet simple metoder til beregning af kantsømme baseret på plasticitetsteorien.

I dag baseres statiske beregninger på et delvist empirisk brudkrav, hvor de effektive sømspændinger bestemmes som middelværdien af spændingerne i halssnittet uden kendskab til hele spændingstilstanden i svejsesømmen. I denne afhandling er det vist, at der heldigvis kun er tale om mindre justeringer for at opnå en tilfredsstillende behandling.

De plastiske løsninger er sammenlignet med forsøg vedrørende flydestadiet udført på Danmarks Ingeniørakademi i begyndelsen af halvfemserne og med ældre brudforsøg med kantsømme. De nye bæreevneudtryk er i rigtig god overensstemmelse med forsøg i flydestadiet, hvorimod de er i mindre god overensstemmelse med de ældre brudforsøg.

Derudover præsenteres en beregningsmetode for stålpladedragere med kropsafstivninger påvirket til forskydning. Den kan anvendes til at bestemme bæreevnen eller som en dimensioneringsmetode til bestemmelse af det optimale antal kropsafstivninger.

Den nye metode kaldes *diagonaltrækmetoden*. Den er baseret på plasticitetsteorien og er analog til den såkaldte *diagonaltrykmethode* udviklet til forskydningsarmerede betonbjælker. Der er udviklet mange andre metoder, men metoden der er præsenteret her, afviger fra de øvrige ved at medtage tværafstivningernes styrke, og ved at den forudsætter, at trækbåndene kan passere tværafstivningerne, hvilket ofte er observeret ved forsøg. Andre metoder har kun omfattet ét enkelt pladefelt mellem to afstivninger. Bæreevnen kan bestemmes både ved hjælp af nedreværdisætningen og ved hjælp af øvreværdisætningen. Øvreværdiløsningerne viser en særdeles god overensstemmelse med både ældre og nye forsøg.

I dag beregnes plader påvirket til tryk med den delvist empiriske metode baseret på de såkaldte effektive bredder, som blev udviklet af Winter med flere. Det er velkendt, at plader påvirket til tryk kan bære en belastning, der er væsentlig større end belast-

ningen svarende til den, hvor elastisk foldning opstår. Metoden med effektive bredder medtager den overkritiske bæreevne. En ny metode med effektive bredder er udviklet, baseret på en konsistent teori. Metoden er baseret på plasticitetsteorien, særligt brudlinieteorien. Hovedvægten er lagt på foldningsproblemer relateret til pladedragere. To generelle tilfælde er undersøgt: Plader påvirket til enakset tryk med understøtninger langs alle rande, for eksempel trykflangen i en kassedrager, og plader med én fri rand, for eksempel trykflangen eller kropsafstivningerne i en drager med I-formet tværsnit. De opstillede formler er sammenlignet med Winter's formler. De plastiske løsninger giver stort set samme resultat som Winter's løsninger uden nogen empiriske korrektioner.

Endeligt præsenteres en simpel teori for beregning af stålpladedragere med koncentreret belastning.

Teorien er simplificeret, først og fremmest ved, at den forudsætter, at hele pladefeltet under den koncentrerede last altid er aktivt. Den overkritiske bæreevne for pladefeltet bestemmes ud fra princippet vedrørende effektive bredder. Spændingerne i de effektive bredder vil fordele sig jævnt ud under flangen, og de påføres i flange-mekanismen, som beregnes separat.

Løsningerne er opstillet selvstændigt for henholdsvis pladedragere med kvadratiske pladefelter og med rektangulære pladefelter.

Begge løsninger er sammenlignet med forsøg, og teorien stemmer fint overens med forsøgene, specielt for dragerne med rektangulære pladefelter.

Yderligere er det vist, at teorien også er i stand til at behandle fænomenet *flangeindskydning*.

**TABLE OF CONTENTS**

**NOTATION ..... XIII**

**1 INTRODUCTION ..... 1**

1.1 STATE OF THE ART ..... 2

*Welded Connections* ..... 2

*Steel Plate Girders*..... 2

*Stability Problems*..... 3

*Fracture Mechanics*..... 3

1.2 AIM AND MOTIVATION ..... 4

1.3 OUTLINE OF THE THESIS ..... 4

**2 THEORY OF PLASTICITY..... 6**

2.1 EXTREMUM PRINCIPLES FOR RIGID-PLASTIC MATERIALS ..... 7

*The Lower-Bound Theorem* ..... 7

*The Upper-Bound Theorem* ..... 7

*The Uniqueness Theorem* ..... 7

2.2 DISSIPATION FORMULAS ..... 8

**PART I – PLASTICITY THEORY OF FILLET WELDS ..... 9**

**1 INTRODUCTION ..... 11**

1.1 HISTORICAL OVERVIEW ..... 12

1.2 ASSUMPTIONS ..... 14

**2 LOWER-BOUND SOLUTIONS FOR SYMMETRIC FILLET WELDS ..... 16**

2.1 SHEAR PARALLEL TO THE AXIS OF THE WELD ..... 16

2.2 UNIAXIAL TENSION PERPENDICULAR TO THE THROAT SECTION ..... 17

2.3 SHEAR PERPENDICULAR TO THE AXIS OF THE WELD..... 20

2.4 YIELD SURFACES FOR SYMMETRIC FILLET WELDS ..... 21

2.5 COMPARISON WITH EXPERIMENTAL RESULTS ..... 22

**3 LOWER-BOUND SOLUTIONS FOR SINGLE FILLET WELDS..... 25**

3.1 SHEAR ON THE THROAT SECTION PERPENDICULAR TO THE AXIS OF THE WELD..... 25

3.2 YIELD SURFACES FOR SINGLE FILLET WELDS ..... 27

3.3 COMPARISON WITH EXPERIMENTAL RESULTS ..... 29

3.4 REDUCTION OF THE LOAD-CARRYING CAPACITY..... 32

**4 CONCLUSION..... 34**

**5 REFERENCES..... 35**

**6 NOTATION..... 36**

**PART II – THE PLASTIC TENSION FIELD METHOD ..... 37**

**1 INTRODUCTION ..... 39**

1.1 OTHER METHODS ..... 40

## TABLE OF CONTENTS

<b>2</b>	<b>LOAD-CARRYING CAPACITY.....</b>	<b>44</b>
2.1	LOWER-BOUND SOLUTION.....	45
2.2	UPPER-BOUND SOLUTION FOR CONCENTRATED LOADING.....	48
	<i>Contribution from the Web Plate</i> .....	49
	<i>Contribution from the Flanges</i> .....	51
	<i>Contribution from the Internal Stiffeners</i> .....	51
	<i>Load-Carrying Capacity</i> .....	52
2.3	UPPER-BOUND SOLUTION FOR DISTRIBUTED LOADING.....	58
<b>3</b>	<b>DESIGN METHOD.....</b>	<b>68</b>
3.1	CIRCULAR FAN SOLUTIONS.....	68
3.2	APPLICATION OF CIRCULAR FAN STRESS FIELDS.....	72
3.3	PRACTICAL DESIGN METHOD.....	74
	<i>Example</i> .....	76
3.4	OTHER LOADING CASES.....	80
3.5	END PANELS.....	81
<b>4</b>	<b>EXPERIMENTAL RESULTS FROM THE LITERATURE.....</b>	<b>83</b>
<b>5</b>	<b>NEW PLATE GIRDER EXPERIMENTS.....</b>	<b>88</b>
5.1	THE TEST GIRDERS.....	88
	<i>Girder Dimensions</i> .....	89
	<i>Steel Properties</i> .....	90
	<i>Critical Web Buckling Stresses</i> .....	92
	<i>Deflections</i> .....	93
5.2	TESTS ON PLATE GIRDERS SUBJECTED TO CONSTANT SHEAR.....	94
	<i>Ultimate Loads and Deflections</i> .....	95
	<i>Strain Measurements on the Web</i> .....	102
	<i>Strain Measurements on the Flanges and Stiffeners</i> .....	104
5.3	TESTS ON PLATE GIRDERS SUBJECTED TO DISTRIBUTED LOADING.....	107
	<i>Ultimate Loads</i> .....	108
	<i>Strain Measurements on the Web</i> .....	111
	<i>Strain Measurements on the Flanges and Stiffeners</i> .....	111
<b>6</b>	<b>CONCLUSION.....</b>	<b>113</b>
<b>7</b>	<b>REFERENCES.....</b>	<b>114</b>
<b>8</b>	<b>NOTATION.....</b>	<b>116</b>
<b>PART III – POST-BUCKLING STRENGTH OF PLATES IN COMPRESSION.....</b>		<b>119</b>
<b>1</b>	<b>INTRODUCTION.....</b>	<b>121</b>
1.1	HISTORICAL OVERVIEW.....	122
<b>2</b>	<b>POST-BUCKLING THEORY FOR PLATES IN COMPRESSION.....</b>	<b>124</b>
2.1	YIELD LINE THEORY.....	124
2.2	EFFECT OF DEFLECTIONS.....	125
2.3	COLUMN EXAMPLE.....	126
<b>3</b>	<b>PLATES SUPPORTED ALONG ALL EDGES.....</b>	<b>130</b>
3.1	SQUARE PLATES.....	130
3.2	RECTANGULAR PLATES.....	136

3.3	COMPARISON WITH EXPERIMENTAL RESULTS .....	138
<b>4</b>	<b>PLATES WITH ONE FREE EDGE.....</b>	<b>140</b>
4.1	RECTANGULAR PLATES .....	140
4.2	COMPARISON WITH EXPERIMENTAL RESULTS .....	142
4.3	SQUARE PLATES .....	143
<b>5</b>	<b>IMPERFECTIONS.....</b>	<b>146</b>
<b>6</b>	<b>OTHER APPLICATIONS OF THE THEORY .....</b>	<b>149</b>
<b>7</b>	<b>CONCLUSION.....</b>	<b>150</b>
<b>8</b>	<b>REFERENCES.....</b>	<b>151</b>
<b>9</b>	<b>NOTATION.....</b>	<b>152</b>
 <b>PART IV – PATCH LOADING ON PLATE GIRDERS .....</b>		<b>153</b>
<b>1</b>	<b>INTRODUCTION .....</b>	<b>155</b>
1.1	OTHER METHODS .....	156
<b>2</b>	<b>ASSUMPTIONS .....</b>	<b>158</b>
<b>3</b>	<b>PLATE GIRDERS WITH SQUARE WEB PANELS.....</b>	<b>160</b>
3.1	THE WEB MECHANISM.....	160
3.2	THE FLANGE MECHANISM.....	162
3.3	COMPARISON WITH EXPERIMENTAL RESULTS .....	164
<b>4</b>	<b>PLATE GIRDERS WITH RECTANGULAR WEB PANELS .....</b>	<b>167</b>
4.1	THE WEB MECHANISM FOR RECTANGULAR PANELS.....	167
4.2	LOAD-CARRYING CAPACITY .....	170
4.3	COMPARISON WITH EXPERIMENTAL RESULTS .....	173
<b>5</b>	<b>FLANGE INDUCED BUCKLING .....</b>	<b>177</b>
<b>6</b>	<b>THE EFFECT OF UNIAXIAL TENSION STRESSES IN THE WEB.....</b>	<b>180</b>
6.1	SQUARE WEB PANELS WITH UNIAXIAL TENSION AT 45° .....	180
6.2	RECTANGULAR WEB PANELS WITH UNIAXIAL TENSION AT 45° .....	182
6.3	WEB PANELS WITH UNIAXIAL TENSION IN AN ARBITRARY DIRECTION .....	185
<b>7</b>	<b>CONCLUSION.....</b>	<b>186</b>
<b>8</b>	<b>REFERENCES.....</b>	<b>187</b>
<b>9</b>	<b>NOTATION.....</b>	<b>188</b>
 <b>CONCLUSION .....</b>		<b>191</b>
	<i>Recommendations for Future Work.....</i>	192
 <b>REFERENCES.....</b>		<b>193</b>

TABLE OF CONTENTS

<b>APPENDIX A</b> .....	<b>201</b>
<b>APPENDIX B</b> .....	<b>202</b>
<b>APPENDIX C</b> .....	<b>203</b>
<b>APPENDIX D</b> .....	<b>207</b>
<b>APPENDIX E</b> .....	<b>215</b>
<b>APPENDIX F</b> .....	<b>220</b>
<b>APPENDIX G</b> .....	<b>228</b>
<b>APPENDIX H</b> .....	<b>232</b>
<b>APPENDIX I</b> .....	<b>234</b>
<b>APPENDIX J</b> .....	<b>238</b>

## NOTATION

### Lower case Latin letters

$a$	throat thickness; length
$b$	width; constant stiffener spacing
$b_e$	total effective width
$b_s$	width of effective strip
$c$	length; length of patch load
$d$	girder depth, i.e. depth of the web plate
$f$	yield condition
$f_y$	yield stress
$f_u$	ultimate tensile strength
$k$	elastic buckling coefficient; factor
$l, m, n$	coordinates of a unit vector
$m$	bending capacity of a yield line per unit length; fictitious moment
$m_b$	bending moment per unit length in a yield line
$m_p$	plastic yield moment per unit length
$n$	non-dimensional generalised normal force; number of stiffeners; normal force per unit length
$n_p$	load-carrying capacity per unit length in pure compression or tension
$p$	load per unit area; patch load per unit length; surface vector
$q$	load per unit length; non-dimensional generalised shear force
$r$	radial distance
$r_0$	radius of curvature of tension coupons
$t$	thickness
$u$	relative displacement; deflection
$u_m$	deflection at maximum load
$v$	angle
$x, y, z$	coordinates in a Cartesian $x,y,z$ -system of coordinates
$x$	length; web plate depth included in the internal beam
$x_f$	web plate depth included in the internal beam from flange yielding
$y_0$	vertical distance from the bottom face of a girder

### Upper case Latin letters

$A$	area
$C$	compressive flange force (positive as compression); pole of fan; empirical coefficient
$D$	diameter
$E$	Young's modulus
$G$	shear modulus
$I$	moment of inertia
$L$	weld length; length of shear zone; column length
$L_0, L_c$	original gauges length and parallel length of tension coupons
$M$	moment
$M_p$	plastic yield moment; plastic yield moment of internal beam
$N$	normal force
$N_p$	normal force, load-carrying capacity in pure compression or tension
$P$	force, load
$Q$	shear force
$R_x$	resultant of the $\sigma_x$ -stresses
$S_0$	original cross-section area of tension coupons
$T$	tensile flange force (positive as tension)
$V$	volume
$W$	plastic work
$W_e, W_i$	external work and dissipation, respectively
$W_l$	dissipation per unit length
$X, Y$	free optimisation parameters

## NOTATION

### Lower case Greek letters

$\alpha$	angle; angle of circular fan; angle between yield line and relative displacement; parameter (shape of curvature function); imperfection factor; length
$\beta$	correlation factor; angle of uniaxial web stress; length
$\beta_w$	correlation factor according to EC3
$\delta$	relative displacement; displacement increment
$\varepsilon$	strain
$\varepsilon_y$	yield strain
$\phi$	change of angle
$\gamma$	angle of weld
$\gamma_{Mw}$	partial coefficient according to EC3
$\eta$	non-dimensional parameter measuring flange stiffness
$\varphi$	stiffener ratio
$\kappa, \kappa_{xy}$	curvature and torsional curvature, respectively
$\lambda$	non-dimensional parameter; indeterminate factor
$\lambda_r$	non-dimensional slenderness ratio according to EC3
$\mu$	empirical coefficient
$\nu$	Poisson's ratio; effectiveness factor
$\theta$	angle; angle of uniaxial concrete stress; angle in failure mechanism
$\rho$	radius of curvature
$\sigma$	normal stress
$\sigma_i$	failure load for welded connection
$\tau$	shear stress
$\upsilon$	angle
$\psi$	mechanical degree of stiffening; relative deflection increment

### Upper case Greek letters

$\Delta$	difference
$\Phi$	EC3 parameter for calculation of columns

### Subscripts

0	indication for parallel direction
1, 2, 3	principal directions
90	indication for perpendicular direction
<i>A, B</i>	points
<i>bf</i>	bottom face
<i>c</i>	concrete; compression
<i>cr</i>	elastic critical value
<i>d</i>	design value
<i>e</i>	edge; end panel
<i>EC3</i>	index for value determined by EC3
<i>eff</i>	effective
<i>exp</i>	experimental value
<i>f</i>	flange
<i>F</i>	circular fan
<i>FEM</i>	index for value determined by FEM model
<i>h</i>	rotated throat section
<i>H</i>	homogeneous region
<i>i</i>	imperfection; initial
max	maximum value
min	minimised value
<i>r, \alpha</i>	coordinates in a polar system of coordinates
<i>s</i>	stiffener
<i>t</i>	tensile
<i>tf</i>	top face
<i>u</i>	ultimate; theoretical value
<i>v</i>	vertical
<i>w, web</i>	web

$x, y, z$  coordinates in a Cartesian  $x,y,z$ -system of coordinates

### Superscripts

+ upper-bound value  
- lower-bound value  
\* virtual load



## 1 INTRODUCTION

There is a century-long tradition in Denmark of deriving theories for civil engineering structures of concrete based on the theory of plasticity.

The theory of plasticity utilises the load-carrying capacity reserve that occurs when yielding of the construction material is utilised, i.e. the material will deform heavily without any significant change in the stresses. It is a well-known fact that many steel grades have such yielding properties. On the contrary is the theory of elasticity, where the stresses and strains are assumed to be proportional.

In Denmark, not much emphasis has been attached to the development of theories for steel structures based on the theory of plasticity. Worldwide however, a great deal of emphasis has been attached to applying the theory of plasticity to steel structures and other materials with yielding properties.

A failure theory for concrete structures began when Ingerslev (1923) and later Johansen (1943), based on German tests, developed yield line theories for plates based on the upper-bound theorem, which was proven by Johansen.

Later, the Russian Gvozdev (1938) derived a complete theory including the lower-bound theorem. Drucker et al. (1952) from the USA, developed an analogue to Gvozdev's theory. In Denmark however, a lower-bound theory had already been developed by Lundgren (1949) for cylindrical shells (the stringer theory).

From the 1960's to date, the work regarding failure theories for concrete structures has been continued by Nielsen (1998).

The theories for concrete are at a level where a large number of prevalent structures may be designed with the developed hand-calculation methods.

In Denmark, the research of steel structures has mainly been concentrated on studying the fatigue properties of ordinary steel and high strength steel, respectively.

Theory of plasticity for steel structures has been particularly developed in England, e.g. (Baker et al. 1956), and in USA in the 1950's and 1960's at Lehigh University. Through this research, plasticity theories for frame structures were more or less clarified.

As previously mentioned, the theory of plasticity has been applied on concrete structures in Denmark. Even though the material steel shows, to a much larger extent, perfectly plastic behaviour, not much emphasis have been attached to applying the theory of plasticity to steel structures. This might be due to the fact that steel structures are often very slender, so that stability failure, e.g. buckling, might occur instead of failure by initiation of yielding.

However, there are a large number of construction elements, especially construction joints, where stability problems do not play an important role. Additionally, it is also possible to study stability problems by taking into account yielding, as will be shown in this thesis.

In Danish consulting companies, the theory of plasticity is applied to a large extent as a useful tool in the daily design of civil engineering structures. Hence, the obtained results may easily be implemented within the companies.

The theory of plasticity for steel structures deviates little from the theory of plasticity for concrete structures in the form developed in Denmark. Thus, the present project is a natural extension of the century-long development of concrete structures in Denmark.

### 1.1 State of the Art

In this research project, four main topics were originally chosen. The four topics are denoted *welded connections*, *steel plate girders*, *stability problems* and *fracture mechanics*, and they are briefly described below.

#### WELDED CONNECTIONS

Structural steel joints based on welding became commonplace during and after the Second World War. In the inter-war period, empirical formulae for predicting the load-carrying capacity of the most common welded connections were already developed. In these formulae, the effective weld stress is determined by calculating the mean stresses on the throat section, without knowledge of the entire stress field.

Currently, calculations of fillet welds are still based on the old semi-empirical formulae, with only a few modifications.

It seems obvious to attempt to establish simple methods for calculation of fillet welds based on the theory of plasticity, where the stress field in the whole weld is included, thereby establishing a safe and statically admissible stress distribution.

Development of calculation methods for welded connections based on the theory of plasticity was initiated by Nielsen and Pilegaard Hansen (1971), and was followed up by Jensen (1991). For various reasons the work was never completed. The tasks remaining within this topic are to derive simple methods for calculation of fillet welds and further experimental verification.

#### STEEL PLATE GIRDERS

As previously mentioned, plasticity theories for beam and frame structures were developed in England after the Second World War by Baker et al. (1956) among others. The yielding behaviour is taken into consideration by the assumption that the load-carrying capacity is reached by the formation of a number of plastic yield hinges, i.e. regions where large plastic deformations occur, and thereby also large mutual angular rotations. In the 1960's and 1970's, investigations were conducted at Lehigh University in the USA in order to obtain practical recommendations, based on the theory of plasticity, for the structural design, i.e. determination of plate thicknesses, etc. They showed that often, large plate thicknesses are required to ensure that plastic yield hinges will develop. In practical design, it is often preferred to apply smaller plate thicknesses, so failure due to stability might occur instead of failure by initiation of yielding, hence the yielding capacity is not fully utilised.

These circumstances are especially pronounced for steel plate girders, where the thickness of the web plate is often taken to be very small, thus according to a linear elastic calculation, failure due to buckling of the web plate will occur before the yielding capacity is fully utilised. However, it is a well-known fact that until the buckling load is reached, a web plate subjected to shear will develop identical principal stresses at an angle of  $45^\circ$  and  $135^\circ$  to the flanges, respectively. When the web buckles, it practically loses its capacity to sustain the compressive principal stresses, hence a new way of carrying the load arises, where the shear forces are carried by inclined tensile bands.

Many other theories, both empirical and theoretical, have been developed based on the observed tension field action. These methods have in common the fact that they are only dealing with a single web field between two stiffeners.

Preliminary investigations of a fully plastic theory for predicting the post-buckling strength of plate girders in shear were conducted by Nielsen and Christensen (1982).

### STABILITY PROBLEMS

When the full yielding capacity is utilised, one must ensure that no localised failure due to stability will occur, e.g. buckling of the compression flange or buckling at concentrated loads.

An accurate calculation of such phenomena requires an advanced computer program. However, simple semi-empirical formulae for determination of the post-buckling strength of plates in compression have been derived long ago by Winter (1947) based on the effective width concept suggested by Kármán et al. (1932). Roberts (1983) developed practical semi-empirical formulae for predicting the load-carrying capacity of steel plate girders subjected to concentrated loads.

The theory of plasticity in its simplest form does not take into account the effect of change of geometry, but it is often possible to do so by estimating the deformations. This idea was introduced by Murray (1984) in Australia.

### FRACTURE MECHANICS

During the industrial evolution, sudden and inexplicable brittle failures often occurred. These brittle failures often occurred with cyclic loading, therefore they were often denoted as *fatigue failures*. Empirical investigations began, but with a lack of understanding of the complex nature of the fatigue failure, more and more brittle failures occurred, for instance when welded connections became common. The many brittle failures in the welds of the *Liberty Ships* during the Second World War are well-known, as are the crashes of de Havillands *Comet jet airplanes*, where the window openings were unfavourably designed, causing large stress concentration to occur.

An understanding of brittle fracture began with the work of Griffith (1921, 1924) in England. He examined failures in glass, and showed that existing initial cracks induced large stress concentrations, which led to crack growth with consumption of the existing elastic energy without further supply of energy.

In the USA, Irwin (1948) and Orowan (1948) modified Griffith's theory to a form useful for metallic materials. They showed that the plastic work in the vicinity of the crack tip has to be taken into account, which is by far the most important contribution for metallic materials. Furthermore, Irwin introduced the notation *stress intensity factors*.

Finally, Paris et al. (1961) showed that crack growth due to cyclic loading may be described by the variation of the stress intensity factors at the crack tip.

The topic of fracture mechanics is not directly related to the main subject of the thesis, but the theory of plasticity assumes that the yielding capacity of the material is sufficient. If not, the load-carrying capacity might be reached by a brittle failure before the plastic load-carrying capacity is fully utilised. Therefore, fracture mechanics is indeed relevant.

## 1.2 Aim and Motivation

The research within civil engineering structures has changed considerably along with the development of computer programs. Consequently, this development has resulted in academic research being concentrated on deriving theories that, with great accuracy, may calculate a complicated stress distribution on the basis of correct constitutive equations. This shift in research at universities has caused the development of simple hand-calculation methods to cease more or less completely. This is not optimal for consulting companies, since the computer programs are often too heavy to work with, within normal design projects. Only for very large and important structures may the use of heavy computer programs be justified.

Therefore, the aim of this research project is to derive simple hand-calculation methods within the chosen topics, and thereby create a coherent basis corresponding to that already existing for concrete structures.

## 1.3 Outline of the Thesis

The four chosen research topics cover a wide field, hence the main content of the thesis is subdivided into four individual parts. These parts cover three of the original research topics. The first part covers welded connections while the second covers steel plate girders. Both the third and the fourth part concern stability problems. The topic of fracture mechanics is not included in this thesis.

The four individual parts are briefly presented below.

PART I deals with simple methods for the calculation of fillet welds based on the theory of plasticity. In developing the solutions, the lower-bound theorem is used. The welding material and parts of the base material are subdivided into triangular regions with homogeneous stress fields; thereby a safe and statically admissible stress distribution is established. The plasticity solutions are compared with tests carried out at The Engineering Academy of Denmark, Lyngby, in the early 1990's, and with old fillet weld tests.

PART II describes a calculation method for steel plate girders with transverse web stiffeners subjected to shear. It may be used for predicting the failure load or, as a design method, to determine the optimal number of transverse web stiffeners.

The new method is called *the plastic tension field method*. The method is based on the theory of plasticity and is analogous to the so-called *diagonal compression field method* developed for reinforced concrete beams with transverse stirrups.

As further verification of the theory, new experiments with plate girders subjected to shear were conducted at The Technical University of Denmark during the present study.

Many other theories have been developed, but the method presented differs from these theories by incorporating the strength of the transverse stiffeners and by the assumption that the tensile bands may pass the transverse stiffeners, something that is often observed in tests. Other methods have only dealt with a single web field between two stiffeners.

PART III presents new effective width equations, which are derived on the basis of a consistent theory.

It was realised many years ago that the elastic buckling theory is not able to account accurately for the real strength. The main reason is that in a large parameter interval,

the ultimate load is reached after yielding of the plate. This fact was pointed out by Kármán et al. (1932), who suggested a modification of the elastic solution by an empirical coefficient. This idea was taken up by Winter (1947), who developed accurate formulae based on the effective width concept, taking the post-buckling capacity into account.

The new method rests on the theory of plasticity, particularly the yield line theory. The emphasis is attached to buckling problems related to plate girders. Two general cases are studied: Plates in uniaxial compression supported along all edges, e.g. the compressed flange in a box girder, and plates with one free edge, e.g. the compressed flange and the internal web stiffeners in an I-shaped girder.

PART IV concerns a simplified theory for calculating the load-carrying capacity of steel plate girders subjected to concentrated loads based on the theory of plasticity.

When designing a steel plate girder, it is usually recommended to add transverse web stiffeners where concentrated loads act. However, this is not always possible to fulfil in practice, as the plate girder may for instance be subjected to wheel loads, loads from purlins and roller loads during construction. It is therefore necessary to check the unstiffened web under the edge compressive loading to ensure no localised failure will occur. This kind of loading on plate girders is commonly known as *patch loading*.

Finally in this part, the phenomenon *flange induced buckling* is touched upon.

Each part may, in general, be considered as individual reports. However, PART IV contains references to both PART II and PART III, hence it may not stand completely alone.

The four individual parts roughly follow a chronological time line, except the new plate girder experiments described in PART II, which were conducted at the end of the study.

A description of the general notation used is found in the previous chapter. However, the notation used for the different topics is also given at the end of each part together with a list of references. Each of the four parts contains a concluding section. After the individual parts, the general conclusions are drawn together with recommendations for future work. Furthermore, a general list of references covering the whole thesis is found.

PART I only contains a summary of the obtained results. The research done within the topic of welded connections is fully described in a separate report, cf. (Hansen 2004). Furthermore, a brief summary is presented in a conference paper cf. (Hansen 2005).

The design method presented in PART II is also described in a conference paper cf. (Hansen and Nielsen 2005). The derivation of the effective width equations, cf. PART III, is also presented in a conference paper cf. (Hansen and Nielsen 2006). It has been extended and will be submitted as a full journal paper to the *International Journal of Advanced Steel Construction* in the form presented in PART III, with only a few alterations in the layout.

The work presented in PART IV has not been published elsewhere.

## 2 THEORY OF PLASTICITY

A complete description of the basic principals of the theory of plasticity will not be given here. Only the main assumptions, the extremum principles and the relevant dissipation formulae are mentioned. A complete description may be found in (Nielsen et al. 2000) or in (Nielsen 1998), where the emphasis is on concrete structures.

The assumed material model is shown in Figure 2.1. The figure shows a stress-strain curve in the uniaxial case. The yield stress, for which arbitrary large strains are possible, is denoted  $f_y$ . The yield stresses for tensile and compressive actions are assumed equal. For stresses below the yield stress, it is seen that no strains occur. A material behaving as shown in the figure, is denoted a *rigid-plastic material*.

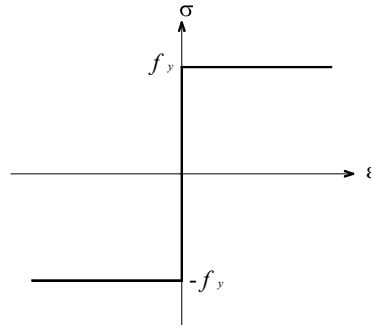


**Figure 2.1:** Uniaxial stress-strain relation for a rigid-plastic material

The maximum work hypothesis by von Mises states that the stresses corresponding to a given strain field assume such values that the plastic work,  $W$ , becomes as large as possible. The plastic work in a three-dimensional, isotropic continuum is given by

$$W = \sigma_1 \varepsilon_1 + \sigma_2 \varepsilon_2 + \sigma_3 \varepsilon_3 \quad (2.1)$$

Here  $\sigma_1$ ,  $\sigma_2$  and  $\sigma_3$  are the principal stresses, and  $\varepsilon_1$ ,  $\varepsilon_2$  and  $\varepsilon_3$  are the corresponding principal strains.

For isotopic materials, the yield point is assumed to be determined by a yield condition, e.g.

$$f(\sigma_1, \sigma_2, \sigma_3) = 0 \quad (2.2)$$

Stresses rendering  $f < 0$  correspond to stresses that may be sustained by the material. Stresses giving  $f > 0$  cannot occur. Furthermore, it is assumed that the yield surface is convex.

The relations between the principal stresses and strains may, with the assumptions mentioned, be expressed by *von Mises' flow rule*:

$$(\varepsilon_1, \varepsilon_2, \varepsilon_3) = \lambda \left( \frac{\partial f}{\partial \sigma_1}, \frac{\partial f}{\partial \sigma_2}, \frac{\partial f}{\partial \sigma_3} \right) \quad (2.3)$$

The indeterminate factor,  $\lambda$ , must satisfy the condition  $\lambda \geq 0$ .

The strain vector is an outward-directed normal to the yield surface, hence Equation (2.3) is also named the *normality condition*.

## 2.1 Extremum Principles for Rigid-Plastic Materials

The *load-carrying capacity* is defined as the load on a body causing deformations without further increase of the load. The terms *yield load* and *failure load* will also be used.

With the above-mentioned assumptions, it is possible to determine the load-carrying capacity by applying the extremum principles for rigid-plastic materials.

When applying these principles in the simplest form, the effect of change of geometry is not taken into account. However, it is not a general assumption in this thesis, since the effect of change of geometry is taken into consideration by estimating the deformations.

### THE LOWER-BOUND THEOREM

Nielsen (1998) expresses the lower-bound theorem thus:

*“If the load has such a magnitude that it is possible to find a stress distribution corresponding to stresses within the yield surface and satisfying the equilibrium conditions and the statical boundary conditions for the actual load, then this load will not be able to cause collapse of the body.”*

A stress distribution such as this is denoted a *safe and statically admissible stress distribution*.

A *lower-bound solution* is found by considering a statically admissible stress field corresponding to the stresses within or on the yield surface.

### THE UPPER-BOUND THEOREM

About the upper-bound theorem Nielsen (1998) concludes for proportional loading:

*“If various geometrically possible strain fields are considered, the work equation can be used to find values of the load-carrying capacity that are greater than or equal to the true one.”*

An *upper-bound solution* is found by considering a *geometrically possible failure mechanism* and by solving the work equation. In the general form, the work equation is normally derived for the undeformed body. However, in this thesis the work equation will be derived for the deformed body in some cases.

### THE UNIQUENESS THEOREM

The uniqueness theorem expresses that a load-carrying capacity corresponding to a geometrically possible failure mechanism, to which a safe and statically admissible stress distribution may be attributed, is equal to the true collapse load.

An *exact solution* requires construction of a statically admissible stress field corresponding to stresses within or on the yield surface in the whole body, as well as verification that a geometrically possible strain field, satisfying the constitutive equations, corresponds to this stress field.

It should be noted that neither the stress field nor the strain field at collapse is uniquely determined.

## 2.2 Dissipation Formulas

In the theory of plasticity it is necessary to operate with discontinuity planes or lines along which jumps in the displacements occur. These discontinuity lines will be denoted *yield lines*.

By far, the most commonly used yield condition for steel is von Mises' yield criterion. In the condition of plane strain, the only possible deformation condition is pure change of angle for a von Mises material. Hence the dissipation in a yield line per unit length,  $W_l$ , is given by

$$W_l = \frac{1}{\sqrt{3}} f_y u t \quad (2.4)$$

where  $f_y$  is the yield stress,  $t$  the thickness of the considered element, and  $u$  is the relative displacement of the two rigid bodies on each side of the yield line.

Steel structures may also be calculated by applying Tresca' yield criterion. For a Tresca material, the dissipation in a yield line per unit length is also given by Equation (2.4), except with the factor  $1/\sqrt{3}$  changed to  $1/2$ , i.e.

$$W_l = \frac{1}{2} f_y u t \quad (2.5)$$

In the condition of plane stress, which for instance occurs in thin plates, the dissipation in a yield line per unit length for a von Mises material is given by

$$W_l = \frac{2}{\sqrt{3}} f_y u t \sqrt{\sin^2 \alpha + \frac{1}{4} \cos^2 \alpha} \quad (2.6)$$

For a Tresca material, the dissipation in a yield line per unit length is given by

$$W_l = \frac{1}{2} f_y u t (1 + \sin |\alpha|) \quad (2.7)$$

In both Equations (2.6) and (2.7),  $\alpha$  is the angle between the relative displacement,  $u$ , and the yield line. As before,  $t$  is the thickness of the considered element. In the condition of plane strain,  $\alpha$  is equal to zero, thus the failure in plane strain is always a pure sliding failure.

The derivation of the above-mentioned dissipation formulae for steel may be found in (Nielsen et al. 2000).

---

# **PART I**

---

## **PLASTICITY THEORY OF FILLET WELDS** **– Lower-Bound Solutions for Static Loading**



# PLASTICITY THEORY OF FILLET WELDS

## – Lower-Bound Solutions for Static Loading

### 1 INTRODUCTION

Currently, static calculations of fillet welds, according to EC3 (2005) and the Danish Code for Steel Structures, DS 412 (1999), are based on a semi-empirical failure condition, which resembles von Mises' yield criterion. The effective weld stress is determined by calculating the mean stresses on the throat section, whereby the failure condition is used without knowledge of the entire stress field.

The aim of this part of the thesis is to establish simple methods for calculation of fillet welds based on the theory of plasticity, where the stress field in the whole weld is included. In developing the solutions, the lower-bound theorem is used. The welding material and parts of the base material are subdivided into triangular regions with homogeneous stress fields; thereby a safe and statically admissible stress distribution is established.

A development of calculation methods for welded connections based on the theory of plasticity was initiated by Nielsen and Pilegaard Hansen (1971), and was followed up by Jensen (1991). The work that remains within this topic is to derive simple methods for calculation of fillet welds and further experimental verification.

Jensen (1991) derived solutions for calculation of fillet welds in the yield stage based on the theory of plasticity. He derived the theories by applying the upper and lower bound theorems based on Tresca's yield criterion. The solutions must be found numerically. In this thesis von Mises' yield criterion is applied, as it more readily allows the establishment of hand-calculation methods.

In relation to the development of Jensen's theoretical solutions, he carried out yield load tests at the Engineering Academy of Denmark, Lyngby, in the early nineties. These experimental results are used to verify the theory here.

Nielsen and Pilegaard Hansen (1971) were also dealing with simple calculation methods based on the theory of plasticity. They determined the stresses in the welds by referring to a section appearing after a rotation of the throat section to one of the faces of the weld, which was previously common practice. Their method is based on the assumption that the welded connection consists of two symmetrical fillet welds. Hence, it cannot be used to calculate single fillet welds. Some parts of their work may still be applied, as will be seen in this thesis.

In Chapter 2, lower-bound solutions for connections with symmetrical fillet welds are presented. This topic is more or less covered by the solutions of Nielsen and Pilegaard Hansen (1971). Therefore, the chapter primarily contains a summary of their solutions. Furthermore, the solutions are verified with experimental results from yield load tests found in the literature.

In Chapter 3, lower-bound solutions for single fillet welds are derived, and the solutions are verified with experiments mainly carried out by Jensen (1991).

### 1.1 Historical Overview

Kist (1936) formulated an expression for determination of the failure load for a welded connection:

$$\sqrt{\sigma^2 + 3\tau^2} = \sigma_i \quad (1.1)$$

Here  $\sigma$  and  $\tau$  are the mean values of the normal stress and the shear stress on the throat section respectively. The expression resembles von Mises' yield criterion for plane stress. It was verified by Kist's own experiments and by experiments made by Jensen (1934).

Kist assumed that failure occurs in the smallest section of the weld (usually the throat section). The stress distribution may be chosen freely if the equilibrium conditions are satisfied, since the stress distribution will adjust so that the maximum load-carrying capacity is reached (the lower-bound theorem of the theory of plasticity). However, there is no guarantee that (both) the equilibrium and boundary conditions will be satisfied, when the stress field of the entire weld is not considered. Thus the stresses on the throat section do not always give a safe statically admissible stress distribution all over the weld. Finally, it is observed that von Mises' yield criterion is applied as a failure criterion.

After the Second World War, van der Eb (1952) conducted new failure tests. These tests did not coincide well with the expression of Kist, cf. Equation (1.1). This led to the following modifications of the expression: I.S.O's modified formula

$$\sqrt{\sigma^2 + 1.8\tau^2} = \sigma_i \quad (1.2)$$

and the  $\beta$ -formula

$$\beta\sqrt{\sigma^2 + 3\tau^2} = \sigma_i \quad (1.3)$$

In these formulae,  $\sigma$  and  $\tau$  are the mean values of the stresses on the throat section, which are only subjected to loads perpendicular to the axis of the weld.

Based on very few failure load tests by Ligtenberg and van Melle (1964), the formulae were modified in order to make them valid for three-dimensional cases.

Despite the weaknesses of the formulae, it was recommended by IIW<sup>1</sup> in 1974 that the  $\beta$ -formula became the basis of revision of the codes, which was going on in many countries, cf. (Jensen 1991). Today, it is also the  $\beta$ -formula that is adopted in EC3 (2005) as well as the Danish Code for Steel Structures, DS 412 (1999).

According to EC3, the effective weld stress has to satisfy the failure condition:

---

<sup>1</sup> International Institute of Welding

$$\sigma_{eff} = \sqrt{\sigma_{90}^2 + 3(\tau_0^2 + \tau_{90}^2)} \leq \frac{f_{ud}}{\beta_w} \quad (1.4)$$

The parameters,  $\sigma_{90}$ ,  $\tau_{90}$ , and  $\tau_0$ , are average, normal and shear stresses along the throat section respectively, see Figure 1.1. Index 0 is parallel and index 90 is perpendicular to the axis of the weld.  $f_{ud}$  is the design value ( $f_u/\gamma_{Mw}$ ) of the ultimate tensile strength of the weaker material.  $\beta_w$  is the appropriate, so-called correlation factor taking into account the correlation between the base material and the weld material. The  $\beta_w$ -value is determined empirically to be between 0.8 and 1.0 depending on the strength of the material, see (ECCS 1989).

In Figure 1.2, Equation (1.4) is compared with the tests made by Jensen (1934) and Kist (1936) respectively. Similarly, the equation is compared with the tests of van der Eb (1952) in Figure 1.3.

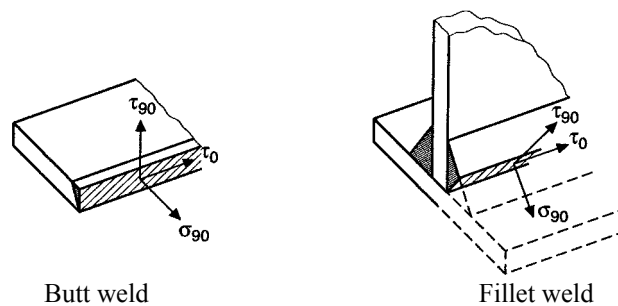


**Figure 1.1:** Stresses on the throat section of a butt weld and a fillet weld according to EC3<sup>2</sup>

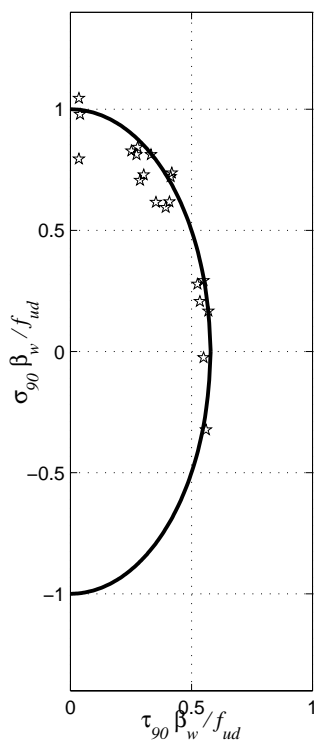


**Figure 1.2:** Comparison with experimental results by Kist and Jensen

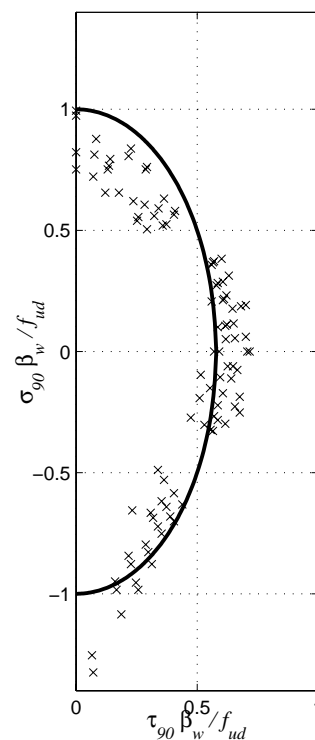


**Figure 1.3:** Comparison with experimental results by van der Eb

<sup>2</sup> The figure is taken from (Bonnerup and Jensen 2003)

The experimental results shown in the figures above are used many times in the literature, e.g. (Bonnerup and Jensen 2003) as a verification of the failure condition in EC3 (2005). It should be noted here that the stress  $\tau_0$  is equal to zero in all of the experiments, hence a complete experimental verification based on these tests will not be sufficient.

In Appendix A, the original test results from Jensen (1934) and Kist (1936) are shown together with sketches of the applied test specimens. In a similar way, the test results and sketches of the test specimens from van der Eb (1952) are shown in Appendix B. From these appendices it is seen that a large number of the specimens are only supplied with one single fillet weld.

In Figure 1.2 there is a good correlation between EC3 (2005) and the experimental results. However, the number of tests is limited, especially for the compressed specimens. The number of tests is much greater in Figure 1.3. These tests show a remarkable difference between the load-carrying capacity in compression and tension. EC3 seems to overestimate the load-carrying capacity for the tensile specimens, and the opposite seems to be the case for the compressed specimens

From the two figures it is also seen that the scatter of the test series is large, especially for the tests by van der Eb. This is due to the fact that the material properties are not well documented, especially in the heat-affected zone.

What is unsatisfactory regarding the approach in EC3 (2005), at least from an academic point of view, is that a yield criterion, here von Mises' criterion, is used without knowledge of the entire stress field. In this thesis it is shown that fortunately, only small corrections are needed according to a consistent treatment.

Only a detailed summary of the achieved results is presented below. The work done within this topic is fully described in a separate report in Danish, see (Hansen 2004).

## 1.2 Assumptions

Welds are normally categorised as either butt welds or as fillet welds, cf. Figure 1.1. Butt welds may be calculated as the remaining structure, thus it is not necessary to consider the welds as long as a sufficient level of quality is ensured. An overview of the different welding methods and the amount of required control is given in (Gath 1997).

Therefore, this part of the thesis deals only with fillet welds, although the derived solutions are also valid for butt welds. Furthermore, welds subjected to fatigue are not considered here.

The cross-section of a fillet weld is assumed to form a right-angled isosceles triangle along the full length of the weld. The height of the cross-section is called the *throat section* and the dimensions of the weld are characterised by the *throat thickness*,  $a$ , and the length,  $L$ . Since  $L \gg a$ , plane strain is assumed. Furthermore, the special boundary conditions in the end zones of the weld are neglected.

The base materials and welding material are assumed homogeneous, isotropic and perfectly plastic. Hence it is possible to apply the extremum principles for rigid-plastic materials, i.e. the lower-bound theorem and the upper-bound theorem. Deriving a simple calculation method is most easily done by applying the lower-bound theorem, hence this is mainly used in the following. In some cases, the upper-bound theorem is applied in order to compare the results obtained by both theorems.

As a yield criterion, von Mises' yield criterion is applied in the form:

$$(\sigma_x - \sigma_y)^2 + (\sigma_y - \sigma_z)^2 + (\sigma_z - \sigma_x)^2 + 6(\tau_{xy}^2 + \tau_{xz}^2 + \tau_{yz}^2) = 2 f_y^2 \quad (1.5)$$

Here  $\sigma_x$ ,  $\sigma_y$ ,  $\sigma_z$ ,  $\tau_{xy}$ ,  $\tau_{xz}$ , and  $\tau_{yz}$  are the stress components in a Cartesian  $x,y,z$ -system of coordinates and  $f_y$  is the yield stress of the weaker material.

In some cases, Tresca's yield criterion is applied in the form:

$$|\sigma_1 - \sigma_3| = f_y \quad (1.6)$$

Here,  $\sigma_1$  is the principal major stress and  $\sigma_3$  is the principal minor stress.

The assumption of plastic materials usage gives the possibility to choose the stress distribution in the weld freely. In general, the stresses are calculated as uniformly distributed on the throat section with the directions, as in EC3 (2005), shown in Figure 1.1. It should be stated that these uniformly distributed stresses on the throat section are a part of the full stress field in the weld, not only the mean stresses on the throat section as defined in EC3. The stress component,  $\sigma_0$ , is, in the following, assumed equal to zero.

In some cases the stresses are determined in the welds by referring to a section appearing after a rotation of the throat section to one of the faces of the weld.

In almost all tests found in the literature, only the failure load has been measured. Since von Mises' yield criterion has never been proved valid as a failure criterion, a comparison to these tests will not be sufficient. Thus in this situation, tests where the yield load is measured are used to verify the theories. Therefore the failure conditions shown are expressed as a function of the yield stress,  $f_y$ , instead of  $f_{ud}/\beta_w$  as in Equation (1.4).

## 2 LOWER-BOUND SOLUTIONS FOR SYMMETRIC FILLET WELDS

With regard to welded connections with two symmetric fillet welds, it was formerly common practice to determine the stresses in the welds by referring to a section appearing after a rotation of the throat section to one of the faces of the weld as described by Nielsen and Pilegaard Hansen (1971). This approach is used in the following, thus to some extent the text in Sections 2.1 – 2.3 follows the text in (Nielsen and Pilegaard Hansen 1971).

A common form of connection is a plate welded to another construction element by two symmetric fillet welds, see Figure 2.1. The dimensions of the welds are given by the throat thickness,  $a$ , and the length,  $L$ .

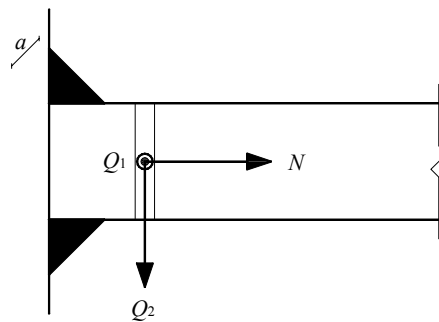


Figure 2.1: Welded connection with two symmetric fillet welds

The connection is subjected to a normal force,  $N$ , and two shear forces,  $Q_1$  and  $Q_2$ . The three load cases are studied one by one, using the lower-bound theorem.

### 2.1 Shear Parallel to the Axis of the Weld

In this case, the shear force,  $Q_1$ , is sustained by uniformly distributed shear stresses,  $\tau$ , on each face of the weld, see Figure 2.2.

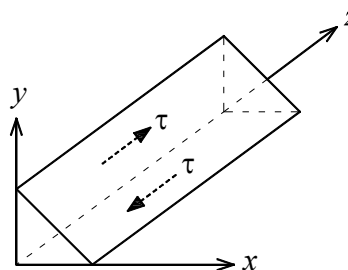


Figure 2.2: Fillet weld subjected to shear

Thereby, a simple statically admissible stress distribution is established. Referring to a Cartesian  $x,y,z$ -system of coordinates, cf. Figure 2.2, the homogeneous stresses are

$$\tau_{xz} = -\tau \quad \tau_{yz} = \tau \quad (2.1)$$

All other stress components are equal to zero. The stress field satisfies the equilibrium conditions since it is homogeneous. The unloaded boundary of the weld has the normal

$$(l, m, n) = \frac{1}{\sqrt{2}} (1, 1, 0) \quad (2.2)$$

Applying the boundary conditions, the stress components  $p_x$ ,  $p_y$  and  $p_z$  will be

$$\begin{bmatrix} p_x \\ p_y \\ p_z \end{bmatrix} = \begin{bmatrix} \sigma_x & \tau_{xy} & \tau_{xz} \\ \tau_{xy} & \sigma_y & \tau_{yz} \\ \tau_{xz} & \tau_{yz} & \sigma_z \end{bmatrix} \begin{bmatrix} l \\ m \\ n \end{bmatrix} = \frac{1}{\sqrt{2}} \begin{bmatrix} 0 & 0 & -\tau \\ 0 & 0 & \tau \\ -\tau & \tau & 0 \end{bmatrix} \begin{bmatrix} 1 \\ 1 \\ 0 \end{bmatrix} = \begin{bmatrix} 0 \\ 0 \\ 0 \end{bmatrix} \quad (2.3)$$

Thus the stresses, cf. Equation (2.1), correspond to an unloaded surface. Inserting Equation (2.1) into von Mises' yield criterion, cf. Equation (1.5), the load-carrying capacity may be expressed by the shear stress on the rotated throat section, see Figure 2.3, as

$$\tau_{1h} = \sqrt{2} \tau = \frac{1}{\sqrt{3}} f_y \cong 0.58 f_y \quad (2.4)$$

where  $f_y$  is the yield stress of the weld material. It is seen that the shear capacity is the highest possible for a von Mises material. The stress on the throat section is also given by Equation (2.4).

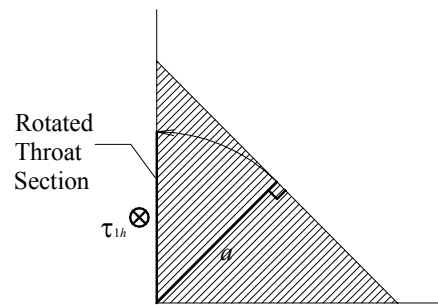


Figure 2.3: Rotated throat section

## 2.2 Uniaxial Tension Perpendicular to the Throat Section

In this case, a safe statically admissible stress distribution may be established by assuming that each weld is subjected to uniaxial tension perpendicular to the throat section. Thereby, equilibrium with the normal force,  $N$ , is obtained through the black area, see Figure 2.4.

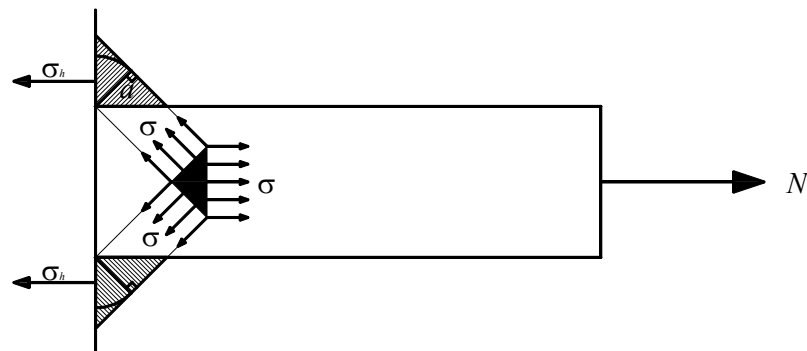


Figure 2.4: Fillet welds subjected to uniaxial tension perpendicular to the throat sections. The black area is under hydrostatic tension

Referring to a Cartesian  $x,y$ -system of coordinates, cf. Figure 2.2, the homogeneous stresses are

$$\sigma_x = \frac{1}{2}\sigma = \frac{\sqrt{2}}{2}\sigma_h \quad \sigma_y = \frac{1}{2}\sigma = \frac{\sqrt{2}}{2}\sigma_h \quad \tau_{xy} = -\frac{1}{2}\sigma = -\frac{\sqrt{2}}{2}\sigma_h \quad (2.5)$$

The load-carrying capacity, expressed by the normal stress on the rotated throat section, is given by

$$\sigma_h = \frac{\sqrt{2}}{2} f_y \cong 0.71 f_y \quad (2.6)$$

It is assumed that the inclined stresses through the welds may be carried further by the base material. If it is not possible to develop the inclined stresses through the welds, the load-carrying capacity must be reduced.

Figure 2.5 (a) shows a connection where the stress field is more complicated.

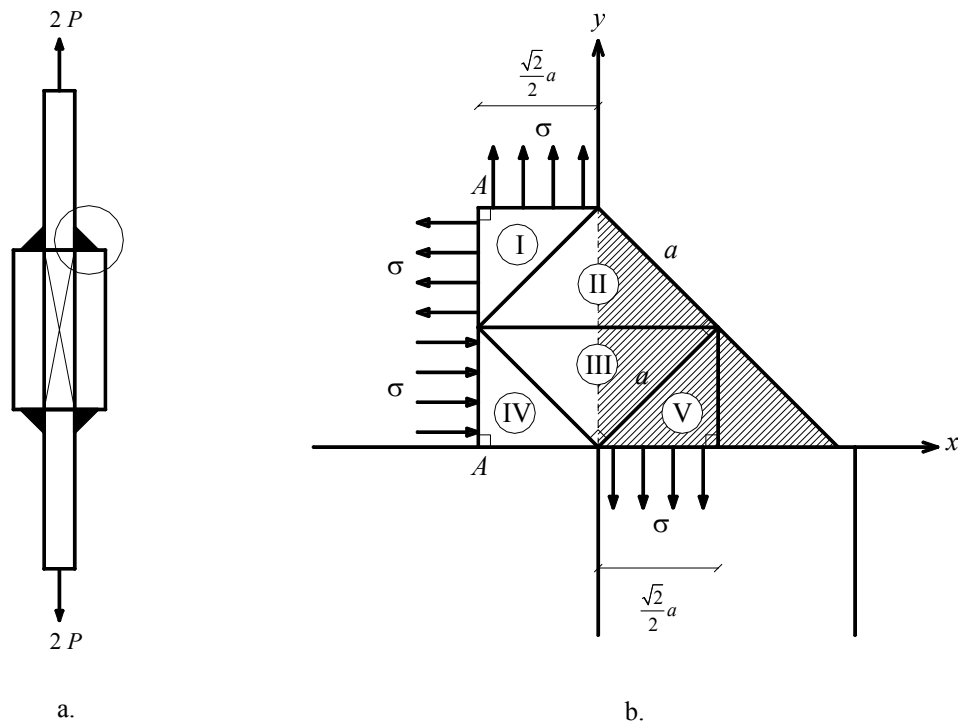


**Figure 2.5:** Stress field where inclined stresses through the weld cannot be established

Figure 2.5 (b) shows a statically admissible stress distribution. The uniform stress,  $\sigma$ , in the strips of width  $\frac{\sqrt{2}}{2} a$ , correspond to half of the load,  $2 P$ . It is assumed that the plate thickness is at least twice the width of the single strip. The stress is transferred to the splice piece by a bending moment in section  $A-A$ . Region I is subjected to hydrostatic tension, region II and V to uniaxial tension, and region IV is subjected to uniaxial compression. For the most critical region III, the stresses are

$$\sigma_x = -\frac{1}{2}\sigma = -\frac{\sqrt{2}}{2}\sigma_h \quad \sigma_y = \frac{1}{2}\sigma = \frac{\sqrt{2}}{2}\sigma_h \quad \tau_{xy} = -\frac{1}{2}\sigma = -\frac{\sqrt{2}}{2}\sigma_h \quad (2.7)$$

By applying von Mises' yield criterion, cf. Equation (1.5), it is found that the load-carrying capacity must be reduced to

$$\sigma_h = \frac{\sqrt{2}}{2} \sigma = \frac{\sqrt{2}}{2} \sqrt{\frac{2}{3}} f_y = \frac{1}{\sqrt{3}} f_y \cong 0.58 f_y \quad (2.8)$$

In this case, a simple upper-bound value is easily found. Consider Figure 2.6 showing a geometrically possible failure mechanism. A pure sliding failure in the yield lines is assumed.

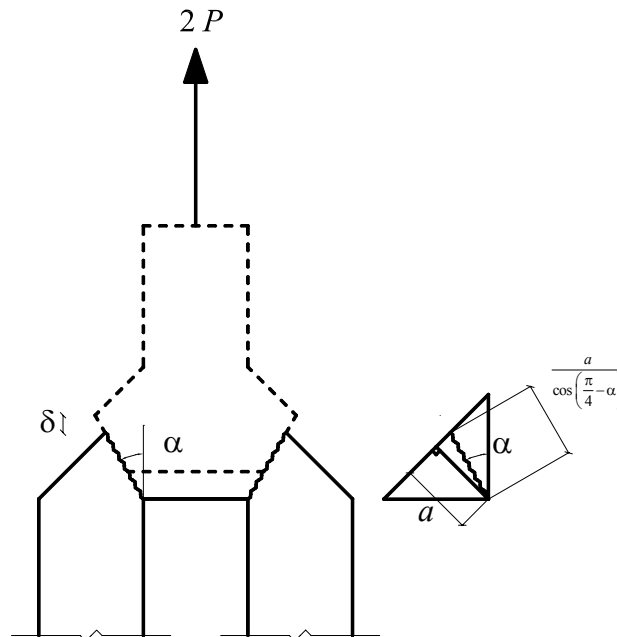


**Figure 2.6:** Geometrically possible failure mechanism

The dissipation per unit length for a von Mises material is given by, cf. (Nielsen et al. 2000),

$$W_l = \frac{1}{\sqrt{3}} f_y u t \quad (2.9)$$

Here, plane strain is assumed,  $u$  is the relative displacement and  $t$  is the thickness. For a Tresca material, the factor  $1/\sqrt{3}$  is simply substituted by a factor of  $1/2$ .

The work equation equals

$$2P\delta = \frac{1}{\sqrt{3}} f_y \frac{\delta}{\cos \alpha} L \cdot 2 \frac{a}{\cos\left(\frac{\pi}{4} - \alpha\right)} \quad (2.10)$$

Minimum of  $P$  is found for  $\alpha = \pi/8$ , thus

$$P = \frac{1}{\cos^2\left(\frac{\pi}{8}\right)} \frac{1}{\sqrt{3}} a L f_y \cong 1.17 \frac{1}{\sqrt{3}} a L f_y \quad (2.11)$$

In the rotated throat section this corresponds to

$$\sigma_h = 1.17 \frac{1}{\sqrt{3}} f_y \cong 0.68 f_y \quad (2.12)$$

Thus the difference between the lower-bound value, cf. Equation (2.8), and the upper-bound value, cf. Equation (2.12), is not larger than the difference between using Tresca's or von Mises' yield criterion. On the safe side, the lower-bound value for  $\sigma_h$ , given by Equation (2.8), is applied in the following.

### 2.3 Shear Perpendicular to the Axis of the Weld

In the same way, a safe statically admissible stress distribution may be established in load case,  $Q_2$ . The only difference is that the uniaxial stresses have opposite signs, see Figure 2.7. The black area is now subjected to pure shear, which is the same as pure tension and pure compression under 45 degrees, respectively.

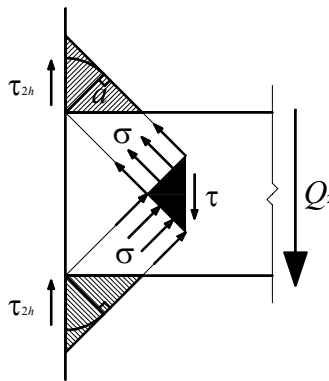


**Figure 2.7:** Fillet welds subjected to uniaxial tension and compression, respectively. The black area is under pure shear

In the Cartesian  $x,y$ -system of coordinates, cf. Figure 2.2, the homogeneous stresses are

$$\sigma_x = \frac{1}{2} \sigma = \frac{\sqrt{2}}{2} \tau_{2h} \quad \sigma_y = \frac{1}{2} \sigma = \frac{\sqrt{2}}{2} \tau_{2h} \quad \tau_{xy} = -\frac{1}{2} \sigma = -\frac{\sqrt{2}}{2} \tau_{2h} \quad (2.13)$$

The load-carrying capacity, expressed by the shear stress on the rotated throat section, is the same as for  $\sigma_h$  in Equation (2.6), i.e.

$$\tau_{2h} = \frac{\sqrt{2}}{2} f_y \cong 0.71 f_y \quad (2.14)$$

As in Section 2.2, it is assumed that the inclined stresses through the welds may be carried further by the base material.

## 2.4 Yield Surfaces for Symmetric Fillet Welds

Superimposing and applying von Mises' yield criterion, cf. Equation (1.5), the three single lower-bound solutions, cf. Equations (2.1), (2.5) and (2.13), lead to a yield condition for the load-carrying capacity for symmetric fillet welds, which may be written:

$$2\left(|\sigma_h| + |\tau_{2h}|\right)^2 + 3\tau_{1h}^2 \leq f_y^2 \quad (2.15)$$

In connections where uniaxial stresses through the welds cannot be established, the factor 2 in Equation (2.15) may be substituted with 3, cf. (Nielsen and Pilegaard Hansen 1971), which gives

$$3\left(|\sigma_h| + |\tau_{2h}|\right)^2 + 3\tau_{1h}^2 \leq f_y^2 \quad (2.16)$$

With this modification, Equation (2.16) gives the same result as Equation (2.8), that is  $\sigma_h = f_y/\sqrt{3}$  for  $\tau_{1h} = \tau_{2h} = 0$ .

The yield conditions may be expressed in a more convenient way as non-dimensional generalised forces. In this way Equation (2.15) is written:

$$\frac{1}{2}\left(|n| + |q_2|\right)^2 + \frac{3}{4}q_1^2 \leq 1 \quad (2.17)$$

Here the non-dimensional forces are given by

$$n = \frac{N}{aL f_y} \quad q_1 = \frac{Q_1}{aL f_y} \quad q_2 = \frac{Q_2}{aL f_y} \quad (2.18)$$

With the same modification as in Equation (2.16), the yield condition for symmetric fillet welds, where the inclined uniaxial stresses cannot be established, is given by

$$\frac{3}{4}\left(|n| + |q_2|\right)^2 + \frac{3}{4}q_1^2 \leq 1 \quad (2.19)$$

If  $\sigma_{90} = \tau_{90}$  and  $f_y = f_{ud}/\beta_w$  are introduced into the failure condition in EC3 (2005), cf. Equation (1.4), this equation may be expressed exactly as in Equation (2.17), since

$$\tau_0 = \tau_{1h} \quad , \quad \sigma_{90} = \tau_{90} = \frac{\sqrt{2}}{2}\sigma_h = \frac{\sqrt{2}}{2}\tau_{2h} \quad (2.20)$$

Inserting (2.20) into Equation (1.4) gives

$$\sigma_{eff}^2 = 2\left(|\sigma_h| + |\tau_{2h}|\right)^2 + 3\tau_{1h}^2 \leq f_y^2 \quad (2.21)$$

However, according to EC3 (2005), the failure condition is the same for any weld, and no reduction of the load-carrying capacity is necessary in any cases.

## 2.5 Comparison with Experimental Results

Tests in the yield stage, with specimens (see Figure 2.8) where uniaxial stresses through the welds cannot be established, have been made at the Engineering Academy of Denmark (Jensen 1991). The specimens were cut out of a steel plate, which means that the welds were only marked by the geometry. Thereby, the number of unknown parameters was reduced. The failure load was also measured in the experiments in order to verify whether there was a relation between the final failure and the yield zones. This did not turn out to be the case. The failures of some selected specimens are shown in Figure 2.9.

The data for the experiments may be found in Appendix C.

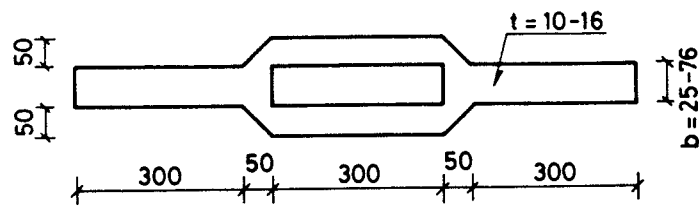


Figure 2.8: Test specimens (measures in mm) on yield tests<sup>3</sup>

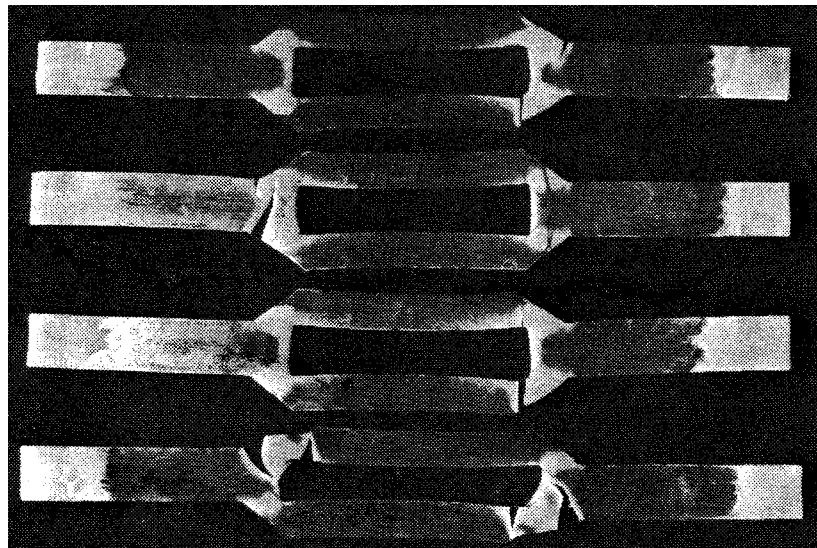


Figure 2.9: Failure of test specimens<sup>4</sup>

In these tests the specimens are subjected to a normal force,  $N$ , cf. Figure 2.1, which means that  $Q_1$  and  $Q_2$  are equal to zero. In this case, the lower-bound solution gives, cf. Equation (2.19),

$$N^- = \frac{2}{\sqrt{3}} a L f_y \cong 1.155 a L f_y \quad (2.22)$$

The upper-bound solution, assuming plane strain, gives, cf. Equation (2.12),

$$N^+ = 1.17 \frac{2}{\sqrt{3}} a L f_y \cong 1.351 a L f_y \quad (2.23)$$

<sup>3</sup> The figure is taken from (Jensen 1991)

<sup>4</sup> The figure is taken from (Jensen 1991)

In the Hansen (2004) report, assuming plane stress, an upper-bound solution is studied. The upper-bound determined is  $N^+ = 1.320 a L f_y$ . If  $f_y$  is set equal to  $f_{ud}/\beta_w$ , the failure condition in EC3 (2005), cf. Equation (1.4), gives

$$N_{EC3} = \sqrt{2} a L f_y \cong 1.414 a L f_y \quad (2.24)$$

The lower-bound value, the upper-bound value (assuming plane stress), and the value from EC3 are shown in Figure 2.10 together with the experimental results. The mean value of the tests is  $N = 1.170 a L f_y$ , which is close to the lower-bound solution.

The mean value of the ratios,  $N/N_{exp}$ , is found to be 0.988 with a standard deviation of 3.4 %.

Furthermore it is seen that EC3 overestimates the load-carrying capacity in this case.

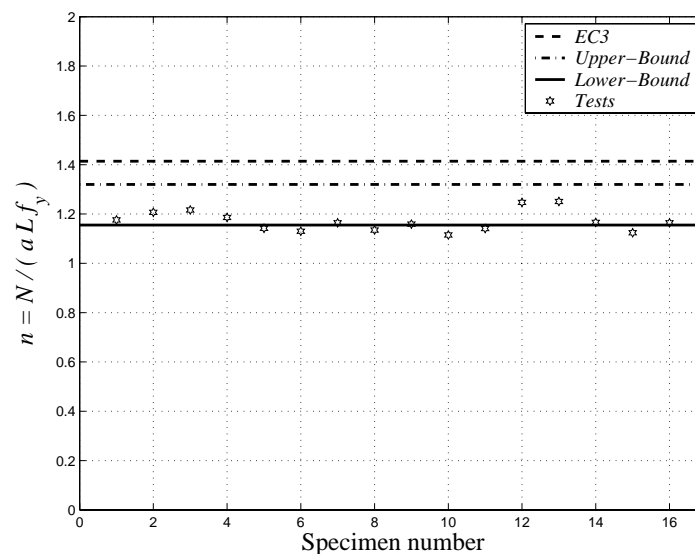


**Figure 2.10:** Comparison of theory and test results

Experiments in the yield stage, where uniaxial stresses through the welds may develop, are conducted by Butler and Kulak (1971), Swannell (1981), Clark (1972) and by Miazga and Kennedy (1989). March (1985) did tests with aluminium welds. The theory for  $q_2 = 0$ , cf. Equation (2.17), is compared with the experimental results in Figure 2.11, where  $n_1$  is shown as a function of  $q_1$ .

There is a relatively large scatter in the test results, nevertheless they appear to verify the theory. By taking the square root of the left-hand side of Equation (2.17), the effective weld stress  $\sigma_{exp}$  for each test result is found. The theory gives  $\sigma_{eff}/f_y = 1$ , then the mean value of the ratios,  $\sigma_{eff}/\sigma_{exp}$ , is 1.020 and the standard deviation is 12.4 % of all the tests in the figure.

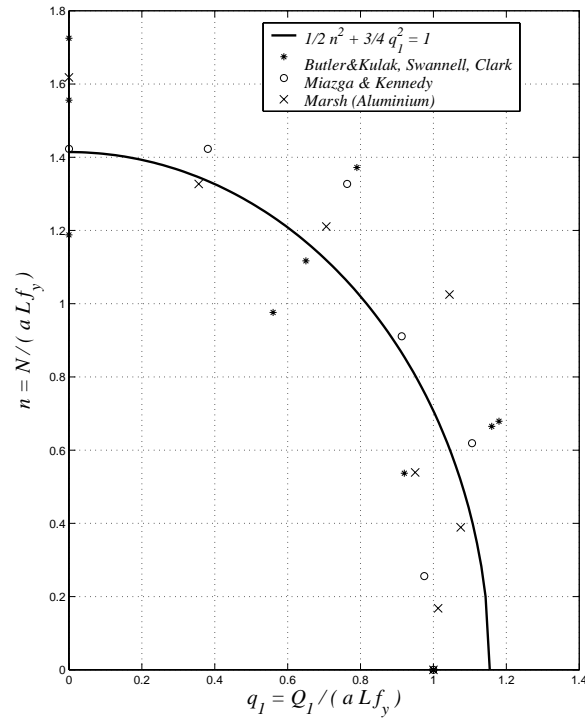


Figure 2.11: Relationship between  $n_1$  and  $q_1$ , theory and test results

Swannell and Skewes (1978) made a limited number of tests with combined load case  $N$  and  $Q_1$ , where uniaxial stresses through the welds could not be established. In these tests,  $N$  is in compression, which has no influence on the verification of the theory at yielding. The theory for  $q_2 = 0$ , cf. Equation (2.19), is compared with the experimental results in Figure 2.12, where  $n_1$  is shown as a function of  $q_1$ .

The theory seems to underestimate the load-carrying capacity in pure compression, and the opposite seems to be the case at pure shear.

The mean value of the ratios,  $\sigma_{eff}/\sigma_{exp}$ , is 1.065 and the standard deviation is 10.0 % of the tests in the figure.

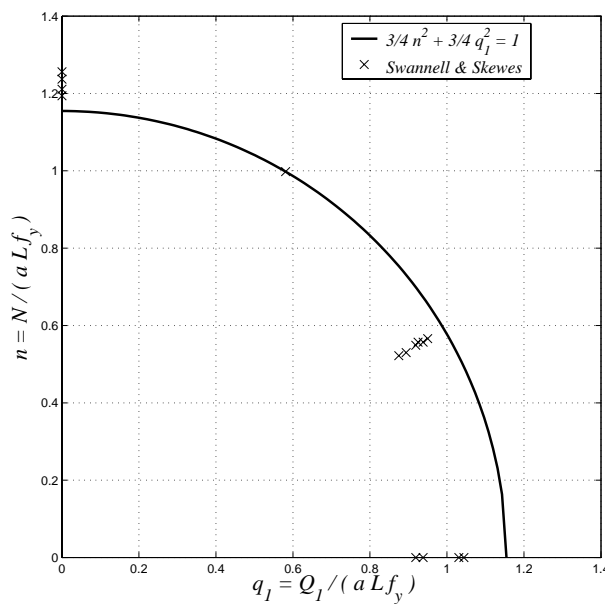


Figure 2.12: Relationship between  $n_1$  (compression) and  $q_1$ , where the uniaxial stresses cannot be established, theory and test results

### 3 LOWER-BOUND SOLUTIONS FOR SINGLE FILLET WELDS

The lower-bound solutions given in Sections 2.1 and 2.2 are also valid for connections with a single fillet weld. However, the solution given in Section 2.3 is only valid for connections with two symmetric fillet welds, as both uniaxial tension and compression must be established. Therefore new lower-bound solutions are necessary.

#### 3.1 Shear on the Throat Section Perpendicular to the Axis of the Weld

The solutions needed refer to shear (in the plane of the throat section) that is perpendicular to the axis of the weld. Again, this is done by establishing a safe, statically admissible stress distribution, see Figure 3.1. In this figure, the welding material and parts of the base material are subdivided into four triangular regions with homogeneous stress fields. Equilibrium with the shear stress on the throat section is obtained by the two boundary stresses. In the lower half (the dashed lines) the signs of the stresses are opposite to the stresses in the upper half.

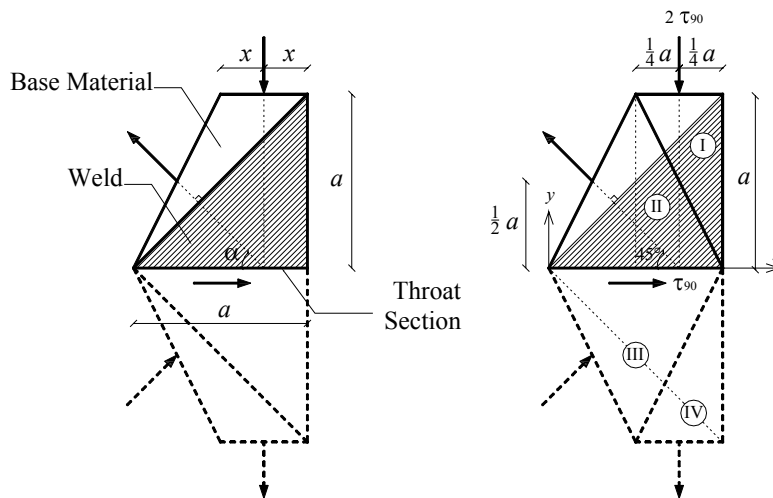


Figure 3.1: Statically admissible stress distribution for  $x = \frac{1}{4} a$

The horizontal part,  $2x$ , of the base material is included. By choosing  $x = \frac{1}{4} a$ , the maximum value of the shear stress on the throat section is found. The vertical boundary stress will then be  $2\tau_{90}$ . Region I is subjected to uniaxial compression. In the Cartesian  $x,y$ -system of coordinates, cf. Figure 3.1, the homogeneous stresses are

$$\sigma_x = 0 \quad \sigma_y = -2\tau_{90} \quad \tau_{xy} = 0 \quad (3.1)$$

The load-carrying capacity for region I is given by, cf. Equation (1.5),

$$\tau_{90} = \frac{1}{2} f_y \quad (3.2)$$

In region II the stresses are given by

$$\sigma_x = \frac{1}{2} \tau_{90} \quad \sigma_y = 0 \quad \tau_{xy} = -\tau_{90} \quad (3.3)$$

The load-carrying capacity for region II is given by, cf. Equation (1.5),

$$\tau_{90} = \frac{2}{\sqrt{13}} f_y \cong 0.56 f_y \quad (3.4)$$

Region III and IV render the same load-carrying capacity as in Equations (3.2) and (3.4) respectively.

From Equation (3.4) it is seen that it is not fully possible to reach the maximum shear load-carrying for a von Mises material ( $\sim 0.58 f_y$ ). It is also seen that region I is the critical region, hence the load-carrying capacity is given by Equation (3.2). The stress fields in the two regions are illustrated in Figure 3.2 by applying Mohr's circle.

When Tresca's yield criterion, cf. Equation (1.6), is applied, region II will be the critical one, as  $\tau_{90}$  in region I will still be given by Equation (3.2), while for region II  $\tau_{90} = 0.49 f_y$  is found.

It is not convenient to have region I as the critical one, hence the statically admissible stress distribution in Figure 3.3, with  $x = \frac{1}{2} a$ , is chosen.

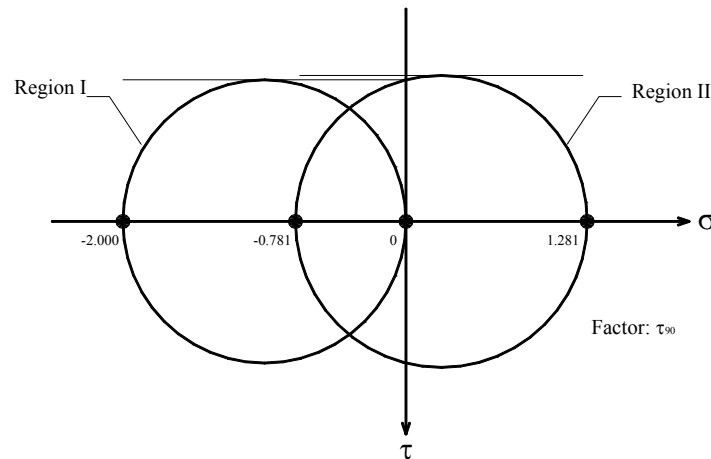


Figure 3.2: Mohr's circle applied on the two stress fields

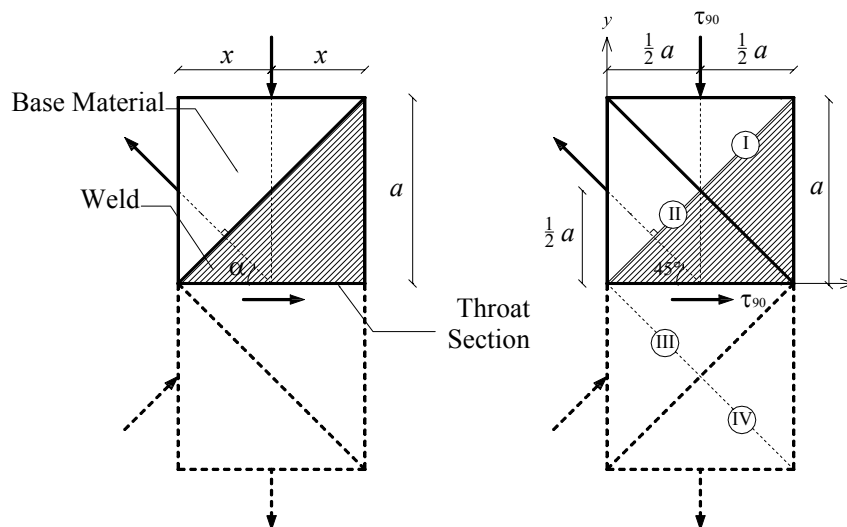


Figure 3.3: Statically admissible stress distribution for  $x = \frac{1}{2} a$

Only region III and IV influence the load-carrying capacity. In the Cartesian  $x,y$ -system of coordinates, cf. Figure 3.3, the homogeneous stresses in region III are

$$\sigma_x = -\tau_{90} \quad \sigma_y = 0 \quad \tau_{xy} = -\tau_{90} \quad (3.5)$$

and in region IV

$$\sigma_x = 0 \quad \sigma_y = \tau_{90} \quad \tau_{xy} = 0 \quad (3.6)$$

The load-carrying capacity (region III) is then given by  $\tau_{90} = 0.50 f_y$ , which is lower than the maximum shear capacity of a von Mises material ( $\sim 0.58 f_y$ ).

For region IV  $\tau_{90} = f_y$  is found, hence region III is now decisive. The stress fields in all four regions are illustrated in Figure 3.4 by applying Mohr's circle. The circles for region III and IV correspond to the circles for regions I and II mirrored at the  $\tau$ -axis, respectively.

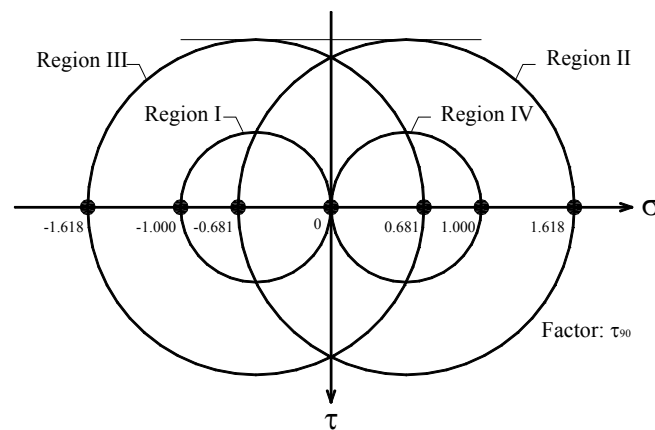


Figure 3.4: Mohr's circle applied on the four stress fields

### 3.2 Yield Surfaces for Single Fillet Welds

To be able to compare the solutions with the failure conditions used in EC3 (2005), cf. Equation (1.4), the notation of the stresses in the above three solutions are harmonised with the EC3 notation. It is seen that  $\tau_{1h} = \tau_0$  in Equation (2.4) and  $\sigma = \sigma_{90}$  in Equation (2.5). Equations (3.5) and (3.6) are already expressed by  $\tau_{90}$ . It must be clearly stated that  $\sigma_{90}$ ,  $\tau_{90}$  and  $\tau_0$  are uniformly distributed stresses on the throat section, and are in agreement with the stress field as a whole, and not just the average stresses on the throat section as in EC3. Superimposing the three lower-bound solutions, after transforming them to the same system of coordinates, see Figure 3.5, then leads to a yield surface for the load-carrying capacity of single fillet welds, see Figures 3.6 and 3.7. The superimposed stresses referred to in the Cartesian  $x,y,z$ -system of coordinates, cf. Figure 3.5, are given in Table 3.1. Region V – VIII is given by the solution for  $\tau_{90}$ , cf. Equations (3.5) and (3.6), so they will not influence the superimposed load-carrying capacity.

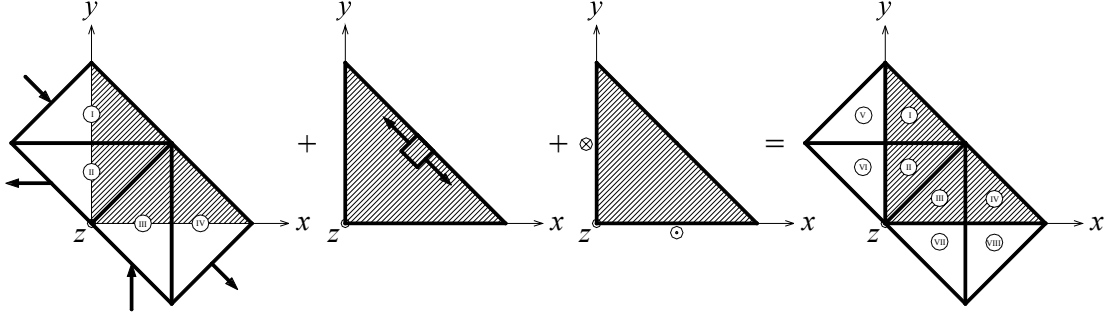


Figure 3.5: Superposition of the three solutions for  $\sigma_{90}$ ,  $\tau_{90}$  and  $\tau_0$ , respectively

Region	$\sigma_x$	$\sigma_y$	$\tau_{xy}$	$\tau_{xz}$	$\tau_{yz}$
I	$-\frac{1}{2} \tau_{90} + \frac{1}{2} \sigma_{90}$	$-\frac{1}{2} \tau_{90} + \frac{1}{2} \sigma_{90}$	$\frac{1}{2} \tau_{90} - \frac{1}{2} \sigma_{90}$	$-\frac{\sqrt{2}}{2} \tau_0$	$\frac{\sqrt{2}}{2} \tau_0$
II	$\frac{3}{2} \tau_{90} + \frac{1}{2} \sigma_{90}$	$-\frac{1}{2} \tau_{90} + \frac{1}{2} \sigma_{90}$	$\frac{1}{2} \tau_{90} - \frac{1}{2} \sigma_{90}$	$-\frac{\sqrt{2}}{2} \tau_0$	$\frac{\sqrt{2}}{2} \tau_0$
III	$\frac{1}{2} \tau_{90} + \frac{1}{2} \sigma_{90}$	$-\frac{3}{2} \tau_{90} + \frac{1}{2} \sigma_{90}$	$-\frac{1}{2} \tau_{90} - \frac{1}{2} \sigma_{90}$	$-\frac{\sqrt{2}}{2} \tau_0$	$\frac{\sqrt{2}}{2} \tau_0$
IV	$\frac{1}{2} \tau_{90} + \frac{1}{2} \sigma_{90}$	$\frac{1}{2} \tau_{90} + \frac{1}{2} \sigma_{90}$	$-\frac{1}{2} \tau_{90} - \frac{1}{2} \sigma_{90}$	$-\frac{\sqrt{2}}{2} \tau_0$	$\frac{\sqrt{2}}{2} \tau_0$

Table 3.1: Homogeneous stresses in region I – IV

There are two surfaces as there are two regions that influence the load-carrying capacity, cf. Figure 3.3. The yield surfaces are given by:

$$\sigma_{90}^2 + 4\tau_{90}^2 + |\sigma_{90}\tau_{90}| + 3\tau_0^2 \leq f_y^2 \quad (3.7)$$

$$(|\sigma_{90}| + |\tau_{90}|)^2 + 3\tau_0^2 \leq f_y^2 \quad (3.8)$$

The load-carrying capacity is governed by the equation that gives the smaller value on the left hand side of the equations. For  $|\sigma_{90}| > 0.75 f_y$ , Equation (3.8) is valid, otherwise Equation (3.7) is referred to. The absolute value of the product,  $\sigma_{90}\tau_{90}$ , indicates that the product will always reduce the load-carrying capacity.

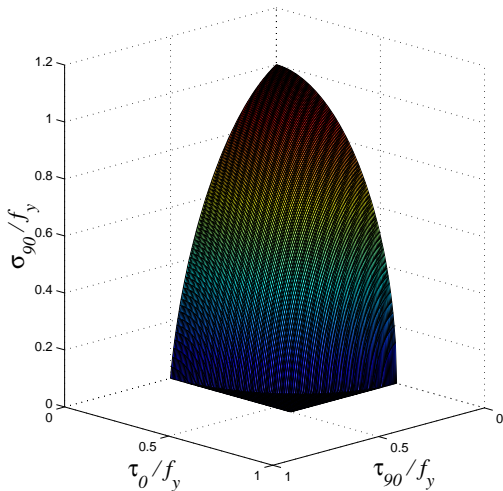


Figure 3.6: Yield surface given by Equation (3.7)

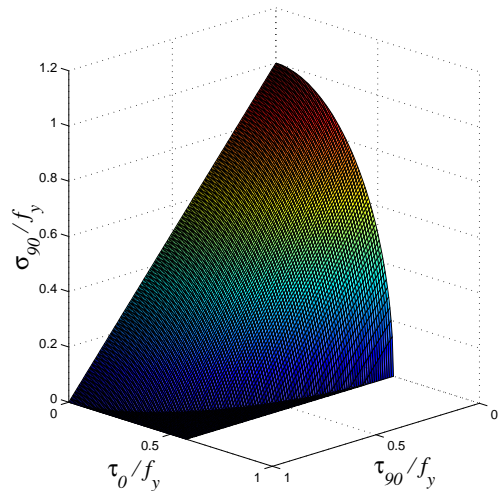


Figure 3.7: Yield surface given by Equation (3.8)

### 3.3 Comparison with Experimental Results

The yield surfaces are compared with tests made by Jensen (1991) and by Ligtenberg and van Melle (1964). In the special case  $\tau_0 = 0$ , see Figure 3.8, the best agreement with the theory is achieved for series S02. Here, the specimens are cut out of a steel plate; hence the number of unknown parameters is reduced, since the specimens are not welded. The larger deviation from theory is achieved for series 323.18. The specimens in these tests are loaded to failure; therefore the yield load is inaccurately determined. The specimens for series S02 are shown in Figure 3.9, and for series 323.14 and 323.18 in Figure 3.10.

The effective weld stress for  $|\sigma_{90}| \leq 0.75 f_y$  is given by, cf. Equation (3.7),

$$\sigma_{eff} = \sqrt{\sigma_{90}^2 + 4\tau_{90}^2 + |\sigma_{90}\tau_{90}|} \leq f_y \quad (3.9)$$

For  $|\sigma_{90}| > 0.75 f_y$ , the effective weld stress is given by, cf. Equation (3.8),

$$\sigma_{eff} = |\sigma_{90}| + |\tau_{90}| \leq f_y \quad (3.10)$$

The mean value of the ratios,  $\sigma_{eff}/\sigma_{exp}$ , is 1.052 and the standard deviation is 10.8 % of all the tests in the figure.

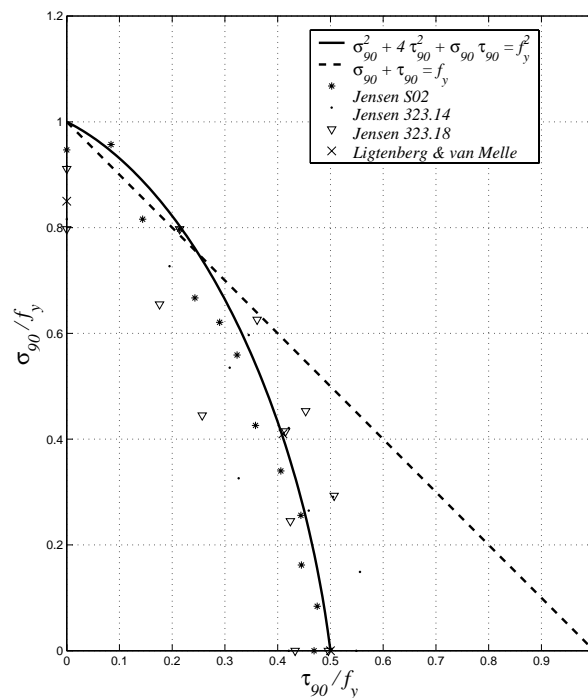


Figure 3.8: Theory and test for  $\tau_0 = 0$

Ligtenberg and van Melle (1964) also conducted experiments at the yield stage with some relatively strange looking specimens, see Figure 3.11.

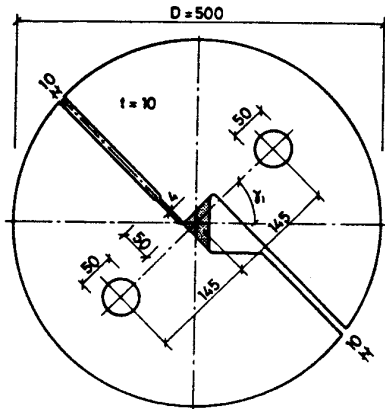


Figure 3.9: Test specimens for series S02 (measures in mm)<sup>5</sup>

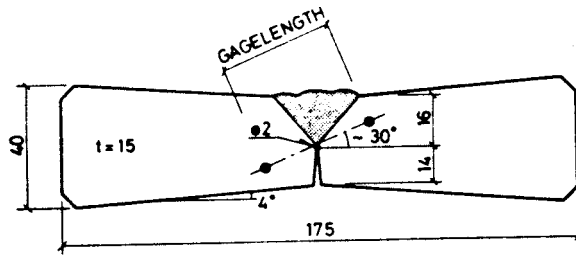


Figure 3.10: Test specimens for series 323.14 and 323.18 (measures in mm)<sup>6</sup>

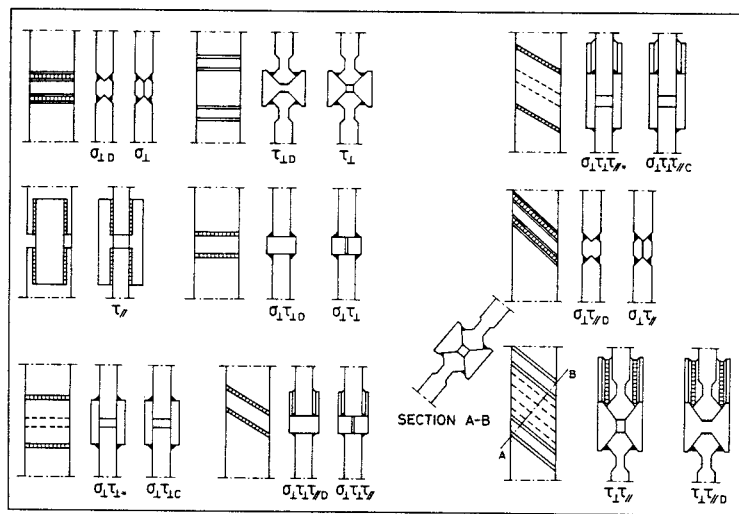


Figure 3.11: Specimens for series by Ligtenberg and van Melle (1964)<sup>7</sup>

In the special case  $\tau_{90} = 0$ , the two yield surfaces give the same result, see Figure 3.12. The specimens for series 323.23 are shown in Figure 3.13 and the effective weld stress is given by, cf. Equations (3.7) and (3.8),

$$\sigma_{eff} = \sqrt{\sigma_{90}^2 + 3\tau_0^2} \leq f_y \quad (3.11)$$

There is very good agreement with the tests. The mean value of the ratios,  $\sigma_{eff}/\sigma_{exp}$ , is 0.973 and the standard deviation is 5.4 % of all the tests in the figure.

<sup>5</sup> The figure is taken from (Jensen 1991)

<sup>6</sup> The figure is taken from (Jensen 1991)

<sup>7</sup> The figure is taken from (Witteveen and van Douwen 1966)

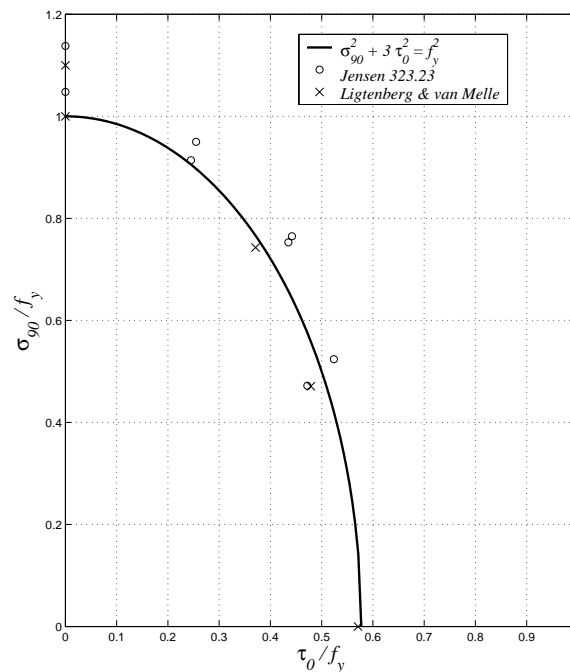


**Figure 3.12:** Theory and test for  $\tau_{90} = 0$

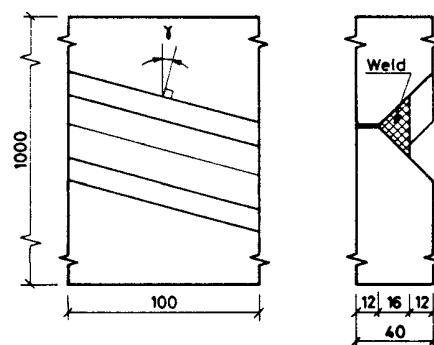


**Figure 3.13:** Test specimens for series 323.23 (measures in mm)<sup>8</sup>

In the special case  $\sigma_{90} = 0$ , almost no tests have been found in the literature, see Figure 3.14. Here the points represent the mean value for five tests each. The effective weld stress is given by, cf. Equation (3.7),

$$\sigma_{eff} = \sqrt{4\tau_{90}^2 + 3\tau_0^2} \leq f_y \quad (3.12)$$

The data for all experiments by Jensen (1991) may be found in Appendix C. For the individual test series shown in Figures 3.8, 3.12 and 3.14, the following mean values and standard deviations are obtained:

- Jensen S02: Mean 1.042, standard deviation 3.6 %.
- Jensen 323.14: Mean 1.046, standard deviation 13.2 %.
- Jensen 323.18: Mean 1.068, standard deviation 14.3 %.
- Jensen 323.23: Mean 0.957, standard deviation 5.3 %.
- Ligtenberg and van Melle: Mean 1.038, standard deviation 7.6 %.

<sup>8</sup> The figure is taken from (Jensen 1991)

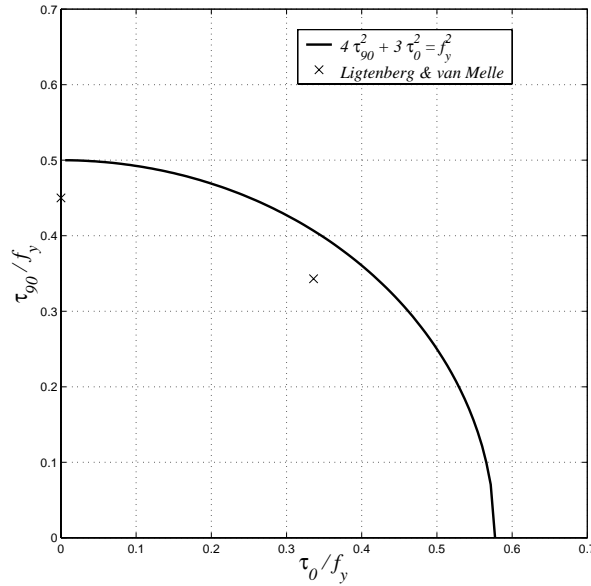


Figure 3.14: Theory and test for  $\sigma_{90} = 0$

### 3.4 Reduction of the Load-Carrying Capacity

As described in Section 2.2, the load-carrying capacity has to be reduced if inclined uniaxial stresses through the weld cannot be established. Superimposing the two shear solutions and the reduced normal stress solution, cf. Equation (2.7), leads to a reduced yield surface for a single fillet weld:

$$\frac{3}{2}\sigma_{90}^2 + 4\tau_{90}^2 + \frac{9}{2}|\sigma_{90}\tau_{90}| + 3\tau_0^2 \leq f_y^2 \quad (3.13)$$

Here, only one region, cf. Figure 3.3, influences the load-carrying capacity. Therefore the yield surface is given by only one expression. No tests have been found to verify the theory, so it is compared to the solution given by Equation (3.7), see Figures 3.15 and 3.16. It is seen that the load-carrying capacity is reduced by up to 18%. In the special case  $\sigma_{90} = 0$ , the yield surfaces give the same result, as no reduction is needed.

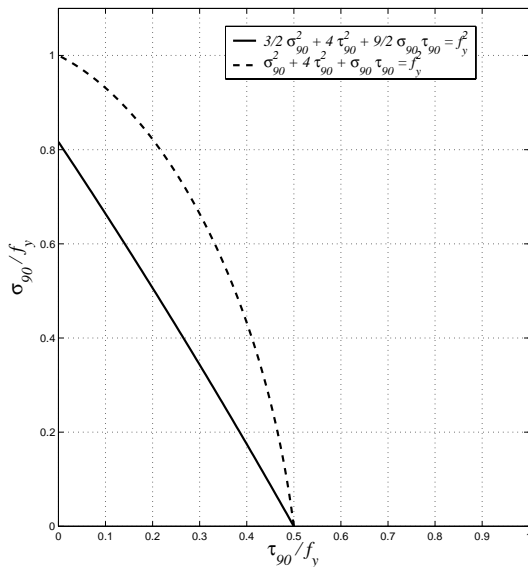


Figure 3.15: Relationship between  $\sigma_{90}$  and  $\tau_{90}$

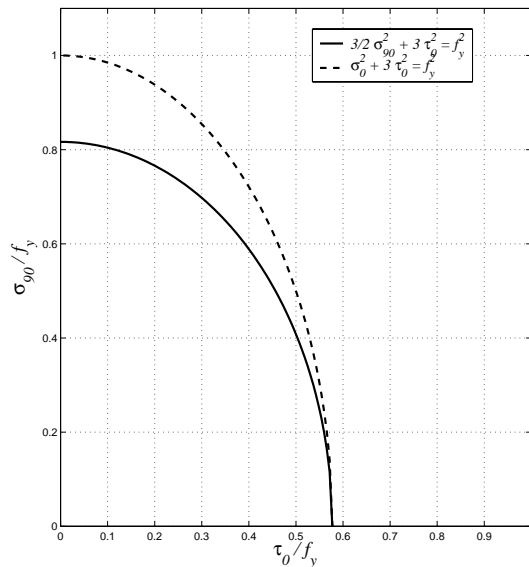
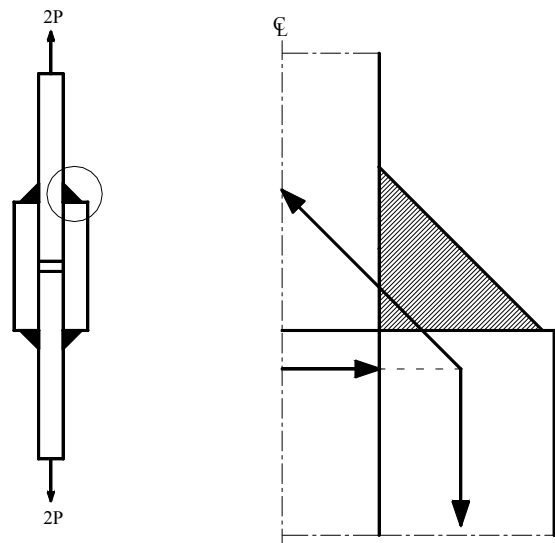


Figure 3.16: Relationship between  $\sigma_{90}$  and  $\tau_0$

In a splice piece joint like that shown in Figure 3.17, the welds may be subjected to uniaxial tension through the welds, as the inclined tensile stress may be transferred to the splice pieces by compression in the adjacent plates. Hence the load-carrying capacity is not reduced in this case. The “clamping” phenomenon is illustrated in Figure 3.17.

If the thickness of the splice pieces is at least twice the throat thickness, the load-carrying capacity is given by Equation (2.15), as the joint contains two symmetric fillet welds.

However, for a given welded connection, it may be difficult to evaluate whether the “clamping” phenomenon is present or not. Hence, there is some associated doubt when including this phenomenon in the calculations.



**Figure 3.17:** Splice piece joint

## 4 CONCLUSION

Yield conditions are determined for symmetric fillet welds and single fillet welds, respectively. The yield conditions for joints with two symmetrical fillet welds are derived by referring to a section appearing after a rotation of the throat section to one of the faces of the weld. The obtained solution gives the same result as the failure criterion in EC3 as long as the inclined uniaxial stress through the welds may be carried further by the base material.

If inclined uniaxial stress through the welds cannot be established, the load-carrying capacity must be reduced.

The yield condition of a joint with a single fillet weld is determined by the smaller value of two yield surfaces.

The derived yield conditions are compared to tests where emphasis is attached to the determination of the yield load instead of the failure load. There is very good agreement with these tests. The best agreement is obtained with tests where the specimens have been cut out of a steel plate; hence the welds are only marked by the geometry. In that way the number of unknown parameters is reduced.

## 5 REFERENCES

- BONNERUP, B and JENSEN, B. C. (2003). *Stålkonstruktioner efter DS 412* (1. udg.). København: Ingeniøren/Bøger.
- BUTLER, L. J. and KULAK, G. L. (1971). Strength of Fillet Welds as a Function of Direction of Load. *Welding Journal Supplement*, **36(5)**, 231-234.
- CLARK, P. J. (1972). Basis of Design for Fillet-Welded Joints Under Static Loading. *Proceedings, Conference on Welding Product Design*. Vol. 2. Welding Institute, Abington U.K., 85-96.
- DANSK STANDARD (1999). *DS 412: Norm for stålkonstruktioner* (3. udg.). København: Dansk Standard.
- EB VAN DER, W. J. (1952). The Testing of End Fillet Welds. *Vorbereich 4. Kongress Int. Ver. für Brückenbau und Hockbau*, 459-474.
- EUROPEAN COMMITTEE FOR STANDARDISATION (EC3 2005). *Eurocode 3: Design of Steel Structures – Part 1-8: Design of Joints*. EN 1993-1-8: 2005. Brussels: CEN.
- EUROPEAN CONVENTION FOR STRUCTURAL STEELWORK (ECCS 1989). *Background Documentation to Eurocode 3-1-1*. Chapter 6, Document 6.05.
- GATH, J. (1997). *Stålkonstruktioner: Beregning af svejsesamlinger i fågangspåvirkede stålkonstruktioner*. Lyngby: BYG•DTU, Danmarks Tekniske Universitet.
- HANSEN, T. (2004). *Plasticitetsteori for svejsesømme: Nedreværdiløsninger for statisk last*. R-144. Lyngby: BYG•DTU, Danmarks Tekniske Universitet.
- JENSEN, C. D. (1934). Combined Stresses in Fillet Welds. *Journal of the American Welding Society*, **13**, pp 17-21.
- JENSEN, Aa. P. (1991). *Svejsesømmes styrke*. Lyngby: Danmarks Ingeniørakademi.
- KIST, N. C. (1936). Berechnung der Schweissnähte unter Berücksichtigung konstanter Gestaltänderungsenergie. *Vorbereich 2. Kongress Int. Ver. für Brückenbau und Hochbau*.
- LIGTENBERG, F. K. and VAN MELLE, F. (1964). Onderzoek naar de Vervorming van statisch belaste hoekklasse. *Heron*, **12(1)**.
- MARSH, C. (1985). Strength of Aluminum Fillet Welds. *Welding Journal, Welding Research Supplement*, 335-338.
- MIAZGA, G. S. and KENNEDY, D. L. J. (1989). Behaviour of Fillet Welds as a Function of the Angle Loading. *Canadian Journal of Civil Engineering*, **6**, 583-599.
- NIELSEN, M. P. and PILEGAARD HANSEN, L. (1971). *AM 1.1. Stålkonstruktioner: Materialer og samlinger*. Aalborg: Danmarks Ingeniørakademi.
- NIELSEN, M. P., PILEGAARD HANSEN, L. and RATHKJEN, A. (2000). *Mekanik 2.2 del 2: Rumlige spændings- og deformationstilstande*. Aalborg/København: Institut for Bærende Konstruktioner og Materialer, Danmarks Tekniske Universitet.
- SWANNELL, P. (1981). Rational Design of Weld Groups. *Journal of Structural Division. ASCE*, **107(ST5)**, 789-802.
- SWANNELL, P. and SKEWES, I. C. (1978). The Design of Welded Brackets Loaded in Plane: (General Theoretical ultimate load techniques and experimental program). *Australian Welding Research Association Report P6-1-78. Australian Welding Research*, **7**, 55-70.
- WITTEVEEN, J. and VAN DOUWEN, A. A. (1966). Voorstel tot Wijziging van de I.S.O.-formule voor lasberekningen in een op de vloeihypothese van Huber-Hencky aansluitende formule. *Overdruk uit Lastechniek*, **32e (6)**, Uitgevers Wyt-Rotterdam.

## 6 NOTATION

$a$	throat thickness
$b$	width of test specimen
$f_u$	characteristic value of the ultimate tensile strength
$f_{ud}$	design value of the ultimate tensile strength
$f_y$	yield stress
$l, m, n$	coordinates of a unit vector
$n$	non-dimensional generalised normal force
$p_x, p_y, p_z$	coordinates of a surface vector
$q_1, q_2$	non-dimensional generalised shear forces
$t$	thickness
$u$	relative displacement
$D$	diameter of test specimen
$L$	weld length
$N$	normal force
$N^+$	normal force, upper-bound value
$N^-$	normal force, lower-bound value
$N_{exp}$	normal force, test
$N_{EC3}$	normal force, EC3
$P$	force, load
$Q_1$	shear force in the 1-direction
$Q_2$	shear force in the 2-direction
$W_l$	dissipation per unit length
$x, y, z$	coordinates in a Cartesian $x,y,z$ -system of coordinates
$x$	length
$\alpha$	angle
$\beta$	correlation factor
$\beta_w$	correlation factor according to EC3
$\delta$	relative displacement
$\gamma$	angle of weld
$\gamma_{Mw}$	partial coefficient according to EC3
$\sigma$	normal stress
$\sigma_0$	normal stress on the throat section parallel to the axis of the weld
$\sigma_1, \sigma_3$	principal stresses
$\sigma_{90}$	normal stress on the throat section perpendicular to the axis of the weld
$\sigma_{eff}$	effective weld stress, theory
$\sigma_{exp}$	effective weld stress, test
$\sigma_h$	normal stress on the rotated throat section
$\sigma_i$	failure load for welded connection
$\sigma_x, \sigma_y, \sigma_z$	normal stresses referred to a Cartesian $x,y,z$ -system of coordinates
$\tau$	shear stress
$\tau_0$	shear stress on the throat section parallel to the axis of the weld
$\tau_{1h}$	shear stress on the rotated throat section in the 1-direction
$\tau_{2h}$	shear stress on the rotated throat section in the 2-direction
$\tau_{90}$	shear stress on the throat section perpendicular to the axis of the weld
$\tau_{xy}, \tau_{xz}, \tau_{yz}$	shear stresses referred to a Cartesian $x,y,z$ -system of coordinates

---

## **PART II**

---

### **THE PLASTIC TENSION FIELD METHOD** **- Post-Buckling Strength of Plate Girders Subjected to Shear**



# THE PLASTIC TENSION FIELD METHOD

## - Post-Buckling Strength of Plate Girders Subjected to Shear

### 1 INTRODUCTION

This part of the thesis describes a calculation method for steel plate girders with transverse web stiffeners subjected to shear. It may be used for predicting the failure load or, as a design method, to determine the optimal number of internal web stiffeners. The load-carrying capacity of a plate girder may be determined by applying the lower-bound theorem as well as the upper-bound theorem of the plastic theory. As a design method the lower-bound theorem is the easiest of the two to apply.

The method is called *the plastic tension field method*. It is based on the theory of plasticity and is analogous to the so-called *diagonal compression field method* developed for reinforced concrete beams with transverse stirrups, which was adopted in EC2 (2004).

The work was started by Nielsen and Christensen (1982). They derived lower-bound and upper-bound solutions for plate girders subjected to constant shear. This was followed up by Tolderlund (2000) who derived an upper-bound solution for simply supported plate girders with constant stiffener spacing subjected to a uniformly distributed load. In this thesis, Tolderlund's results are further developed and corrected.

In a concrete beam with transverse stirrups, the shear forces are carried by inclined compression in the concrete, see (Nielsen 1998). Along the tensile zone and the compressive zone of the beam, the transverse components of the inclined compression are transferred to the stirrups, which are thus subjected to tension. The principal for concrete beams is illustrated in Figure 1.1.

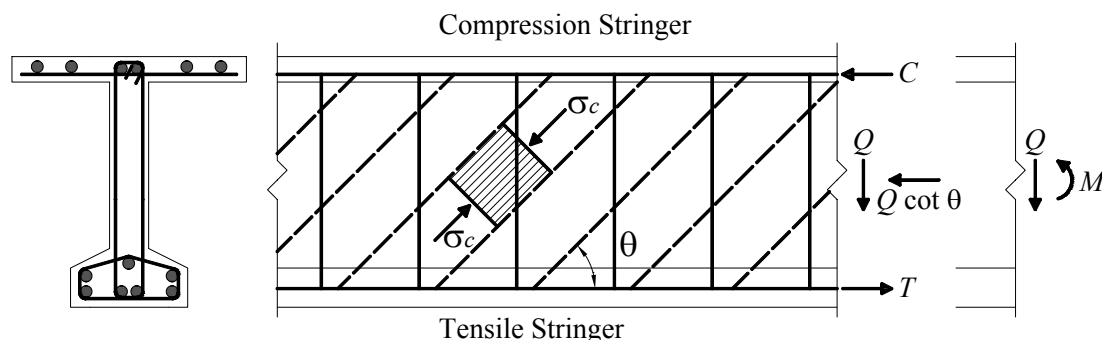


Figure 1.1: Diagonal compression stress field in a concrete beam

In a steel plate girder with transverse web stiffeners, the forces are carried in an analogous way after the web has buckled. Until the buckling load is reached, a web plate subjected to shear will develop identical principal stresses at an angle of  $45^\circ$  and  $135^\circ$  to the flanges, respectively. When the web buckles, it practically loses its capacity to sustain the compressive principal stresses, hence a new way of carrying the load arises, where the shear forces are carried by inclined tensile bands.

Many other theories have been developed, but the method presented differs from these theories by incorporating the strength of the transverse stiffeners and by the assumption that the tensile bands may pass the transverse stiffeners, which is often observed in tests. Other methods have only dealt with a single web field between two stiffeners.

In Chapter 2, a description is given for determining the load-carrying capacity of a plate girder subjected to constant shear by applying both the lower bound theorem as well as the upper-bound theorem. A new upper-bound solution, for simply supported girders subjected to uniform loading, is presented in Section 2.3.

The work conducted by Nielsen and Christensen (1982) only deals with determination of the load-carrying capacity; hence a practical design method is needed. The derived design method is presented in Chapter 3.

Nielsen and Christensen (1982) stated that further experimental verification of the plastic tension field theory was required. In Chapter 4, the theory is verified with experimental results found in the literature. During the present study, two M.Sc. thesis students conducted a test series of eight plate girder specimens as further verification of the theory, see (Øskan and Bak 2006). These experiments are presented in Chapter 5.

### 1.1 Other Methods

Subsequent to buckling, the stress distribution in the web of a plate girder changes and considerable post-buckling strength may be realised due to the diagonal tension that develops. This is commonly called the *tension-field action*. Even without transverse web stiffeners, a plate girder may develop a shear stress at the ultimate load several times the elastic critical shear buckling stress. The stress distribution of the tension field that develops in a plate girder with transverse stiffeners was first verified experimentally by Basler et al. (1960).

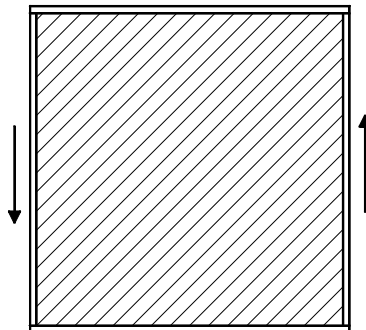
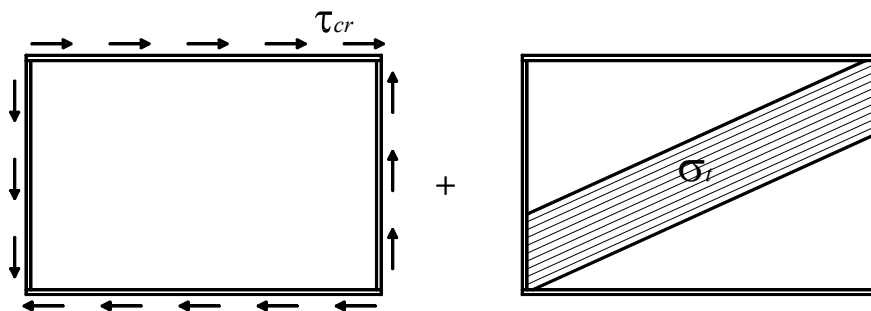


Figure 1.2: Pure tension field by Wagner

However, Wagner (1929) had already used a complete, uniform tension field to determine the post-buckling strength of a panel in pure shear, see Figure 1.2. He assumed the flanges to be rigid and the web to be very thin. This method is suitable for aircraft structures where extremely thin plates attached to very rigid boundary elements are encountered. Hence, it is of little practical use in civil engineering structures.

Basler (1961) was the first to derive a successful method for plate girders with slender webs and transverse stiffeners of the type used in civil engineering structures. He assumed that the flanges of most plate girders are too flexible to provide an anchorage for the tension field, so that the tension field shown in Figure 1.3 determines the shear strength. He further assumed that the shear stress in buckling  $\tau_{cr}$  would remain active all over the web, also after buckling occurs.



**Figure 1.3:** Combined critical shear buckling and tensile band by Basler

It was first shown, cf. (Selberg 1963), by Gaylord (1963) and later by Fujii et al. (1971) that, by means of a mistake, Basler's method gives the shear strength for a complete tension field instead of the limited band in Figure 1.3. Therefore, the method overestimates the shear strength of a girder whose flanges are incapable of providing anchorage for the tension field.

Many variations of the post-buckling tension field have been developed since Basler published his work. Only the different types of method will be mentioned in the following. For a detailed historical view, see (Galambos 1988).

Rockey and Skaloud (1971) showed that for girders with ordinary dimensions, the bending stiffness of the flanges is very significant for the post-buckling strength.

Fujii et al. (1971) derived a method with beam mechanisms in each flange with interior yield hinge at the midpoints, see Figure 1.4.

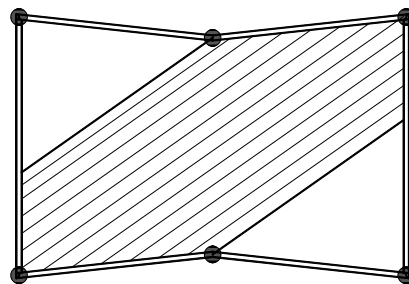


**Figure 1.4:** Tension field with yield hinge in the flange midpoints by Fujii et al.

Ostapenko and Chern (1971) proposed a tension field, where the principal band is determined by yielding, taking into account the stress that exists at buckling. A frame mechanism was assumed in the flanges, see Figure 1.5.

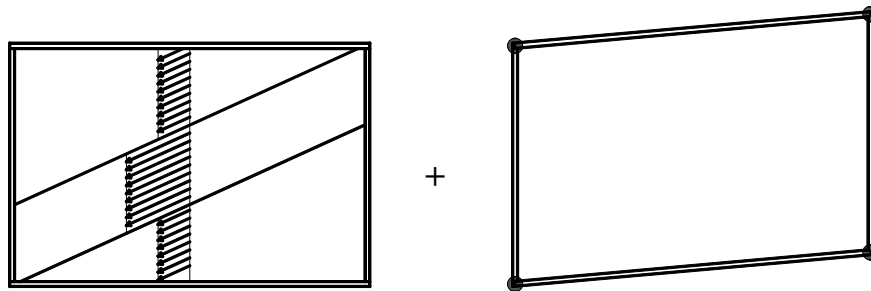


Figure 1.5: Tension field action and frame mechanism by Ostapenko and Chern

Komatsu (1971) derived a method where he determined the position of the interior yield hinges and found that the inclination of the tensile band varied with the dimensions of the flange and web, respectively.

Calladine (1973) formulated a pure plastic solution, where he showed that the position of the yield hinges as well as the inclination of the tensile band varied with the flange stiffness, see Figure 1.6. Calladine's solution is a special case (girders without internal stiffeners, i.e.  $\psi = 0$ ) of the general solution presented in Section 2.2.

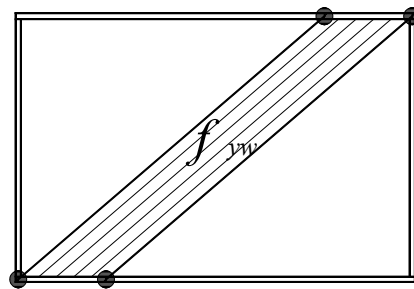


Figure 1.6: Pure plastic solution by Calladine

The tension field of Porter et al. (1975) consists of a single tensile band, and is a development of that suggested by Rockey and Skaloud (1971). The tensile membrane stress, together with the buckling stress, causes yielding, and failure occurs when hinges develop in the flanges to produce a combined mechanism, see Figure 1.7.

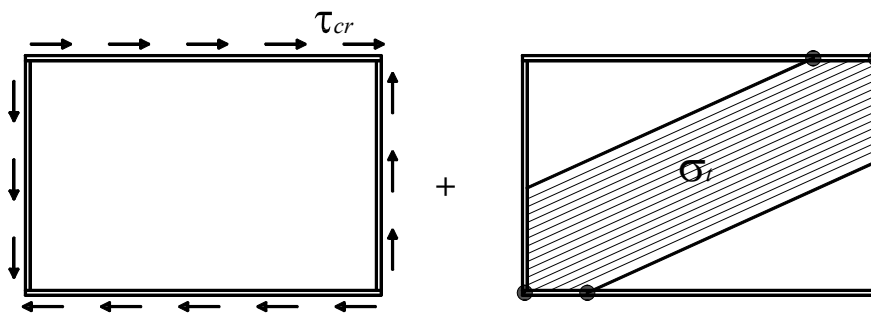


Figure 1.7: Combined critical shear buckling and tensile band by Porter et al.

In all the methods illustrated in Figures 1.2 – 1.7, only a web panel between two stiffeners is considered.

Many other researchers have dealt with the problem, e.g. Sakai et al. (1966), Bergfelt (1973), Höglund (1973), Dubas (1974) and Herzog (1974).

The solution by Porter et al. (1975) is the one adopted in the 1993-edition of Eurocode 3 (EC3 1993), with some further modification not treated here.

In the newest edition (2006) of Eurocode 3 (EC3 2006), the method by Porter et al. (1975) has been removed and substituted with another method, which is based on the rotated stress field developed by Höglund (1973). The rotated stress field is illustrated in Figure 1.8. Höglund has modified his own theory several times. The newest version of the rotated stress field theory is found in (Höglund 1995), which is adopted in EC3 (2006) with few empirical modifications. A description of the method in EC3 (2006) is given in (Johansson et al. 2001).

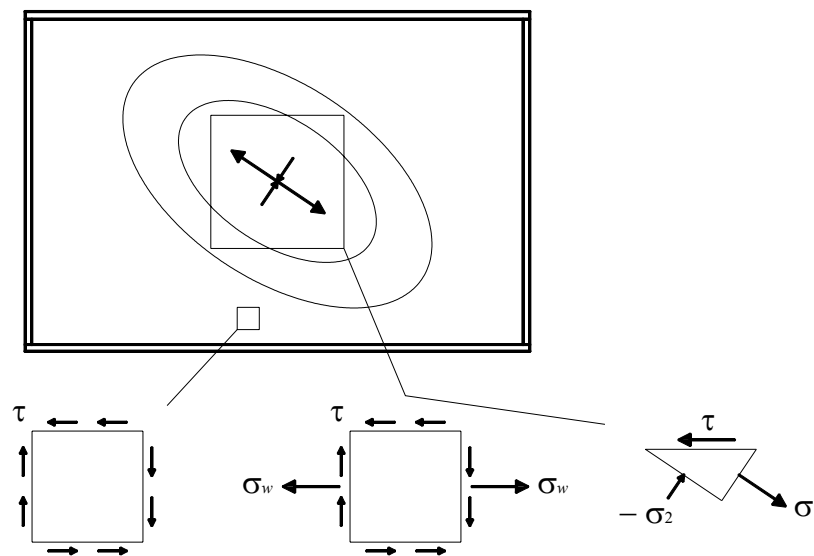


**Figure 1.8:** Rotated stress field by Höglund

## 2 LOAD-CARRYING CAPACITY

The post-buckling strength of a given steel plate girder with transverse stiffeners may be determined by the lower-bound theorem as well as the upper-bound theorem of the theory of plasticity.

In both the lower-bound solution and the upper-bound solution presented in the following two sections, a horizontal, simply supported steel plate girder with double-symmetrical I-section and transverse web stiffeners is considered. The plate girder is subjected to two symmetrical, concentrated forces, see Figure 2.1.

In Section 2.3, an upper-bound solution for girders with uniform load is presented. The assumptions related to uniform loading are mentioned in Section 2.3.

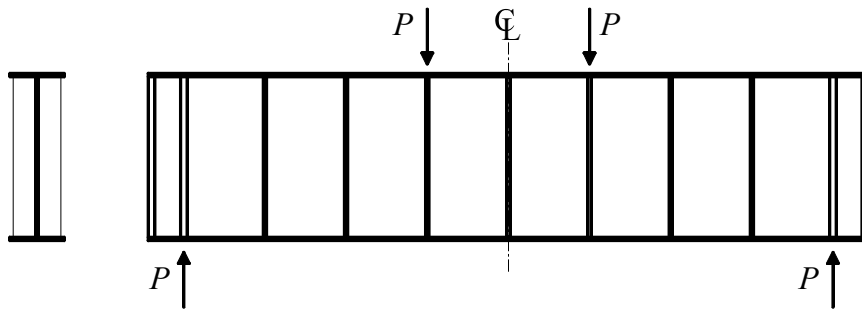


Figure 2.1: Considered steel plate girder

In the calculations, the following general assumptions are made: The web plate has no compressive strength, i.e. the yield criterion is as shown in Figure 2.2 with the solid lines. In the figure,  $\sigma_1$  and  $\sigma_2$  are the principal stresses and  $f_{yw}$  is the tensile yield stress. Even though the web plate has buckled, some diagonal compression stresses may be sustained by the web, especially due to stabilising effects of the large tensile stresses. This is on the safe side neglected.

Furthermore, the materials are assumed to be perfectly plastic.

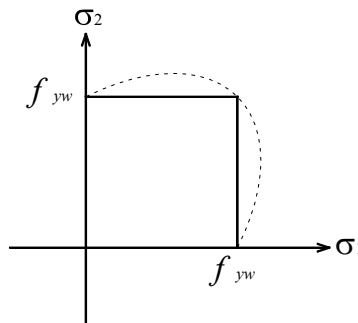


Figure 2.2: Yield criterion for the web plate

The assumed yield criterion is identical to Tresca's yield criterion without the compressive parts. It might appear more natural to apply a yield criterion such as the elliptical von Mises' yield criterion without the compressive parts, which is indicated by the dashed lines in the figure. However, the main reason for choosing the simplified yield criterion is to keep the theory as simple as possible. Choosing the yield criterion with the dashed line will lead to far more complicated solutions than presented in the following. In general, von Mises' yield criterion is the most accepted for steel structures, but it is not guaranteed that it is also valid in cases of materials

without compressive strength. As shown in Chapters 4 and 5, the theory based on the simplified yield criterion coincides closely with both the old and the new experimental results.

Furthermore, the largest difference between Tresca's and von Mises' yield criterion is obtained in the case of pure shear. Here, it is the uniaxial tensile strength that is utilised, where the two criteria give the same solution, hence it is not at all certain that applying the yield criterion, shown with the dashed lines in Figure 2.2, will increase the load-carrying capacity.

Moreover, the internal stiffeners are assumed subjected to compression. There are stiffeners at the reactions and at the concentrated forces, and the girder has constant dimensions, i.e. plate thicknesses and plate widths. The web plate is assumed simply supported at the boundaries, i.e. at the flanges and external stiffeners. Furthermore, imperfections and changes of geometry until failure are disregarded.

The equations in Sections 2.1 and 2.2 were originally derived by Nielsen and Christensen (1982). In order to compare the theory with the experimental result later on, the theory is represented in the following, and to some extent it follows the text in (Nielsen and Christensen 1982).

## 2.1 Lower-Bound Solution

Consider a horizontal, simply supported steel plate girder with double-symmetrical I-section and transverse web stiffeners subjected to constant shear, see Figure 2.3. The web is assumed to have no compressive strength, and the stiffeners are assumed subjected to compression, cf. Figure 2.2. The compression flange is idealised as a stringer carrying a force,  $C$  (positive as compression), and the tensile flange is idealised as a stringer carrying a force,  $T$  (positive as tension). Furthermore, the flanges are assumed to have no bending stiffness.

A statically admissible stress field in the web consists of uniaxial tension,  $\sigma_w$ , at an angle,  $\beta$ , to the girder axis. The stress field carries the following stresses referred to a Cartesian  $x,y$ -system of coordinates, cf. Figure 2.3,

$$\sigma_{xx} = \sigma_w \cos^2 \beta = \tau \cot \beta \quad (2.1)$$

$$\sigma_{yy} = \sigma_w \sin^2 \beta = \tau \tan \beta \quad (2.2)$$

$$\tau = -\tau_{xy} = \sigma_w \cos \beta \sin \beta \quad (2.3)$$

Here, index,  $w$ , refers to the web and  $\tau$  is the average shear stress in the section. Normal stresses in the web are positive as tension. The sign of shear stresses is as usual related to the system of coordinates. The relation between the average shear stress and the shear force,  $P = Q$ , is:

$$\tau = \frac{Q}{d t_w} \quad (2.4)$$

where  $d$  is the depth (distance between  $C$  and  $T$ ) of the girder and  $t_w$  is the web thickness. The stringer forces,  $C$  and  $T$ , are assumed to act at the midpoint of the

flange, hence  $d$  should be replaced by  $d$  plus  $t_f$ , when  $d$  denotes the depth of the web plate only, as it does in general in this thesis. Throughout Section 2.1 this is neglected.

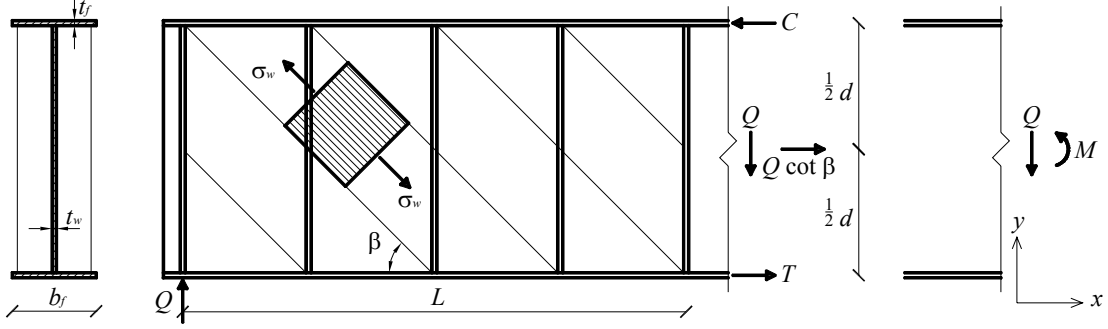


Figure 2.3: Diagonal tension stress field

The internal stiffeners are assumed to be closely spaced along the entire shear span; hence the stiffener forces may be replaced by an *equivalent stiffener stress*,  $\sigma_{sy}$  (positive as compression), equal to the forces in the stiffeners distributed over the web area. Thus for a girder with  $A_s$  being the total cross-sectional area of a single stiffener,  $n$  the number of internal stiffeners,  $L$  the shear zone length,  $\varphi$  the *stiffener ratio* and  $f_{ys}$  the ultimate stress of the stiffeners (either the buckling stress or the yield stress, the lower being decisive), the equivalent stiffener stresses are given by

$$\sigma_{sy} = \frac{A_s n}{L t_w} f_{ys} = \varphi f_{ys} \quad ; \quad \sigma_{sx} = \tau_{sxy} = 0 \quad (2.5)$$

Determining the buckling stress of the stiffeners is treated in PART III, Section 4.1.

The boundary conditions along the stringers for the total stress is  $\sigma_y = \sigma_{wy} - \sigma_{sy} = 0$ . Therefore the number of internal stiffeners is determined by

$$\varphi f_{ys} = \tau \tan \beta \quad (2.6)$$

The uniaxial web stress is:

$$\sigma_w = \frac{\tau}{\cos \beta \sin \beta} = \tau (\tan \beta + \cot \beta) \leq f_{yw} \quad (2.7)$$

The web stresses have to satisfy the condition  $\sigma_w \leq f_{yw}$  ( $f_{yw}$  being the yield stress of the web).

The normal stress,  $\sigma_{wx}$ , is equivalent to a longitudinal force,  $Q \cot \beta$ , acting in the middle of the cross-section. This force must equilibrate the flange forces. The forces in the flanges are correspondingly:

$$T = \frac{M}{d} - \frac{1}{2} Q \cot \beta \quad (2.8)$$

$$C = \frac{M}{d} + \frac{1}{2} Q \cot \beta \quad (2.9)$$

Equation (2.9) is only valid if  $C$  does not exceed the buckling load of the compression flange. Determination of the buckling load of the compression flange is treated in PART III, Section 4.1.

Timoshenko and Gere (1961) derived the same expressions for the flange forces, cf. Equations (2.8) and (2.9), using the tension field by Wagner (1929), cf. Figure 1.2.

To express the number and strength of the stiffeners, a non-dimensional parameter, the *mechanical degree of stiffening*, is introduced:

$$\psi = \varphi \frac{f_{ys}}{f_{yw}} = \frac{A_s n f_{ys}}{L t_w f_{yw}} \quad (2.10)$$

Again,  $A_s$  is the total cross-sectional area of a single stiffener,  $L$  is the shear zone length,  $n$  the number of internal stiffeners,  $\varphi$  the *stiffener ratio*,  $f_{yw}$  the yield stress of the web, and  $f_{ys}$  is the ultimate stress of the stiffeners (either the buckling stress or the yield stress, the lower being decisive).

Then the load-carrying capacity may be expressed by the following non-dimensional value,  $\tau/f_{yw}$ , by a formula identical to the concrete solution, cf. (Nielsen 1998),

$$\frac{\tau}{f_{yw}} = \begin{cases} \sqrt{\psi(1-\psi)} & \text{for } \psi < \frac{1}{2} \\ \frac{1}{2} & \text{for } \psi \geq \frac{1}{2} \end{cases} \quad (2.11)$$

It is interesting to note that the effectiveness factor,  $v$ , equals unity. This will be verified with experimental results in Chapters 4 and 5.

The solution is derived from Equations (2.6) and (2.7) assuming that the web yields in tension and the stiffeners yield in compression at the same time. If the buckling load of the stiffeners is valid, then it is furthermore assumed that the stiffeners “yield” at the buckling load.

The ratio,  $\tau/f_{yw}$ , as a function of  $\psi$  is shown in Figure 2.4. It is seen that Equation (2.11) forms a circle for  $0 \leq \psi \leq 0.5$  and a straight line for  $\psi > 0.5$ , corresponding to the constant value  $\tau/f_{yw} = 0.5$ .

If the yield criterion, signified by the dashed lines in Figure 2.2, had been applied, the lower-bound solution would be exactly the same as presented above.

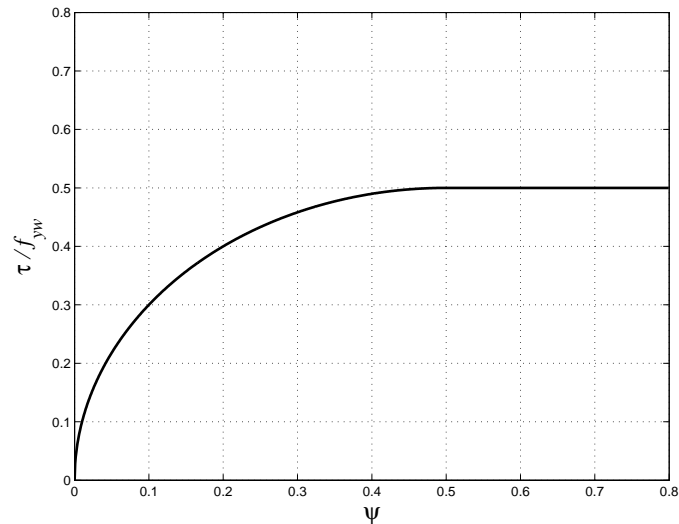


Figure 2.4: Lower-bound solution

### 2.2 Upper-Bound Solution for Concentrated Loading

In the upper-bound solution, the bending stiffness of the flanges may easily be taken into account.

The failure mechanism shown in Figure 2.5 is assumed, where the girder is subjected to constant shear. Until the buckling load is reached, the web plate will develop identical principal stresses at an angle of  $45^\circ$  and  $135^\circ$  to the flanges, respectively. Thereafter, the load is sustained by membrane forces, which will induce inwards bending of the flanges. Further loading will lead to yielding in the web, and yield hinges in the flanges will develop.

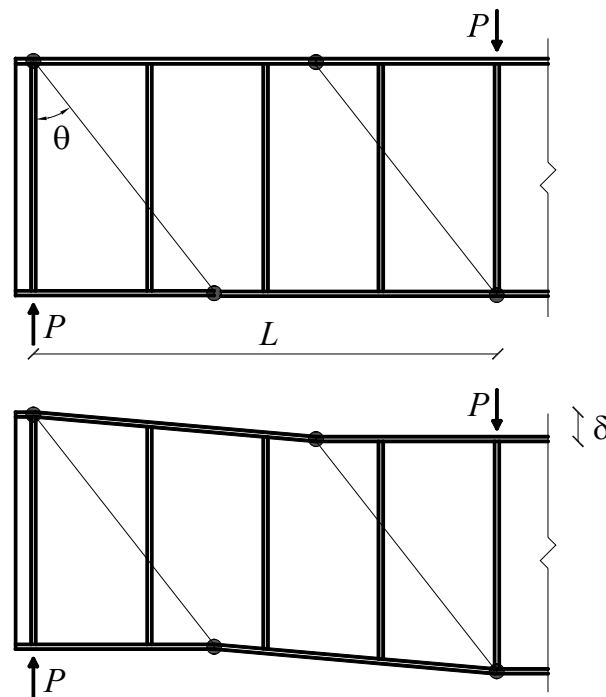


Figure 2.5: Failure mechanism for concentrated loading

There is yielding in the web in a parallelogram-shaped area, “yielding” in the internal stiffeners and yield hinges in the flanges. The yield hinges in the flanges at the end of the length,  $L$  (at the reaction,  $P$ , and at the concentrated force,  $P$ ), are fixed, while the position of the internal yield hinges varies with the different parameters. The load-carrying capacity is calculated by the work equation, where the girder is given a displacement,  $\delta$ , in transverse direction.

The external work,  $W_e$ , is given by

$$W_e = P\delta \quad (2.12)$$

The internal work, i.e. the dissipation, consists of three contributions; deformation of the web in the parallelogram-shaped area, bending of the flanges and compression of the internal stiffeners. In the following, these three contributions are treated separately.

### CONTRIBUTION FROM THE WEB PLATE

The two triangular regions,  $AEC$  and  $BDF$ , see Figure 2.6, are idealised as rigid, since the rotation of the hinges in the flanges will not lead to any change of strain. Elastic strains will occur in the two regions, but at collapse, the change of elastic strain is zero.

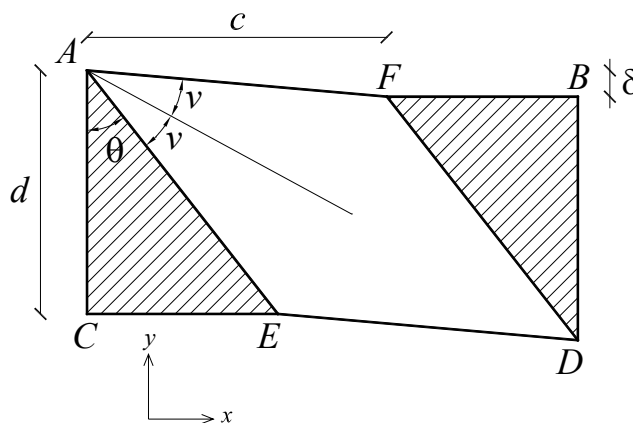


Figure 2.6: Deformation of the web plate

The parallelogram-shaped region,  $AEDF$ , gets plastic deformations. The plane strain field, referred to the Cartesian  $x,y$ -system of coordinates, cf. Figure 2.6, is given by

$$\varepsilon_x = 0 \quad (2.13)$$

$$\varepsilon_y = -\frac{\delta}{c} \tan \theta \quad (2.14)$$

$$\phi_{xy} = -\frac{\delta}{c} \quad (2.15)$$

Here,  $\varepsilon_x$  and  $\varepsilon_y$  are the longitudinal strains and  $\phi_{xy}$  is the change of angle. The length,  $c$ , the angle,  $\theta$ , and the displacement,  $\delta$ , are illustrated in Figure 2.6. The strains are illustrated by applying Mohr's circle in Figure 2.7.

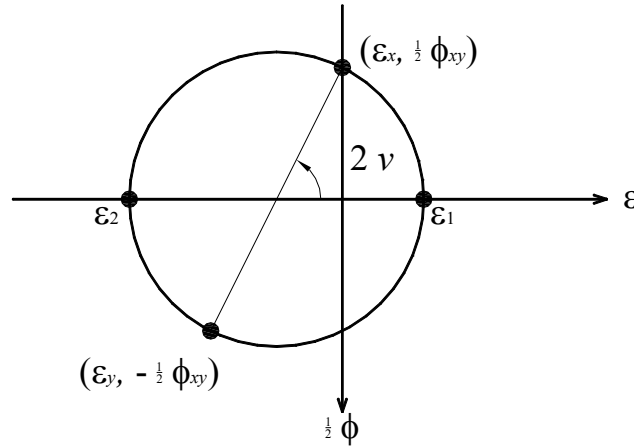


Figure 2.7: Strain field illustrated by Mohr's circle

The principal strains,  $\varepsilon_1$  and  $\varepsilon_2$ , are found by

$$\left. \begin{array}{l} \varepsilon_1 \\ \varepsilon_2 \end{array} \right\} = \frac{1}{2}(\varepsilon_x + \varepsilon_y) \pm \sqrt{\frac{1}{4}(\varepsilon_x - \varepsilon_y)^2 + \frac{1}{4}\phi_{xy}^2} \quad (2.16)$$

The principal major strain renders

$$\varepsilon_1 = \frac{1}{2} \frac{\delta}{c} \frac{1}{\cos \theta} (1 - \sin \theta) \quad (2.17)$$

and the principal minor strain is

$$\varepsilon_2 = -\frac{1}{2} \frac{\delta}{c} \frac{1}{\cos \theta} (1 + \sin \theta) \quad (2.18)$$

The angle,  $\nu$ , between the  $x$ -axis and the major principal axis is determined by, cf. Figure 2.7,

$$\tan 2\nu = -\frac{\frac{1}{2}\phi_{xy}}{\frac{1}{2}(\varepsilon_x + \varepsilon_y)} = \cot \theta \quad (2.19)$$

It is seen that the direction of the principal strain is the angular bisector of the parallelogram, cf. Figure 2.6, since the angle,  $\nu$ , is given by

$$\nu = \frac{1}{2} \left( \frac{\pi}{2} - \theta \right) \quad (2.20)$$

In the mechanism, there is yielding in the whole parallelogram shaped area,  $AEDF$ , with the tensile yield stress parallel to the angular bisector. According to the assumed yield criterion, cf. Figure 2.2, compressive stresses in the second principal direction are equal to zero. Thus the contribution from the web plate to the dissipation becomes

$$W_{i,web} = \int_V \varepsilon_1 f_{yw} dV = \int_A \frac{1}{2} \frac{\delta}{c} \frac{1}{\cos \theta} (1 - \sin \theta) f_{yw} t_w dA \quad (2.21)$$

$$W_{i,web} = \frac{1 - \sin \theta}{2 \cos \theta} f_{yw} t_w d \delta$$

Here,  $\varepsilon_1$  is the principal strain given by Equation (2.17),  $f_{yw}$  the yield stress of the web material,  $d$  the girder depth,  $t_w$  the web plate thickness and the length,  $c$ , the displacement,  $\delta$ , and the angle,  $\theta$ , are illustrated in Figure 2.6.

### CONTRIBUTION FROM THE FLANGES

The flanges yield in the four points  $A$ ,  $E$ ,  $D$  and  $F$ , where the plastic yield hinges develop, see Figure 2.8.

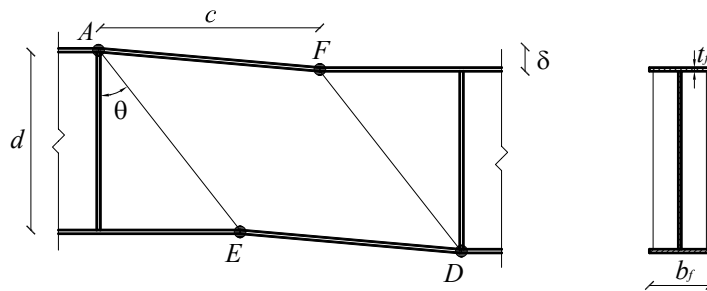


Figure 2.8: Bending of the flanges

Each flange is assumed to bend around its innermost point. Hence, the yield moment of the flange,  $M_{pf}$ , is given by

$$M_{pf} = \frac{1}{2} b_f t_f^2 f_{yf} \quad (2.22)$$

Here,  $b$  is width,  $t$  thickness and  $f_y$  is the yield stress or the buckling stress, the lower one being decisive. Index,  $f$ , refers to the flange. If the buckling stress is valid for the compression flange, the following Equation (2.23) is invalid, hence here and below it is assumed that the buckling stress of the compression flange is larger than the yield stress of the flange material.

The contribution from the flanges to the dissipation, when the rotation,  $\delta/c$ , of the yield hinges takes place at the deformation, becomes

$$W_{i,flange} = 4 \frac{\delta}{c} M_{pf} = 2 \frac{b_f t_f^2}{c} f_{yf} \delta \quad (2.23)$$

### CONTRIBUTION FROM THE INTERNAL STIFFENERS

As in the lower-bound solution, cf. Section 2.1, the internal stiffeners are assumed closely spaced along the entire shear span. Hence, the *equivalent stiffener stress*,  $\sigma_{sy}$  (positive as compression), cf. Equation (2.5), is given by

$$\sigma_{sy} = \frac{A_s n}{L t_w} f_{ys} \quad (2.24)$$

where  $A_s$  is the total cross-sectional area of a single stiffener,  $L$  the shear zone length,  $n$  the number of internal stiffeners,  $\varphi$  the *stiffener ratio*, and  $f_{yw}$  the yield stress of the web. Again, the ultimate stress of the stiffeners,  $f_{ys}$ , is either the buckling stress or the yield stress. If the buckling stress is valid, the stiffeners are assumed to yield at the buckling stress in the following calculations. Determination of the buckling stress of the stiffeners is treated in PART III, Section 4.1.

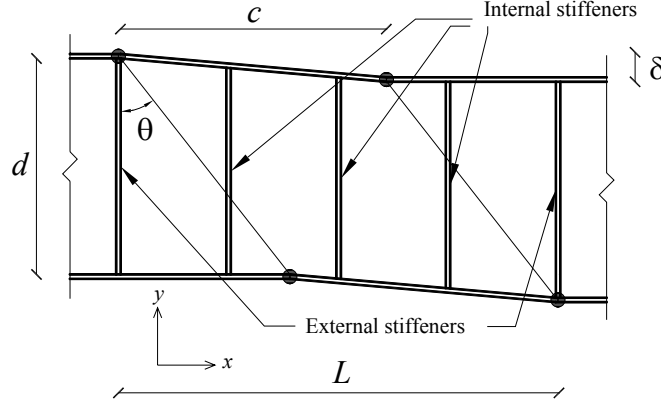


**Figure 2.9:** Compression of the internal stiffeners

The deformation leads to a strain,  $\varepsilon_y$ , corresponding to compression of the internal stiffeners in the  $y$ -direction, see Figure 2.9, given by Equation (2.14). The external stiffeners do not contribute to the dissipation. Thus, contribution from the stiffeners to the dissipation is

$$W_{i,stiffener} = \int_V \varepsilon_y \sigma_{sy} dV = \int_A \frac{\delta}{c} \tan \theta t_w \sigma_{sy} dA \quad (2.25)$$

$$W_{i,stiffener} = \frac{A_s n d}{L} \tan \theta f_{ys} \delta$$

Here,  $\sigma_{sy}$  is the equivalent stiffener stress given by Equation (2.24) and  $t_w$  is the web plate thickness. The length,  $c$ , the displacement,  $\delta$ , and the angle,  $\theta$ , are illustrated in Figure 2.9.

### LOAD-CARRYING CAPACITY

The total dissipation is then found by adding the three contributions given by Equations (2.21), (2.23) and (2.25), respectively.

Equalising the total dissipation and the external work, cf. Equation (2.12), gives

$$P^+ = \frac{1 - \sin \theta}{2 \cos \theta} f_{yw} t_w d + 2 \frac{b_f t_f^2}{c} f_{yf} + \frac{A_s n d}{L} \tan \theta f_{ys} \quad (2.26)$$

The load-carrying capacity may be expressed by the same non-dimensional value,  $\tau/f_{yw}$ , as the lower-bound solution, where  $\tau$  is given by Equation (2.4), i.e.

$$\frac{\tau}{f_{yw}} = \frac{1 - \sin \theta}{2 \cos \theta} + 2 \frac{b_f t_f^2}{c d t_w} \frac{f_{yf}}{f_{yw}} + \frac{A_s n}{L t_w} \frac{f_{ys}}{f_{yw}} \tan \theta \quad (2.27)$$

As a measure for the bending stiffness of the flanges, the non-dimensional parameter,  $\eta$ , is introduced as

$$\eta = 4 \frac{M_{pf}}{d^2 t_w f_{yw}} = 2 \frac{b_f t_f^2 f_{yf}}{d^2 t_w f_{yw}} \quad (2.28)$$

In the above equations,  $f_y$  is yield stress,  $t$  thickness and  $b$  width. Index,  $f$ , refers to the flange, index,  $w$ , refers to the web, and index,  $s$ , refers to the stiffeners. Notice that  $f_{ys}$  is either the yield stress or the buckling stress of the stiffeners. Furthermore,  $d$  is the girder depth,  $A_s$  the total cross-sectional area of a single stiffener,  $L$  the shear zone length,  $n$  the number of internal stiffeners and  $M_{pf}$  is the plastic yield moment of the flange, cf. Equation (2.22). The length,  $c$ , and the angle,  $\theta$ , are illustrated in Figure 2.9.

Introducing  $\eta$  and the *mechanical degree of stiffening*,  $\psi$ , cf. Equation (2.10), and utilising  $c = L - d \tan \theta$ , the load-carrying capacity may be expressed as

$$\frac{\tau}{f_{yw}} = \frac{1}{2} \left( \sqrt{1 + \tan^2 \theta} - \tan \theta \right) + \frac{\eta}{L/d - \tan \theta} + \psi \tan \theta \quad (2.29)$$

Due to the geometry,  $0 \leq \tan \theta \leq L/d$  is required.

When dealing with upper-bound solutions, the load-carrying capacity should be minimised with regard to the free parameter, here  $\theta$ . Minimising Equation (2.29) regarding  $\tan \theta$  leads to

$$\frac{d}{d \tan \theta} \left( \frac{\tau}{f_{yw}} \right) = 0 \Rightarrow \frac{1}{2} \frac{\tan \theta}{\sqrt{1 + \tan^2 \theta}} - \frac{1}{2} + \frac{\eta}{(L/d - \tan \theta)^2} + \psi = 0 \quad (2.30)$$

It has not been possible to find an analytical expression for the load-carrying capacity, so it must be found by numerical methods.

From Equation (2.30), it is seen that  $\tan \theta$  is equal to zero for

$$\psi \geq \frac{1}{2} - \left( \frac{d}{L} \right)^2 \quad (2.31)$$

Thus

$$\frac{\tau}{f_{yw}} = \frac{1}{2} + \eta \frac{d}{L} \quad \text{for} \quad \psi \geq \frac{1}{2} - \left( \frac{d}{L} \right)^2 \quad (2.32)$$

Hence, if the value of  $\psi$  given by Equation (2.31) is valid, adding more or stronger stiffeners would not increase the load-carrying capacity.

The ratio,  $\tau/f_{yw}$ , as a function of  $\psi$  is shown in Figures 2.10 – 2.12 for different values of  $\eta$  and the length-to-depth ratio,  $L/d$ . In the figures, the lower-bound solution, cf. Equation (2.11), is also shown.

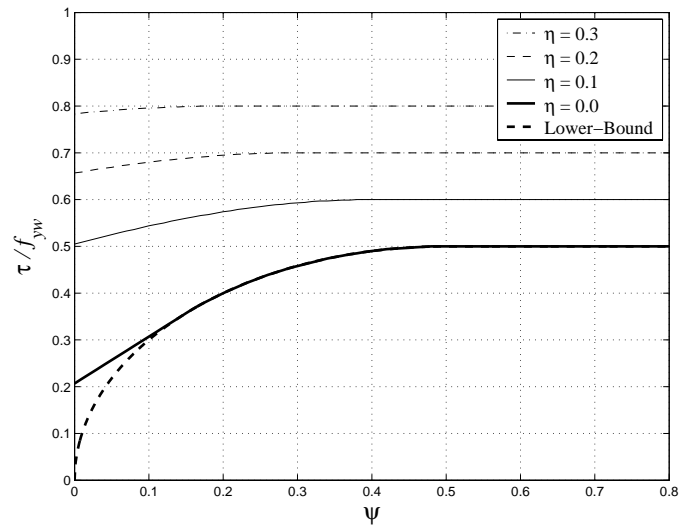


Figure 2.10: Upper-bound solution for  $L/d = 1.0$

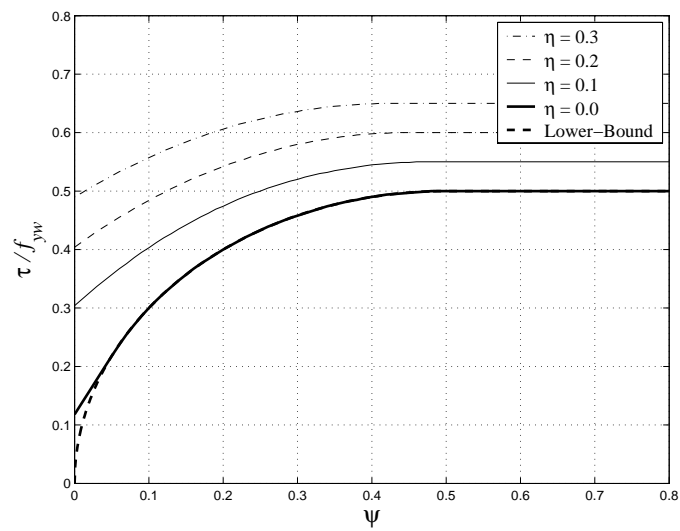


Figure 2.11: Upper-bound solution for  $L/d = 2.0$

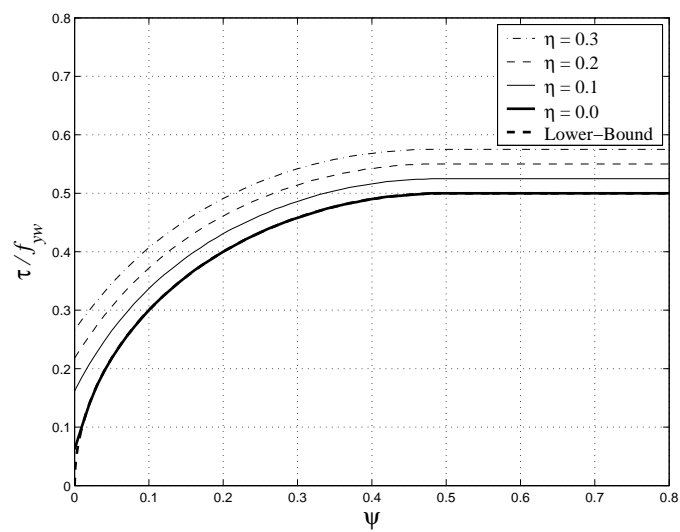
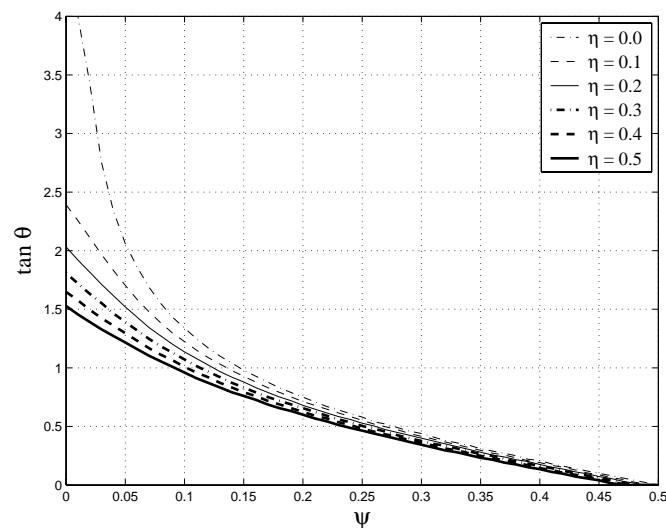


Figure 2.12: Upper-bound solution for  $L/d = 4.0$

From the figures it is seen that for short girders, i.e. low  $L/d$ -ratio, the internal stiffeners have less influence on the load-carrying capacity, as the flanges will sustain the main part of the load, so the load-carrying capacity is heavily dependant on the bending stiffness of the flange, i.e. the  $\eta$ -value. For slender flanges, i.e. small  $\eta$ -value, the upper-bound solution moves closer to the lower-bound solution. By increasing  $L/d$ -ratio, the load-carrying capacity is reduced, as the contribution from the flanges decreases compared to the contribution from the web and internal stiffeners, respectively. Hence, the upper-bound solution also moves closer to the lower-bound solution in this case.

In the tests presented in Chapter 5, the ratio  $L/d = 4.0$  is applied. For this ratio,  $\tan \theta$  as a function of  $\psi$  is shown in Figure 2.13 and as a function of  $\eta$  in Figure 2.14. For increasing values of  $\psi$ ,  $\tan \theta$  decreases to zero for  $\psi = 1/2$ , i.e. the yield hinges move towards the external stiffeners, at the reaction and at the concentrated load, whereby the yield band will broaden. For increasing values of  $\eta$ , the yield hinges also moves towards the external stiffeners.



**Figure 2.13:**  $\tan \theta$  as a function of  $\psi$  for  $L/d = 4.0$

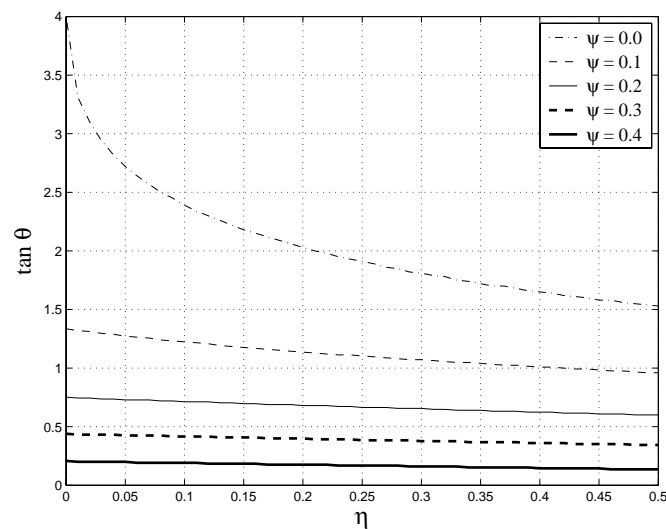


**Figure 2.14:**  $\tan \theta$  as a function of  $\eta$  for  $L/d = 4.0$

In the special case  $\eta = 0$ , i.e. girders with very low bending stiffness of the flanges, the load-carrying capacity is determined by

$$\frac{\tau}{f_{yw}} = \frac{1}{2} \left( \sqrt{1 + \tan^2 \theta} - \tan \theta \right) + \psi \tan \theta \quad (2.33)$$

Again,  $0 \leq \tan \theta \leq L/d$  is required.

By minimising Equation (2.33) regarding  $\tan \theta$ , and with the requirement,  $\tan \theta \leq L/d$ , it is found that

$$\tan \theta_{\min} = \min \begin{cases} \frac{1-2\psi}{2\sqrt{\psi(1-\psi)}} \\ \frac{L}{d} \end{cases} \quad (2.34)$$

Inserting Equation (2.34) into Equation (2.33) gives

$$\frac{\tau}{f_{yw}} = \begin{cases} \sqrt{\psi(1-\psi)} & \text{for } \frac{1}{2} \left( 1 - \frac{1}{\sqrt{1+(d/L)^2}} \right) \leq \psi \leq \frac{1}{2} \\ \frac{1}{2} \sqrt{1 + \left( \frac{L}{d} \right)^2} + \left( \psi - \frac{1}{2} \right) \frac{L}{d} & \text{for } 0 \leq \psi < \frac{1}{2} \left( 1 - \frac{1}{\sqrt{1+(d/L)^2}} \right) \end{cases} \quad (2.35)$$

With the assumptions made, the load-carrying capacity given by the upper expression is an exact solution, as it corresponds to the lower-bound solution, cf. Equation (2.11). The lower expression forms a straight line with the slope,  $L/d$ , which is tangent to the circle, cf. Figures 2.10 – 2.12.

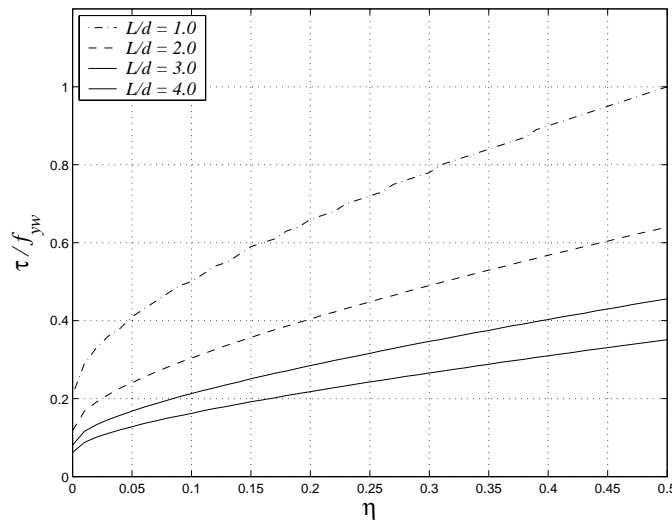


Figure 2.15: Upper-bound solution for  $\psi = 0$

In the special case of  $\psi = 0$ , i.e. girders without internal web stiffeners, the load-carrying is determined by

$$\frac{\tau}{f_{yw}} = \frac{1}{2} \left( \sqrt{1 + \tan^2 \theta} - \tan \theta \right) + \frac{\eta}{L/d - \tan \theta} \quad (2.36)$$

It has also not been possible to find an analytical solution in this case. The ratio,  $\tau/f_{yw}$ , as a function of  $\eta$  is shown in Figure 2.15 for different values of the ratio,  $L/d$ .

So far the derived theory is only valid for plate girders with relatively slender web plates, i.e. the critical buckling load of the web plate is less than the yield load of the web.

The elastic critical buckling stress,  $\tau_{cr}$ , of a single web panel is given by, cf. (Timoshenko and Gere 1961),

$$\tau_{cr} = k \frac{\pi^2 E}{12(1-\nu^2)} \left( \frac{t_w}{d} \right)^2 \quad (2.37)$$

where the buckling coefficient,  $k$ , is found from

$$k = \begin{cases} 5.35 + 4 \left( \frac{d}{b} \right)^2 & \text{for } \frac{d}{b} \geq 1 \\ 5.35 \left( \frac{d}{b} \right)^2 + 4 & \text{for } \frac{d}{b} < 1 \end{cases} \quad (2.38)$$

Here,  $d$  is the depth of the girder,  $t_w$  the web plate thickness,  $b$  the length between two adjacent stiffeners,  $E$  is Young's modulus, and  $\nu$  is Poisson's ratio. Furthermore, it is assumed that the web plate is simply supported at the flanges and at the stiffeners.

For plate girders with  $\tau_{cr} \geq f_{yw}/\sqrt{3}$ , buckling of the web will not occur according to the elastic buckling theory. Hence, no tensile yield band will develop as previously assumed, but a mechanism corresponding to yielding over the entire shear zone and yield hinges in the corners will develop, see Figure 2.16.

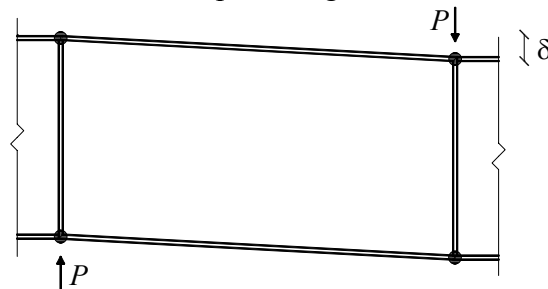


Figure 2.16: Failure mechanism for girders with thick web plates

The load-carrying capacity for this mechanism, when von Mises' yield criterion is applied, is

$$P^+ = \frac{f_{yw}}{\sqrt{3}} d t_w + \frac{4 M_{pf}}{c} \quad (2.39)$$

Here  $f_{yw}$  is the yield stress of the web material,  $t_w$  the web plate thickness,  $d$  the girder depth,  $M_{pf}$  the plastic yield moment of the flange, cf. Equation (2.22), and  $c$  is the length between the yield hinges at the supplied loads and at the internal yield hinges.

The load-carrying capacity may be expressed by the non-dimensional value,  $\tau/f_{yw}$ , utilising Equation (2.28) and  $c = L - d \tan \theta$  ( $L$  being the length of the shear zone), as

$$\frac{\tau}{f_{yw}} = \frac{1}{\sqrt{3}} + \frac{\eta}{L/d - \tan \theta} \quad (2.40)$$

Minimising with regard to  $\tan \theta$  renders  $\tan \theta$  equal to zero, i.e. the yield hinges in the flanges will develop in the corners as shown in Figure 2.16. Thus

$$\frac{\tau}{f_{yw}} = \frac{1}{\sqrt{3}} + \eta \frac{d}{L} \quad (2.41)$$

where  $\eta$  is given by Equation (2.28).

The stiffeners are not incorporated in the load-carrying capacity expression. The stiffeners should be included in the calculation of the buckling load, considering the entire shear zone, but this has not yet been done.

If Tresca's yield criterion is applied, the factor  $1/\sqrt{3}$  should be replaced by  $1/2$  in Equations (2.39) – (2.41).

### 2.3 Upper-Bound Solution for Distributed Loading

In the case of a simply supported girder, the failure mechanism shown in Figure 2.17 is assumed, where the girder is subjected to a load,  $q$ , per unit length acting on the top flange. Again, a double-symmetrical I-section with constant dimensions is assumed. The stiffeners are assumed subjected to compression and the yield criterion for the web plate is given by Figure 2.2.

There is yielding in the web in two parallelogram-shaped areas, “yielding” in the internal stiffeners and yield hinges in the flanges. The yield hinges in the flanges at the end of the length,  $L$  (at the reaction  $\frac{1}{2} q L$ ), are fixed, while the position of the internal yield hinges varies with the different parameters. The length,  $x$ , between the two yield hinges, cf. Figure 2.17, is assumed to be the same in both the top and bottom flange.

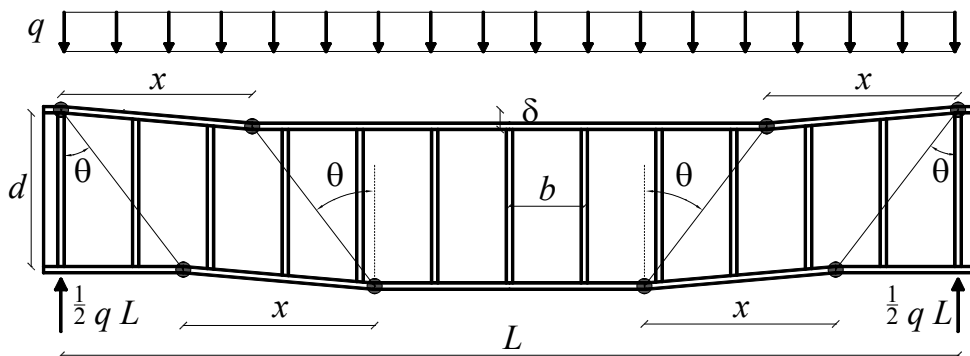


Figure 2.17: Failure mechanism for a simply supported girder with distributed loading

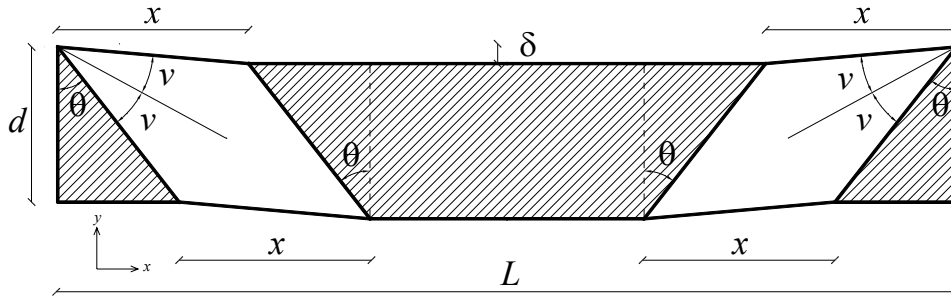


Figure 2.18: Deformation of the web plate

Only the two parallelogram-shaped areas get plastic deformations in the failure mechanism. The remaining web areas (the hatched areas in Figure 2.18) are idealised as rigid, since the rotation of the hinges in the flanges will not lead to any chance of strain here. Thus the dissipation from one parallelogram shaped web area is the same as for concentrated loading, cf. Equation (2.21). The contribution to the dissipation from the web of the girder in Figure 2.18 then becomes

$$W_{i,web} = 2 \int_V \varepsilon_1 f_{yw} dV = 2 \int_A \frac{1}{2} \frac{\delta}{x} \frac{1}{\cos \theta} (1 - \sin \theta) f_{yw} t_w dA \quad (2.42)$$

$$W_{i,web} = \frac{1 - \sin \theta}{\cos \theta} f_{yw} t_w d \delta$$

Here,  $\varepsilon_1$  is the principal strain given by Equation (2.17),  $f_{yw}$  the yield stress of the web material,  $d$  the girder depth and  $t_w$  is the web plate thickness. The length,  $x$ , the displacement,  $\delta$ , and the angle,  $\theta$ , are illustrated in Figure 2.18.

The only difference between this equation and the dissipation in Equation (2.21) is a factor of two. Also, the hinge spacing is now called  $x$  instead of  $c$ . This is done because  $c$  may be expressed by the angle,  $\theta$ , cf. Figure 2.6. The hinge spacing,  $x$ , is independent of the angle,  $\theta$ , cf. Figure 2.18.

The contribution to the dissipation from the flanges is determined in the same way by multiplying with a factor of two and substituting  $c$  with  $x$ , cf. Equation (2.23),

$$W_{i,flange} = 8 \frac{\delta}{x} M_{pf} = 4 \frac{b_f t_f^2}{x} f_{yf} \delta \quad (2.43)$$

Here  $b$  is width,  $t$  is thickness and  $f_y$  is the yield stress or the buckling stress, the lower one being decisive. Index,  $f$ , refers to the flange. As in Section 2.2, it is here assumed that the buckling stress of the compression flange is larger than the yield stress of the flange material.

Only the stiffeners located along the two lengths,  $x + d \tan \theta$ , except the stiffeners at the supports, will be compressed. It is here assumed that all the stiffeners are placed with a constant spacing,  $b$ . Hence the *equivalent stiffener stress*,  $\sigma_{sy}$  (positive as compression), cf. Equation (2.24), may be determined by ( $A_s$  being the total cross-sectional area of a single stiffener and  $t_w$  the web plate thickness)

$$\sigma_{sy} = \frac{A_s}{b t_w} f_{ys} \quad (2.44)$$

Again, the ultimate stress of the stiffeners,  $f_{ys}$ , is either the buckling stress or the yield stress. If the buckling stress is valid, the stiffeners are assumed to yield at the buckling stress in the following calculations. Determination of the buckling stress of the stiffeners is treated in PART III, Section 4.1.

With the assumption of constant stiffener spacing, it is not necessary to evaluate how many stiffeners are located along the two lengths,  $x + d \tan \theta$ . The contribution to the dissipation from the stiffeners is then determined by, cf. Equation (2.25),

$$\begin{aligned} W_{i,stiffener} &= 2 \int_V \varepsilon_y \sigma_{sy} dV = 2 \int_A \frac{\delta}{x} \tan \theta t_w \sigma_{sy} dA \\ W_{i,stiffener} &= 2 \frac{A_s d}{b} \tan \theta f_{ys} \delta \end{aligned} \quad (2.45)$$

The total dissipation is then found by adding the three contributions given by Equations (2.42), (2.43) and (2.45), respectively. This gives

$$W_i = \frac{1 - \sin \theta}{\cos \theta} f_{yw} t_w d \delta + 4 \frac{b_f t_f^2}{x} f_{yf} \delta + 2 \frac{A_s d}{b} \tan \theta f_{ys} \delta \quad (2.46)$$

The external work is given by

$$W_e = q(L - x)\delta \quad (2.47)$$

where  $q$  is the supplied load per unit length and  $L$  is the length of the shear zone. The length,  $x$ , and the displacement,  $\delta$ , are shown in Figure 2.18.

It should be stated here that the solution will be different if the girder is subjected to a uniformly distributed load along the bottom face, as the external work will not be given by Equation (2.47) in this case.

Equalising the total dissipation and the external work gives

$$q^+ = \frac{1 - \sin \theta}{\cos \theta} \frac{f_{yw} t_w d}{L - x} + 4 \frac{b_f t_f^2}{(L - x)x} f_{yf} + 2 \frac{A_s d}{b(L - x)} \tan \theta f_{ys} \quad (2.48)$$

The load-carrying capacity may be expressed by the non-dimensional value,  $\tau/f_{yw}$ , where  $\tau$  is given by

$$\tau = \frac{1}{2} \frac{qL}{d t_w} \quad (2.49)$$

The load-carrying capacity then becomes

$$\frac{\tau}{f_{yw}} = \frac{1}{2} \frac{1 - \sin \theta}{\cos \theta} \frac{L}{L - x} + 2 \frac{b_f t_f^2}{d t_w} \frac{f_{yf}}{f_{yw}} \frac{L}{(L - x)x} + \frac{A_s}{b t_w} \frac{f_{ys}}{f_{yw}} \frac{L}{L - x} \tan \theta \quad (2.50)$$

Introducing  $\eta$  as a measure for the bending stiffness of the flanges, given by Equation (2.28), and the *mechanical degree of stiffening*,  $\psi$ , cf. Equation (2.10), the load-carrying capacity may be expressed as

$$\frac{\tau}{f_{yw}} = \frac{1}{2} \frac{\sqrt{1 + \tan^2 \theta} - \tan \theta}{1 - x/L} + \frac{d}{x} \frac{\eta}{1 - x/L} + \frac{\psi \tan \theta}{1 - x/L} \quad (2.51)$$

Due to the geometry the following condition must be satisfied:

$$0 \leq \tan \theta \leq \frac{1}{2} \frac{L}{d} - \frac{x}{d} \quad (2.52)$$

In Equations (2.48) - (2.52),  $f_y$  is yield stress and  $t$  is thickness with index  $f$  for flange,  $w$  for web and  $s$  for stiffener. Again,  $f_{ys}$  is either the yield stress or the buckling stress of the stiffeners. Furthermore,  $b_f$  is the flange width,  $b$  the constant stiffener spacing,  $d$  the girder depth,  $A_s$  the total cross-sectional area of a single stiffener,  $L$  the shear zone length, and  $n$  is the number of internal stiffeners. The length,  $x$ , and the angle,  $\theta$ , are illustrated in Figure 2.18.

Tolderlund (2000) derived the same solution as Equation (2.51), but he did not include the restriction on  $\tan \theta$ , cf. Equation (2.52), therefore his result is incorrect.

The load-carrying capacity should be minimised with regard to the free parameters. In the case of concentrated loading, cf. Section 2.2, only the angle,  $\theta$ , is a free parameter. In this case however, there are two, i.e.  $\theta$  and  $x$ . Minimising Equation (2.51) regarding  $\tan \theta$  leads to

$$\frac{d}{d \tan \theta} \left( \frac{\tau}{f_{yw}} \right) = 0 \Rightarrow \frac{1}{2} \frac{\sqrt{1 + \tan^2 \theta} \tan \theta - \tan^2 \theta - 1}{1 - x/L} + \frac{\psi (1 + \tan^2 \theta)}{1 - x/L} = 0 \quad (2.53)$$

In this case it is possible to find an analytical expression for the load-carrying capacity, as Equation (2.53) turns out to be independent of  $x$ . It is in fact also independent of the bending stiffness of the flanges, i.e.  $\eta$ , and the ratio,  $d/L$ . The angle,  $\theta_{\min}$ , leading to a minimum for  $\tau/f_{yw}$  is given by

$$\tan \theta_{\min} = \begin{cases} \frac{1 - 2\psi}{2\sqrt{\psi(1-\psi)}} & \text{for } \psi < \frac{1}{2} \\ 0 & \text{for } \psi \geq \frac{1}{2} \end{cases} \quad (2.54)$$

Inserting this value of  $\tan \theta$  for  $\psi < 1/2$  into Equation (2.51) and minimising regarding  $x$ , the length,  $x$ , is found to be determined by

$$\frac{x}{L} = \frac{\sqrt{\eta \frac{d}{L} \left( \eta \frac{d}{L} + \sqrt{\frac{\psi}{1-\psi}} - \psi \sqrt{\frac{\psi}{1-\psi}} \right)} - \eta \frac{d}{L}}{\sqrt{\psi(1-\psi)}} \quad (2.55)$$

The analytical expression for the load-carrying capacity is found by inserting  $\tan \theta$ , cf. Equation (2.54), and  $x/L$ , cf. Equation (2.55), into Equation (2.51). This corresponds to what Tolderlund (2000) did. If the restriction due to geometry, cf. Equation (2.52), is included, then  $\tan \theta$  is determined by

$$\tan \theta_{\min} = \min \begin{cases} \frac{1-2\psi}{2\sqrt{\psi(1-\psi)}} \\ \frac{1}{2} \frac{L}{d} - \frac{x}{d} \end{cases} \quad (2.56)$$

By inserting the lower expression into Equation (2.51) and minimising regarding  $x$  leads to

$$\begin{aligned} \frac{d}{dx} \left( \frac{\tau}{f_{yw}} \right) = 0 \Rightarrow & \frac{-\frac{1}{2} \frac{L}{d} - \frac{x}{d}}{\sqrt{1 + \left( \frac{1}{2} \frac{L}{d} - \frac{x}{d} \right)^2}} + \frac{1}{d} + \frac{\sqrt{1 + \left( \frac{1}{2} \frac{L}{d} - \frac{x}{d} \right)^2} - \frac{1}{2} \frac{L}{d} + \frac{x}{d}}{2(1-x/L)^2 L} \\ & + \frac{\eta d}{(1-x/L)^2 x L} - \frac{\eta d}{(1-x/L)x^2} - \frac{\psi}{(1-x/L)d} + \frac{\psi \left( \frac{1}{2} \frac{L}{d} - \frac{x}{d} \right)}{(1-x/L)^2 L} = 0 \end{aligned} \quad (2.57)$$

It has not been possible to find an analytical expression for the ratio,  $x/L$ , so it must be found by numerical methods.

The ratio,  $\tau/f_{yw}$ , as a function of  $\psi$  is shown in Figures 2.19 – 2.21 for different values of  $\eta$  and the length-to-depth ratio,  $L/d$ .

It is seen that  $\tan \theta$  is equal to zero for  $\psi \geq 1/2$ , cf. Equation (2.56). Thus

$$\frac{\tau}{f_{yw}} = \frac{1}{2} \frac{1}{1-x/L} + \frac{d}{x} \frac{\eta}{1-x/L} \quad \text{for } \psi \geq \frac{1}{2} \quad (2.58)$$

where the ratio,  $x/L$ , for  $\psi = 1/2$  is given by, cf. Equation (2.55),

$$\frac{x}{L} = \sqrt{2\eta \frac{d}{L} \left( 2\eta \frac{d}{L} + 1 \right)} - 2\eta \frac{d}{L} \quad (2.59)$$

Hence if  $\psi \geq 1/2$ , adding stronger or more stiffeners would not increase the load-carrying capacity.

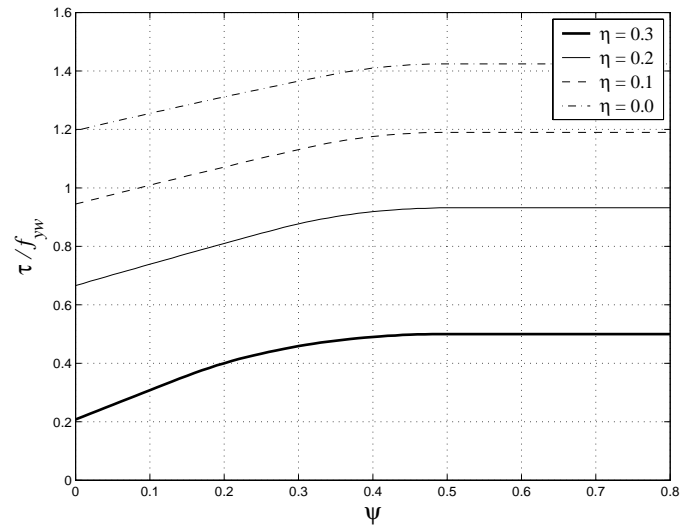


**Figure 2.19:** Upper-bound solution for  $L/d = 2.0$

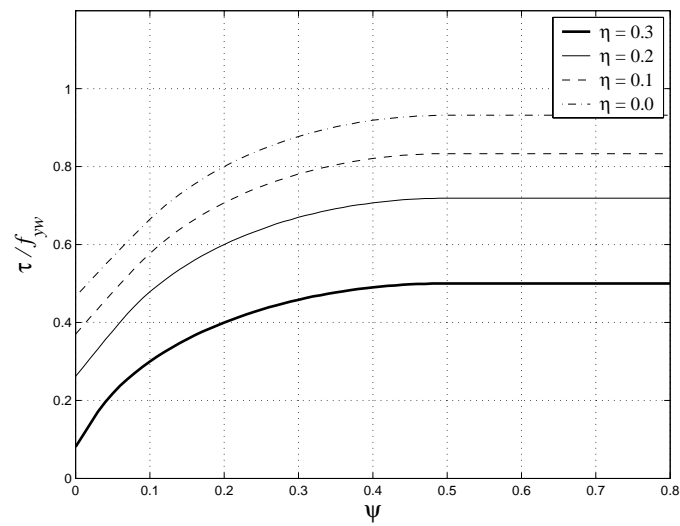


**Figure 2.20:** Upper-bound solution for  $L/d = 6.0$

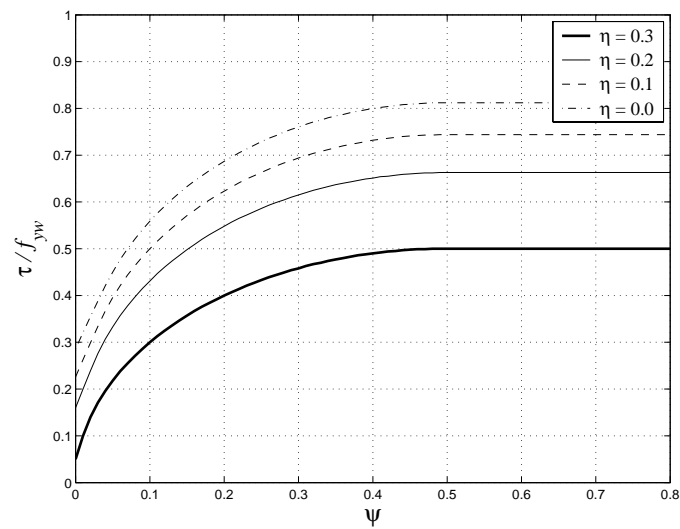


**Figure 2.21:** Upper-bound solution for  $L/d = 10.0$

From the figures it is seen that the flange stiffness, i.e. the  $\eta$ -value, has a larger influence on the load-carrying capacity compared to the solution for constant shear, cf. Figures 2.10 – 2.12, as the flanges will sustain the main part of the load. By increasing  $L/d$ -ratio, the load-carrying capacity is reduced since the contribution from the flanges decreases compared to the contribution from the web and internal stiffeners, respectively. But for  $L/d = 10$ ,  $\eta = 0.3$  and  $\psi \geq 1/2$ , cf. Figure 2.21, the load-carrying capacity is still 62 % greater than the load-carrying capacity for  $\eta = 0.0$ . For constant shear, the load-carrying capacity for  $L/d = 4$ ,  $\eta = 0.3$  and  $\psi \geq 1/2$ , cf. Figure 2.12, is only 15 % greater than the load-carrying capacity for  $\eta = 0.0$ .

In the special case  $\eta = 0$ , i.e. girders with very low bending stiffness of the flanges, the load-carrying capacity is determined by

$$\frac{\tau}{f_{yw}} = \frac{1}{2} \frac{\sqrt{1 + \tan^2 \theta} - \tan \theta}{1 - x/L} + \frac{\psi \tan \theta}{1 - x/L} \quad (2.60)$$

Again, the following condition must be satisfied:

$$0 \leq \tan \theta \leq \frac{1}{2} \frac{L}{d} - \frac{x}{d} \quad (2.61)$$

By minimising Equation (2.60) regarding  $x$ , it is found that  $x$  is equal to zero when  $\eta$  equals zero. By minimising regarding  $\tan \theta$ , and with the requirement in Equation (2.61), it is found that

$$\tan \theta_{\min} = \min \begin{cases} \frac{1 - 2\psi}{2\sqrt{\psi(1-\psi)}} \\ \frac{1}{2} \frac{L}{d} \end{cases} \quad (2.62)$$

Inserting Equation (2.62) and  $x = 0$  into Equation (2.60) gives

$$\frac{\tau}{f_{yw}} = \begin{cases} \sqrt{\psi(1-\psi)} & \text{for } \frac{1}{2} \left( 1 - \frac{1}{\sqrt{1+4(d/L)^2}} \right) \leq \psi \leq \frac{1}{2} \\ \frac{1}{2} \sqrt{1 + \frac{1}{4} \left( \frac{L}{d} \right)^2} + \frac{1}{2} \left( \psi - \frac{1}{2} \right) \frac{L}{d} & \text{for } 0 \leq \psi < \frac{1}{2} \left( 1 - \frac{1}{\sqrt{1+4(d/L)^2}} \right) \end{cases} \quad (2.63)$$

The result,  $x = 0$  for  $\eta = 0$ , is indicating that no parallelogram-shaped yield area develops in the web. Then the dissipation from the parallelogram-shaped region should correspond to the dissipation in a single yield line. In order to verify this fact, the mechanism consisting of a single yield line in the web shown in Figure 2.22 is calculated.

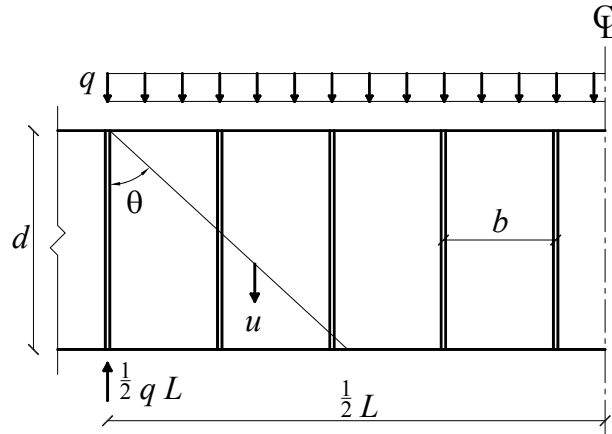


**Figure 2.22:** Failure mechanism for a simply supported girder with low flange bending stiffness

The mechanism is most simply calculated with the reaction ( $R = \frac{1}{2} q L$ ) as the active load. Then, due to the symmetry, only one half of the girder is considered. The external work,  $W_e$ , is then given by

$$W_e = \frac{1}{2} q L u \quad (2.64)$$

With the assumed yield criterion for plane stress, cf. Figure 2.2, the dissipation in the yield line per unit length,  $W_l$ , is given by, cf. (Nielsen et al. 2000),

$$W_l = \frac{1}{2} f_y t u (1 - \sin \alpha) \quad (2.65)$$

Here,  $q$  is the supplied load per unit length,  $L$  the total length of the girder,  $f_y$  the yield stress,  $t$  the thickness and  $\alpha$  is the angle between the relative displacement,  $u$ , and the yield line. From Figure 2.22 it is seen that  $\alpha$  is equal to  $\theta$ . Again, the stiffeners are assumed placed with a constant spacing,  $b$ . The total dissipation,  $W_i$ , without any contribution from the flanges is given by

$$W_i = \frac{1}{2} f_{yw} t_w u (1 - \sin \theta) \frac{d}{\cos \theta} + \frac{A_s}{b} f_{ys} u d \tan \theta \quad (2.66)$$

Equalising the total dissipation and the external work gives

$$q^+ = \frac{1 - \sin \theta}{\cos \theta} \frac{f_{yw} t_w d}{L} + 2 \frac{A_s d}{b L} f_{ys} \tan \theta \quad (2.67)$$

In Equations (2.66) and (2.67),  $f_{yw}$  is the web yield,  $t_w$  the web thickness, and  $f_{ys}$  is either the yield stress or the buckling stress of the stiffeners. Furthermore,  $b$  is the constant stiffener spacing,  $d$  the girder depth,  $A_s$  the total cross-sectional area of a single stiffener,  $L$  the total girder length, and  $n$  is the number of internal stiffeners. The relative displacement,  $u$ , and the angle,  $\theta$ , are illustrated in Figure 2.22.

Utilising  $\tau$  given by Equation (2.49) and  $\psi$ , cf. Equation (2.10), the load-carrying capacity may be expressed by the non-dimensional value,  $\tau/f_{yw}$ , as

$$\frac{\tau}{f_{yw}} = \frac{1}{2} \left( \sqrt{1 + \tan^2 \theta} - \tan \theta \right) + \psi \tan \theta \quad (2.68)$$

This is identical to Equation (2.60) for  $x$  equals zero, hence the load-carrying capacity for the mechanism with the parallelogram-shaped region for  $x$  equals zero gives the same result as a mechanism with a single yield line. Also, minimising regarding  $\tan \theta$  leads to Equation (2.62).

If the flanges are included in the mechanism, cf. Figure 2.22, the inclined yield line in the web plate will be followed by a vertical yield line in each flange, inducing a pure shear failure of the flanges. The contribution to the dissipation from one flange will be, cf. Equation (2.65), where  $\alpha$  is equal to zero,

$$W_{i,flange} = \frac{1}{2} f_{yf} t_f b_f u \quad (2.69)$$

Here,  $u$  is the relative displacement,  $b$  the width,  $t$  the thickness and  $f_y$  is the yield stress or the buckling stress, the lower of the two being decisive. Index,  $f$ , refers to the flange.

It is seen that the flange will give a relatively large contribution to the dissipation, hence the mechanism, cf. Figure 2.22, is only valid for girders with low bending stiffness of the flanges. It should here be stated that extremely wide flanges with extremely small thickness may provide a considerable contribution to the dissipation, cf. Equation (2.69), even though the bending stiffness of such flanges will be very low.

For concrete beams, cf. (Nielsen 1998), the solution will be identical to the solution for steel plate girders with  $\eta$  equals zero subjected to concentrated loading, cf. Equation (2.33). For distributed loading, the solution will be different for steel plate girders and concrete beams, respectively.

In the special case  $\psi = 0$ , i.e. girders without internal web stiffeners, the load-carrying capacity is determined by

$$\frac{\tau}{f_{yw}} = \frac{1}{2} \frac{\sqrt{1 + \tan^2 \theta} - \tan \theta}{1 - x/L} + \frac{d}{x} \frac{\eta}{1 - x/L} \quad (2.70)$$

Here,  $\tan \theta$  is given by cf. Equation (2.56),

$$\tan \theta = \frac{1}{2} \frac{L}{d} - \frac{x}{d} \quad (2.71)$$

It has not been possible to find an analytical solution in this case either. The ratio,  $\tau/f_{yw}$ , as a function of  $\eta$  is shown in Figure 2.23 for different values of the ratio,  $L/d$ .

From Equation (2.71) it is seen that the two yield hinges in the bottom flange will both develop in the midpoint of the bottom flange, cf. Figure 2.17, i.e. only one plastic yield hinge will develop.

For low  $\eta$ -values,  $x$  will be close to zero and the length,  $d \tan \theta$ , close to  $\frac{1}{2} L$ . For increasing  $\eta$ -values,  $x$  increases and the length,  $d \tan \theta$ , decreases.

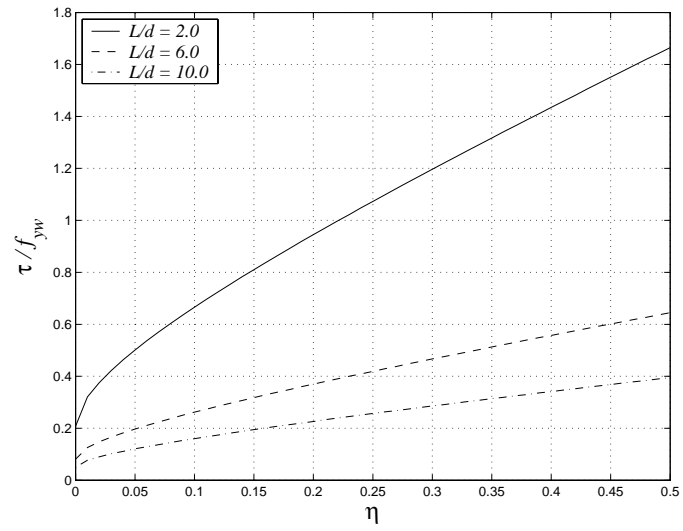


**Figure 2.23:** Upper-bound solution for  $\psi = 0$



$$\sigma_{wx} = \sigma_r \sin^2 \alpha \quad (3.1)$$

$$\sigma_{wy} = \sigma_r \cos^2 \alpha \quad (3.2)$$

$$|\tau_{wxy}| = \sigma_r \cos \alpha \sin \alpha \quad (3.3)$$

Note that the angle,  $\alpha$ , equals  $\pi/2 - \beta$ , where  $\beta$  is the angle introduced in Figure 2.3. At the bottom face of the circular fan in Figure 3.1, the web stress is equal to the stress from the uniform load at the bottom face of the girder plus a possible contribution from the transverse stiffeners needed in the region on the right-hand side of the circular fan. To satisfy the boundary condition at the top face ( $\sigma_y = 0$ ), the stiffeners in the circular fan must, as described in Section 2.1, correspond to

$$\varphi f_{ys} = \sigma_{wy,tf} = \sigma_{sy,tf} \quad (3.4)$$

Here and in the following, index, *tf*, refers to top face and index, *bf*, refers to bottom face. Furthermore, index, *w*, refers to web and index, *s*, refers to stiffeners.  $\varphi$  is the stiffener ratio and  $f_{ys}$  is either the yield stress or the buckling stress of the stiffeners. Determination of the buckling stress is treated in PART III, Section 4.1.

These stiffeners will add an extra tensile stress to the web stress in the region on the left-hand side of the circular fan. If  $a$  is the vertical distance from the pole,  $C$ , of the fan to the bottom face, then  $r = a/\cos\alpha$  along the bottom face and the radial web stress,  $\sigma_r$ , in any point of the circular fan is given by

$$\sigma_r = \frac{\sigma_{wy,bf} a}{\cos^3 \alpha r} \quad (3.5)$$

Along any other horizontal line the web stress,  $\sigma_{wy}$ , may be determined by the following formula, where  $y_0$  is the vertical distance from the bottom face of the girder to the particular horizontal line considered, cf. Figure 3.1,

$$\sigma_{wy} = \sigma_{wy,bf} \frac{a}{a - y_0} \quad (3.6)$$

By Equations (3.2) and (3.3), the shear stress,  $\tau_{wxy}$ , along the bottom face is found to be

$$\tau_{wxy} = \sigma_{wy,bf} \tan \alpha \quad (3.7)$$

Along any other horizontal line  $\tau_{wxy}$  is

$$\tau_{wxy} = \sigma_{wy,bf} \frac{a}{a - y_0} \tan \alpha \quad (3.8)$$

Thus  $\tau_{wxy}$  is a linear function of  $x$  along a horizontal line.

In the same way it is found that  $\sigma_{wx}$  along any horizontal line is given by

$$\sigma_{wx} = \sigma_{wy,bf} \frac{a}{a - y_0} \tan^2 \alpha \quad (3.9)$$

Unfortunately, the stress field in a circular fan becomes strongly inhomogeneous if the angle between the two inclined faces limiting the circular fan becomes large. This is evident from Equation (3.5). Since  $\sigma_r \rightarrow \infty$  for  $r \rightarrow 0$ , the pole cannot belong to the region considered. The largest value of the web stress ( $\sigma_w = \sigma_r$ ) is found when  $\alpha$  is as large as possible and  $r$  as small as possible. Thus the point with maximum stress (as well as the point with minimum stress) is as shown in Figure 3.1.

In general, the stresses in a fan may be found by Equations (3.1) - (3.3). Solving one of these equations for  $\sigma_r$  and inserting into one of the other equations, the relationship between the three stress components may be expressed as shown in Box 1.

$\sigma_x = \tau_{xy} \tan \alpha$	$\tau_{xy} = \sigma_x \cot \alpha$	$\sigma_x = \sigma_y \tan^2 \alpha$
$\sigma_y = \tau_{xy} \cot \alpha$	$\tau_{xy} = \sigma_y \tan \alpha$	$\sigma_y = \sigma_x \cot^2 \alpha$

**Box 1:** Relationship between  $\sigma_x$ ,  $\sigma_y$  and  $\tau_{xy}$ .

The equations in Box 1 are in fact valid for any uniaxial stress field. To make them valid for the circular fan solutions,  $\sigma_y$  must, as previously mentioned, be constant along horizontal lines.

The variation of the flange forces,  $T$  and  $C$ , follow from the shear stress,  $\tau$ , along the flanges, i.e.

$$\frac{dT}{dx} = \frac{dC}{dx} = \tau t_w \quad (3.10)$$

where  $t_w$  is the web thickness and  $x$  is the girder axis.

If the shear stress is constant, the flange forces will be linear functions. When circular fans are applied, the shear stress varies linearly along the stringers in each fan, thus the flange forces will be parabolic. It becomes apparent that the traditional equations for the flange forces, Equations (2.8) and (2.9), may still be used with the following modifications:

$$T_B = \frac{M}{d} - \frac{1}{2} Q \tan \alpha_{left} \quad (3.11)$$

$$C_A = \frac{M}{d} + \frac{1}{2} Q \tan \alpha_{right} \quad (3.12)$$

Here,  $Q$  is the shear force and  $M$  is the moment in the section considered ( $AB$ ). Indexes,  $A$  and  $B$ , refer to the points marked in Figure 3.2. The angles,  $\alpha_{left}$  and  $\alpha_{right}$ , are the angles of the left- and right-hand side of the fan considered, respectively. Notice, that  $\tan \alpha = \cot \beta$ , cf. Figure 2.1.

Again, Equation (3.12) is only valid if  $C_A$  does not exceed the buckling load of the compression flange. Determination of the buckling load of the compression flange is treated in PART III, Section 4.1.

As described in Section 2.1,  $d$  in Equation (3.11) and Equation (3.12) should be replaced by  $d$  plus  $t_f$ . This is also neglected in this section.

The flange forces must equilibrate the normal stresses,  $\sigma_{wx}$ , in a vertical section. In Figure 3.2, a circular fan ( $A$ ,  $B$ ,  $C$  and  $D$ ) is shown. The web normal stress,  $\sigma_{wx}$ , along the vertical line,  $AB$ , as a function of the vertical distance,  $y_0$ , from the bottom face may be determined by, cf. Box 1,

$$\sigma_{wx} = \sigma_{wy,bf} \frac{a^3}{(a - y_0)^3} \tan^2 \alpha_{left} \quad (3.13)$$

The  $\sigma_{wx}$ -distribution along the vertical section ( $AB$ ) is also illustrated in Figure 3.2.

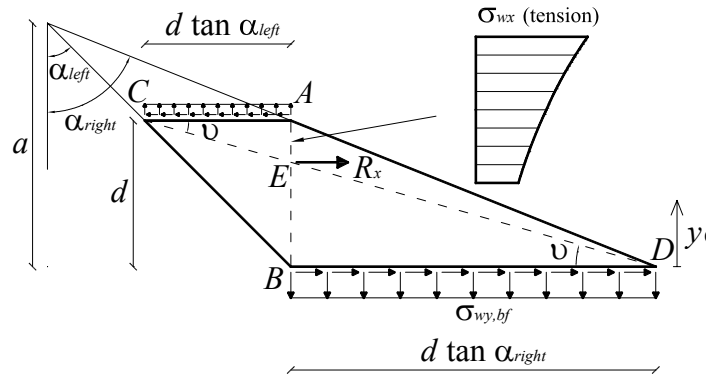


**Figure 3.2:** Normal stress along a vertical section in a circular fan

Due to equilibrium with the flange forces,  $T_B$  and  $C_A$ , cf. Equations (3.11) and (3.12), the resultant of the  $\sigma_{wx}$ -stresses along a vertical section in any circular fan is given by

$$R_x = \frac{1}{2} Q (\tan \alpha_{right} + \tan \alpha_{left}) \quad (3.14)$$

This resultant acts on the point  $E$ , cf. Figure 3.2, i.e. the point where the diagonals ( $AB$ ) and ( $CD$ ) intersect. This may be verified by applying the moment equilibrium equation on point  $E$ . The lever arm for  $T_B$ , i.e. length between  $B$  and  $E$ , is given by

$$|BE| = d \tan \alpha_{right} \tan \nu = d \frac{\tan \alpha_{right}}{\tan \alpha_{left} + \tan \alpha_{right}} \quad (3.15)$$

The lever arm for  $C_A$ , i.e. length between  $A$  and  $E$ , is given by

$$|AE| = d \tan \alpha_{left} \tan \nu = d \frac{\tan \alpha_{left}}{\tan \alpha_{left} + \tan \alpha_{right}} \quad (3.16)$$

The following criterion is then always fulfilled, cf. Equations (3.11) and (3.12).

$$C_A |AE| + T_B |BE| = M \quad (3.17)$$

Equation (3.14) is also found by the equations in Box 1, when the mean value of  $\tau_{xy}$  and  $\sigma_x$  in section ( $AB$ ) is considered.

It is now evident that the flange forces calculated by the Equations (3.11) and (3.12) are valid for the four points  $A$ ,  $B$ ,  $C$  and  $D$  in Figure 3.2 in any circular fan. Along the compression flange, a jump in the shear stress,  $\tau_{wxy}$ , in point  $A$  (and in point  $C$ ) will occur, hence the compressive flange force curve will have a slope discontinuity at this point. This is also the case for the tensile flange force at point  $B$  (and  $D$ ). Between the points  $A$  and  $C$  (and between  $D$  and  $B$ ), the flange forces are parabolic functions.

### 3.2 Application of Circular Fan Stress Fields

As mentioned above, since the stress field in a circular fan becomes strongly inhomogeneous if the angle between the two inclined faces limiting the circular fan becomes large, more than one circular fan must normally be applied. The optimal subdivision may be found by requiring the web stress,  $\sigma_r$ , in the point with maximum stress in each fan to be equal to the yield stress,  $f_{yw}$ .

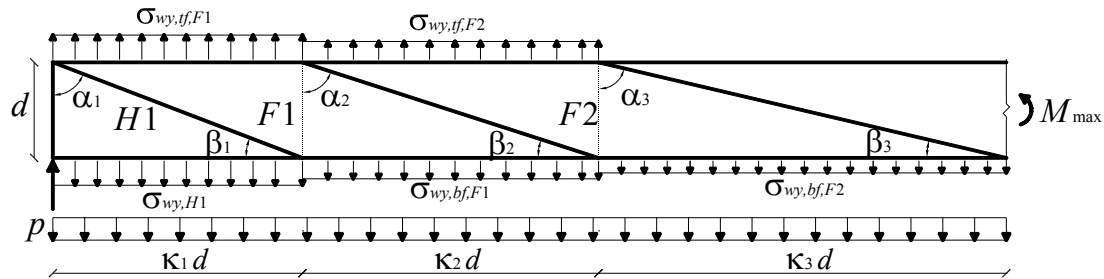


Figure 3.3: Steel plate girder subdivided into circular fans

Consider Figure 3.3, which shows a part of a steel plate girder, uniformly loaded (note that  $p$  is a load per unit area) at the bottom face, from a maximum moment point to a support. The girder is modelled by one homogeneous stress region,  $H1$ , and two circular fans,  $F1$  and  $F2$ . Denoting  $\kappa_i = \tan\alpha_i = \cot\beta_i$ , the parameter,  $\kappa_1$ , and thereby the length,  $\kappa_1 d$ , and the angles,  $\alpha_1$  and  $\beta_1$ , are determined by, cf. Equation (2.7),

$$\kappa_1 = \frac{1}{2} \frac{f_{yw}}{\tau} \left( 1 + \sqrt{1 - \left( \frac{\tau}{\frac{1}{2} f_{yw}} \right)^2} \right), \quad \tau \leq \frac{1}{2} f_{yw} \quad (3.18)$$

The shear stress at the support is inserted into this equation as the  $\tau$ -value. The web stress,  $\sigma_{wy,H1}$ , in the  $y$ -direction in  $H1$  is then determined by Equation (2.2), i.e.

$$\sigma_{wy,H1} = \frac{\tau}{\kappa_1} \quad (3.19)$$

To satisfy the boundary conditions along the bottom face of region  $H1$ , the web stress,  $\sigma_{wy,H1}$ , must correspond to the load at the bottom face of the girder plus a contribution from the stiffeners needed in the circular fan,  $F1$ . The stresses for web and stiffeners, respectively, in the  $y$ -direction at the top face of  $F1$ , are then given by

$$\sigma_{sy,tf,F1} = \sigma_{wy,tf,F1} = \sigma_{wy,H1} - p = \left( \varphi f_{ys} \right)_{\kappa_1 d} \quad (3.20)$$

The stresses determine the number of stiffeners ( $\varphi f_{ys}$ ) along the length,  $\kappa_1 d$ .

The optimal value of the angle,  $\alpha_2$  (and thereby the length,  $\kappa_2 d$ ), may be found by setting  $\sigma_r$  equal to  $f_{yw}$  and  $\sigma_{wy}$  equal to  $\sigma_{wy,tf,F1}$  in Equation (3.2). This gives

$$\alpha_2 = \text{Arc cos} \sqrt{\frac{\sigma_{wy,tf,F1}}{f_{wy}}} \quad (3.21)$$

When the angle,  $\alpha_2$ , is known, the length,  $\kappa_1 d$ , at the bottom face of  $F1$  is given by

$$\kappa_2 d = d \tan \alpha_2 = d \cot \beta_2 \quad (3.22)$$

The two limiting faces of  $F1$  are now known, hence the position of the pole may be found by simple geometry considering Figure 3.4:

$$\tan \alpha_1 = \frac{x_1}{a_1} \quad \text{and} \quad \tan \alpha_2 = \frac{x_1}{a_1 - d} \quad (3.23)$$

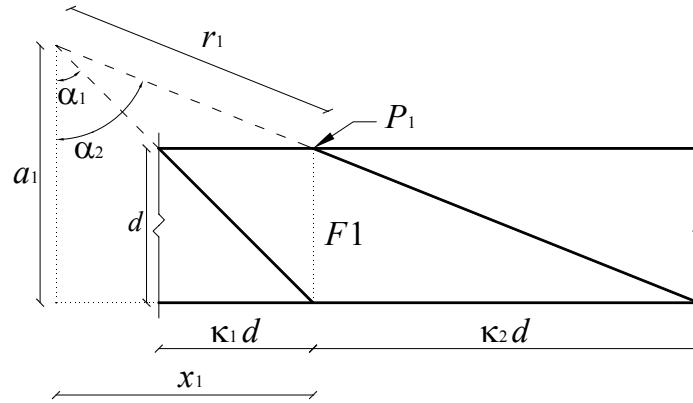


**Figure 3.4:** Geometry of circular fan,  $F1$

Solving one of the equations for  $x_1$  and inserting into the other one, gives

$$a_1 = d \frac{\cos \alpha_1 \sin \alpha_2}{\cos \alpha_1 \sin \alpha_2 - \sin \alpha_1 \cos \alpha_2} \quad (3.24)$$

The radial distance,  $r_1$ , from the pole to the point,  $P_1$ , with maximum stress is given by

$$r_1 = \frac{a_1 - d}{\cos \alpha_2} \quad (3.25)$$

Due to equilibrium, the web stress,  $\sigma_{wy,bf,F1}$ , at the bottom face of  $F1$  must be equal to

$$\sigma_{wy,bf,F1} = \sigma_{wy,tf,F1} \frac{\kappa_1}{\kappa_2} \quad (3.26)$$

All necessary information is now available and the equations in Box 1 or Equation (3.5) may be used to calculate the stresses at any point of the circular fan,  $F1$ .

Now consider circular fan,  $F2$ , where  $\kappa_2$ ,  $\alpha_2$  and  $\beta_2$  are already known. The length along the top face must be equal to the length at the bottom face of fan,  $F1$ , which is  $\kappa_2 d$ . Along the top face, the stress in the  $y$ -direction is given by, cf. Equation (3.20) valid for fan,  $F1$ ,

$$\sigma_{sy,tf,F2} = \sigma_{wy,tf,F2} = \sigma_{wy,bf,F1} - p = (\varphi f_{ys})_{\kappa_2 d} \quad (3.27)$$

The stresses determine the number of stiffeners ( $\varphi f_{ys}$ ) along the length,  $\kappa_2 d$ .

The optimal value of the angle,  $\alpha_3$ , is given by Equation (3.21) only with new indexes. The same is valid for Equations (3.22) - (3.26), whereby the stresses at any point of the circular fan,  $F2$ , may be determined. If the optimal value of the angle,  $\alpha_3$ , leads to passing of the end point, then the angle corresponding to the end point is applied.

In the remaining triangular region, all stresses are equal to zero. Hence, no stiffeners are supplied in this region, i.e. along the length,  $\kappa_3 d$ .

Hereby, a safe, statically admissible stress field is established for the whole girder part in Figure 3.3.

### 3.3 Practical Design Method

In practise, where it is simply a case of designing the internal stiffeners and checking the web stresses, the calculations may be done in a quick and easy manner when the shear stress diagram is given.

As shown in the previous section, the number of web stiffeners ( $\varphi f_{ys}$ ) in a homogeneous stress region as well as in a circular fan, is determined by

$$\varphi f_{ys} = \sigma_{sy,tf} \quad (3.28)$$

where  $\sigma_{sy,tf}$  is the stress in the  $y$ -direction at the top face sustained by the stiffeners.

The number of internal stiffeners in homogeneous stress regions or in circular fans may alternatively be determined by

$$\varphi f_{ys} = \frac{\tau}{\kappa} \quad (3.29)$$

where the  $\tau$ -value to be used is shown in Figure 3.5. The  $\kappa$ -value is determined by the angle,  $\beta$ , on the left-hand side of the fan. This means that

$$\sigma_{sy,tf} = \sigma_{wy,tf} = \frac{\tau}{\kappa} \quad (3.30)$$

It may be useful to illustrate further the validity of this equation. Consider Figure 3.5, which shows a circular fan such as  $F1$  or  $F2$  in Figure 3.3. In the vertical section shown, the shear stresses,  $\tau_{wxy}$ , as a function of the vertical distance,  $y_0$ , from the bottom face may be determined by, cf. the equations in Box 1,

$$\tau_{wxy} = \sigma_{wy,bf} \frac{a^2}{(a - y_0)^2} \tan \alpha_{left} = \sigma_{wy,bf} \frac{(a - d + y_0)^2}{a^2} \tan \alpha_{right} \quad (3.31)$$

Thus the shear stresses are parabolic along vertical lines. They are illustrated in the figure. The mean value of these  $\tau_{wxy}$ -stresses is equal to the  $\tau$ -value taken from the shear stress diagram for the section considered. By equilibrium it follows that

$$\sigma_{sy,tf} \kappa d t_w = \tau d t_w \Rightarrow \sigma_{sy,tf} = \frac{\tau}{\kappa} \quad (3.32)$$

remembering that  $\kappa = \cot \beta = \tan \alpha_{left}$  and that  $d$  is the girder depth and  $t_w$  the web thickness.

The equations for the fan solutions are summarised below. Consider Figure 3.6, where a steel plate girder and the corresponding shear stress diagram are shown.

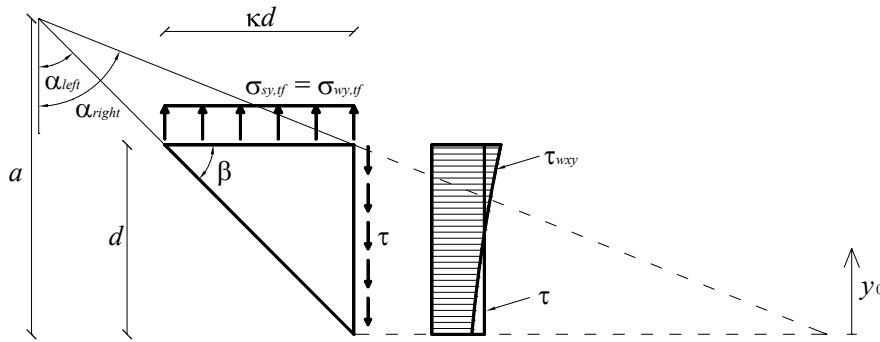


Figure 3.5: Shear stress in a vertical section of a circular fan

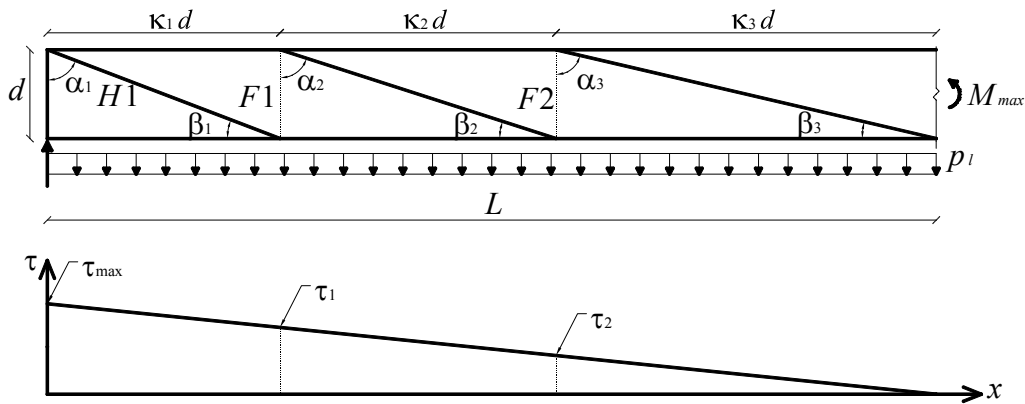


Figure 3.6: Uniformly loaded girder with the corresponding shear stress diagram

1. Introduce a triangular homogeneous stress region at the support. Determine  $\kappa_1$  ( $= \tan \alpha_1 = \cot \beta_1$ ) by Equation (3.18):

$$\kappa_1 = \frac{1}{2} \frac{f_{yw}}{\tau_{max}} \left( 1 + \sqrt{1 - \left( \frac{\tau_{max}}{\frac{1}{2} f_{yw}} \right)^2} \right), \quad \tau \leq \frac{1}{2} f_{yw} \quad (3.33)$$

2. The number of internal stiffeners along the length,  $\kappa_1 d$ , is, cf. Equation (3.29):

$$\left( \varphi f_{ys} \right)_{\kappa_1 d} = \frac{\tau_1}{\kappa_1} \quad (3.34)$$

3. Since  $\sigma_{sy,tf} = \sigma_{wy,tf} = \tau/\kappa$ ,  $\kappa_2$  is determined by Equation (3.21):

$$\alpha_2 = \text{Arc cos} \sqrt{\frac{\tau_1 / \kappa_1}{f_{yw}}} \quad (3.35)$$

$$\kappa_2 = \tan \alpha_2 \quad (3.36)$$

4. The number of internal stiffeners along the length,  $\kappa_1 d$ , is then:

$$\left( \varphi f_{ys} \right)_{\kappa_2 d} = \frac{\tau_2}{\kappa_2} \quad (3.37)$$

5. Continue by determining the  $\kappa_i$ -values and the required number of stiffeners along the lengths,  $\kappa_i d$ , until the cross-section with the maximum moment point is reached.
6. In a triangular region at the right end of the girder considered, all stresses are equal to zero. No stiffeners are needed.
7. If the girder is not loaded at the bottom face, extra stiffeners capable of transferring the load to the bottom face are supplied.

The use of circular fan solutions is illustrated in the following by calculating a specific example.

**EXAMPLE**

A simply supported girder with a double-symmetrical I-shaped cross-section is considered.

The girder has the web dimensions  $t_w = 5$  mm,  $d = 1500$  mm and  $L = 30000$  mm. The geometry of the girder is shown in Figure 3.7. Due to the symmetry, only one half of the girder is considered in the following.

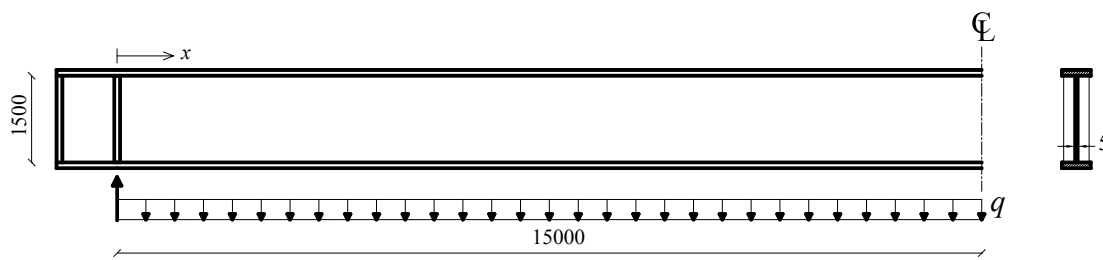


Figure 3.7: Geometry of the considered girder (measures in mm)

The girder is uniformly loaded at the bottom face corresponding to the load intensity of  $q = 40$  N/mm. The yield stresses of the web material along with the stiffener material are  $f_{ys} = f_{yw} = 240$  MPa (for the stiffeners the yield stress is assumed to be valid). The task is to design the required number of transverse web stiffeners.

The shear stress  $\tau$  is given by

$$\tau(x) = \frac{Q(x)}{t_w d} = \frac{40 \cdot (15000 - x)}{5 \cdot 1500} \quad (3.38)$$

The shear force at  $x$ ,  $Q(x)$ , is in Newton. The depth,  $d$ , and the thickness of the web,  $t_w$ , are in millimetres.

The girder is subdivided into two different circular fans and two triangular homogeneous stress regions, leading to three lengths,  $\kappa_i d$ , in the  $x$ -direction along the bottom face of the girder, see Figure 3.8. The maximum shear stress is

$$\tau(x_1) = \frac{40 \cdot (15000 - 0)}{5 \cdot 1500} = 80 \text{ MPa} < \frac{1}{2} f_{yw} = \frac{1}{2} \cdot 240 = 120 \text{ MPa} \quad (3.39)$$

The calculations follow the procedure given in Section 3.3.

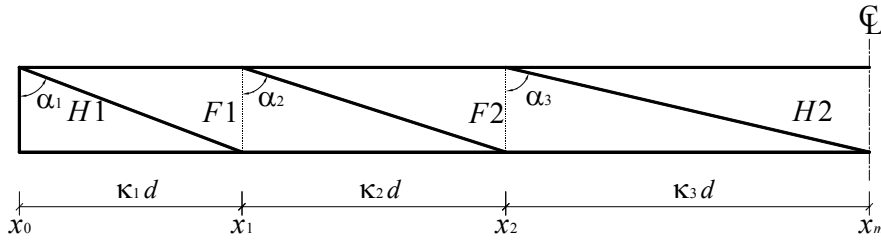


**Figure 3.8:** Subdivision of circular fans and triangular homogeneous stress fields

#### Length $\kappa_1 d$

For  $x = x_0 = 0$  mm:

$$\kappa_1 = \frac{1}{2} \frac{240}{80} \left( 1 + \sqrt{1 - \left( \frac{80}{\frac{1}{2} \cdot 240} \right)^2} \right) = 2.618 \quad (3.40)$$

$$x_1 = \kappa_1 d = 2.618 \cdot 1500 = 3927 \text{ mm} \quad (3.41)$$

$$\tau(x_1) = \frac{40(15000 - 3927)}{5 \cdot 1500} = 59 \text{ MPa} \quad (3.42)$$

$$\varphi_{\kappa_1 d} = \frac{\tau(x_1)}{\kappa_1 f_{ys}} = \frac{59}{2.618 \cdot 240} = 9.4 \cdot 10^{-2} = \underline{9.4\%} \quad (3.43)$$

#### Length $\kappa_2 d$

For  $x = x_1 = 3927$  mm:

$$\alpha_2 = \text{Arc cos} \sqrt{\frac{\tau(x_1) / \kappa_1}{f_{yw}}} = \text{Arc cos} \sqrt{\frac{59 / 2.618}{240}} = 72.15^\circ \quad (3.44)$$

$$\kappa_2 = \tan \alpha_2 = \tan 72.15^\circ = 3.105 \quad (3.45)$$

$$\kappa_2 d = 3.105 \cdot 1500 = 4657 \text{ mm} \quad (3.46)$$

$$x_2 = x_1 + \kappa_2 d = 3927 + 4657 = 8584 \text{ mm} \quad (3.47)$$

$$\tau(x_2) = \frac{40(15000 - 8584)}{5 \cdot 1500} = 34 \text{ MPa} \quad (3.48)$$

$$\varphi_{\kappa_2 d} = \frac{\tau(x_2)}{\kappa_2 f_{ys}} = \frac{34}{3.105 \cdot 240} = 4.6 \cdot 10^{-2} = \underline{4.6\%} \quad (3.49)$$

### Length $\kappa_3 d$

For  $x = x_2 = 8584$  mm:

$$\alpha_3 = \text{Arc cos} \sqrt{\frac{\tau(x_2)/\kappa_2}{f_{yw}}} = \text{Arc cos} \sqrt{\frac{34/3.105}{240}} = 77.67^\circ \quad (3.50)$$

$$\kappa_3 = \tan \alpha_3 = \tan 77.67^\circ = 4.575 \quad (3.51)$$

$$\kappa_3 d = 4.575 \cdot 1500 = 6863 \text{ mm} \quad (3.52)$$

$$x_3 = x_2 + \kappa_3 d = 8584 + 6863 = 15447 \text{ mm} > x_m = 15000 \text{ mm} \quad (3.53)$$

Hence, the value of  $\kappa_3 d = 15000 - 8584 = 6416$  mm is applied. Along this length no stiffeners are needed.

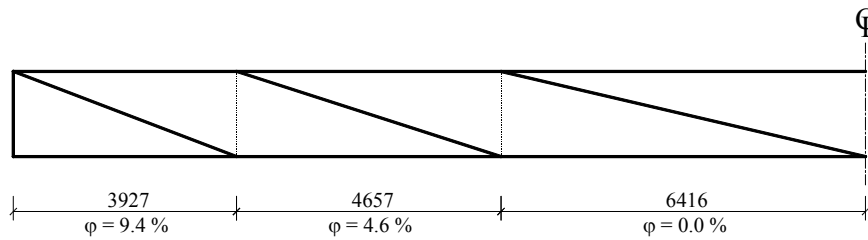


**Figure 3.9:** Transverse web stiffener ratios,  $\varphi$  (lengths in mm)

The designed number of transverse web stiffeners for each region is shown in Figure 3.9. The results obtained are also summarised in Table 3.1 together with the flange forces,  $T$  and  $C$ , calculated in the vertical sections corresponding to  $x_0$ ,  $x_1$ ,  $x_2$  and  $x_m$  by applying Equations (3.11) and (3.12). The flange force curves are shown in Figure 3.10. From the figure it is seen that the flange force curves have a slope discontinuity in the points corresponding to  $x_1$  and  $x_2$ , respectively. This is due to the jump in the shear stresses in these points, cf. Section 3.1. In between the points marked \*, the flange force curves are parabolic functions, and they curve opposite to the moment curve.

Region	$\tau_i$ [MPa]	$\kappa$ [ ]	$\varphi$ [%]	$A_s n$ [mm <sup>2</sup> ]	$C$ [kN]	$T$ [kN]
$H1(x_0)$	80	2.618	9.4	7049	785	-785
$F1(x_1)$	59	3.105	4.6	3444	2053	785
$F2(x_2)$	34	4.277	0.0	0	3000	2053
$H2(x_m)$	0	-	0.0	0	3000	3000

**Table 3.1:** Data for girder example

The total cross-sectional areas,  $A_s n$  ( $A_s$  being the cross-sectional area of a single stiffener and  $n$  the number of stiffeners), of the stiffeners along the lengths,  $\kappa_i d$ , corresponding to the calculated  $\phi$ -values are also shown in table.

Figure 3.11 shows the web normal stresses in the y-direction,  $\sigma_{wy}$ , at the top face and at the bottom face, respectively. Here the web normal stresses in the x-direction,  $\sigma_{wx}$ , in the vertical sections corresponding to  $x_0$ ,  $x_1$ ,  $x_2$  and  $x_m$  are also shown. In a similar way, Figure 3.12 shows the absolute values of the web shear stresses,  $\tau_{wxy}$ .

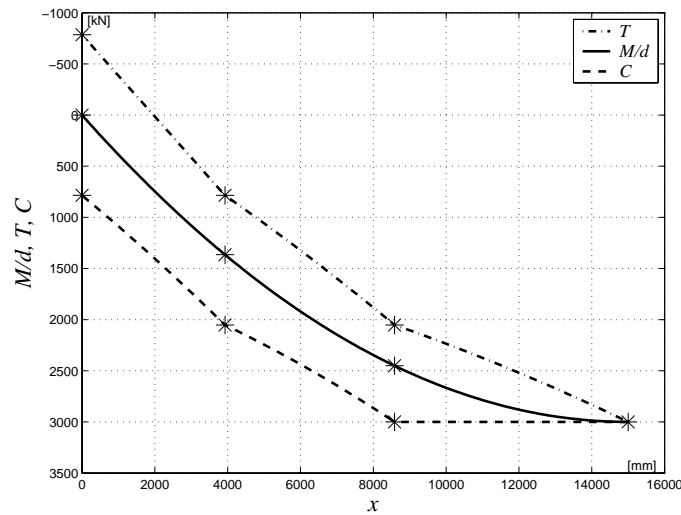


Figure 3.10: Flange force curves

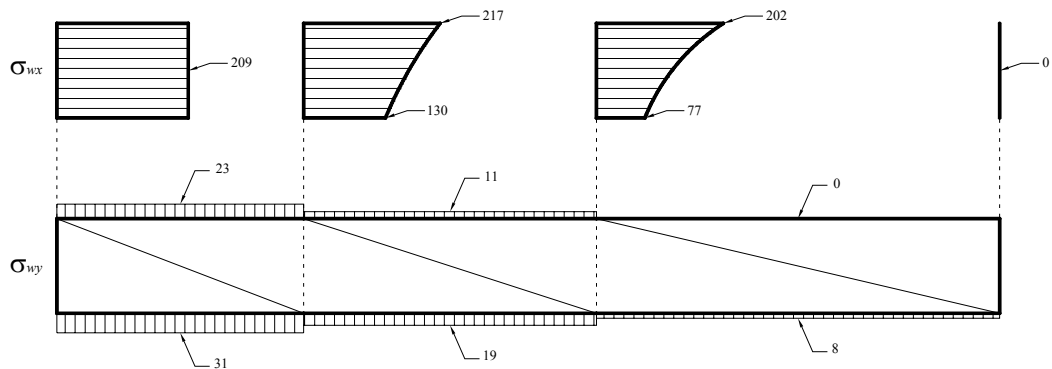


Figure 3.11: Web normal stresses,  $\sigma_{wx}$  and  $\sigma_{wy}$  (stresses in MPa)

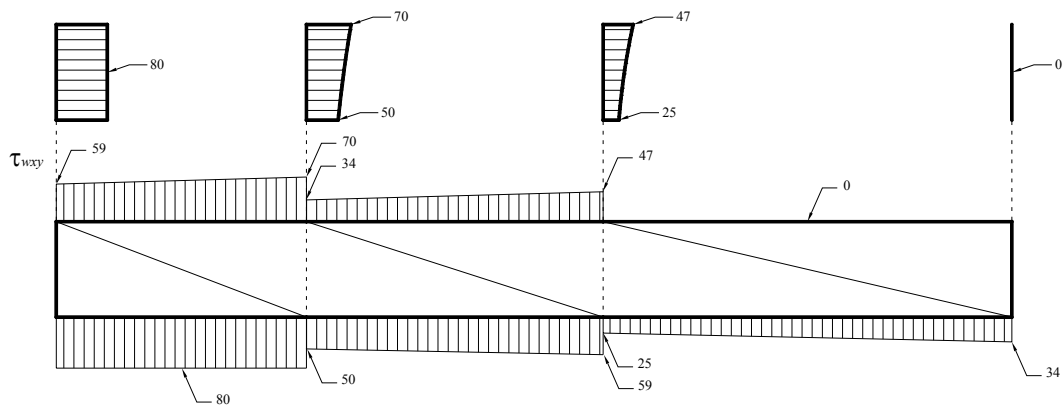


Figure 3.12: Absolute values of the web shear stresses,  $\tau_{wxy}$  (stresses in MPa)

### 3.4 Other Loading Cases

Thus far, the presented design method has only dealt with girders subjected to constant shear or to a uniformly distributed load at the bottom face. Girders loaded at the top, or at a level between the top and the bottom, may be treated as girders loaded at the bottom face, if extra transverse stiffeners capable of transferring the load to the bottom are supplied.

The design method described may also be used for girders subjected to uniform loading with piecewise constant load intensity along each of the lengths,  $\kappa_i d$ .

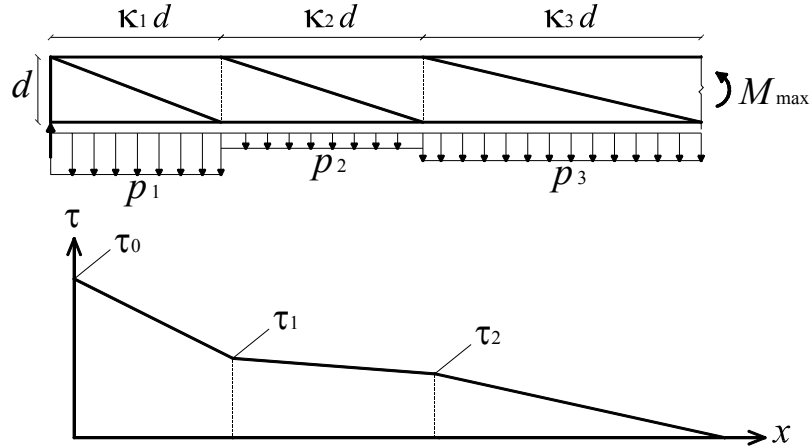


Figure 3.13: Simply supported plate girder with uniform loading, constant in each region

In Figure 3.13, a simply supported girder is modelled using triangular homogeneous regions and circular fans. The girder is subjected to a uniform load with three different load intensities ( $p_1$ ,  $p_2$  and  $p_3$ ). Each of the load intensities is constant along the lengths,  $\kappa_i d$ .

The stresses in the  $y$ -direction are:

$$\sigma_{wy,H1} = \frac{\tau_0}{\kappa_1} \quad (3.54)$$

$$\sigma_{sy,tf,F1} = \sigma_{wy,tf,F1} = \sigma_{wy,H1} - p_1 = \frac{\tau_1}{\kappa_1} \quad (3.55)$$

$$\sigma_{wy,bf,F1} = \sigma_{wy,tf,F1} \frac{\kappa_1}{\kappa_2} \quad (3.56)$$

$$\sigma_{sy,tf,F2} = \sigma_{wy,tf,F2} = \sigma_{wy,bf,F1} - p_2 = \frac{\tau_2}{\kappa_2} \quad (3.57)$$

$$\sigma_{wy,bf,F2} = \sigma_{wy,tf,F2} \frac{\kappa_2}{\kappa_3} = p_3 \quad (3.58)$$

Note that  $p_1$ ,  $p_2$  and  $p_3$  are normal stresses (positive as tension) at the bottom face, not loads per unit length.

The number of stiffeners may then be calculated in exactly the same way as for uniform load using the shear stress diagram, cf. the procedure of Section 3.3. Thus

$$\left(\varphi f_{ys}\right)_{\kappa_i d} = \frac{\tau_i}{\kappa_i} \quad (3.59)$$

If  $\kappa_i > \kappa_{i+1}$ , the pole of the fan is placed below the girder, however the solution is still valid if  $\sigma_w$  does not exceed  $f_{yw}$ . Systems with poles on either side of the girder will not be treated further here.

Since the design method applying circular fan solutions may be used for uniform loading, the intensity of which varies from region to region but which is constant within each region, the method can deal approximately with almost any load case by superposition. To treat combinations of continuous loading and concentrated loads, superposition may also be used.

The design method may also be applied to steel plate girders with other cross-sections e.g. single-symmetrical I-section, box girders, etc.

Girders with variable depth may be treated in the same way as concrete beams with variable depth, see (Nielsen 1998).

### 3.5 End Panels

The end panels differ from the other panels because the tensile band is not equilibrated by the stresses in an adjacent panel. The horizontal component of the uniaxial tensile band must therefore be anchored in the end panel. Hence, the end panel must be designed such that it is able to sustain these forces. One way of doing so is illustrated in the following.

The stresses from the tensile band will act as a uniform load on the end panel, which may be considered a vertical beam. Thus the transverse web stiffeners will act as the top and bottom flange respectively. Furthermore, the flanges of the girder will act as stiffeners in the vertical beam, see Figure 3.14. If necessary, the end panel may be supplied with extra horizontal web stiffeners, as shown by the dashed lines in the figure.

The beam is assumed simply supported by the flanges. The shear force from the girders will be transferred directly to the support. Hence, the only shear stress that must be sustained by the end panel is that due to the uniform load from the tensile band.

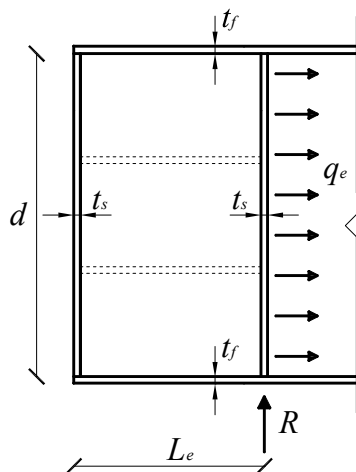


Figure 3.14: Design of end panel

The load per unit length,  $q_e$ , on the end panel is given by, cf. Equation (2.1),

$$q_e = t_w \tau \cot \beta \quad (3.60)$$

where  $\tau$  is the shear stress in the considered section,  $\beta$  the angle of the uniaxial tensile stresses with the girder axis, and  $t_w$  the web plate thickness, which is assumed to be constant throughout the entire girder.

The shear force and the moment is then determined by ( $d$  being the girder depth)

$$Q_e = \frac{1}{2} q_e d \quad (3.61)$$

$$M_e = \frac{1}{8} q_e d^2 \quad (3.62)$$

With the above notation and  $L_e$  being the length of the end panel, the shear stress,  $\tau_e$ , in the end panel is found to be

$$\tau_e = \frac{Q_e}{t_w L_e} \quad (3.63)$$

The maximum normal stress in the transverse web stiffener, i.e. the flanges of the vertical beam, is given by

$$\sigma_e = \frac{M_e}{A_s (t_s + L_e)} \quad (3.64)$$

where  $A_s$  is the cross-sectional area of the stiffener and  $t_s$  is the thickness of the stiffener.

The length of the end panel,  $L_e$ , must be chosen so the shear stress given by Equation (3.63) may be sustained by the end panel, and the normal stress given by Equation (3.64) should not exceed the yield stress or the buckling stress of the transverse web stiffeners. Determination of the buckling stress of the stiffeners is treated in PART III, Section 4.1.

## 4 EXPERIMENTAL RESULTS FROM THE LITERATURE

Many researchers have conducted tests to investigate the shear capacity of steel plate girders.

The aim of the tests was to verify the different theories, as all the researchers who have conducted the tests also have their own theory. Therefore, it is not always the same parameters that have been varied, as would be ideal for the present theory. The parameter,  $\psi$ , in particular (number and strength of the stiffeners) has only been varied in a few test series found in the literature. This is due to the fact that all the other theories only deal with a single web panel between two stiffeners. Hence in many of the tests, no stiffeners were supplied between the reaction and the applied load. Unfortunately, the parameter,  $\psi$ , would be the most relevant to vary in order to verify the present theory, as it is here that the theory differs from the other theories. Therefore, new experiments have been made with varying  $\psi$ -values, see Chapter 5.

In some of the tests found in the literature, internal stiffeners are supplied, but since they are not included in the other theories, information about the stiffeners is not given in sufficient detail.

In some of the tests, longitudinal stiffeners are supplied. In other cases, different stiffener arrangements are used, e.g. small ribs or angle bars. These results cannot be directly used to verify the present theory.

The yield stresses may be defective in some cases, as a value of the yield stress is given without any information on how this value was obtained. The main problem is the yield stress of the stiffeners, where no value is given in some cases. The only information provided is that the stiffeners were cut out of the same plate as the web or the flanges.

Another problem with some of the old tests is that the stiffeners are not welded to the bottom flange. This is done in order to make the design of the specimens easier. However, this will have no significant influence on the load-carrying capacity, as the stiffeners will be pushed towards the bottom flange during the loading. This fact was verified experimentally by Basler et al. (1960).

In total, 77 tests found in the literature may be used to verify the present theory. These tests were performed in ten different research laboratories. Different test setups and load arrangements were used. They are illustrated in Appendix D, where the dimensions of each specimen are also given.

The tests G6T1 – G9T2 were done by Basler et al. (1960), C4 – A4 by Longbottom and Heymann (1956), S1 and S2 by Lew et al. (1969), H1-T1 – H2-T2 by Cooper et al. (1964), WB-1 – WB-10 by Lyse and Godfrey (1935), G1 – G8 by Nishino and Okumura (1968), TG1 – TG5' by Skaloud (1971), LST1 by d'Apice et al. (1966), G1 – G9 by Sakai et al. (1966) and TG1 – TG10 were done by Rockey and Skaloud (1971).

Primarily, the variation of the load-carrying capacity in shear with  $d/t_w$ ,  $L/d$  and the bending stiffness of the flanges have been investigated in the tests. The parameters vary in the interval:

- $d/t_w$ : 50 – 400 (depth-to-thickness ratio)
- $L/d$ : 1.0 – 4.29 (length-to-depth ratio)
- $\psi$ : 0.000 – 0.405 (mechanical degree of stiffening)
- $\eta$ : 0.005 – 1.084 (bending stiffness and strength of the flanges)

All these experimental results are categorised in three groups as follows:

- *Thin web plates*, i.e.  $d/t_w \geq 150$ . The load-carrying capacity is given by the post-buckling strength, cf. Equation (2.29), which is minimised regarding  $\theta$ ,

$$\frac{\tau_1}{f_{yw}} = \frac{1}{2} \left( \sqrt{1 + \tan^2 \theta} - \tan \theta \right) + \frac{\eta}{L/d - \tan \theta} + \psi \tan \theta \quad (4.1)$$

- *Thick web plates*, i.e.  $d/t_w \leq 70$ . Buckling of the web does not occur, so the load-carrying capacity is given by, cf. Equation (2.41),

$$\frac{\tau_2}{f_{yw}} = \frac{1}{\sqrt{3}} + \eta \frac{d}{L} \quad (4.2)$$

- *Intermediate web plates*, i.e.  $70 < d/t_w < 150$ . The load-carrying capacity is found by interpolation. Thus

$$\frac{\tau_3}{f_{yw}} = \frac{\tau_2}{f_{yw}} - \left( \frac{\tau_2}{f_{yw}} - \frac{\tau_1}{f_{yw}} \right) \frac{d/t_w - 70}{80} \quad (4.3)$$

Table 4.1 shows the predicted load-carrying capacity,  $\tau_u/f_{yw}$ , together with the load-carrying capacity,  $\tau_{exp}/f_{yw}$ , obtained by the experiments. It also shows the parameters  $d/t_w$ ,  $L/d$ ,  $\psi$  and  $\eta$ .

	Girder	$d/t_w$	$L/d$	$\psi$	$\eta$	$\tau_1/f_{yw}$	$\tau_2/f_{yw}$	$\tau_3/f_{yw}$	$\tau_{exp}/f_{yw}$	$\frac{\tau_u/f_{yw}}{\tau_{exp}/f_{yw}}$
Basler et al.	G6T1	259	3.0	0.081	0.031	<b>0.293</b>	-	-	0.328	0.893
	G6T2	259	3.0	0.243	0.031	<b>0.442</b>	-	-	0.424	1.042
	G6T3	259	3.0	0.405	0.030	<b>0.502</b>	-	-	0.500	1.004
	G7T1	255	3.0	0.159	0.030	<b>0.380</b>	-	-	0.389	0.977
	G7T2	255	3.0	0.159	0.030	<b>0.380</b>	-	-	0.400	0.950
	G8T1	254	3.0	0.000	0.030	<b>0.146</b>	-	-	0.226	0.646
	G8T2	254	3.0	0.076	0.030	<b>0.285</b>	-	-	0.267	1.067
	G8T3	254	3.0	0.076	0.030	<b>0.285</b>	-	-	0.311	0.916
	G9T1	382	3.0	0.000	0.039	<b>0.156</b>	-	-	0.165	0.945
G9T2	382	3.0	0.098	0.039	<b>0.320</b>	-	-	0.257	1.245	
Longbottom & Heymann	C4	241	1.48	0.075	0.022	<b>0.327</b>	-	-	0.328	0.997
	A1	94	1.29	0.000	0.090	0.412	0.647	<b>0.577</b>	0.587	0.982
	A2	94	2.05	0.000	0.090	0.287	0.621	<b>0.521</b>	0.495	1.052
	A3	94	4.29	0.000	0.090	0.146	0.598	<b>0.463</b>	0.303	1.527
	A4	85	2.10	0.000	0.147	0.340	0.647	<b>0.590</b>	0.585	1.008
Lew & d'Apice	S1	190	2.5	0.117	0.046	<b>0.355</b>	-	-	0.417	0.851
	S2	190	2.5	0.117	0.046	<b>0.355</b>	-	-	0.389	0.913
	LST1	256	3.0	0.100	0.084	<b>0.348</b>	-	-	0.400	0.870
Cooper et al.	H1-T1	127	3.0	0.000	0.035	0.152	0.589	<b>0.278</b>	0.297	0.935
	H1-T2	127	3.0	0.064	0.035	0.271	0.589	<b>0.362</b>	0.362	1.001
	H2-T1	128	3.0	0.128	0.146	0.407	0.626	<b>0.467</b>	0.427	1.094
	H2-T2	128	3.0	0.321	0.146	0.522	0.626	<b>0.551</b>	0.524	1.051

**Table 4.1:** Calculated data for the test specimens found in the literature (*continues on next page*)

	Girder	$d/t_w$	$L/d$	$\psi$	$\eta$	$\tau_1/f_{yw}$	$\tau_2/f_{yw}$	$\tau_3/f_{yw}$	$\tau_{exp}/f_{yw}$	$\tau_u/f_{yw} / \tau_{exp}/f_{yw}$
Lyse & Godfrey	WB-1	56	3.0	0	0.602	-	<b>0.778</b>	-	0.721	1.079
	WB-2	55	3.0	0	0.543	-	<b>0.758</b>	-	0.765	0.991
	WB-3	59	3.0	0	0.401	-	<b>0.711</b>	-	0.700	1.016
	WB-6	70	3.0	0	0.500	-	<b>0.744</b>	-	0.661	1.126
	WB-7	60	3.0	0	0.643	-	<b>0.792</b>	-	0.736	1.076
	WB-8	60	3.0	0	0.700	-	<b>0.811</b>	-	0.861	0.942
	WB-9	50	3.0	0	1.077	-	<b>0.936</b>	-	0.972	0.963
	WB-10	50	3.0	0	1.084	-	<b>0.939</b>	-	1.000	0.939
Nishino & Okumura	G1	60	2.69	0	0.130	-	<b>0.626</b>	-	0.588	1.064
	G2	60	2.69	0	0.095	-	<b>0.613</b>	-	0.554	1.106
	G3	77	2.64	0	0.070	0.210	0.604	<b>0.569</b>	0.483	1.179
	G4	78	2.64	0	0.058	0.197	0.599	<b>0.559</b>	0.455	1.229
	G5	100	2.62	0	0.046	0.186	0.595	<b>0.442</b>	0.402	1.098
	G6	101	2.62	0	0.034	0.171	0.590	<b>0.428</b>	0.358	1.195
	G7	119	2.64	0	0.031	0.165	0.589	<b>0.329</b>	0.340	0.969
	G8	121	2.64	0	0.024	0.156	0.586	<b>0.312</b>	0.307	1.016
Skaloud	TG1	400	1.0	0	0.005	<b>0.264</b>	-	-	0.303	0.871
	TG1'	400	1.0	0	0.005	<b>0.264</b>	-	-	0.233	1.133
	TG2	400	1.0	0	0.023	<b>0.337</b>	-	-	0.320	1.053
	TG2'	400	1.0	0	0.023	<b>0.337</b>	-	-	0.278	1.212
	TG3	400	1.0	0	0.061	<b>0.430</b>	-	-	0.381	1.129
	TG3'	400	1.0	0	0.061	<b>0.430</b>	-	-	0.380	1.132
	TG4	400	1.0	0	0.091	<b>0.488</b>	-	-	0.438	1.114
	TG4'	400	1.0	0	0.091	<b>0.488</b>	-	-	0.414	1.179
	TG5	400	1.0	0	0.248	<b>0.720</b>	-	-	0.618	1.165
	TG5'	400	1.0	0	0.248	<b>0.720</b>	-	-	0.601	1.198
Sakai et al.	G1	55	2.61	0	0.177	-	<b>0.645</b>	-	0.529	1.220
	G2	55	2.61	0	0.222	-	<b>0.662</b>	-	0.542	1.222
	G3	60	2.63	0	0.110	-	<b>0.619</b>	-	0.502	1.233
	G4	70	3.57	0	0.171	-	<b>0.625</b>	-	0.492	1.271
	G5	70	2.68	0	0.171	-	<b>0.641</b>	-	0.543	1.181
	G6	70	1.25	0	0.171	-	<b>0.714</b>	-	0.608	1.175
	G7	70	2.68	0	0.171	-	<b>0.641</b>	-	0.543	1.181
	G9	90	2.78	0	0.104	0.232	0.615	<b>0.519</b>	0.466	1.114
	Rockey & Skaloud	TG1	225	1.0	0	0.005	<b>0.264</b>	-	-	0.276
TG1'		225	1.0	0	0.005	<b>0.264</b>	-	-	0.293	0.901
TG2		225	1.0	0	0.008	<b>0.280</b>	-	-	0.308	0.909
TG2'		225	1.0	0	0.008	<b>0.280</b>	-	-	0.287	0.976
TG3		225	1.0	0	0.032	<b>0.362</b>	-	-	0.345	1.049
TG3'		225	1.0	0	0.032	<b>0.362</b>	-	-	0.330	1.097
TG4		225	1.0	0	0.055	<b>0.418</b>	-	-	0.388	1.077
TG4'		225	1.0	0	0.055	<b>0.418</b>	-	-	0.370	1.130
TG13		233	1.0	0	0.135	<b>0.562</b>	-	-	0.461	1.219
TG5		233	1.5	0	0.038	<b>0.283</b>	-	-	0.259	1.093
TG5'		233	1.5	0	0.038	<b>0.283</b>	-	-	0.287	0.986
TG14		316	2.0	0.230	0.023	<b>0.438</b>	-	-	0.389	1.126
TG15		316	2.0	0.230	0.055	<b>0.460</b>	-	-	0.450	1.022
TG16		316	2.0	0.230	0.110	<b>0.497</b>	-	-	0.477	1.042
TG17		316	2.0	0.230	0.208	<b>0.561</b>	-	-	0.597	0.940
TG18		316	2.0	0.230	0.391	<b>0.671</b>	-	-	0.771	0.870
TG19		316	2.0	0.230	0.495	<b>0.731</b>	-	-	0.832	0.879
TG20		150	2.0	0.110	0.011	<b>0.327</b>	-	-	0.360	0.908
TG9		233	2.0	0	0.040	<b>0.226</b>	-	-	0.269	0.840
TG9'		233	2.0	0	0.040	<b>0.226</b>	-	-	0.263	0.859
TG10	235	2.0	0	0.105	<b>0.308</b>	-	-	0.281	1.096	

The theory seems to correlate very well with the experimental results, see Figure 4.1. The mean value of  $(\tau_u/f_{yw})/(\tau_{exp}/f_{yw})$  for all the tests is 1.048 and the standard deviation is 13.4 %. For the individual test series the following results are obtained:

- Basler et al., G6T1 – G9T2: Mean 0.969, standard deviation 15.1 %.
- Longbottom & Heymann, C4 – A4: Mean 1.113, standard deviation 23.3 %.
- Lew & d’Apice, S1, S2 & LST1: Mean 0.878, standard deviation 3.1 %.
- Cooper et al., H1-T1 – H2T2: Mean 1.020, standard deviation 6.8 %.
- Lyse & Godfrey, WB1 – WB10: Mean 1.016, standard deviation 7.0 %.
- Nishino & Okumura, G1 – G8: Mean 1.107, standard deviation 9.0 %.
- Skaloud, TG1 – TG5’: Mean 1.119, standard deviation 9.8 %.
- Sakai et al., G1 – G9: Mean 1.200, standard deviation 4.8 %.
- Rockey & Skaloud, TG1 – TG10: Mean 0.999, standard deviation 10.7 %.

It is seen that the best mean value is obtained for the tests conducted by Rockey and Skaloud (1971), which is also the largest of all the series. The tests by Sakai et al. (1966) are those deviating most from the theory. All the specimens in this series have thick web plates. Nielsen and Christensen (1982) calculated this series by applying Tresca’s yield condition, i.e. the factor  $1/\sqrt{3}$  is substituted by  $1/2$  in Equation (4.2). With Tresca’s yield criterion, a mean value of 1.057 and a standard deviation of 2.7 % is obtained for the tests by Sakai et al. (1966).

In order to illustrate the correlation between the tests and the load-carrying capacity curve, all test values,  $\tau_{exp}/f_{yw}$ , for the tests by Basler et al. (1960), where  $d/t_w \geq 150$ ,  $\eta \approx 0.03$  and  $L/d = 3.0$  are shown as a function of  $\psi$  in Figure 4.2.

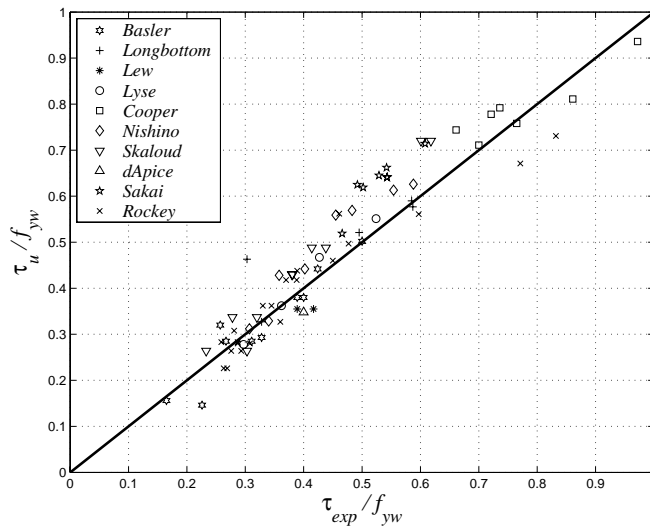
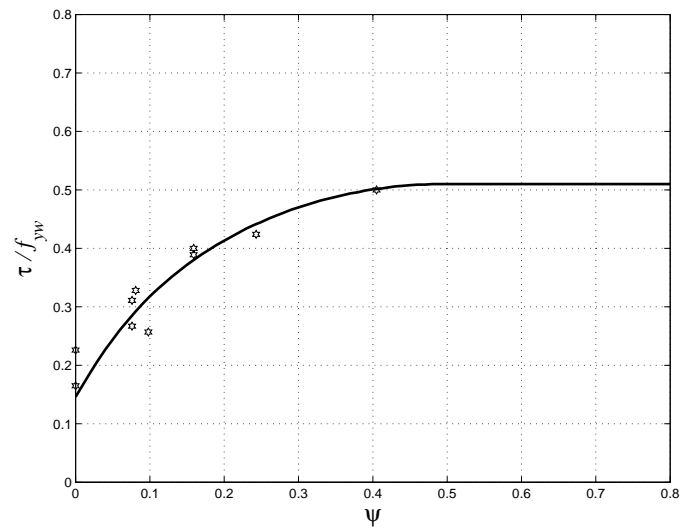


Figure 4.1: Comparison of theory and experimental results

When subdividing the test results into the three groups thin, thick and intermediate web plates, respectively, the following mean values and standard deviations are obtained:

- Thin web plates: Mean 1.011, standard deviation 12.7 %.
- Thick web plates: Mean 1.105, standard deviation 10.8 %.
- Intermediate web plates: Mean 1.097, standard deviation 14.7 %.



**Figure 4.2:** Theory versus tests  $L/d = 3.0$  and  $\eta \approx 0.03$

When designing a shear reinforced concrete beam according to the diagonal compression field method, one has to introduce an effectiveness factor,  $v$ , as tests have shown that it is not fully possible to utilise the concrete compressive strength. For steel plate girders, there is no need to introduce an effectiveness factor, as it is possible to fully utilise the tensile yield strength, cf. Figure 4.2.

## 5 NEW PLATE GIRDER EXPERIMENTS

As previously mentioned, Nielsen and Christensen (1982) stated that further experimental verification of the theory is required. In relation to the present study, a M.Sc. project was carried out at the Technical University of Denmark, cf. (Øskan and Bak 2006). The project was supervised by the author. The objective of their study was to determine the post-buckling strength of thin web plate girders in order to verify the theory. The experimental program contained tests on eight plate girder specimens. All the test specimens were sponsored by DS Stålkonstruktion A/S.

The experimental program and the results obtained are presented below.

### 5.1 The Test Girders

The experimental program contained tests on eight plate girder specimens, which may be classified into the following two groups:

- Constant shear tests, plate girders G1, G2, G3, G4, G5 and G6.
- Distributed loading tests, plate girders G7 and G8.

In the first group, the six specimens were subjected to constant shear in order to verify the lower-bound solution, cf. Section 2.1, as well as the upper-bound solution, cf. Section 2.2. The same test setup was used as shown in Figure 5.1. This figure also gives the shear force diagram, and the corresponding moment diagram. The specimens contained three sections, the middle section being denoted the *Test Section*, with a length of 2.0 m, i.e.  $L = 2.0$  m. The two adjacent sections, denoted the *End Sections* with a length of 1.0 m, were made relatively rigid in order to ensure failure in the test section. The only difference between the six test specimens was the number of transverse web stiffeners in the test section. The girders were supplied with zero to five transverse web stiffeners with an increment of one stiffener, i.e. for G1, no transverse web stiffeners were supplied; for G2, one stiffener was supplied, and for G6, five stiffeners were supplied. In all girders, the transverse web stiffeners in the test section were placed with constant spacing.

The second group contained two specimens designed as cantilever girders and subjected to a uniformly distributed load. The specimens contained two different sections, the test section with a length of 3.0 m, i.e.  $L = 3.0$  m, and the fixed boundary conditions were established by an adjacent section, the end section, with two simple supports, see Figure 5.2. This figure also shows the shear force diagram and the corresponding moment diagram, which is the same for both girders G7 and G8. As in the first group, the only difference between the designs of the two test specimens was the number of transverse web stiffeners supplied in the test section.

Four jacks provided the uniform load. Between the girder and the jacks, wooden blocks were applied in order to distribute the load from the jacks. For girder G8, the load was subjected to the bottom flange as a uniform compressive load. For girder G7, the load was subjected to the top flange as a uniform tensile load. This setup was rather complicated, as the same four jacks were used. The jacks acted on specially designed frames, which transferred the compression from the jacks to tension on the top flange.

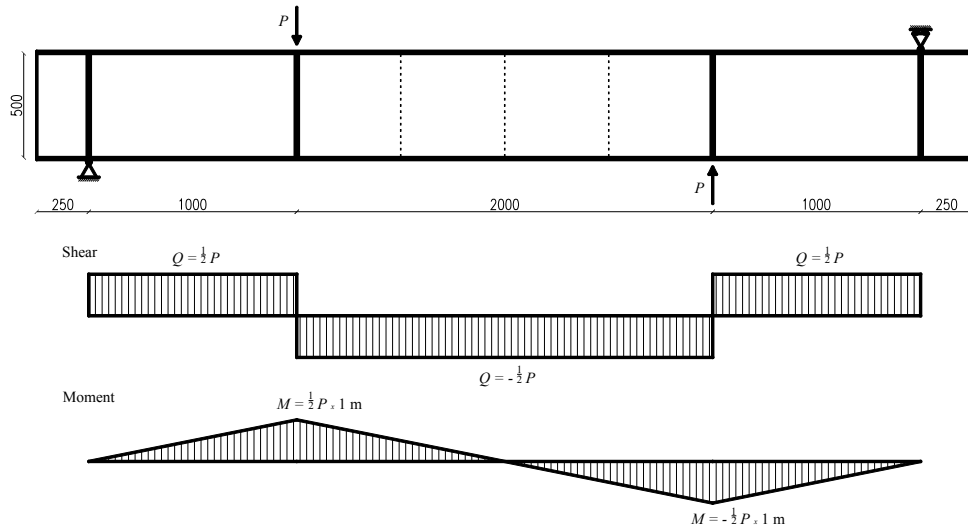


**Figure 5.1:** Shear force diagram and moment diagram for constant shear tests (measures in mm)

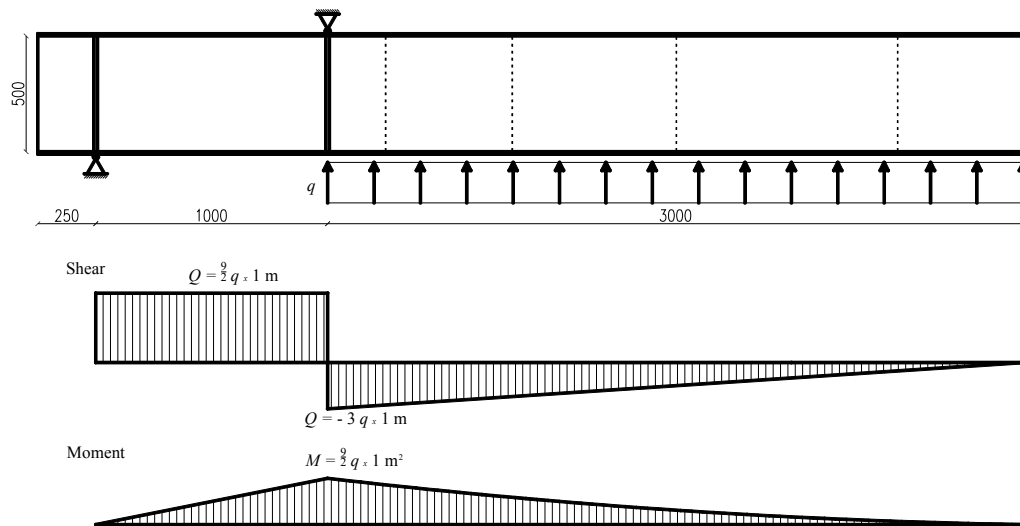


**Figure 5.2:** Shear force diagram and moment diagram for distributed loading tests (measures in mm)

## GIRDER DIMENSIONS

All the test specimens had a double-symmetrical I-shaped cross-section. The top and bottom flanges had constant dimensions throughout their entire length. The flange thickness was  $t_f = 10$  mm and the flange width was  $b_f = 200$  mm for all specimens. The girders all had a constant depth of the web plate of  $d = 500$  mm, so the length-to-depth ratio was  $L/d = 4.0$  for the constant shear tests and  $L/d = 6.0$  for the tests with distributed loading.

The thickness of the web plate for all specimens was  $t_w = 2.0$  mm in the test section and  $t_w = 10.0$  mm in the end sections. This gave a slenderness ratio of  $d/t_w = 250$  in the test sections.

In practical design of conventional steel plate girders, a web plate thickness smaller than  $t_w = 5.0$  mm is seldom used. However, a very small web plate thickness was chosen in order to reduce the size of the specimens, especially the length and the depth of the girders. With  $t_w$  equal to, say, 5.0 mm, the depth of the web plate would have to exceed a depth of 1000 mm in order to obtain a more conventional slenderness ratio.

The transverse stiffeners at the supports and at the concentrated load had a thickness of  $t_s = 15.0$  mm, and  $t_s = 3.0$  mm was applied for all the transverse web stiffeners in the test sections.

The different girder cross-sections used are shown in Figure 5.3. Detailed design drawings of all the girder specimens may be found in Appendix E.

With a plate thickness of 2.0 mm, one might expect welding to be a problem. However, in no cases did the welds fracture prior to ultimate load. The supplier of the girder specimens used TIG<sup>1</sup>-welding, which turned out to be suitable for the job.

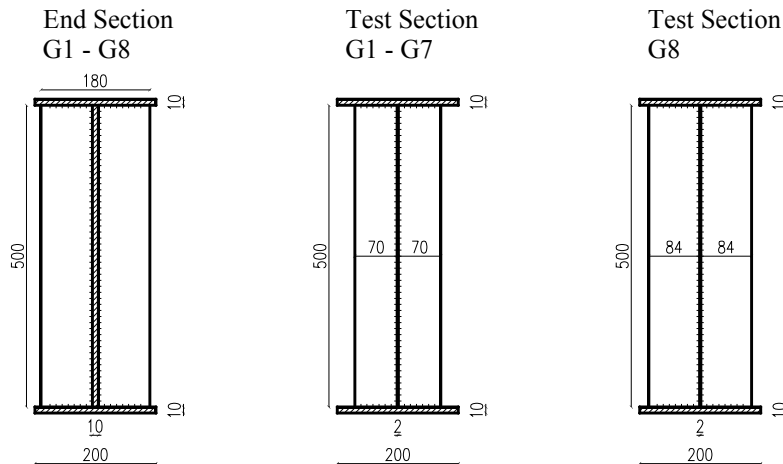


Figure 5.3: Girder cross-sections

### STEEL PROPERTIES

Tests on tension coupons made from the material under consideration were conducted to determine the yield level. The supplier of the girder specimens delivered steel plates with a width of 40 mm and a length of 300 mm together with the girder specimens. These plates were cut out of the same plates as used for the girder specimens. Out of each plate, tension coupons according to EN (2001) were made, see Figure 5.4. Four coupons were made with a thickness of 2.0 mm corresponding to the material used for the web plates in the test sections, four coupons with a thickness of 3.0 mm corresponding to the material used for the transverse web stiffeners in the test sections, two coupons with a thickness of 10.0 mm corresponding to the material used for the flanges and the web plates in the end sections, and two coupons with a thickness of 15.0 mm corresponding to the material used for the transverse web stiffeners in the end sections.

The load-displacement curves for each of the tests are shown in Figures 5.5 – 5.8. The determined material properties are given in Table 5.1.

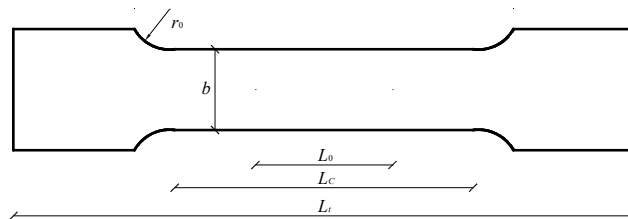


Figure 5.4: Tension coupons

<sup>1</sup> Tungsten Inert Gas welding

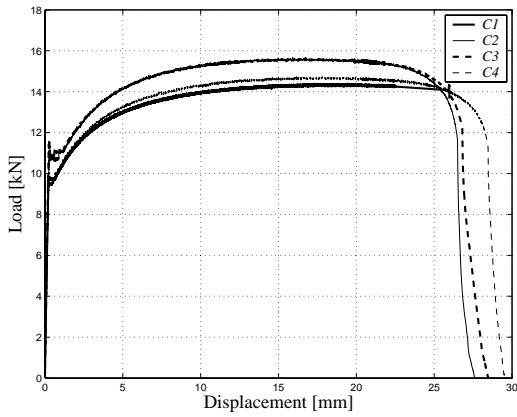


Figure 5.5: Load-displacement curves for 2.0 mm coupons

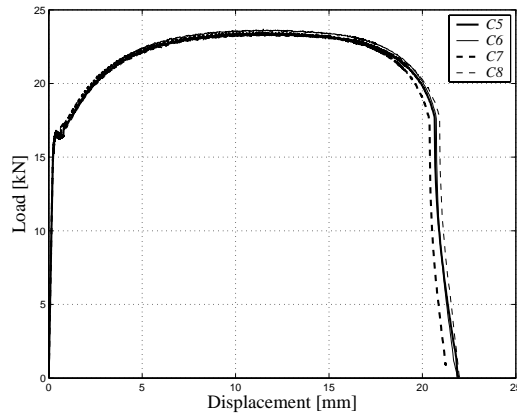


Figure 5.6: Load-displacement curves for 3.0 mm coupons

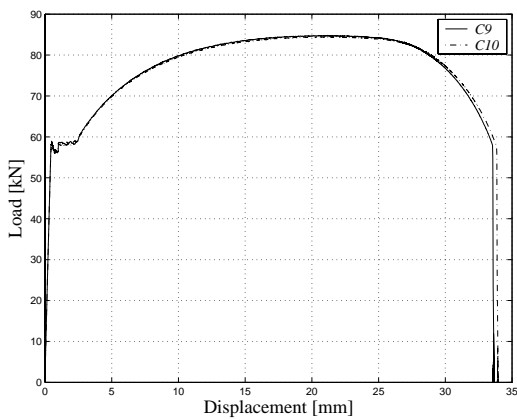


Figure 5.7: Load-displacement curves for 10.0 mm coupons

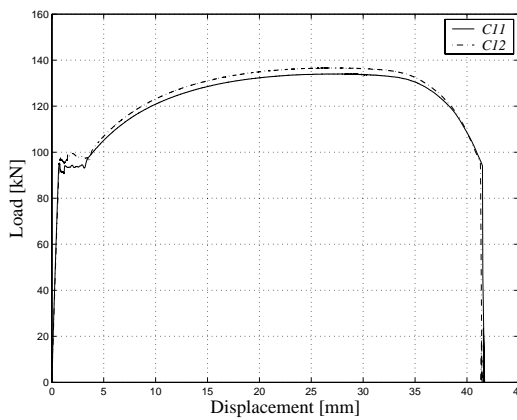


Figure 5.8: Load-displacement curves for 15.0 mm coupons

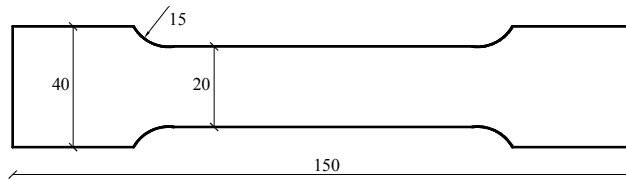


Figure 5.9: Additional tension coupons (measures in mm)

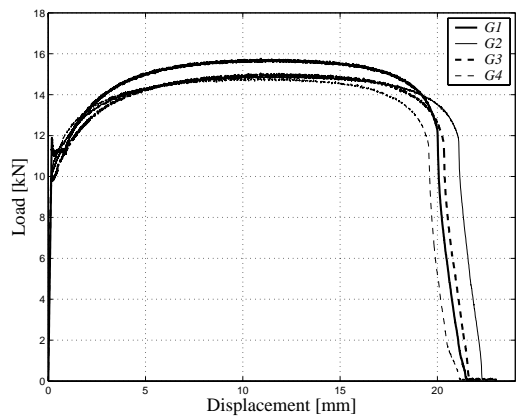


Figure 5.10: Load-displacement curves for additional 2.0 mm coupons, G1 – G4

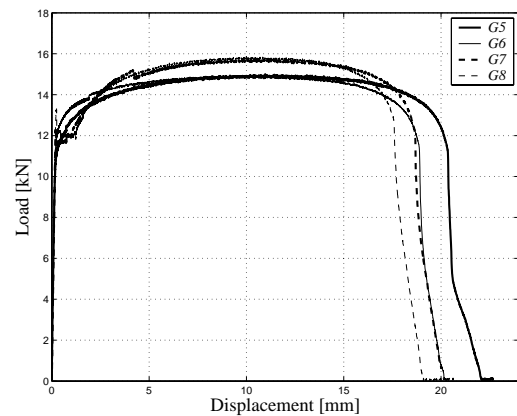


Figure 5.11: Load-displacement curves for additional 2.0 mm coupons, G5 – G8

The same notation as in (EN 2001) is used. Here,  $a$  is the coupon thickness and  $S_0$  is the original cross-sectional area. For all tension coupons,  $r_0 = 15$  mm, cf. Figure 5.4, is applied. The meaning of the notation  $b$ ,  $L_0$  and  $L_c$  is also shown in Figure 5.4.

The table also shows the mean values of the yield stress,  $f_y$ , and the ultimate tensile strength,  $f_u$ . From the figures and the table it is seen that the results from each coupon test with the same thickness coincide closely, except for the 2.0 mm thick coupons, i.e. coupons C1 – C4. For C1 and C4, the mean value was  $f_y = 237$  MPa. For C2 and C3 the mean value was  $f_y = 267$  MPa.

The results from the tests with coupons of thickness 2.0 mm indicate that the web plates of the girder specimens were cut out of two different steel plates. Therefore, additional tests on tension coupons were conducted. The coupons were cut out of the web plate after testing the girders in a location where the buckling deflections of the web plate were limited. Before testing the coupons, the specimens were flattened. The dimensions of the additional tension coupons did not fully satisfy the requirements in (EN 2001), as the total length was reduced, see Figure 5.9. However, this is considered of minor importance.

The load-displacement curves are shown in Figures 5.10 and 5.11. The determined material properties are given in Table 5.2.

The yield stresses determined by the additional coupon tests are found to be larger than the yield stresses given in Table 5.1. This is probably due to strain hardening during the testing of the girders. The main purpose of the additional coupon tests was to evaluate whether it was possible to identify from which of the two steel plates the web plate of each girders specimens were made of. Unfortunately, this may not be clearly seen from the additional coupon tests. Therefore in the following, the yield stresses of the web material determined by the additional tension coupons are applied cf. Table 5.2. For the other materials, the values given in Table 5.1 are used.

Coupon	No. of tests	$a$ [mm]	$b$ [mm]	$S_0$ [mm <sup>2</sup> ]	$L_0$ [mm]	$L_c$ [mm]	$f_y$ [MPa]	$f_u$ [MPa]
C1 – C4	4	2	20	40	34	74	252	378
C5 – C8	4	3	20	60	42	58	255	388
C9 – C10	2	10	20	200	76	104	293	422
C11 – C12	2	15	20	300	94	130	323	450

**Table 5.1** Data for tests on tension coupons

Coupon	G1	G2	G3	G4	G5	G6	G7	G8
$f_y$ [MPa]	280	238	247	250	239	256	249	282
$f_u$ [MPa]	393	373	375	369	373	373	393	395

**Table 5.2:** Data for additional tests on 2.0 mm tension coupons

### CRITICAL WEB BUCKLING STRESSES

An additional reference value, with which an experimental ultimate load may be compared, is the conventionally computed elastic critical buckling stress or load of the web.

The general equation for the ideal critical buckling stress of an isolated web panel is

$$\tau_{cr} = k \frac{\pi^2 E}{12(1-\nu^2)} \left( \frac{t_w}{d} \right)^2 \quad (5.1)$$

Here,  $d$  is the depth of the girder,  $b$  is the length between two adjacent stiffeners,  $t_w$  the web plate thickness,  $E$  is Young's modulus ( $E = 210,000$  MPa), and  $\nu$  is Poisson's ratio ( $\nu = 0.3$ ). Furthermore, it is assumed that the web plate is simply supported at the flanges and at the stiffeners. The buckling coefficient,  $k$ , is then given by, cf. (Timoshenko and Gere 1961),

$$k = \begin{cases} 5.35 + 4 \left( \frac{d}{b} \right)^2 & \text{for } \frac{d}{b} \geq 1 \\ 5.35 \left( \frac{d}{b} \right)^2 + 4 & \text{for } \frac{d}{b} < 1 \end{cases} \quad (5.2)$$

The elastic critical buckling load,  $P_{cr}$ , for girders G1 – G6 is evaluated from  $\tau_{cr} = Q_{cr} / (d t_w)$ , where  $Q_{cr} = \frac{1}{2} P_{cr}$  as seen from Figure 5.1. The critical buckling stress for girders G7 and G8 is calculated for the second web panel, counted from the supported end, as it is the critical one.

In Table 5.3, the critical stresses and loads for all girder specimens are summarised.

Girder	$b/d$ [ ]	$d/t_w$ [ ]	$k$ [ ]	$\tau_{cr}$ [MPa]	$P_{cr}$ [kN]
G1	4.00	250	4.33	13.1	26.2
G2	2.00	250	5.34	16.2	32.4
G3	1.33	250	7.00	21.3	42.6
G4	1.00	250	9.35	28.4	56.8
G5	0.80	250	11.60	35.2	70.4
G6	0.66	250	14.35	43.6	87.2
G7	1.09	250	9.49	25.8	<sup>1)</sup> 11.7
G8	1.09	250	9.49	25.8	<sup>1)</sup> 11.7

1)  $q_{cr}$  in kN/m.

**Table 5.3:** Elastic critical stresses and loads

## DEFLECTIONS

In order to test the elastic behaviour of the girders, their predicted deflections are evaluated below. The maximum deflections are given at the two loading points for girders G1 – G6, and at the free end for girders G7 and G8.

The method of virtual work is used to obtain all the deflections. In this method, a fictitious unit load is applied to the girder at the point where the deflection is desired, and the resulting moment,  $M^*$ , and shear,  $Q^*$ , diagrams from the fictitious load are drawn. Then, the deflection is calculated as the sum of the bending and shear contributions as follows:

$$u = \int \frac{M M^*}{E I} dx + \int \frac{Q Q^*}{G A_w} dx \quad (5.3)$$

In this equation,  $M$  and  $Q$  are the moment and shear force due to the actual load,  $I$  the moment of inertia,  $A_w$  the cross-sectional area of the web plate,  $E$  Young's modulus and  $G$  is the shear modulus ( $G = 81,000$  MPa for  $\nu = 0.3$  and  $E = 210,000$  MPa).

A summary of the girder deflections, calculated from Equation (5.3), is given in Table 5.4, where the bending and shear components of the total deflection are also listed. As a matter of interest, the percentage of the shear contribution to the total deflection is included. The deflections for girders G1 – G6 are evaluated for a load corresponding to  $P_{exp}$ , see the following Section 5.2. The deflections for girders G7 and G8 are evaluated for a load per unit length corresponding to  $q_{exp}$ , see Section 5.3 below.

Girder	Load [kN]	Deflection due to			Shear/Total [%]
		Bending [mm]	Shear [mm]	Total [mm]	
G1	132.2	0.95	1.14	2.09	54.6
G2	158.9	1.14	1.37	2.51	54.6
G3	180.7	1.30	1.56	2.86	54.6
G4	211.0	1.52	1.82	3.34	54.6
G5	226.0	1.62	1.95	3.58	54.6
G6	243.1	1.75	2.10	3.85	54.6
G7	<sup>1)</sup> 48.6	16.92	3.06	19.98	15.3
G8	<sup>1)</sup> 47.8	16.64	3.01	19.65	15.3

1) load in kN/m.

**Table 5.4:** Calculated girder deflections

## 5.2 Tests on Plate Girders Subjected to Constant Shear

The six constant shear tests were done with a test setup as illustrated in Figure 5.12. As seen from the figure, a system of UNP-profiles was used in order to ensure that no failure due to lateral stability occurred.

As previously mentioned, all girder specimens were identical except for the number of transverse stiffeners in the web. The number of stiffeners varied from zero to five. It should here be noted that one stiffener refers to a pair of stiffeners on each side of the web plate.

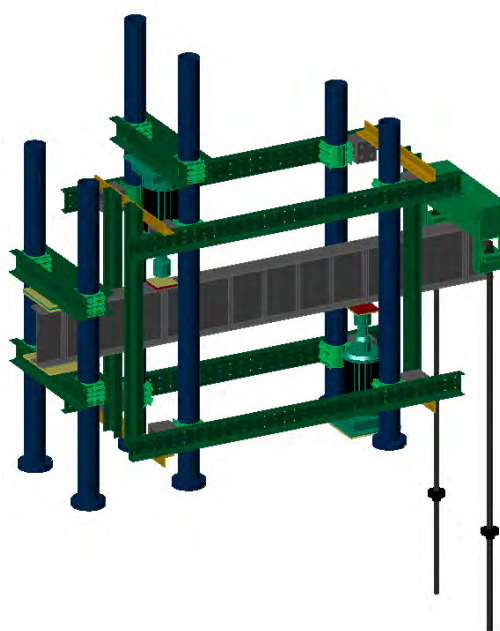


**Figure 5.12:** Illustration of test setup for constant shear tests

## ULTIMATE LOADS AND DEFLECTIONS

All the experiments were made with a load-controlled system, and the uploading was done manually. Thus, it was impossible to have the same uploading speed for all the tests. Therefore, the testing history of each girder is presented in a load-deflection curve. If a displacement-controlled system had been applied, it would have been possible to have the same uploading speed for all tests, and the testing histories might be compared in a load-time curve. However the laboratory facilities, especially the test setup and the applied jacks, made it impossible to use a displacement-controlled system. Furthermore, it could not be guaranteed that the load on each of the two jacks were exactly the same when applying a load-controlled system. This would have been possible if a displacement-controlled system had been used.

The deflections of each girder specimen were measured by two displacement transducers denoted D1 and D2, respectively. The deflections were measured in the two sections where the loads acted, see Figure 5.13.

The load-deflection curves for each girder specimen, with the deflections measured by displacement transducers D1 and D2, are shown in Figure 5.14 and Figure 5.15, respectively. No curves are shown for girder G2, as the handle on the hydraulic station locked and the jacks continued loading, so the maximum load was reached before the measurements were started. Hence, the only useful result from this test is the maximum load read from the hydraulic station.

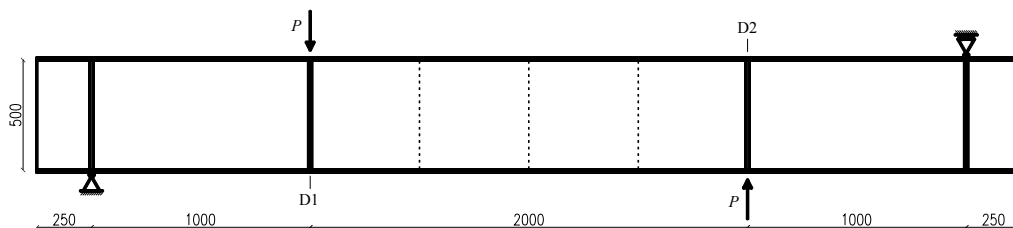


Figure 5.13: Location of displacement transducers D1 and D2

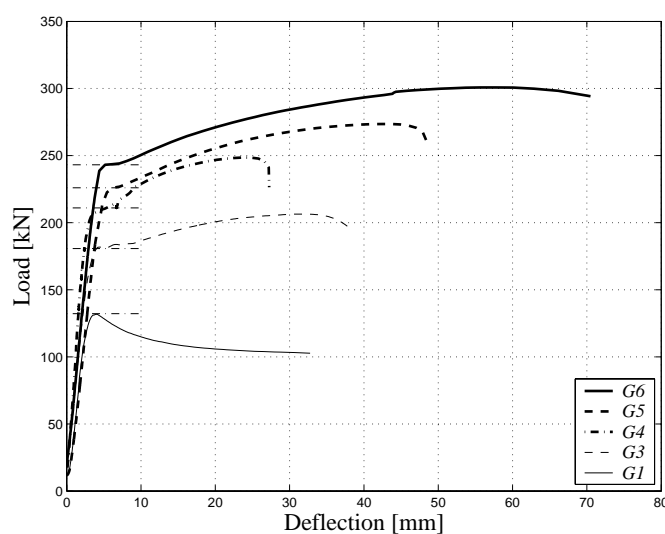
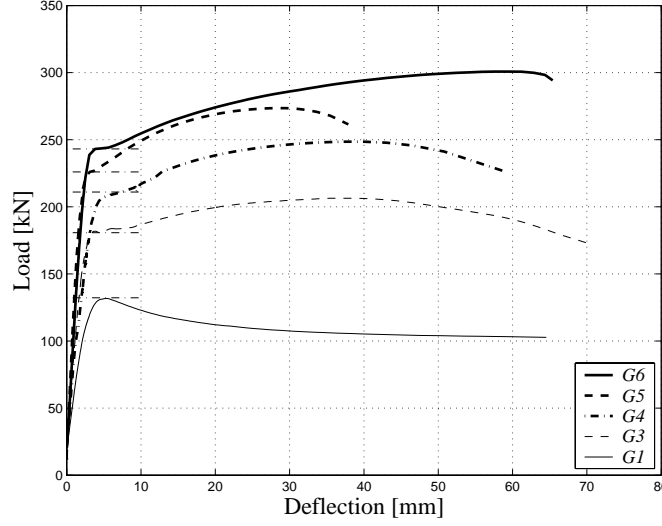


Figure 5.14: Load-deflection curves, deflection measured by displacement transducer D1



**Figure 5.15:** Load-deflection curves, deflection measured by displacement transducer D2

The theoretical and experimental values are shown in Table 5.5. The elastic critical buckling load,  $P_{cr}$ , is given in Table 5.3. The lower-bound value,  $P_u^-$ , is given by, cf. Equation (2.11),

$$\frac{\tau}{f_{yw}} = \begin{cases} \sqrt{\psi(1-\psi)} & \text{for } \psi < \frac{1}{2} \\ \frac{1}{2} & \text{for } \psi \geq \frac{1}{2} \end{cases} \quad (5.4)$$

The upper-bound value,  $P_u^+$ , is determined by, cf. Equation (2.29),

$$\frac{\tau}{f_{yw}} = \frac{1}{2} \left( \sqrt{1 + \tan^2 \theta} - \tan \theta \right) + \frac{\eta}{L/d - \tan \theta} + \psi \tan \theta \quad (5.5)$$

The values of  $P_u$  are found by the following relationship involving the shear stress,  $\tau$ , according to Equations (5.4) and (5.5), respectively:

$$P_u = 2 \tau d t_w \quad (5.6)$$

In Equations (5.4) – (5.6), the mechanical degree of stiffening is found by, cf. Equation (2.10),

$$\psi = \frac{A_s n f_{ys}}{L t_w f_{yw}} \quad (5.7)$$

The non-dimensional parameter,  $\eta$ , is determined by, cf. Equation (2.28),

$$\eta = 2 \frac{b_f t_f^2 f_{yf}}{d^2 t_w f_{yw}} \quad (5.8)$$

Here,  $f_{yw}$  is the yield stress of the web material,  $f_{yf}$  the yield stress of the flange material,  $L$  the length of the test section,  $d$  the depth of the web plate,  $t_w$  the web plate

thickness,  $t_f$  the flange thickness,  $A_s$  the cross-sectional area of a single stiffener,  $n$  the number of stiffeners and  $b_f$  is the width of the flanges.

For the stiffeners, the buckling stress is valid, as the effective width,  $b_e$ , of the stiffeners is found by Equation (4.6) in PART III to be  $b_e = 0.70 b$ , where  $b$  is the total width of a single stiffener. Thus in Equation (5.7),  $f_{ys}$  is the buckling stress of the stiffeners.

In Equation (5.5), the angle  $\theta$ , cf. Figure 2.5, is the free parameter for which the load should be minimised with regard to.

The parameters  $L$ ,  $d$ ,  $t_w$ ,  $A_s$ ,  $f_{ys}$ ,  $b_f$ ,  $t_f$  and  $f_{yf}$  are constant for all girder specimens. Thus, only the parameters  $\theta$ ,  $n$  and  $f_{yw}$ , and thereby  $\psi$  and  $\eta$ , vary from girder to girder.

In Table 5.5, two experimental loads,  $P_{exp}$  and  $P_{max}$ , are shown.  $P_{max}$  is the maximum load for each curve, cf. Figures 5.14 and 5.15.  $P_{exp}$  is the load measured where the slope discontinuity of the curves occur. The slope discontinuity identifies the load for which the assumed failure mechanism develops. For most of the tests it is seen that the load increases considerably after the value of  $P_{exp}$  is reached. However for girder G1, the load decreases after  $P_{exp}$  is reached, i.e.  $P_{max}$  is equal to  $P_{exp}$ . As previously mentioned only the value of  $P_{max}$  was measured for girder G2. From Figures 5.14 and 5.15, it is seen that the difference between the value of  $P_{max}$  and  $P_{exp}$  increases with an increasing number of transverse web stiffeners. Hence, it might be expected that  $P_{exp}$  is equal to  $P_{max}$ , or at least not much smaller than  $P_{max}$  for girder G2. Therefore,  $P_{exp}$  is taken as equal to  $P_{max}$  for girder G2 in Table 5.5.

From the table it appears that the experimentally determined post-buckling strength is found to be up to five times larger than the calculated elastic critical web buckling load.

Girder	Theoretical			Experimental		$P_u^+ / P_{exp}$ [ ]	$P_u^+ / P_{max}$ [ ]
	$P_{cr}$ [kN]	$P_u^-$ [kN]	$P_u^+$ [kN]	$P_{exp}$ [kN]	$P_{max}$ [kN]		
G1	26.2	-	85.2	132.2	132.2	0.645	0.645
G2	32.4	128.1	146.7	158.9	158.9	0.923	0.923
G3	42.6	177.3	192.7	180.7	206.3	1.066	0.934
G4	56.8	208.9	222.8	211.0	249.2	1.056	0.894
G5	70.4	221.9	234.9	226.0	274.2	1.039	0.857
G6	87.2	246.7	259.3	243.1	301.4	1.066	0.860

**Table 5.5:** Summary of theoretical and experimental loads

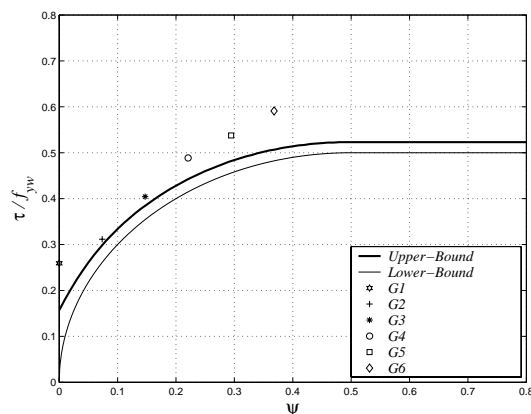


**Figure 5.16:**  $\tau/f_{yw}$  as a function of  $\psi$ , theory versus tests ( $P_{max}$ )

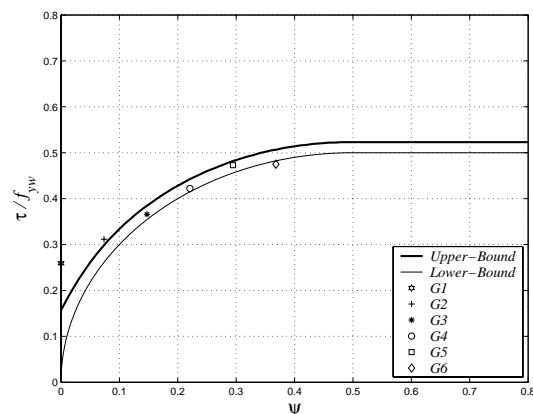


**Figure 5.17:**  $\tau/f_{yw}$  as a function of  $\psi$ , theory versus tests ( $P_{exp}$ )

The theoretical curves, i.e.  $\tau/f_{yw}$  as a function of  $\psi$ , cf. Equations (5.4) and (5.5), are shown in both Figure 5.16 and Figure 5.17. In Figure 5.16, the test values of the ratio,  $\tau/f_{yw}$ , are calculated using  $P_{max}$ . Similarly, the test values of  $P_{exp}$  are applied in Figure 5.17. In order to illustrate the theory with smooth curves, the mean value of the yield stresses of the web material,  $f_{yw}$ , is applied when drawing the curves. In both figures, the experimental values of the non-dimensional ratio,  $\tau/f_{yw}$ , are calculated by applied the correct values of  $f_{yw}$ .

From Figure 5.16 it appears that all test results are above the upper-bound curve. In particular, the results from girders G1, G5 and G6 are found to be considerably larger than the corresponding upper-bound values. However, Figure 5.17 shows that by applying the values of  $P_{exp}$  instead of  $P_{max}$ , the results from girders G3 – G5 are found to be between the curves corresponding to the upper-bound solution and the lower-bound solution, respectively. Moreover, the result from girder G6 is found to be slightly below the lower-bound solution. This indicates that the theory is not able to determine the additional load-carrying capacity, i.e. the difference between  $P_{max}$  and  $P_{exp}$ . In fact this seems natural, as the additional load-carrying capacity mainly stems from the effect of change of geometry and possible strain hardening of the materials. In the theory, the work equation is derived on the basis of the undeformed girder, and it does not take the effect of stain hardening into account.

It may be noticed that applying the values of  $P_{exp}$  instead  $P_{max}$ , agrees with what Basler et al. (1960) did when they compared their tests to their theory.

In both Figure 5.16 and Figure 5.17, girder G1 (the specimen without interior stiffeners) shows a much larger post-buckling strength than predicted by the theory. One might imagine that this is because the flanges will carry part of the tensile band loads when the web plate is heavily deformed. However, this does not seem to be the case when considering the load-deflection curves in Figures 5.14 and 5.15, where there is no increase of the load for increasing deflections after the slope discontinuity. Sooner the reason must be that the stiffeners under the loads are not taken into account in the theory. However, taking these stiffeners into account would affect all the other tests as well, but girder G1 is clearly the one deforming most from its original shape, see the photos in Appendix F. The more deformed the test girder is, the more active the stiffeners at the loads might become; hence this will become more pronounced for girder G1. In the tests by Basler et al. (1960), the same tendency was observed. As seen from Figure 4.1, the girders without interior stiffeners showed a considerably larger load-carrying capacity than that predicted by the theory. However, this is not valid for all tests without internal web stiffeners, presented in Chapter 4. Applying plastic yield hinges in the stiffeners at the loads may be able to take this effect into account. However, the calculations would require another failure mechanism and this has not yet been done.

The theoretical upper-bound values of  $\tau_u/f_{yw}$ , cf. Equations (5.5) and (5.6), are shown together with the experimental values of  $\tau_{max}/f_{yw}$  in Figure 5.18 and with the experimental values of  $\tau_{exp}/f_{yw}$  in Figure 5.19. The ratios,  $P_u^+/P_{exp}$  and  $P_u^+/P_{max}$ , for each test are given in Table 5.5. For the ratio,  $P_u^+/P_{max}$ , a mean value of 0.852 and a standard deviation of 10.7 % are obtained. For the ratio,  $P_u^+/P_{exp}$ , a mean value of 0.966 and a standard deviation of 16.7 % are obtained. The large standard deviation is due to girder G1. If the result from girder G1 is not included, a mean value of 1.030 and a standard deviation of 6.1 % are obtained.

As concluded from the older tests in Chapter 4, it is found that there is no need for introducing an effectiveness factor as when calculating a concrete beam with transverse stirrups.

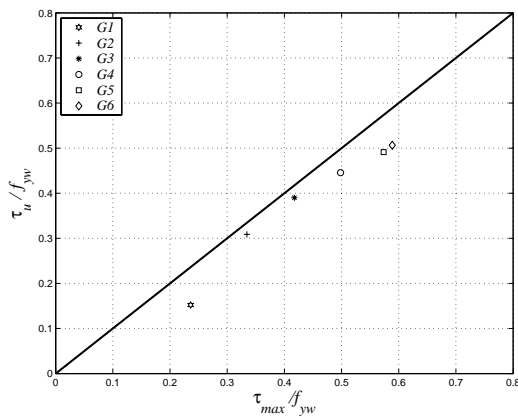


**Figure 5.18:** Comparison of theory and experimental results ( $P_{\max}$ )

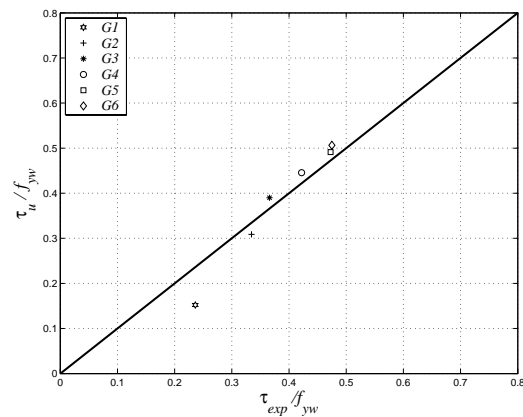


**Figure 5.19:** Comparison of theory and experimental results ( $P_{\exp}$ )

In order to illustrate the theory further, the results obtained by the upper-bound solution are presented for each girder in Figures 5.20 – 5.25. The figures show the extension of the parallelogram shaped yield zone (the hatched areas) and the predicted location of the plastic yield hinges. The location of the plastic yield hinges is given by the length,  $c = d \tan \theta_{\min}$ , where  $d$  is the depth of the web plate and  $\theta_{\min}$  is the angle leading to the minimum value for  $P_u^+$ . Furthermore, the figures give the number of stiffeners,  $n$ , the non-dimensional parameters,  $\psi$  and  $\eta$ , and the yield stress of the web material,  $f_{yw}$ . The angle,  $\nu$ , indicates the major principal strain direction, which is in the angular bisector direction of the acute parallelogram angle, cf. Section 2.2.

In Appendix F, a series of photos for each girder taken before, under and after testing are shown. If the photos are held up against the Figures 5.20 – 5.25, it appears that the location of the plastic yield hinges is found to be more or less as predicted. An exact measurement of the location of the plastic yield hinges has not been done. The measurements, based on the photos, are indicated with the hollow circles in the figures.

According to the theory, the plastic yield hinges will develop in the panel between the applied load and the adjacent transverse web stiffener, except for girder G1, which is of course without stiffeners. This fact correlates with the observations from the photos.

By examining girders G4, G5 and G6 more closely, it appears that the plastic yield hinge in girder G5 develops in the middle of the web panel, adjacent to the load. For girder G6, the yield hinge is found closer to the load, while for girder G4, the yield hinge is found closer to the first intermediate web stiffener from the load. From the photos in Appendix F, the same tendency is observed.

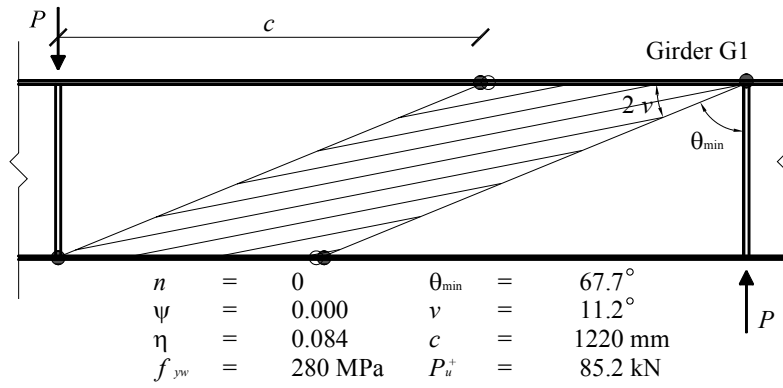


Figure 5.20: Data for girder G1

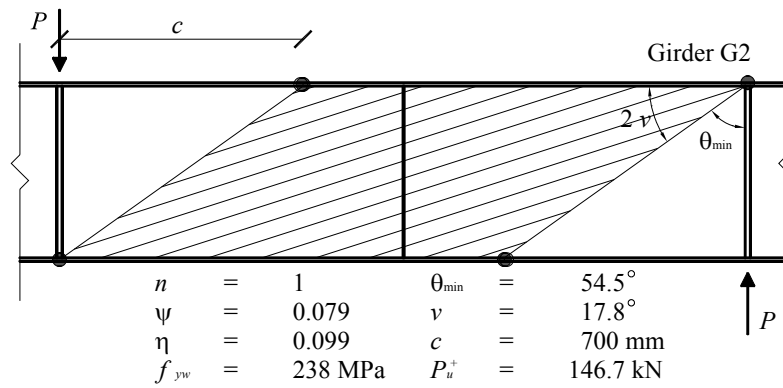


Figure 5.21: Data for girder G2

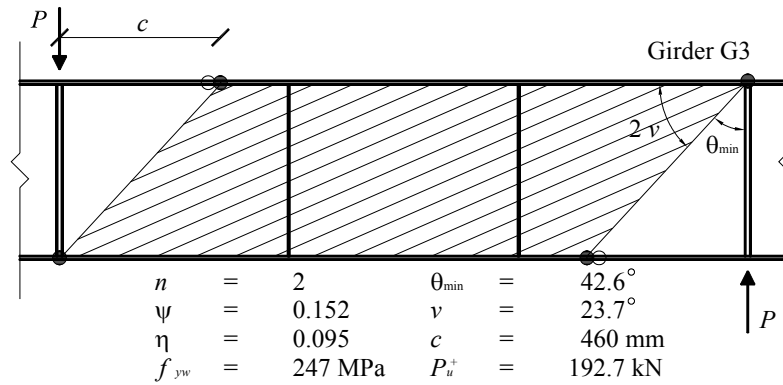


Figure 5.22: Data for girder G3

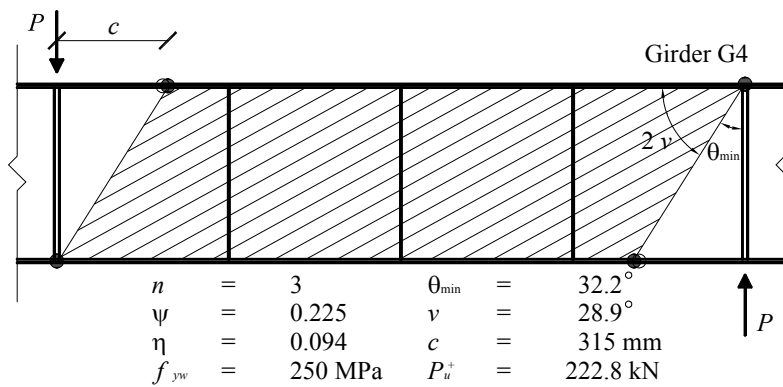


Figure 5.23: Data for girder G4

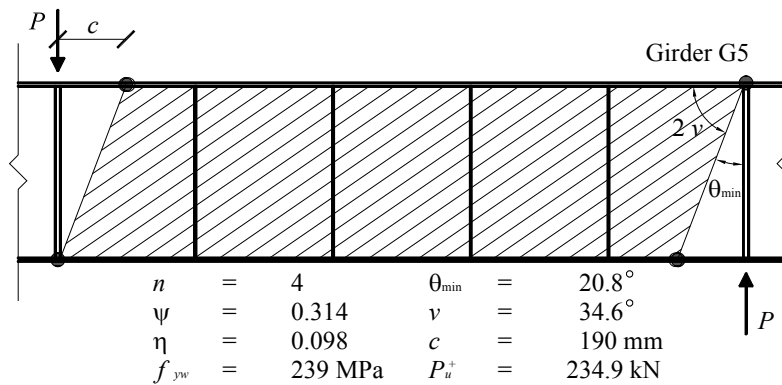


Figure 5.24: Data for girder G5

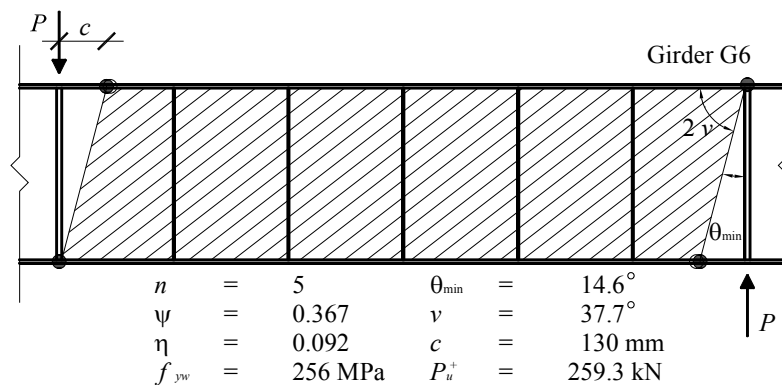


Figure 5.25: Data for girder G6

The results from the FEM model were only available in August 2006, cf. (Øskan and Bak 2006). Due to time limitations, it has not yet been possible to evaluate the results. Therefore the results of the FEM analysis are not included in this thesis. However, the obtained load-carrying capacities are shown in Table 5.6.

The properties of the materials were determined by implementing the real load-displacement curves from the tension coupon tests. It means that the FEM model took the non-linear behaviour of the materials into account as well as the effect of large deformations. Therefore the obtained load-carrying capacities are compared with the experimental values of  $P_{\max}$ .

The imperfections of the web plates in the test sections were measured before testing the girder specimens, but these imperfections were not incorporated directly in the FEM model. However, in order to be able to initiate the buckling process of the web plate, imperfections had to be included. The imperfections were implemented in the model by adding a lateral surface load on the web plate. This surface load acted on the web plate throughout the entire calculation; hence the results from the FEM model are not fully correct. If only the surface load had acted on the web plate in the beginning of the calculation, the results would have been more reliable. It would be preferable to implement the measured imperfections into the model, but this is a rather cumbersome procedure. Although the imperfections were not correctly implemented in the FEM model, this may only have a slight influence on the obtained results.

From Table 5.6 it appears that the FEM results seem to coincide very closely with the measured experimental maximum loads. A mean value of 1.010 and a standard deviation of 4.2 % are obtained for the ratio,  $P_{FEM}/P_{\max}$ .

Girder	G1	G2	G3	G4	G5	G6
$P_{FEM}$ [kN]	143.1	162.1	201.2	254.6	264.5	300.2
$P_{max}$ [kN]	132.2	158.9	206.3	249.2	274.2	301.4
$P_{FEM}/P_{max}$ [ ]	1.082	1.020	0.975	1.022	0.965	0.996

**Table 5.6:** Comparison between FEM model and experimental results

Girder	G1	G2	G3	G4	G5	G6
$P_{EC3}$ [kN]	75.4	112.3	154.2	189.5	210.1	243.2
$P_{exp}$ [kN]	132.2	158.9	180.7	211.0	226.0	243.1
$P_{EC3}/P_{exp}$ [ ]	0.570	0.707	0.853	0.898	0.930	1.000

**Table 5.7:** Comparison between EC3 and experimental results

In Table 5.7, the calculated post-buckling strength according to EC3 (1993) is shown together with the experimental values of  $P_{exp}$ . EC3 (1993) suggests to use a procedure containing twelve equations in order to determine the post-buckling strength of a plate girder in shear. It is not an easy task to follow the physics behind the equations in such a long procedure. However, a helpful description is found in (Dubas and Gehri 1986).

From Table 5.7 it appears that EC3 (1993) seems to underestimate the post-buckling strength of the girders. A mean value of 0.826 and a standard deviation of 15.9 % is obtained for the ratio,  $P_{EC3}/P_{exp}$ .

The large standard deviation is also in this case due to girder G1. If the result from girder G1 is not included, a mean value of 0.878 and a standard deviation of 11.0 % are obtained. As previously mentioned, the upper-bound solution without girder G1 gives a mean value of 1.030 and a standard deviation of 6.1 %.

### STRAIN MEASUREMENTS ON THE WEB

To be able to measure the strains in the web, a photometric measuring equipment called *Aramis* was used. Aramis is a 3D deformation measuring system. It analyses and calculates deformations of the object. Aramis recognises the surface structure, and through pictures from two digital cameras, it gives coordinates to the pixels of the pictures. The pictures, before testing, correspond to the undeformed object. After and under deformation of the object, more pictures are taken, and Aramis uses these pictures to calculate the deflections and strains of the object.

Before testing, the web plates of the girder specimens were painted with non-gloss white paint in the test section. Black dots were then added, corresponding to the size of the pixels in the pictures. Aramis uses these black dots to recognise the pixels and calculate the deflections.

The Aramis equipment was unable to measure the flanges and the transverse stiffeners. Furthermore, the flanges and the stiffeners threw shadows on the web plate, which confused the pictures. In the end, measurements were available from 90 % of the web plate in the test section.

In order to check the results from Aramis, strain rosettes were applied to the web plate. Unfortunately, only a small number of strain rosettes were available. Therefore, only girders G1, G2 and G4 were supplied with strain rosettes. Strain rosettes were applied to the middle of each web panel, i.e. a panel between two stiffeners. In each web panel the strain rosettes were applied to both sides of the web plate in order to be able to compensate for the effect of bending of the plate.

As previously mentioned, the results from girder G2 are of no use. Thus, only results from two girder specimens are available.

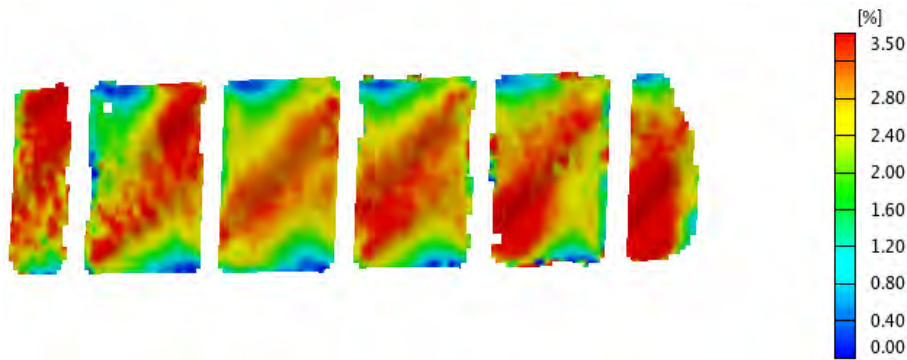


Figure 5.26: Major principal strain plot for girder G6

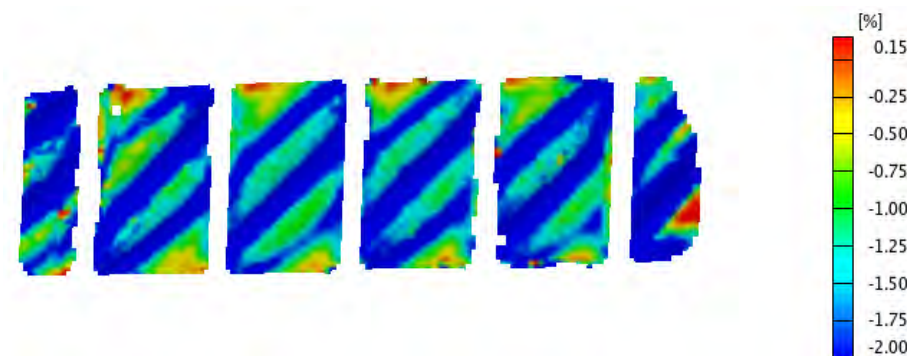


Figure 5.27: Minor principal strain plot for girder G6

The main reason for measuring the strains in the web plate was to verify whether the tensile bands pass the stiffeners or not. Having only strain rosettes on one girder with internal stiffeners made the analysis of the strains measured by the strain rosettes insufficient.

Unfortunately, the Aramis equipment turned out to be unsuitable for verification as well. By using Aramis one might get plots of the major principal strains as well as the minor principal strains. In Figure 5.26, a plot of the major principal strains is shown for girder G6 at a load of  $P = 243.1$  kN corresponding to the value of  $P_{exp}$ . The corresponding minor principal strains are shown in Figure 5.27.

Since Aramis measurements are only taken on one surface of the web, it is not possible to neglect the strains due to the buckling of the web plate. Thus large compressive strains occur at the points where the web plate buckles away from the cameras, see Figure 5.27. Furthermore, it is only possible to measure the magnitude of the strains in each point. It is not possible automatically to deduce the directions of the principal strains. It would have been convenient if the principal strains could have been shown in a vector plot, but with Aramis this is not possible.

Øskan and Bak (2006) performed an analysis of the obtained deformation plots of the web plates in order to verify whether or not the tensile bands may pass the transverse stiffeners. They measured the angle of the developed tensile bands to the girder axis and compared the results with the theoretically determined angles. They found a very good agreement between the measured angles and the calculated ones. Moreover, they concluded that the tensile band might pass the transverse web stiffeners, if any. A summary of their obtained results is presented in Appendix G.



**Figure 5.28:** Photo of G5 after testing

A larger analysis of the problem whether the tensile bands may pass the transverse stiffeners or not is actually unnecessary, as it is easily verified from the photo shown in Figure 5.28 that the bands may do so. The figure shows a photo of girder G5 after testing.

### **STRAIN MEASUREMENTS ON THE FLANGES AND STIFFENERS**

The Aramis equipment could not be used to measure the deformations of the flanges or the transverse web stiffeners. Thus, traditional strain gauges were applied to the flanges and the stiffeners.

On each girder specimen, one pair of strain gauges was placed on both the top and bottom flange. The gauges were placed 20 mm from the web plate on one side of the web plate. One gauge was placed on the top face of each flange and one gauge was placed at the same location on the bottom face of each flange.

Each transverse web stiffener was supplied with a pair of strain gauges on one side of the web plate. In the vertical direction, the gauges were placed in the middle of the stiffeners. In the horizontal direction, the gauges were placed in the middle of the calculated effective width of the stiffeners, i.e. 24 mm from the web plate.

The exact locations of all the strain gauges are given in Appendix H.

In the following, the gauges are termed H1, H2, V1, etc. where H is horizontal, i.e. gauges placed on the flanges, and V is vertical, i.e. gauges placed on the transverse web stiffeners. Furthermore, for all tests, H1 and H2 are the gauges on the top flange, and H3 and H4 are the gauges on the bottom flange.

Figures 5.29 – 5.33 show the load-strain curves for each girder specimen. For each plate, the strains are shown as the mean value of the measured strains from each pair of gauges. This is done in order to compensate for the strains due to bending of the individual plates, thus the strains shown in the figures only correspond to the membrane strains.

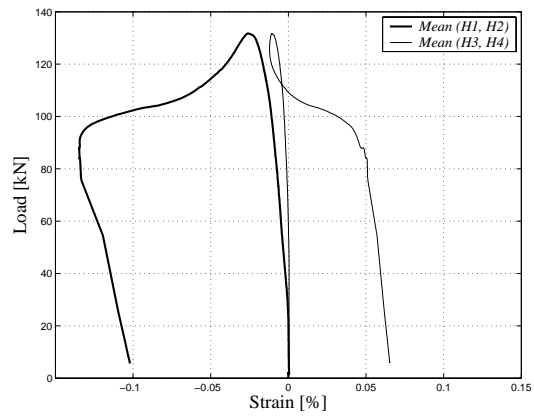


Figure 5.29: Load-strain curves from strain gauges on girder G1

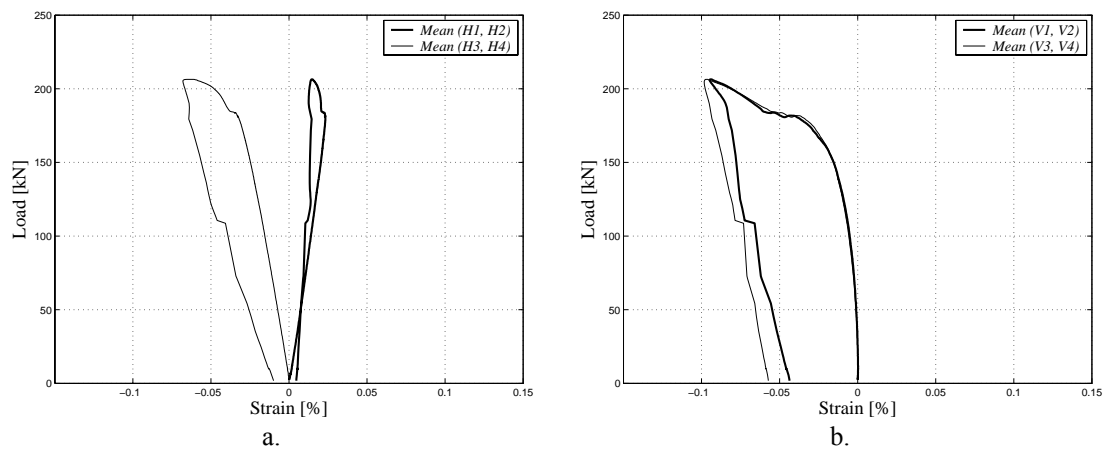


Figure 5.30: Load-strain curves from strain gauges on girder G3

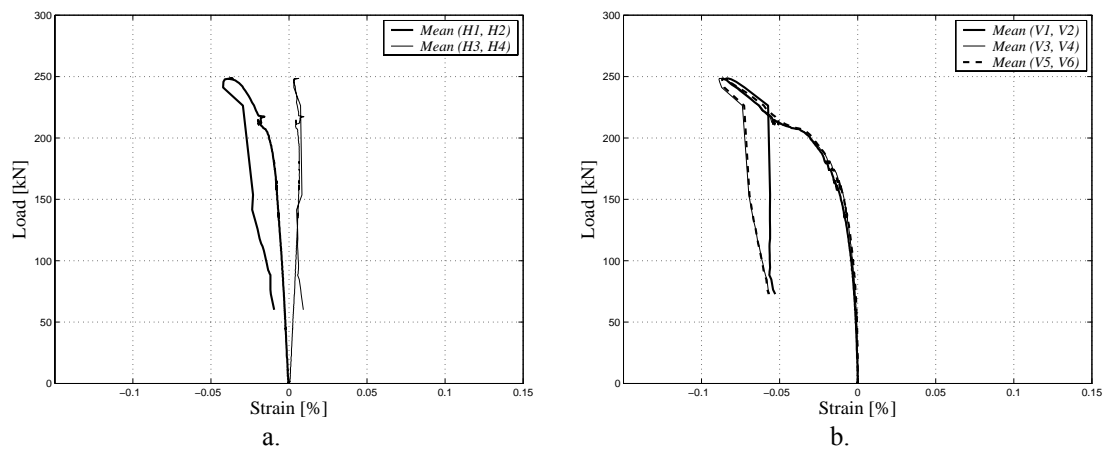


Figure 5.31: Load-strain curves from strain gauges on girder G4

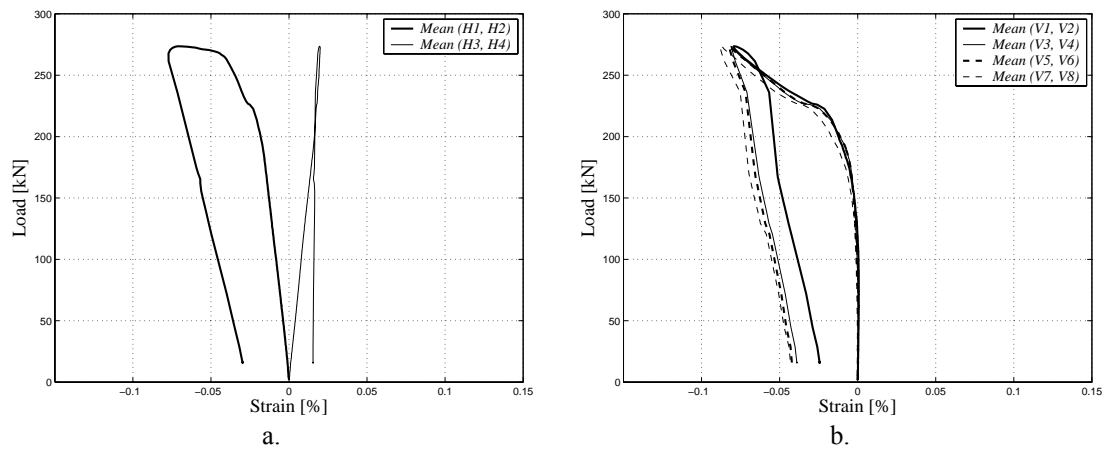


Figure 5.32: Load-strain curves from strain gauges on girder G5

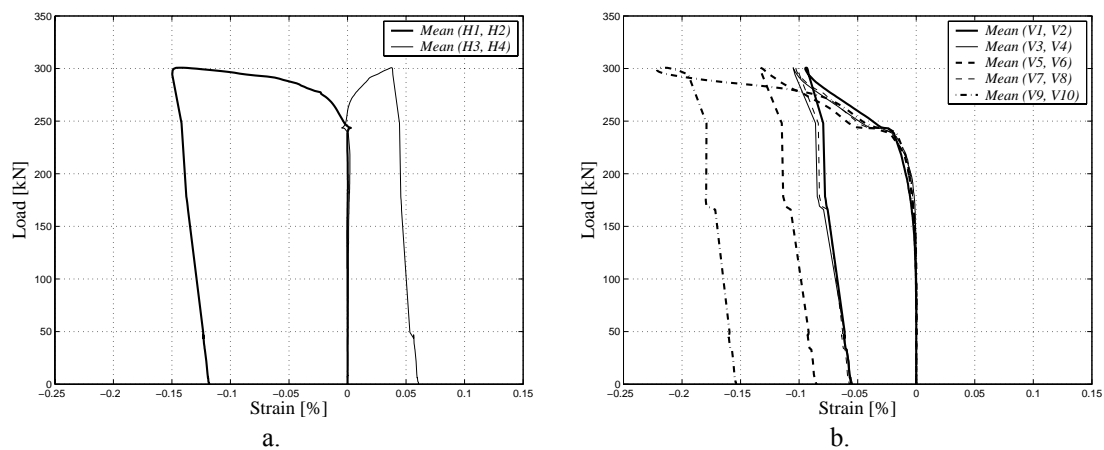


Figure 5.33: Load-strain curves from strain gauges on girder G6

Øskan and Bak (2006) also made an analysis of the measured strains in the flanges and the transverse web stiffeners. They calculated the stresses corresponding to the measured strains and compared the results with the stresses predicted by the lower-bound solution, cf. Section 2.1. They found a relatively good agreement with the compressive stresses in the flange and the transverse web stiffeners, but not so good agreement with the tensile stresses in the flanges. The reason is that this method of determining the stresses is dubious, as the strains are only measured at one point of each plate. For instance, there is no certainty that the stresses in each plate are uniformly distributed. Therefore, when only calculating the stiffener stresses from the strains measured in the middle of the theoretical effective width, one will only get an approximate mean value of the stiffener stresses. Thus, only the load-strain curves shown above are included in this thesis.

The most interesting observation from the load-strain curves is that the measured stiffener strains seem to be approximately constant for each girder test. This is valid for all girders except for girder G6, where two of the stiffeners have strains considerably larger than the other stiffeners. Furthermore, only in these two stiffeners do the measured strains exceed the yield strain. However, this does not ensure that yielding did not occur in any of the other transverse stiffeners.

### 5.3 Tests on Plate Girders Subjected to Distributed Loading

The two distributed loading tests were conducted with a test setup as illustrated in Figure 5.34. As seen from the figure, the same system of UNP-profiles as for the constant shear tests was used in order to ensure that no failure due to lateral stability occurred.

Four jacks established the uniform load. Between the girder and the jacks, wooden blocks were supplied in order to distribute the load from the jacks. These wooden blocks are not shown in the figure.

For girder G8, the load was applied to the bottom flange as a uniform compressive load as shown in Figure 5.34.

For girder G7, the load was applied to the top flange as a uniform tensile load. The setup was used as shown in the figure with the same four jacks as applied for girder G8. The jacks acted on specially designed frames that transferred the compression from the jacks to tension on the top flange. These frames used for the testing of girder G7 are not shown in the figure, but they may be seen in the series of photos presented in Appendix F.

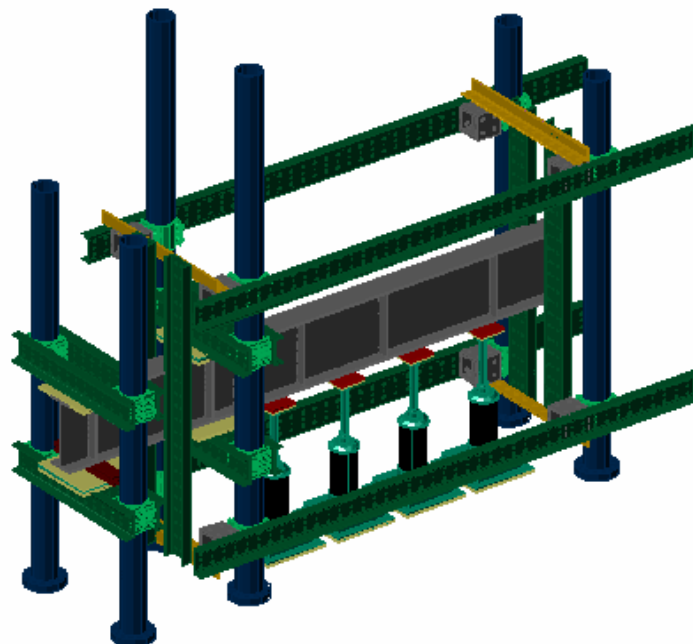


Figure 5.34: Illustration of test setup for distributed loading tests

The two girder specimens were identical except for the cross-sectional area and the number of transverse stiffeners in the web. Øskan and Bak (2006) designed the specimens according to the design method presented in Section 3.3. According to this method, extra stiffeners must be added if the girder is subjected to a compression load on a flange. The extra stiffeners must be able to transfer the compression load to tension along the other flange. Therefore, the design of the stiffeners on girders G7 and G8 are not identical. Girder G7 was supplied with three transverse web stiffeners with a width of 70 mm. Girder G8 was supplied with the same three stiffeners plus an extra one closest to the free end of the girder. All the internal stiffeners in the test section of girder G8 had a width of 84 mm. Again, it should here be noted that one stiffener refers to a pair of stiffeners placed on each side of the web plate.

## ULTIMATE LOADS

In both of the two girder specimens, displacement transducers were placed on the free end of the girders. Unfortunately, due to the large deflections that occurred, the results from these displacement transducers are of no use. Therefore, the testing history is presented in a load-time curve, see Figure 5.35.

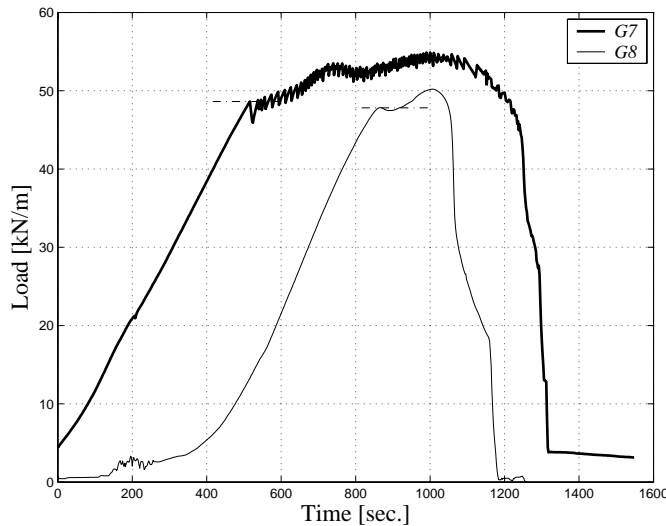


Figure 5.35: Load-time curves for distributed loading tests

In Table 5.8, the two experimental loads per unit length,  $q_{exp}$  and  $q_{max}$ , are shown. Here,  $q_{max}$  is the maximum load and  $q_{exp}$  is the load measured where the slope discontinuity of the curves occur. It is not so clear from the load-time curve when the linear-elastic behaviour stops, but the values of  $q_{exp}$  are taken at the points shown by the two dotted horizontal lines in the figure.

In Table 5.8, the two theoretical loads per unit length,  $q_u^-$  and  $q_u^+$ , are also shown. No general lower-bound solution for cantilever girders subjected to a uniformly distributed load have been derived, so  $q_u^-$  is the design load which the girder specimens are designed for by applying a lower-bound solution, cf. Section 3.3. However in the design of the girders, a value of  $f_y = 235$  MPa was applied to all materials, so the values of  $q_u^-$  in the table are inaccurate.

The values of  $q_u^+$  are the determined upper-bound values. The upper-bound solution for a simply supported girder subjected to a uniformly distributed load may easily be applied for a cantilever girder, cf. Section 2.3. The derived equation will be identical if the value  $2L$  ( $L$  being the length of the test section of the cantilever girders) is inserted for the value of  $L$  in the equations in Section 2.3.

However, this upper-bound solution cannot be used directly to determine the post-buckling strength of girders G7 and G8, as it assumes that constant stiffener spacing is applied, which is not the case. Furthermore, the upper-bound solution is only valid in case of compressive loading, which is not true for girder G7. Hence, new upper-bound solutions are derived.

For girder G8, the only change is the contribution to the dissipation from the internal stiffeners, which will be given by

$$W_{i,stiffener} = \int_V \varepsilon_y \sigma_{sy} dV = \int_A \frac{\delta}{x} \tan \theta t_w \sigma_{sy} dA \quad (5.9)$$

$$W_{i,stiffener} = \frac{A_s n d}{x + d \tan \theta} \tan \theta f_{ys} \delta$$

The contribution to the dissipation from the flanges and from the web plate will be the same as for a simply support girder divided by two, cf. Equations (2.42) and (2.43). The total dissipation then becomes

$$W_i = \frac{1}{2} \frac{1 - \sin \theta}{\cos \theta} f_{yw} t_w d \delta + 2 \frac{b_f t_f^2}{x} f_{yf} \delta + \frac{A_s n d}{x + d \tan \theta} \tan \theta f_{ys} \delta \quad (5.10)$$

Here,  $f_y$  is yield stress and  $t$  is thickness with index  $f$  for flange and  $w$  for web and  $f_{ys}$  is either the yield stress or the buckling stress of the stiffeners.  $b_f$  is the flange width,  $d$  the girder depth and  $A_s$  is the total cross-sectional area of a single stiffener. The length,  $x$ , displacement,  $\delta$ , and the angle,  $\theta$ , are illustrated in Figure 2.18. Moreover,  $n$  is the number of internal stiffeners in the parallelogram-shaped yield zone.

The external work for girder G8 will also be the same as for a simply supported girder divided by two, cf. Equation (2.47). The external work becomes

$$W_e = q \left( L - \frac{1}{2} x \right) \delta \quad (5.11)$$

where  $q$  is the load per unit length and  $L$  is the length of the shear zone. The length,  $x$ , and the displacement,  $\delta$ , are shown in Figure 2.18.

However,  $L$  here is the full length of the test section ( $L = 3.0$  m), so the factor of two only appears if  $L$  is substituted by  $\frac{1}{2} L$  above.

The total dissipation for girder G7 will be the same as for girder G8, cf. Equation (5.10), but the external work will be different because of the tensile loading on the opposite flange. The load acting along the length,  $d \tan \theta$ , closest to the fixed end, will not contribute to the external work, which equals

$$W_e = q \left( L - \frac{1}{2} x - d \tan \theta \right) \delta \quad (5.12)$$

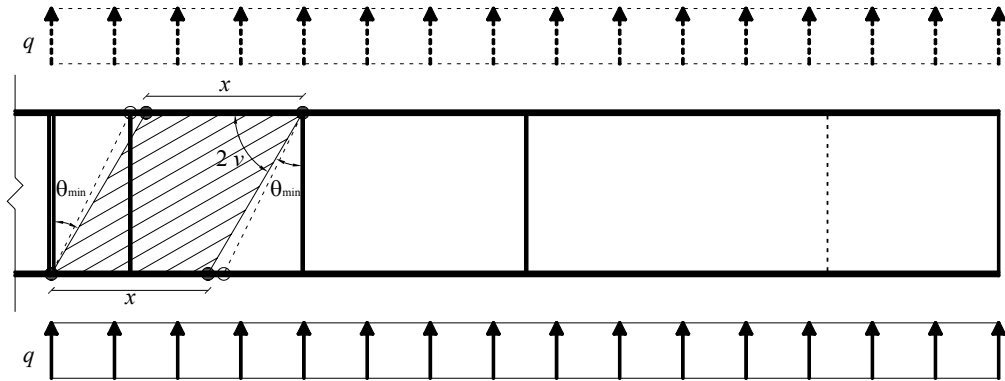
It has not been possible to find analytical expressions in either of the two cases, and furthermore, the calculation procedure is cumbersome because, besides the minimising procedure, iteration must also be used. Therefore, only the dissipation and the external work are shown here.

Iteration is necessary as one must estimate how many transverse web stiffeners are located in the parallelogram-shaped yield zone, cf. Figure 2.17. Thereafter, the geometry of the yield zone is found by minimising the expression for  $q$ , and it is necessary to control whether the estimated number of stiffeners is actually located in the yield zone or not. In the latter case, a new estimate must be made and a recalculation is necessary.

For both girders G7 and G8, only one internal stiffener is found to be located in the yield zone, and the yield zone reaches the second internal stiffener measured from the

fixed support. Figure 5.36 shows the test section on girders G7 and G8, are their predicted yield zones, where  $x = 546$  mm and  $\theta = 26.6^\circ$  for girder G7. For girder G8,  $x = 496$  mm and  $\theta = 31.0^\circ$ .

The predicted location of the yield zones approximately corresponds to the observations in the photos, cf. Appendix F. However, the location of the plastic yield hinges in the flanges did not develop exactly as predicted. In Figure 5.36, the solid circles are the ones calculated for girder G8, and the load is the bottom flange load (solid). The hollow circles are the ones calculated for girder G7, and the load is the top flange load (dashed). The location of the plastic yield hinges are not measured in the experiments.



Girder G7			Girder G8				
$n$	= 1	$\theta_{\min}$	= $26.6^\circ$	$n$	= 1	$\theta_{\min}$	= $31.0^\circ$
$A_s$	= $420 \text{ mm}^2$	$v$	= $31.9^\circ$	$A_s$	= $504 \text{ mm}^2$	$v$	= $29.8^\circ$
$f_{ys}$	= $154 \text{ MPa}$	$x$	= $546 \text{ mm}$	$f_{ys}$	= $179 \text{ MPa}$	$x$	= $496 \text{ mm}$
$f_{yw}$	= $249 \text{ MPa}$	$q_{u^+}$	= $47.9 \text{ kN/m}$	$f_{yw}$	= $282 \text{ MPa}$	$q_{u^+}$	= $50.0 \text{ kN/m}$

Figure 5.36: Data for girders G7 and G8

Girder	Theoretical		Experimental		$q_u^+ / q_{exp}$ [ ]	$q_u^+ / q_{max}$ [ ]
	$q_u^-$ [kN/m]	$q_u^+$ [kN/m]	$q_{exp}$ [kN/m]	$q_{max}$ [kN/m]		
G7	41.5	47.9	48.6	54.9	0.986	0.872
G8	47.0	50.0	47.8	50.2	1.046	0.996

Table 5.8: Summary of theoretical and experimental loads

Although the girders had the same overall dimensions, there were several differences between the two specimens. Firstly, the different loading systems give two slightly different theoretical solutions. Secondly, the width of the internal stiffeners were not the same, i.e.  $t_s = 70$  mm for G7 and  $t_s = 84$  mm for G8. Therefore, the values of  $A_s$  and  $f_{ys}$  are not the same, so the buckling stresses of the internal stiffeners are different. Also, the yield stresses of the web material were far from equal, i.e.  $f_{yw} = 249$  MPa for G7 and  $f_{yw} = 282$  MPa for G8

In the experiments, girder G7 carried a slightly larger load than girder G8. The predicted load-carrying capacities reveal the opposite. The lower-bound value is below the experimentally determined load for both girders. The upper-bound value is below the experimental loads for girder G7 and between the experimental loads for Girder G8.

The experimental results are fairly unreliable, firstly because, during the uploading, both girders began to deflect in lateral direction. As already mentioned, UNP-profiles were applied on both sides of the girders in order to ensure that no failure due to

lateral stability occurred. These UNP-profiles may have influenced the load-carrying capacity due to friction. Secondly, the applied loading system of four jacks turned out to be unsuitable for representing a uniformly distributed load. At the start of the uploading phase it appeared to function correctly, however before reaching the maximum load, the jack nearest the fixed end loosened in both tests, so it was not subjecting any load to the girders at all.

However, the correlation between theory and tests seems to be reasonable.

### STRAIN MEASUREMENTS ON THE WEB

No strain rosettes were added to the web plate of the two girders. The photometric equipment, Aramis, was used to measure the deformations as described in Section 5.2. Due to the larger length of the test section ( $L = 3.0$  m), Aramis only covered approximately 70 % of the web plate on girder G8. On girder G7, only 30 % of the web plate in the test section was covered, because of the special steel frames.

With the same explanation as in Section 5.2, the strains calculated by Aramis were of no real use.

The aim of the two tests was to see whether a buckling pattern occurred with varying direction throughout the girders. The deformation plot from Aramis for girder G8 in Figure 5.37 shows that buckles with different angles with the girder axis indeed did form more or less as expected. The figure shows a plot of the deformations just before the maximum load is reached.

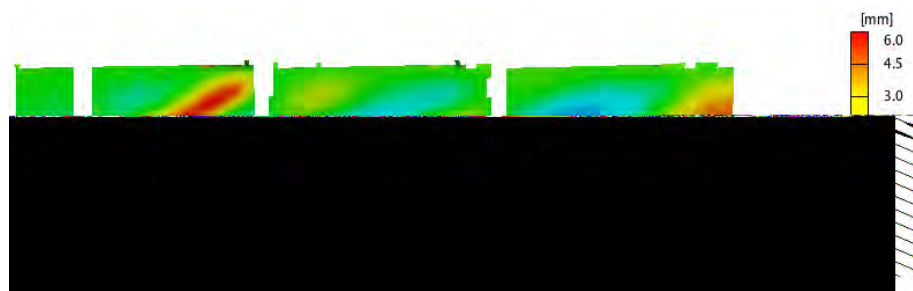


Figure 5.37: Deformation plot for girder G8

### STRAIN MEASUREMENTS ON THE FLANGES AND STIFFENERS

On the two girder specimens, two pairs of strain gauges were applied to the top flange as well as on the bottom flange. The gauges were placed 20 mm from the web plate on one side of the web plate, as in the constant shear tests.

Each transverse web stiffener was equipped with a pair of strain gauges on one side of the web plate. In the vertical direction, the gauges were placed in the middle of the stiffeners. In the horizontal direction, the gauges were placed in the middle of the calculated effective width of the stiffeners. The exact locations of all the strain gauges are given in Appendix H.

The same notation as for the constant shear tests is used, i.e. H1, H2, V1, etc. where H refers to gauges on the flanges, and V to gauges on the transverse web stiffeners.

Figure 5.38 shows the load-strain curves for girder G7, and Figure 5.39 shows the load-strain curves for girder G8. Again, for each plate the strains are shown as the mean value of the measured strains from each pair of gauges, in order to compensate for the strains due to bending of the individual plates.

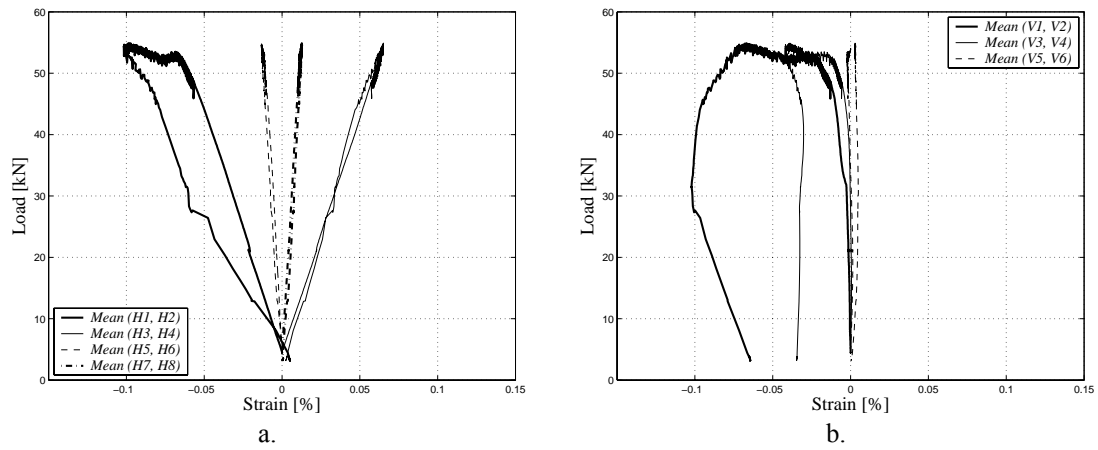


Figure 5.38: Load-strain curves from strain gauges on girder G7

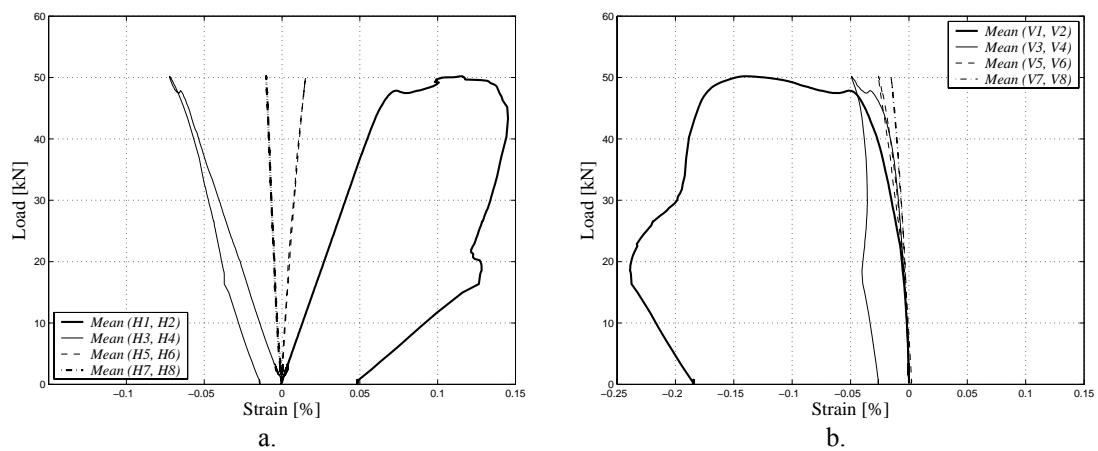


Figure 5.39: Load-strain curves from strain gauges on girder G8

Øskan and Bak (2006) made an analysis of the measured strains in the flanges and the transverse web stiffeners. They calculated the stresses corresponding to the measured strains and compared the results with the stresses predicted by the lower-bound solution, cf. Section 2.1. They found a relatively good agreement with the stresses in the flange and the transverse web stiffeners, determined by the strain gauges closest to the supported end of the girder, but they found less good agreement with measurements from the gauges on the flanges and stiffeners closest to the free end of the girders.

## 6 CONCLUSION

A calculation method, i.e. the plastic tension field method, for steel plate girders with transverse web stiffeners subjected to shear, is presented. The method, which is based on the theory of plasticity, differs from other theories by incorporating the strength of the transverse stiffeners and by the assumption that the tensile bands may pass the transverse stiffeners.

Both the lower-bound theorem and the upper-bound theorem of the theory of plasticity are used.

The theoretical solutions are compared to tests found in the literature as well as new tests conducted at the Technical University of Denmark in 2006. There is in general a very good agreement between theory and the tests. However, the theory seems to underestimate the post-buckling strength for girders without intermediate web stiffeners. This might be due to the fact that the theory does not take the strength of the stiffeners at the loads into account.

A design method for steel plate girders with transverse web stiffeners is also presented. By introducing circular fan solutions, almost any load case may be treated.

## 7 REFERENCES

- BASLER, K. (1961). Strength of Plate Girders in Shear. *Proc. ASCE, J. Struct. Div.* **ST 7**, **87**(2), 151-180.
- BASLER, K., YEN, B., MUELLER and THÜRLIMANN, B. (1960). Web Buckling Tests on Welded Plate Girders. *Welding Research Council, Bulletin No. 64*.
- BERGFELT, A. (1973). Plate Girders with Slender Web-Survey and a Modified Calculation Method. *Report No. 11 2.2*. Oslo: Nordiske forskningsdagar for stålkonstruksjoner.
- CALLADINE, C. R. (1973). A Plastic Theory for Collapse of Plate Girders under Combined Shearing Force and Bending Moment. *The Structural Engineer*, **51**(4), 147-154.
- COOPER, P. B., LEW, H. S. and YEN, B. (1964). Welded Constructional Alloy Steel Plate Girders. *Proc. ASCE, J. Struct. Div.* **ST 1**, **90**, 1-36.
- D'APICE, M. M., FIELDING, D. J. and COOPER, P. B. (1966). Static Tests on Longitudinally Stiffened Plate Girders. *Welding Research Council, Bulletin No. 117*.
- DUBAS, P. (1974). *Zur Erschöpfungslast schubbeanspruchter Stehbleche*. Karlsruhe: Professor Steinhardt Festschrift.
- DUBAS, P. and GEHRI, E. (1986). *Behaviour and Design of Steel Plated Structures: Applied Statics and Steel Structures*. Zürich: ECCS, ETH-Hönggerberg.
- EUROPEAN COMMITTEE FOR STANDARDISATION (EC3 1993). *Eurocode 3: Design of Steel Structures – Part 1-1: General Rules and Rules for Buildings*. EN 1993-1-1: 1993. Brussels: CEN.
- EUROPEAN COMMITTEE FOR STANDARDISATION (EN 2001). *Metallic Materials – Tensile Testing – Part 1: Method of Test at Ambient Temperature*. EN 10002-1. Brussels: CEN.
- EUROPEAN COMMITTEE FOR STANDARDISATION (EC2 2004). *Eurocode 2: Design of Concrete Structures – Part 1-1: General Rules and Rules for Buildings*. EN 1992-1-1: 2004. Brussels: CEN.
- EUROPEAN COMMITTEE FOR STANDARDISATION (EC3 2006). *Eurocode 3: Design of Steel Structures – Part 1-5: Plated Structural Elements*. EN 1993-1-5: 2006. Brussels: CEN.
- FUJII, T., FUKOMOTO, Y., NISHINO, F. and OKUMURA, T. (1971). Research Works on Ultimate Strength of Plate Girders and Japanese Provisions on Plate Girder Design. *IABSE Colloquium*, 21-48.
- GALAMBOS, T. V. (1988). *Guide to Stability Design: Criteria for Metal Structures* (4th ed.). New York: John Wiley & Sons, Inc.
- GAYLORD, E. H. (1963). Discussion of K. Basler 'Strength of Plate Girders in Shear'. *Trans. ASCE*, **128**, Part II, pp. 712.
- HANSEN, T. and NIELSEN M. P. (2005). The Diagonal Compression Field Method using Circular Fans. *Byggningsstatistiske Meddelelser*, **76**(4), 95-124.
- HERZOG, M. (1974). Die Traglast unversteifter und versteifter, dünnwandigen Blechträger unter reinem Schub und Schub mit Biegung nach Versuchen. *Der Bauingenieur*, **49**, 382-389.
- HÖGLUND, T. (1973). *Design of Thin Plate I-Girders in Shear and Bending with Special Reference to Buckling*. No. 94. Stockholm: Kungl. Tekniska Högskolan, Inst. for bygnadsstatik.
- HÖGLUND, T. (1995). *Strength of Steel and Aluminium Plate Girders: Shear Buckling and Overall Web Buckling of Plane and Trapezoidal Webs – Comparison with Tests*. Tech. Report No. 4. Stockholm: Royal Institute of Technology, Department of Structural Engineering.
- JOHANSSON, B., MAQUOI, R. and SEDLACEK, G. (2001). New Design Rules for Plated Structures in Eurocode 3. *Journal of Constructional Steel Research*, **57**, 279-311.
- KOMATSU, S. (1971). Ultimate Strength of Stiffened Plate Girders Subjected to Shear. *IABSE Colloquium*, 49-65.
- LEW, H. S., NATARAJAN, M. and TOPRAC, A. A. (1969). Static Tests on Hybrid Plate Girders. *Welding Research Council, Supplement Vol. 75*, pp. 86.

- LONGBOTTON, E. and HEYMAN, J. (1956). Experimental Verification of the Strength of Plate Girders Designed in Accordance with the Revised British Standard 153: Tests on Full-Size and on Model Plate Girders. *Inst. Civ. Engrs. Proc.*, **5**, 462-486.
- LYSE, I. and GODFREY, H. J. (1935). Investigation of Web Buckling in Steel Beams. *Trans. ASCE*, **100**, 675-695.
- NIELSEN, M. P. (1998). *Limit Analysis and Concrete Plasticity* (2nd ed.). Boca Raton, Florida: CRC Press.
- NIELSEN, M. P. and CHRISTENSEN S. B. (1982). Post-Buckling Strength of Steel Plate Girders Subjected to Shear. *Bygningsstatistiske Meddelelser*, **53(3)**, 95-124.
- NIELSEN, M. P., PILEGAARD HANSEN, L. and RATHKJEN, A. (2000). *Mekanik 2.2 del 2: Rumlige spændings- og deformationstilstande*. Aalborg/ København: Institut for Bærende Konstruktioner og Materialer, Danmarks Tekniske Universitet.
- NISHINO, F. and OKUMURA, T. (1968). Experimental Investigation of Strength of Plate Girders in Shear. *IABSE, Proc. 8th Congr, Final Report*, 451-463.
- OSTAPENKO, A. and CHERN, C. (1971). Ultimate Strength of Longitudinal Stiffened Plate Girders under Combined Loads. *IABSE Colloquium*, 301-313.
- PORTER, D. M., ROCKEY, K. C. and EVANS, H. R. (1975). The Collapse Behavior of Plate Girders Loaded in Shear. *The Structural Engineer*, **53(8)**, 313-325.
- ROCKEY, K. C. and SKALLOUD, M. (1971). The Ultimate Behavior of Plate Girders Loaded in Shear. *IABSE Colloquium*, 1-19.
- SAKAI, F., DOI, K., NISHINO, F. and OKUMURA, T. (1966). *Failure Tests of Plate Girders using Large Sized Models*. Tokyo: Dept. of Civ. Eng., University of Tokyo.
- SELBERG, A. (1963). *Stålkonstruksjoner*. Trondheim: Tapir Forlag.
- SKALLOUD, M. (1971). Ultimate Load and Failure Mechanism of Thin Webs in Shear. *IABSE Colloquium*, 115-127.
- TIMOSHENKO, S. P. and GERE, J. M. (1961). *Theory of Elastic Stability* (2nd ed.). New York: McGraw-Hill Book Co., Inc.
- TOLDERLUND, M. (2000). Plasticitetsteori for ståldragere: Diagonaltrækmetoden (M.Sc. Thesis). Lyngby: BYG•DTU, Danmarks Tekniske Universitet.
- WAGNER, H. (1929). Ebene Blechwandträger mit sehr dünnen Stegblech. *Z. für Flugtechnik und Motorluftschiffahrt*, **20**, 200-207, 227-233, 279-284, 306-314.
- ØSKAN, A. and BAK, C. (2006). Diagonaltrækmetode for ståldragere (M.Sc. Thesis). Lyngby: BYG•DTU, Danmarks Tekniske Universitet.

## 8 NOTATION

$a$	length; thickness of tension coupons
$b$	constant stiffener spacing; width of tension coupons
$b_f$	flange width
$c$	length
$d$	girder depth, i.e. depth of the web plate
$f_u$	ultimate tensile strength
$f_y$	yield stress
$f_{yf}, f_{yw}$	flange yield stress and web yield stress, respectively
$f_{ys}$	stiffener yield stress or buckling stress, the lower one being decisive
$k$	elastic buckling coefficient
$n$	number of stiffeners
$p_1, p_2, p_3$	loads per unit area
$p$	load per unit area
$q$	load per unit length
$q_e$	load per unit length on end panel
$q_{\max}$	experimentally determined maximum load per unit length
$q_u$	theoretical post-buckling load per unit length
$q_u^+$	theoretical post-buckling load per unit length, upper-bound value
$q_u^-$	theoretical post-buckling load per unit length, lower-bound value
$r$	radial distance
$r_0$	radius of curvature on tension coupons
$t$	thickness
$t_f, t_s, t_w$	thickness of flange, stiffener and web, respectively
$u$	relative displacement; deflection
$v$	angle
$x, y$	coordinates in a Cartesian $x, y$ -system of coordinates
$x$	length
$y_0$	vertical distance from the bottom face of a girder
$A$	area
$A_s, A_w$	cross-sectional area of a single stiffener and of the web plate, respectively
$C$	compressive flange force (positive as compression); pole of fan
$E$	Young's modulus
$G$	shear modulus
$I$	moment of inertia
$L$	length of shear zone
$L_0, L_c$	original gauge length and parallel length of tension coupons
$L_e$	length of end panel
$M$	moment
$M^*$	moment from virtual load
$M_e$	maximum moment on end panel
$M_{\max}$	maximum moment
$M_{pf}$	plastic yield moment of flange
$P$	force, load
$P_{cr}$	critical web buckling load
$P_{exp}$	experimentally determined post-buckling load
$P_{EC3}, P_{FEM}$	post-buckling load according to EC3 and FEM model, respectively
$P_{\max}$	experimentally determined maximum load
$P_u$	theoretical post-buckling load
$P_u^+$	theoretical post-buckling load, upper-bound value
$P_u^-$	theoretical post-buckling load, lower-bound value
$Q$	shear force
$Q^*$	shear force from virtual load
$Q_e$	shear force on end panel
$R_x$	resultant of the $\sigma_x$ -stresses
$S_0$	original cross-section area of tension coupons
$T$	tensile flange force (positive as tension)

$V$	volume
$W_e, W_i$	external work and dissipation, respectively
$W_l$	dissipation per unit length
$\alpha$	angle of circular fan; angle between yield line and relative displacement
$\beta$	angle of uniaxial web stress
$\delta$	displacement increment
$\varepsilon_1, \varepsilon_2$	principal strains
$\varepsilon_x, \varepsilon_y$	strains referred to a Cartesian $x,y$ -system of coordinates
$\varepsilon_y$	yield strain
$\phi, \phi_{xy}$	change of angle
$\eta$	non-dimensional parameter measuring flange stiffness
$\varphi$	stiffener ratio
$\nu$	Poisson's ratio; effectiveness factor
$\theta$	angle of uniaxial concrete stress; angle in failure mechanism
$\theta_{\min}$	minimised angle in failure mechanism
$\sigma_1, \sigma_2$	principal stresses
$\sigma_c$	uniaxial concrete stress
$\sigma_e$	normal stress on end panel
$\sigma_r, \sigma_\alpha$	normal stress in radial and circumferential direction, respectively
$\sigma_{sx}, \sigma_{sy}$	equivalent stiffener stresses
$\sigma_t$	tensile band stress
$\sigma_w$	uniaxial web stress
$\sigma_{wx}, \sigma_{wy}$	web normal stresses in a Cartesian $x,y$ -system of coordinates
$\sigma_x$	normal stress in the $x$ -direction
$\sigma_y$	normal stress in the $y$ -direction
$\tau$	shear stress
$\tau_{\max}$	maximum shear stress
$\tau_{cr}$	elastic critical shear buckling stress
$\tau_{exp}$	shear stress measured by experiments
$\tau_u$	theoretically determined shear stress
$\tau_{r\alpha}$	shear stress in polar coordinates
$\tau_{sxy}$	stiffener shear stress
$\tau_{wxy}$	web shear stress
$\tau_u$	ultimate shear load-carrying capacity
$\tau_{xy}$	shear stress in the $xy$ -plane
$\upsilon$	angle
$\psi$	mechanical degree of stiffening

### Subscripts

$bf$	bottom face
$tf$	top face



---

## **PART III**

---

### **POST-BUCKLING STRENGTH OF PLATES IN COMPRESSION**

**- Derivation of Effective Width Equations**



# POST-BUCKLING STRENGTH OF PLATES IN COMPRESSION

## - Derivation of Effective Width Equations

### 1 INTRODUCTION

In PART II it is stated several times that when designing a steel plate girder subjected to shear according to the plastic tension field method, the ultimate stress of the transverse web stiffeners,  $f_{ys}$ , or of the compression flange,  $f_{yf}$ , is either the yield stress or the buckling stress. The lower one is decisive. Therefore the aim of this part of the thesis is to illustrate how one may determine the post-buckling strength of both the transverse web stiffeners and the compression flange.

It was deduced many years ago that the elastic buckling theory is not able to accurately account for the real strength of plates (Schuman and Back 1930). The main reason for this is that, in a large parameter interval, the ultimate load is reached after yielding of the plate. This fact was also pointed out by Kármán et al. (1932), who suggested modifying the elastic solution by an empirical coefficient. This idea was taken up by Winter (1947), who developed accurate formulae for the two important cases considered in the following. Winter's method is an *effective width method*, on which calculations of plates in compression are still based.

Any design method thus has to take into account that plates in compression may carry loads much larger than the load for which elastic buckling will occur. The effective width method takes the post-buckling capacity into account. The aim is here to establish a new effective width method, which is derived on the basis of a consistent theory. The new method rests on the theory of plasticity, particularly the yield line theory. Emphasis is on buckling problems related to plate girders. Two general cases are studied: Plates in uniaxial compression supported along all edges, cf. the compressed flange in a box girder, and plates with one free edge, cf. the compressed flange and the transverse web stiffeners in an I-shaped girder.

The results presented coincide closely with Winter's formulae and with tests.

The basics of the theory are described in Chapter 2. How to take geometrical second order effects into account is illustrated by a simple column example.

Solutions for plates in uniaxial compression supported along all edges are presented in Chapter 3, while solutions for plates with one free edge are treated in Chapter 4. Both chapters contain a comparison between the theory and the experimental results, on which Winter's formulae were based.

The effect of imperfections is touched upon in Chapter 5 and other possible applications of the theory are mentioned in Chapter 6.

### 1.1 Historical Overview

Bryan (1891) was the first to develop a solution for the elastic critical stress of a rectangular plate simply supported along all edges and subjected to a uniform longitudinal compressive stress. Later a large number of solutions using Bryan's equation have been derived, see for instance (Timoshenko and Gere 1961).

In general the elastic critical stress may be expressed as

$$\sigma_{cr} = k \frac{\pi^2 E}{12(1-\nu^2)} \left(\frac{t}{b}\right)^2 \quad (1.1)$$

in which  $E$  is Young's modulus,  $\nu$  Poisson's ratio,  $t/b$  the thickness-to-width ratio and  $k$  is a buckling coefficient, which is a function of plate geometry and boundary conditions. Useful information on  $k$ -factors may be found in a number of references, e.g. (Timoshenko and Gere 1961).

Tests by Schuman and Back (1930) on plates supported by V-grooves along the unloaded edges demonstrated that, for plates of the same thickness, an enhancement of the plate width beyond a certain value did not increase the ultimate load. Wider plates acted as though narrow side portions or "effective load-carrying areas" took most of the load. Furthermore, the ultimate load was found to be up to thirty times larger than the elastic critical buckling load determined by Bryan, cf. Equation (1.1).

It is now well known that the post-buckling resistance of plates is due to redistribution of axial compressive stresses, and to a lesser extent, to tensile membrane effects and to shear that accompany the out-of-plane bending of the plate in both longitudinal and transverse directions. The longitudinal stresses tend to concentrate in the vicinity of the longitudinally supported edges, which are the stiffer parts of the buckled plate. As a result, yielding begins along these edges, which limits the load-carrying capacity.

Several researchers were prompted by the tests of Schuman and Back (1930) to develop expressions for the ultimate strength of such plates. The first to use the effective width concept in handling this problem was Kármán et al. (1932). They derived the following approximate formula for the effective width,  $b_e$ , of plates supported along all edges, based on the assumption that two strips with total width,  $b_e$ , along the sides, each on the verge of buckling, carry the entire load:

$$b_e = \frac{\pi}{\sqrt{3(1-\nu^2)}} t \sqrt{\frac{E}{\sigma_e}} \quad (1.2)$$

Here  $\sigma_e$  is the edge stress along  $b_e$  and the remaining notation is as in Equation (1.1).

As a result of many tests and studies of post-buckling strength, Winter (1947) suggested the following formula for the effective width:

$$b_e = 1.9t \sqrt{\frac{E}{\sigma_e}} \left( 1.0 - 0.574 \frac{t}{b} \sqrt{\frac{E}{\sigma_e}} \right) \quad (1.3)$$

This equation has been modified several times over the past. In the latest version, adopted in EC3 (2006), the formula is written as

$$\frac{b_e}{b} = \sqrt{\frac{\sigma_{cr}}{\sigma_e}} \left( 1.0 - 0.22 \sqrt{\frac{\sigma_{cr}}{\sigma_e}} \right) \quad (1.4)$$

In the calculation of the ultimate compression load, the edge stress,  $\sigma_e$ , is taken to be equal to the yield stress of the plate material. The elastic critical stress,  $\sigma_{cr}$ , is determined by Equation (1.1). Equation (1.4) corresponds to Equation (1.3) if the factor 0.574 is substituted with a factor of 0.415.

For plates supported along only one longitudinal edge, the effective width has been experimentally determined by Winter (1947). The original formula was

$$b_e = 1.25t \sqrt{\frac{E}{\sigma_e}} \left( 1.0 - 0.333 \frac{t}{b} \sqrt{\frac{E}{\sigma_e}} \right) \quad (1.5)$$

This equation has also been modified several times. In the latest version, adopted in EC3 (2006), it is written as

$$\frac{b_e}{b} = \sqrt{\frac{\sigma_{cr}}{\sigma_e}} \left( 1.0 - 0.188 \sqrt{\frac{\sigma_{cr}}{\sigma_e}} \right) \quad (1.6)$$

In the 1993-edition of EC3 (1993), Equation (1.4) is valid in the case of plates supported along all edges and plates with one free edge. Hence, the difference between the two cases is only the value of the buckling coefficient,  $k$ . It is practical and convenient to have only one expression. The reason for changing the factor 0.22 to 0.188, for plates with one free edge, is not yet known to the author. But the adjustment seems to be rather insignificant.

## 2 POST-BUCKLING THEORY FOR PLATES IN COMPRESSION

The basic idea is to use plastic theory in the form of limit analysis on the deflected shape of the plate. The deflected shape has to be estimated which is done by using simple formulae from beam and plate theory. The plastic analysis is carried out using yield line theory.

### 2.1 Yield Line Theory

Yield line theory is an upper-bound method. The mechanisms considered are a system of bending yield hinges along lines, *the yield lines*. The load-carrying capacity is determined by the work equation, equalising external work and dissipation in the yield lines.

It is assumed that the plane stress field existing before buckling is known so that the principal normal forces may be found whereby the corresponding yield moments may be determined. In an unloaded direction, the bending capacity,  $m$ , reaches the full yield moment per unit length in bending,  $m_p$ :

$$m = m_p = \frac{1}{4} t^2 f_y \quad (2.1)$$

where  $t$  is the thickness of the plate and  $f_y$  the yield stress. In the direction of a principal compression or tension (normal force  $n$  per unit length), the bending capacity,  $m$ , is reduced due to the normal force as for beams subjected to combined bending and normal force, i.e.

$$m = m_p \left( 1 - \left( \frac{n}{n_p} \right)^2 \right) \quad (2.2)$$

where  $m_p$  is given by Equation (2.1) and  $n_p = t f_y$  is the load-carrying capacity in pure compression or tension. By determining the yield moments in the two principal directions in this way, the simplification suggested by Johansen (1943) may be used to calculate the bending moment in a yield line,  $m_b$ , as

$$m_b = m_{px} \sin^2 \beta + m_{py} \cos^2 \beta \quad (2.3)$$

where  $\beta$  is the angle between the yield line and the  $x$ -axis. The  $x$ - and  $y$ -axes are directed along the principal directions, and  $m_{px}$  and  $m_{py}$  are the corresponding yield moments per unit length. The plastic yield moments,  $m_{px}$  and  $m_{py}$ , are determined by either Equation (2.1) or (2.2). Equation (2.3) is correct for reinforced concrete slabs in general, which was shown by Nielsen (1998). It is also correct if the yield condition in principal moment space is square or rectangular. For steel plates, such assumptions are dubious, when the slab is acted upon by torsion. Nevertheless, Equation (2.3) is used in the following with surprisingly good results.

A number of different researchers have developed formulae for the plastic moment capacity of inclined yield lines, the first being Murray (1984). Hiriyur and Schafer (2004) and Zhao (2003) have shown that the solutions obtained by the different proposals vary widely, and Zhao (2003) concludes that nothing better than the method suggested by Murray (1984) has been found.

### 2.2 Effect of Deflections

From the general theory of beam-columns, it is known that the equilibrium equations may be derived for the undeformed structure if a fictitious load is included. The fictitious load is a moment per unit length of the beam, equal to

$$m = N \frac{du}{dx} \tag{2.4}$$

where  $N$  is normal force and  $u$  the deflection, transverse to the beam axis,  $x$ . The statical equivalence of  $m$  may be expressed in several ways, but for a given part of a beam subjected to a constant normal force,  $N$ , it may conveniently be expressed in the following simple way: The total moment,  $M$ , on a beam ( $A$ - $B$ ), when  $N$  is constant, is

$$\begin{aligned} M &= \int_A^B m \, dx = \int_A^B N \frac{du}{dx} \, dx = N \int_A^B \frac{du}{dx} \, dx = N(u_B - u_A) \\ &= N \Delta u \end{aligned} \tag{2.5}$$

which may be split into two forces,  $N \Delta u/L$ , in the two end points. The two forces are transverse to the beam as shown in Figure 2.1.

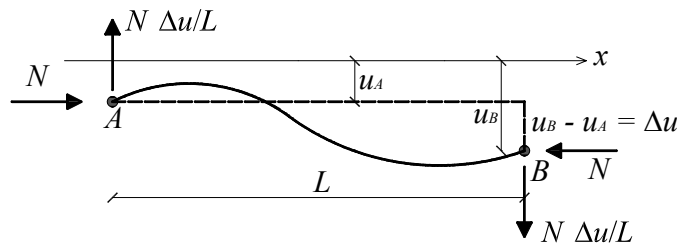


**Figure 2.1:** Part of a beam subjected to a constant normal force,  $N$ , and statically equivalent transverse forces in the end points

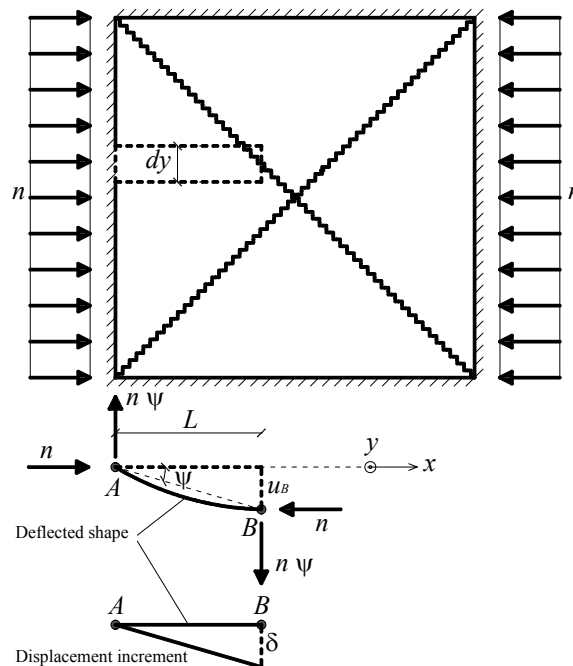


**Figure 2.2:** Plate subdivided into strips with infinitesimal widths

The value of these forces is independent of the deflected shape between the end points,  $A$  and  $B$ . Only the difference in the deflection at the end points is important. The work in a virtual displacement, where the beam considered moves as a rigid body, may then be determined as the work done by the two forces,  $N \Delta u/L$ .

In the simple cases considered, the above result may be used by considering the plate as being subdivided into strips with constant normal force. In Figure 2.2, a simply supported square plate subjected to uniaxial compression is shown.

The strip, marked by the dashed lines, has a normal force,  $n$ , per unit length. The transverse forces are a uniform load,  $n\psi$ , along the lines ( $A$  and  $B$ ) acting upwards in ( $A$ ) (i.e. perpendicular to the  $x,y$ -plane), and a uniform load acting downwards in ( $B$ ). For a displacement increment,  $\delta$ , along the line ( $B$ ), the external work for the strip is given by

$$dW_e = n \psi dy \delta \tag{2.6}$$

where the relative deflection increment,  $\psi = u_B/L$ . The dissipation contribution from the strip is determined by

$$dW_i = m dy \frac{\delta}{L} \tag{2.7}$$

where  $m$  is calculated by Equation (2.2).

### 2.3 Column Example

The procedure is illustrated by a simply supported column, see Figure 2.3. The deflected shape of the column is characterised by the deflection in the midpoint at maximum load,  $u_m$ . The column is centrally loaded by a compressive normal force,  $N$ , and thereby each half is subjected to the forces,  $N\psi$ . In the figure they are only shown in the midpoint.

The column is given a lateral displacement increment,  $\delta$ , at the midpoint, as shown in Figure 2.4, where a plastic yield hinge is formed.

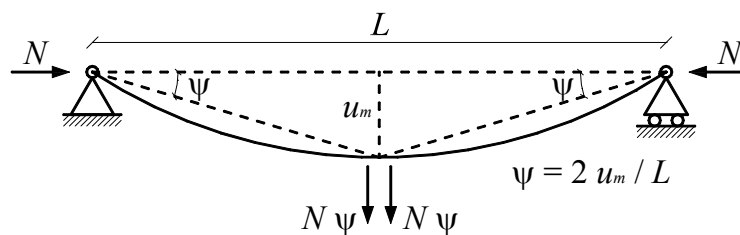


Figure 2.3: Deflected shape of a simply supported column

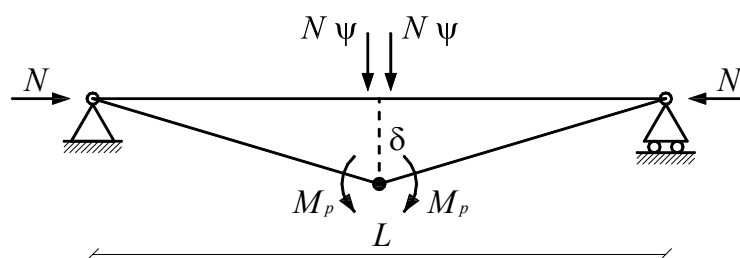


Figure 2.4: Failure mechanism for a lateral displacement increment,  $\delta$

The external work of the mechanism renders

$$W_e = 2 N \psi \delta = 4 N \frac{u_m}{L} \delta \quad (2.8)$$

and the dissipation is

$$W_i = 4 \frac{M_p}{L} \delta \quad (2.9)$$

Here,  $M_p$  is the plastic yield moment, which must be reduced due to the normal force. The work equation equals:

$$N u_m = M_p \quad (2.10)$$

A constant, solid and rectangular cross-section of the column is assumed in order to compare the result with the solutions derived later for plates. Hence, the following solution also corresponds to a rectangular plate with two free unloaded edges. The sides of the rectangular cross-section are denoted  $b$  and  $t$ , respectively, where  $b \geq t$  is assumed. The plastic yield moment, reduced due to the normal force, is then

$$M_p = \frac{1}{4} b t^2 f_y \left( 1 - \left( \frac{N}{N_p} \right)^2 \right) \quad (2.11)$$

$N$  is the normal force,  $f_y$  the yield stress and  $N_p = b t f_y$  is the load-carrying capacity in pure compression or tension.

The next step is to find a good estimate for the deflected shape of the column. The maximum deflection for a beam may in general be determined as

$$u_m = \frac{1}{\alpha} \kappa L^2 \quad (2.12)$$

where  $\kappa$  is the curvature in a selected point,  $L$  the length and  $\alpha$  is a parameter depending on the shape of the curvature function. In the following,  $\alpha = 8$ , corresponding to a constant curvature function, is used.

In a beam or column with yielding, the deflection corresponding to maximum load tends to be reached when the yield strain,  $\varepsilon_y$ , is obtained in one or both faces. Here it is assumed that the deflection at maximum load may be found by assuming that the yield strain,  $\varepsilon_y = f_y/E$  ( $f_y$  is yield stress and  $E$  Young's modulus), is reached in both faces. Thus the curvature is determined by  $2 \varepsilon_y/t$ . The formula is modified as follows:

$$\kappa = \frac{2 \varepsilon_y \mu}{t} \quad (2.13)$$

where the parameter,  $\mu$ , is an empirical coefficient accounting for the effect of imperfections and residual stresses. Hence for the column in Figure 2.3, the deflection equals:

$$u_m = \frac{1}{8} \frac{2\varepsilon_y \mu}{t} L^2 = \frac{1}{4} \mu \frac{f_y}{E} \frac{L^2}{t} \quad (2.14)$$

Inserting Equations (2.11) and (2.14) into Equation (2.10), the load-carrying capacity expressed by the non-dimensional value,  $N / (b t f_y)$ , is found to be

$$\frac{N}{b t f_y} = -\frac{1}{2} \mu \lambda^2 + \sqrt{\frac{1}{4} \mu^2 \lambda^4 + 1} \quad (2.15)$$

where the parameter,  $\lambda$ , has been introduced:

$$\lambda = \frac{L}{t} \sqrt{\frac{f_y}{E}} \quad (2.16)$$

Now this result is compared with the EC3 (2005) formulae. Here a non-dimensional slenderness ratio,  $\lambda_r$ , is introduced as

$$\lambda_r = \sqrt{\frac{A f_y}{N_{cr}}} \quad (2.17)$$

Here,  $A$  is the cross-sectional area and  $N_{cr}$  is the elastic critical buckling force (the Euler-load), see the following Equation (2.21). For a solid, rectangular cross-section where  $\lambda$  is given by Equation (2.16),  $\lambda_r$  may be expressed as,

$$\lambda_r = \frac{\sqrt{12}}{\pi} \sqrt{\frac{f_y}{E}} \frac{L}{t} = \frac{\sqrt{12}}{\pi} \lambda \quad (2.18)$$

The load-carrying capacity according to EC3 (2005) is given by

$$\frac{N_{cr}}{b t f_y} = \frac{1}{\Phi + \sqrt{\Phi^2 - \lambda_r^2}} \quad (2.19)$$

where

$$\Phi = 0.5 \left( 1 + \alpha (\lambda_r - 0.2) + \lambda_r^2 \right) \quad (2.20)$$

The so-called *geometric equivalent imperfection factor*  $\alpha$  in this equation is obtained from Table 2.1. Notice that  $\alpha$  here is not the same as the  $\alpha$  introduced in Equation (2.12).

Buckling curve	$a_0$	$a$	$b$	$c$	$d$
Imperfection factor $\alpha$	0.13	0.21	0.34	0.49	0.76

**Table 2.1:** Imperfection factors for buckling curves according to EC3

The buckling curves according to EC3 (2005), cf. Equation (2.19), and the curve given by Equation (2.15) for  $\mu = 1.4$  are shown in Figure 2.5. It turns out that by choosing a value of  $\mu$  between 1.2 and 1.6, all buckling curves in EC3 (2005) may be

well represented. For  $\mu = 1.4$ , the result coincides very closely with the buckling curve  $b$ . The figure also shows the Euler curve, which for a solid rectangular cross-section is given by

$$\frac{N_{cr}}{bt f_y} = \frac{1}{\lambda_r^2} = \frac{\pi^2}{12} \lambda^{-2} \quad (2.21)$$

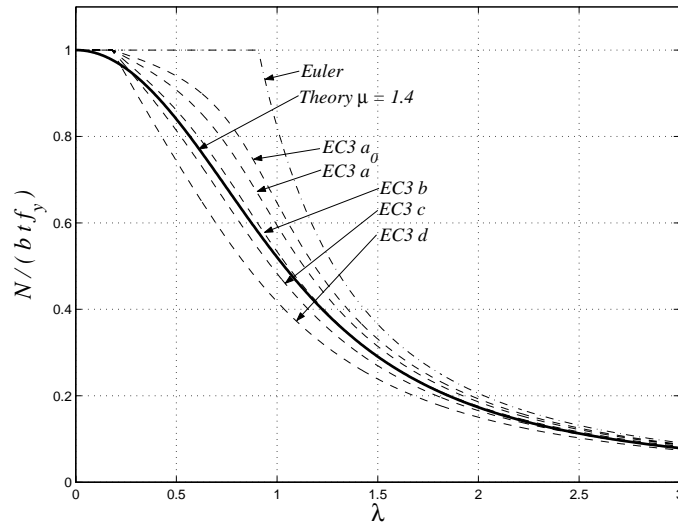


**Figure 2.5:**  $N / (b t f_y)$  as a function  $\lambda$ , plastic theory and EC3

If the column in Figure 2.3 is also subjected to a lateral load,  $q$ , per unit length along the entire length,  $L$ , then this load is easily included in the calculations. The work done by the lateral load is simply added to the external work, thus the work equation becomes, cf. Equation (2.10),

$$N u_m + \frac{1}{8} q L^2 = M_p \quad (2.22)$$

Here,  $u_m$  is the estimated deflection at maximum load,  $N$  the normal force and  $M_p$  is the plastic yield moment which must be reduced due to the normal force.

In a similar way, any load case may be treated. Also other boundary conditions may be considered; however this requires new estimates of the deflected shape.

### 3 PLATES SUPPORTED ALONG ALL EDGES

The design method (the lower-bound solution) presented in PART II is also valid in the case of, for instance, a box-girder. The compression flange in a box-girder may be considered as a plate simply supported along the edges. The ultimate stress of the flange,  $f_{yf}$ , is either the yield stress or the buckling stress, as stated in PART II. Determination of the post-buckling strength of plates supported along all edges is presented below.

#### 3.1 Square Plates

Initially, the square plate in Figure 3.1 is considered. It is simply supported along all four edges and subjected to a uniform load per unit length,  $n$ , along two opposite edges.

The first step is to find a good estimate for the deflected shape of the plate. As stated in Section 2.3, the maximum deflection for a beam may in general be determined as

$$u_m = \frac{1}{\alpha} \kappa L^2 \tag{3.1}$$

where  $\kappa$  is the curvature,  $L$  the length and  $\alpha$  is a parameter depending on the shape of the curvature function. Again  $\alpha = 8$  is used, corresponding to a constant curvature function.

In a plate with yielding, the deflection corresponding to maximum load tends to be reached when the yield strain,  $\epsilon_y$ , is obtained in one or both faces. As in the case of a column, cf. Section 2.3, the deflection at maximum load may be found by assuming the yield strain,  $\epsilon_y = f_y/E$ , is reached in both faces of the plate. Here,  $f_y$  is the yield stress and  $E$  is the Young's modulus. Here  $\mu = 1$  is applied, cf. Equation (2.13), thus the curvature is determined by ( $t$  being the plate thickness)

$$\kappa = \frac{2 \epsilon_y}{t} \tag{3.2}$$

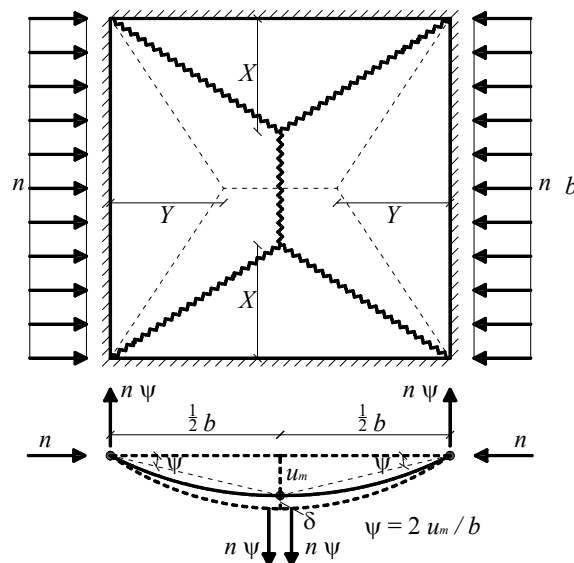


Figure 3.1: Failure mechanism for a simply supported square plate

For a square plate,  $L$  is taken equal to the side length,  $b$ . Hence, for the plate in Figure 3.1, the deflection at maximum load,  $u_m$ , is

$$u_m = \frac{1}{8} \frac{2 \varepsilon_y}{t} b^2 = \frac{1}{4} \frac{f_y}{E} \frac{b^2}{t} \quad (3.3)$$

The next step is to find the optimal failure mechanism (yield line pattern). In Figure 3.1, two different yield line patterns are shown, one with the free parameter,  $X$ , and one with the free parameter,  $Y$  (shown with dashed lines), respectively.

For the mechanism with the free parameter,  $X$ , the external work for a displacement increment,  $\delta$ , equals

$$\begin{aligned} W_e &= 4 X n \frac{2 u_m}{b} \frac{\delta}{2} + 2(b - 2 X) n \frac{2 u_m}{b} \delta \\ W_e &= n u_m \delta \left( 4 - 4 \frac{X}{b} \right) \end{aligned} \quad (3.4)$$

and the dissipation is

$$W_i = 4 m_p \delta \left( 1 - \left( \frac{n}{n_p} \right)^2 \right) + 2 m_p \delta \frac{b}{X} \quad (3.5)$$

Here, the plastic yield moment,  $m_p$ , per unit length is given by Equation (2.1) and  $n_p = t f_y$  is the load-carrying capacity in pure compression or tension.

Equalising the external work and the dissipation and inserting Equations (2.1) and (3.3), the load-carrying capacity, expressed by the non-dimensional parameter,  $n/(t f_y)$ , may be written as

$$\frac{n}{t f_y} = -\frac{1}{2} \lambda^2 \left( 1 - \frac{X}{b} \right) + \sqrt{\frac{1}{4} \lambda^4 \left( 1 - \frac{X}{b} \right)^2 + \frac{1}{2} \left( 2 + \frac{b}{X} \right)} \quad (3.6)$$

where the parameter,  $\lambda$ ,

$$\lambda = \frac{b}{t} \sqrt{\frac{f_y}{E}} \quad (3.7)$$

has been introduced.

Equation (3.6) is the post-buckling load in this case. The value of  $n/(t f_y)$  as a function of  $\lambda$  is shown for different values of  $X$  in Figure 3.2.

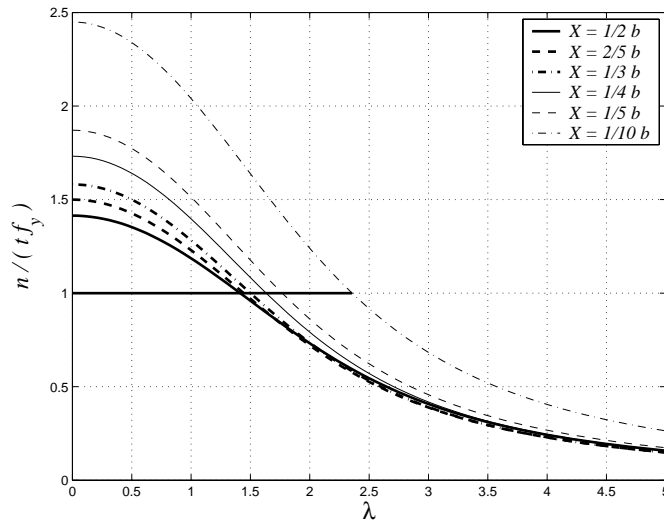


**Figure 3.2:**  $n/(t f_y)$  as a function of  $\lambda$  for different values of  $X$

It is seen that  $n/(t f_y) > 1$  for small values of  $\lambda$ , which is not possible in reality, hence a cut-off at  $n/(t f_y) = 1$  must be introduced. With this cut-off, it appears that almost the same load-carrying capacity is obtained for  $X = 1/2 b$ ,  $X = 2/5 b$  and  $X = 1/3 b$ .

The mechanism with the free parameter,  $Y$ , cf. Figure 3.1, leads to  $Y = 0$  when optimised. However, it must be remembered that the deflected shape is used both as an estimate of the deflection at maximum load and as the basis for a choice of the deflection increment at the yield load. Thus the optimised value for  $Y = 0$  must be disregarded and the mechanism corresponding to  $X = 1/2 b$  ( $Y = 1/2 b$ ) is chosen for the following calculations.

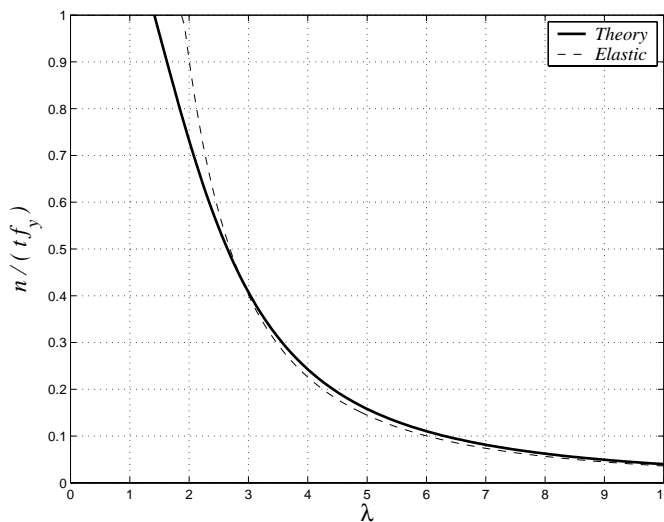


**Figure 3.3:**  $n/(t f_y)$  as a function of  $\lambda$  for  $X = 1/2 b$

In Figure 3.3, the ratio,  $n/(t f_y)$ , as a function of  $\lambda$  for  $X = 1/2 b$  is shown together with the elastic solution, which may be written as, cf. Equation (1.1),

$$\frac{n}{t f_y} = \frac{\pi^2 k}{12(1-\nu^2)} \lambda^{-2} \tag{3.8}$$

where  $k$  is the buckling coefficient and  $\nu$  is Poisson's ratio. Here  $k = 4$  and  $\nu = 0.30$  are used. The parameter,  $\lambda$ , is given by Equation (3.7).

The two curves coincide very closely, but this indicates that no extra post-buckling reserve is found from this approach. According to what has previously been mentioned the result is incorrect. This is, of course, due to the fact that a redistribution of the stresses occurs when the buckling mechanism develops. This is illustrated in Figure 3.4.

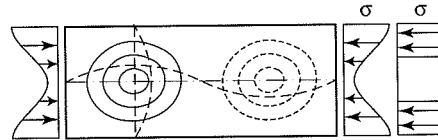


Figure 3.4: Stress distribution in a plate after buckling

As previously mentioned, Kármán et al. (1932) suggested that instead of using the true varying stress distribution, the calculation might be simplified by using an effective area subjected to a uniform stress equal to the yield stress, i.e.  $\sigma = f_y$ , in Figure 3.4. The same simplification will be used here. Hence the plate is subjected to a load per unit length equal to the yield stress multiplied by the thickness of the plate, i.e.  $n = n_p = t f_y$ , which is applied along two strips with the width equal to the unknown length,  $b_s$ , see Figure 3.5.

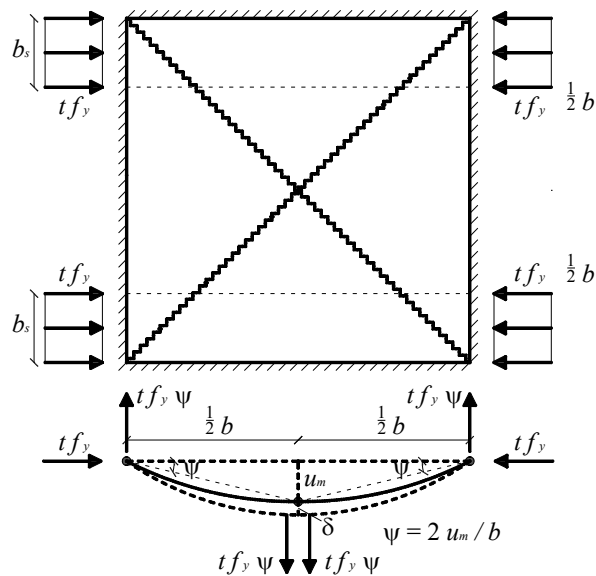


Figure 3.5: Simply supported square plate subjected to uniaxial compression along strips of width  $b_s$

The external work,  $W_e$ , and the dissipation,  $W_i$ , are for  $\delta = 1$ , respectively:

$$W_e = 8 t f_y u_m \frac{b_s^2}{b^2} \tag{3.9}$$

$$W_i = \underbrace{8 m_p \frac{b_s}{b} \left( 1 - \left( \frac{t f_y}{n_p} \right)^2 \right)}_{=0} + 8 m_p \left( 1 - \frac{b_s}{b} \right) = 8 m_p \left( 1 - \frac{b_s}{b} \right) \tag{3.10}$$

Again,  $u_m$  is the deflection at maximum load,  $m_p$  is the plastic yield moment per unit length given by Equation (2.1) and  $n_p = t f_y$  is the load-carrying capacity in pure compression or tension.

The contribution from the part of the yield lines running in the widths,  $b_s$ , is equal to zero, as  $n_p = t f_y$ . Inserting Equations (2.1) and (3.3), and using  $W_i = W_e$ ,  $b_s$  is found to be determined by

$$\frac{f_y}{E} b_s^2 + \frac{t^2}{b} b_s - t^2 = 0 \quad (3.11)$$

Denoting the total effective width  $b_e = 2 b_s$ , it equals

$$\frac{b_e}{b} = -\lambda^{-2} + \sqrt{\lambda^{-4} + 4\lambda^{-2}} \quad (3.12)$$

where  $\lambda$  is given by Equation (3.7).

Equation (3.13) indicated that the average stress relative to the yield stress,  $f_y$ , along the whole width,  $b$ , from the yield force,  $b_e t f_y$ , along  $b_e$  is  $b_e t f_y / (b t f_y) = b_e / b$ . For a solution with uniform load,  $n$ , along the width,  $b$ , the average stress relative to the yield stress is  $n / (t f_y)$ .

$$\frac{b_e}{b} = \frac{n}{t f_y} \quad (3.13)$$

In Figure 3.6,  $b_e/b$ , cf. Equation (3.12), is shown as a function of  $\lambda$ .

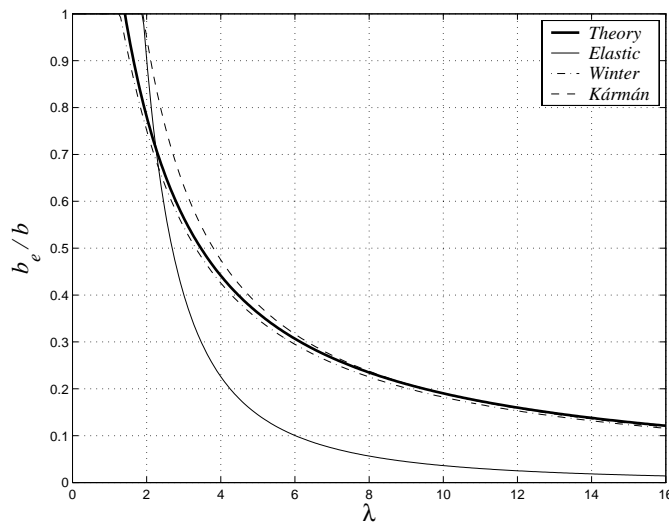


**Figure 3.6:**  $b_e/b$  as a function of  $\lambda$

The elastic buckling load characterised by  $n / (t f_y)$ , cf. Equation (3.8), is also shown. It appears that the plate may carry compressive forces considerably above the elastic buckling load. The first to demonstrate this through tests appear to be Schuman and Back (1930).

The third curve plotted in the figure is the semi-empirical expression derived by Winter (1947). With the introduced parameter,  $\lambda$ , given by Equation (3.7), it may be written as, cf. Equation (1.4),

$$\frac{b_e}{b} = \frac{\pi\sqrt{k}}{\sqrt{12(1-\nu^2)}} \lambda^{-1} \left( 1 - 0.22 \frac{\pi\sqrt{k}}{\sqrt{12(1-\nu^2)}} \lambda^{-1} \right) \quad (3.14)$$

Finally, a cut-off at  $b_e/b = n/(t f_y) = 1$  is introduced.

Winter's formula is a modification of the original formula introduced by Kármán et al. (1932). Kármán et al. stated that the effective width might be determined by

$$\frac{b_e}{b} = C \frac{t}{b} \sqrt{\frac{E}{f_y}} = C \lambda^{-1} \quad (3.15)$$

where  $C$  is an empirical constant. Based on the tests made by Schuman and Back (1930),  $C = 1.9$  was found. Equation (3.15) is also shown in the figure. Regarding Equation (3.15), Winter (1947) argued that  $C$  should depend on the parameter  $\lambda^{-1}$ . Based on his own tests and those made by Sechler (Winter 1947), he found the best fit to be

$$C = 1.9 - 1.09 \frac{t}{b} \sqrt{\frac{E}{f_y}} = 1.9 - 1.09 \lambda^{-1} \quad (3.16)$$

As previously mentioned, this formula has consequently been modified several times. Equation (3.14) is the newest modification and it is adopted in EC3 (2006). Equation (3.14) corresponds, for  $k = 4$  and  $\nu = 0.30$ , to

$$C = 1.9 - 0.42 \lambda^{-1} \quad (3.17)$$

Figure 3.6 shows that the present theoretical result closely follows Winter's semi-empirical solution.

In order to investigate the sensitiveness of the solution, Equation (3.12), to the estimated deflection at maximum load, it is compared with the solution using  $\alpha = 10$  in Figure 3.7.

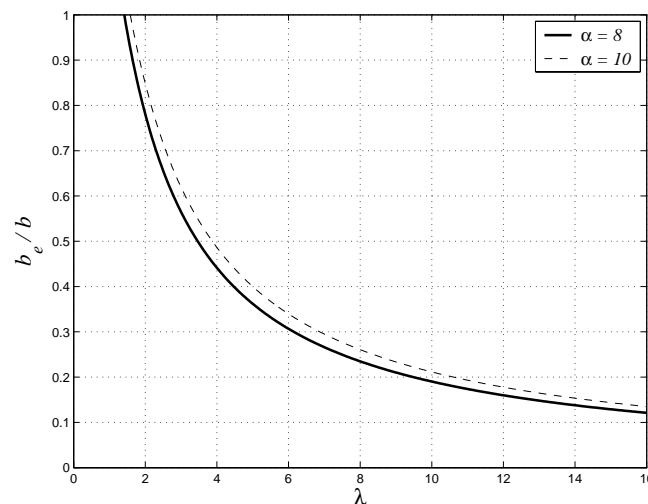


**Figure 3.7:**  $b_e/b$  as a function of  $\lambda$  for  $\alpha = 8$ ,  $\alpha = 10$  and by using von Mises' yield criterion, respectively

Choosing  $\alpha = 10$  in Equation (3.1) approximately corresponds to a sinusoidal curvature function ( $\alpha = \pi^2 \approx 10$ ). For  $\alpha = 10$ , the effective width is determined by

$$\frac{b_e}{b} = -\frac{5}{4}\lambda^{-2} + \sqrt{\frac{25}{16}\lambda^{-4} + 5\lambda^{-2}} \quad (3.18)$$

where  $\lambda$  is still given by Equation (3.7).

Equation (3.18) gives a post-buckling strength up to 11 % larger than that obtained by Equation (3.12) for the  $\lambda$ -interval shown in Figure 3.7. Hence, the theory seems to be relatively insensitive to the estimated deflection at maximum load.

When von Mises' yield criterion is applied,  $m_p$  in Equation (3.10) is simply substituted with  $2 m_p / \sqrt{3}$  if uniaxial strain is supposed. In that case also  $n_p$  should be increased and  $b_e/b$  then will measure  $n$  relative to the increased value of  $n_p$ . Thus it turns out that nothing is changed, since  $b_e/b$  is given by, cf. Equation (3.12),

$$\frac{b_e}{b} = -\lambda^{-2} + \sqrt{\lambda^{-4} + 4\lambda^{-2}} \quad (3.19)$$

In practise one should calculate on the safe side using the uniaxial yield stress and not any increased value, which means that the former solution is applied.

### 3.2 Rectangular Plates

It is a well-known fact that a long rectangular elastic plate subjected to compression in the longitudinal direction buckles into a shape of half waves with a length equal to the plate width, see Figure 3.8. This result is applied for estimating the post-buckling strength. Thus a long plate may be subdivided into a number of square plates where the previous yield line patterns may be applied, cf. Section 3.1. The vertical lines between the square regions will act as simple supports, since if one square region forms a wave downwards, then the adjacent regions will form a wave upwards. Therefore, the post-buckling strength or the effective width for a long rectangular plate is in general given by Equation (3.12).

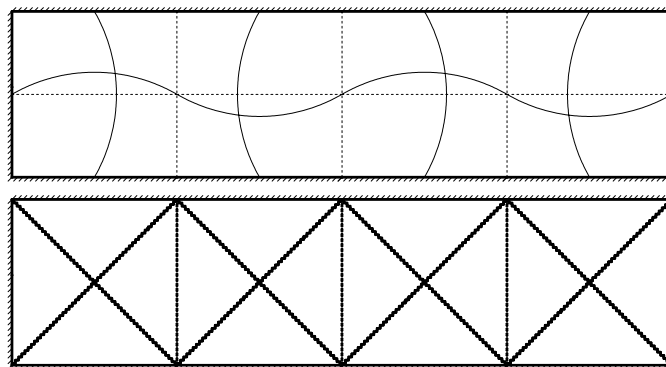


**Figure 3.8:** Deflection shape and failure mechanism for long simply supported rectangular plates

Now consider a rectangular plate with a length somewhat larger than the width. In Figure 3.9, the width is named  $b$  and the length named  $a$ . The plate is subjected to uniaxial compression,  $n_p = t f_y$ , acting on the two strips,  $b_s$ .

The failure mechanism has the free parameter,  $X$ . The maximum deflection,  $u_m$ , is assumed to be given by Equation (3.3). The external work is then for  $\delta = 1$  given by

$$W_e = 4 t f_y \frac{u_m b_s^2}{X b} \quad (3.20)$$

and the dissipation

$$W_i = 2 m_p \left( \frac{b}{X} - 2 \frac{b_s}{X} + 2 \frac{a}{b} \right) \quad (3.21)$$

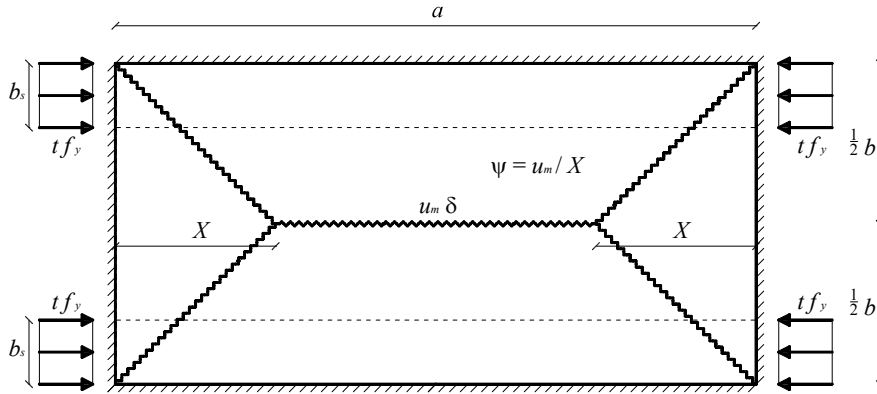


Figure 3.9: Failure mechanism for a short rectangular plate

Hence,  $b_s$  may be determined by

$$\frac{f_y}{E} b_s^2 + \frac{t^2}{b} b_s - t^2 \left( \frac{1}{2} + \frac{X a}{b^2} \right) = 0 \quad (3.22)$$

The effective width,  $b_e$  ( $b_e = 2 b_s$ ), is then found to be

$$\frac{b_e}{b} = -\lambda^{-2} + \sqrt{\lambda^{-4} + 4 \left( \frac{1}{2} + \frac{X a}{b^2} \right) \lambda^{-2}} \quad (3.23)$$

where  $\lambda$  is given by Equation (3.7). Furthermore, in the above equations,  $t$  is the thickness,  $E$  is Young's modulus,  $f_y$  the yield stress,  $m_p$  is the plastic yield moment per unit length given by Equation (2.1), and  $n_p = t f_y$  is the load-carrying capacity in pure compression or tension.

Assuming  $X = \frac{1}{2} b$ , the effective width is determined by

$$\frac{b_e}{b} = -\lambda^{-2} + \sqrt{\lambda^{-4} + 2 \left( 1 + \frac{a}{b} \right) \lambda^{-2}} \quad (3.24)$$

When  $a$  is larger than, or equal to,  $b$ , it appears that Equation (3.24) gives the smallest post-buckling strength if  $a$  is equal to  $b$ . Hence in practice, the yield line pattern for a square plate may be considered as the optimal solution, rather than the pattern shown in Figure 3.9.

Special attention is required for plates where  $a$  is smaller than  $b$ , but they will not be treated here, although the theory may also easily be applied to this case. Solutions for plates where  $a$  is smaller than  $b$  are treated in PART IV, Section 4.1.

### 3.3 Comparison with Experimental Results

Schuman and Back (1930) conducted experiments on individual rectangular flat plates of four different metals, i.e. *Duralumin*, *Stainless Iron*, *Monel Metal* and *Nickel*. Equation (3.12) is compared to these tests in Figure 3.10. The figure also shows the elastic solution, cf. Equation (3.8), Winter's solution cf. Equation (3.14) and the solution by Kármán et al. cf. Equation (3.15). From the figure it appears that all formulae, except the elastic solution, overestimate the post-buckling strength, in some cases considerably. However, it is generally accepted that these experiments are unreliable because of the dubious V-groove supports. Hence, these experiments are not treated further here.

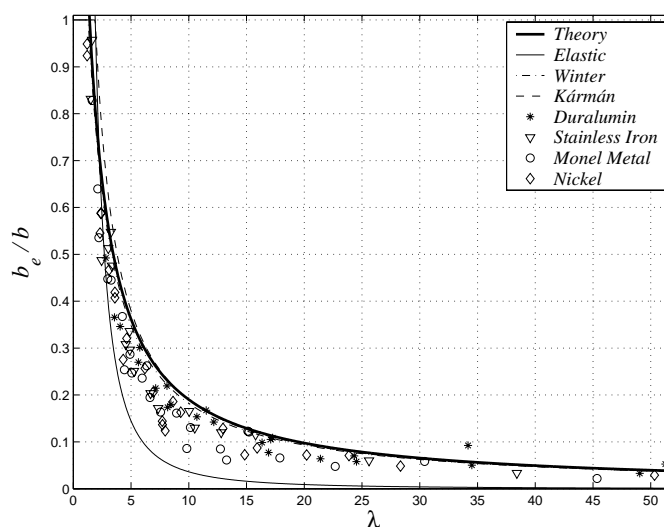


Figure 3.10:  $b_e/b$  as a function of  $\lambda$ , theories compared with tests by Schuman and Back

In Figure 3.11, the theories are compared with more reliable experiments.

The *U-beams* and *I-beams* tests made by Winter (1947) both consisted of specimens made by bolting or welding U-sections together. Winter also used the tests made by *Sechler* (Winter 1947) to verify his method. The specimens in these tests were single plates, unconnected to any adjacent elements. These tests have been shown in Figure 3.11. Furthermore, newer tests by Moxham (1971) are included in the figure. He conducted three test series, denoted *Welded*, *Unwelded* and *Short* in the following. Also, in these tests, all specimens were separate plates. He developed a new test rig, where he could establish the simple support conditions in a reliable way. In the *Welded* series, the longitudinal edges were heat treated in order to induce residual stresses. The *Short* series was conducted on specimens where the loaded edges were slightly longer than the unloaded edges (length-to-width ratio: 0.875). The theoretical effective width of the short specimens is calculated by Equations (4.9) and (4.10) in PART IV. The specimens in the *Welded* and *Unwelded* series all had a length-to-width ratio of 4.0.

The data for all experiments may be found in Appendix I.

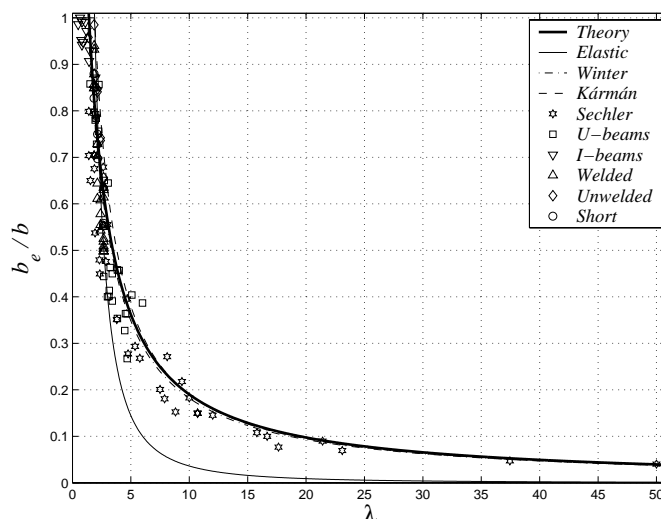


Figure 3.11:  $b_e/b$  as a function of  $\lambda$ , theories and tests

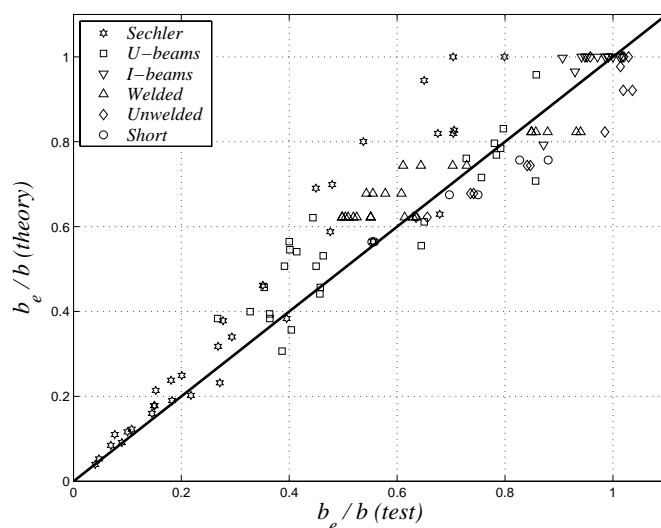


Figure 3.12: Theory versus tests

The agreement with all the tests seems to be very good. In Figure 3.12, the correlation between the present theory and tests is shown in a more illustrative way. For all tests, a mean value of 1.088 and a standard deviation of 16.9 % are obtained. For the separate test series, the following results are obtained:

- *Sechler*: Mean 1.202, standard deviation 17.9 %.
- Winter, *U-beams*: Mean 1.098, standard deviation 18.9 %.
- Winter, *I-beams*: Mean 1.019, standard deviation 4.6 %.
- Moxham, *Welded*: Mean 1.097, standard deviation 12.2 %.
- Moxham, *Unwelded*: Mean 0.931, standard deviation 5.8 %.
- Moxham, *Short*: Mean 0.946, standard deviation 6.4 %.

It may be seen that the tests by *Sechler* deviate somewhat from the theory, especially for  $b_e/b$  close to unity. One explanation for this might be initial imperfections, see Chapter 5. Moreover, he may have applied the same doubtful V-groove supports as Schuman and Back (1930). Without *Sechler*'s tests, a mean value of 1.045 and a standard deviation of 14.4 % are obtained.

## 4 PLATES WITH ONE FREE EDGE

The compressive flange and the transverse web stiffeners in an I-shaped steel plate girder may be considered to be long, rectangular plates simply supported along three of the edges, and free along one longitudinal edge. Determining the post-buckling strength of such plates is presented below.

### 4.1 Rectangular Plates

The considered plate with length  $a$ , width  $b$  and thickness  $t$  is subjected to uniaxial compression,  $n_p = t f_y$ , along an effective width,  $b_e$ , near the supported longitudinal edge.

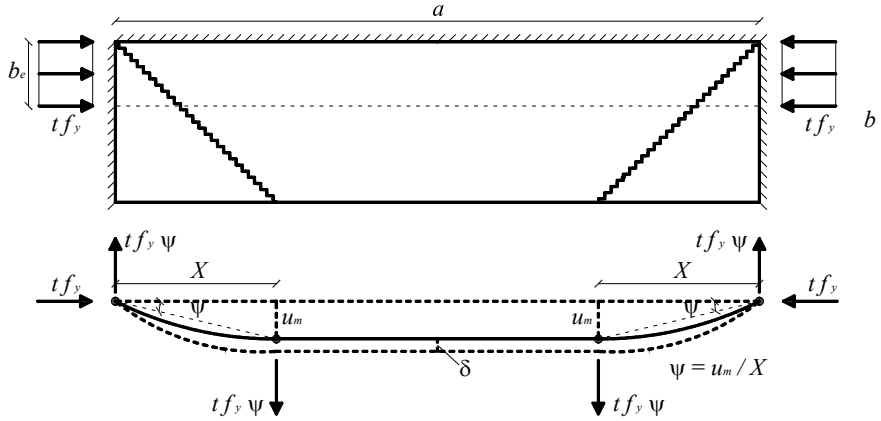


Figure 4.1: Failure mechanism for a rectangular plate with one free edge

The best failure mechanism, with free parameter,  $X$ , is shown in Figure 4.1. It is easily verifiable that plates with length,  $a$ , in the interval,  $2 X \leq a \leq \infty$ , will have the same post-buckling strength. Plates with  $a < 2 X$  require another failure mechanism, which will be treated in Section 4.3.

The two regions with area,  $X b$ , will approximately be subjected to pure torsion. Thus the principal directions are under  $45^\circ$  with the edges, and the principal curvatures are equal, but with opposite sign. In the principal directions, the curvatures are estimated to be, in absolute value, the same as in Equation (3.2). Then the torsional curvature,  $\kappa_{xy}$ , will also be  $\kappa_{xy} = 2 \varepsilon_y / t$  ( $\varepsilon_y = f_y/E$  is the yield strain and  $t$  the thickness), which means that the deflection,  $u_m$ , at the end point of the yield line in the free edge will be

$$u_m = \kappa_{xy} X b = \frac{2 \varepsilon_y}{t} X b = 2 \frac{f_y}{E} \frac{X b}{t} \quad (4.1)$$

For the mechanism shown in Figure 4.1, the external work is for  $\delta = 1$  given by

$$W_e = t f_y \frac{u_m}{X} \frac{b_e^2}{b} \quad (4.2)$$

and the dissipation is

$$W_i = 2 m_p \left( \frac{X}{b} + \frac{b}{X} - \frac{b_e}{X} \right) \quad (4.3)$$

where  $m_p$  is given by Equation (2.1). Hence the effective width,  $b_e$ , may be determined by

$$2 \frac{f_y}{E} b_e^2 + \frac{1}{2} \frac{t^2}{X} b_e - \frac{1}{2} t^2 \left( \frac{X}{b} + \frac{b}{X} \right) = 0 \quad (4.4)$$

The non-dimensional value,  $b_e/b$ , is then given by

$$\frac{b_e}{b} = -\frac{1}{8} \frac{b}{X} \lambda^{-2} + \sqrt{\frac{1}{64} \left( \frac{b}{X} \right)^2 \lambda^{-4} + \frac{1}{4} \left( \frac{X}{b} + \frac{b}{X} \right) \lambda^{-2}} \quad (4.5)$$

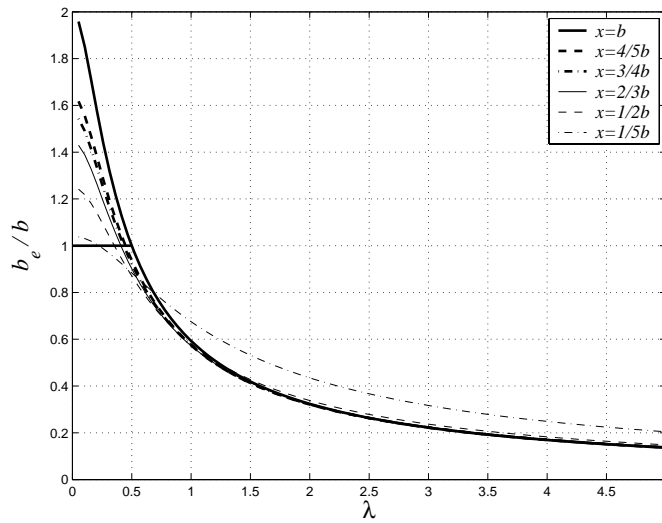


**Figure 4.2:**  $b_e/b$  as a function of  $\lambda$  for different values of  $X$

Equation (4.5) is shown for different values of  $X$  in Figure 4.2. A cut-off at  $b_e/b = 1$  must again be introduced. With this cut-off, it is seen that almost the same load-carrying capacity is obtained for  $X = b$ ,  $X = 4/5 b$  and  $X = 3/4 b$ ; hence  $X = b$  is used in the following calculations.

The effective width for  $X$  equal to  $b$  is found to be

$$\frac{b_e}{b} = -\frac{1}{8} \lambda^{-2} + \sqrt{\frac{1}{64} \lambda^{-4} + \frac{1}{2} \lambda^{-2}} \quad (4.6)$$

which is shown in Figure 4.3. The figure also shows the elastic buckling curve given by Equation (3.8) with  $k = 0.43$ , cf. (Timoshenko and Gere 1961). Again, Poisson's ratio  $\nu = 0.30$  is assumed. The third curve shown is Winter's formula in the form given in EC3 (2006), which may be written as, cf. Equation (1.6),

$$\frac{b_e}{b} = \frac{\pi \sqrt{k}}{\sqrt{12(1-\nu^2)}} \lambda^{-1} \left( 1 - 0.188 \frac{\pi \sqrt{k}}{\sqrt{12(1-\nu^2)}} \lambda^{-1} \right) \quad (4.7)$$

Here,  $k = 0.43$  and  $\nu = 0.30$  are again used. It is found that the theory gives a slightly larger post-buckling strength than Winter's solution.

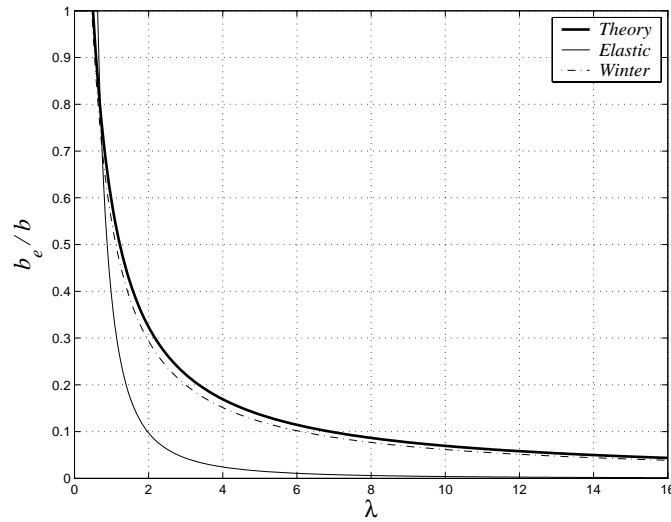


Figure 4.3:  $b_e/b$  as a function of  $\lambda$

### 4.2 Comparison with Experimental Results

Figure 4.4 shows four test series compared with Equation (4.6). The figure also shows the elastic solution cf. Equation (3.8) and Winter's solution cf. Equation (4.7).

In the test series *Plates* (Bambach and Rasmussen 2004), the specimens were single plates, unconnected to any adjacent elements. These authors applied the test rig suggested by Moxham (1971) which enabled them to establish simple support conditions in a reliable way.

The series *Stub-column*, *Beams* (Kalyanaraman et al. 1977) and *I-beams* (Winter 1947) all consisted of specimens made by bolting or welding U-sections together. The data for all experiments may be found in Appendix J.

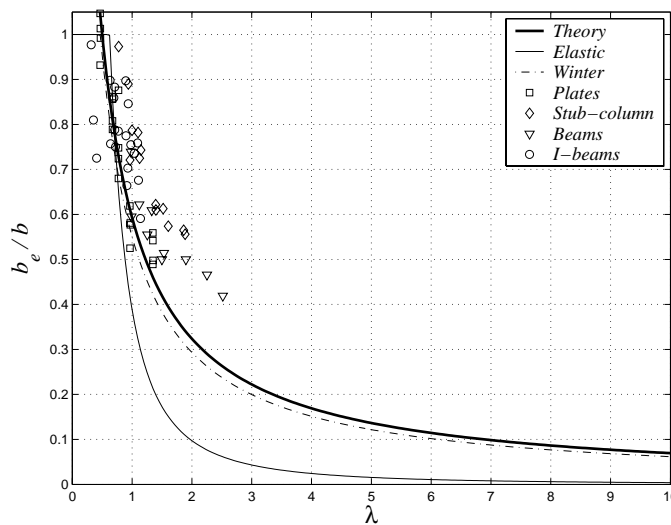
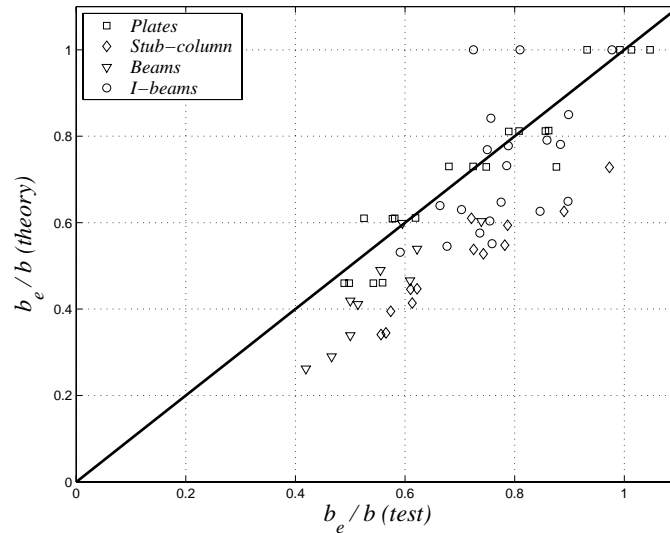


Figure 4.4:  $b_e/b$  as a function of  $\lambda$ , theories and tests



**Figure 4.5:** Theory versus tests

In Figure 4.5, the correlation between theory and test is shown. For all tests, a mean value of 0.877 and a standard deviation of 15.7 % are obtained. For the separate test series, the following results are obtained:

- Bambach & Rasmussen, *Plates*: Mean 0.981, standard deviation 8.5 %.
- Kalyanaraman et al., *Stub-column*: Mean 0.717, standard deviation 6.2 %.
- Kalyanaraman et al., *Beams*: Mean 0.790, standard deviation 12.1 %.
- Winter, *I-beams*: Mean 0.925, standard deviation 16.7 %.

The theory seems to underestimate the post-buckling strength for the tests *Stub-column* and *Beams*. Kalyanaraman et al. (1977) stated that the mean value of the elastic buckling coefficient was measured to be around  $k = 0.85$ . This number shows that the longitudinal edge cannot have been simply supported, since for a plate with a simply supported longitudinal edge  $k = 0.43$ . For a fixed edge  $k = 1.28$  according to the elastic theory, cf. (Timoshenko & Gere 1961). The test series *I-beams* is defected by a large scatter. Winter (1947) gives several explanations for the large scatter. On the other hand, the test series *Plates*, with the most reliably established boundary conditions, shows a very good agreement with the theory.

### 4.3 Square Plates

Square plates in uniaxial compression with one free edge require another failure mechanism than the one shown in Figure 4.1 valid for rectangular plates.

The optimal mechanism for a square plate is drawn in Figure 4.6. It has the free parameter,  $X$ , which is set at  $X = \frac{1}{2} b$ . The plate is again subjected to uniaxial compression,  $n_p = t f_y$ , along an effective width,  $b_e$ , close to the support.

In this case, two work equations must be derived; one corresponding to  $b_e < X$  and one corresponding to  $b_e > X$ , respectively.

The deflection at maximum load,  $u_m$ , is taken as the deflection of a beam in the direction of the uniaxial compression with the curvature given by Equation (3.2). Thus

$$u_m = \frac{1}{8} \frac{2 \varepsilon_y}{t} b^2 = \frac{1}{4} \frac{f_y}{E} \frac{b^2}{t} \quad (4.8)$$

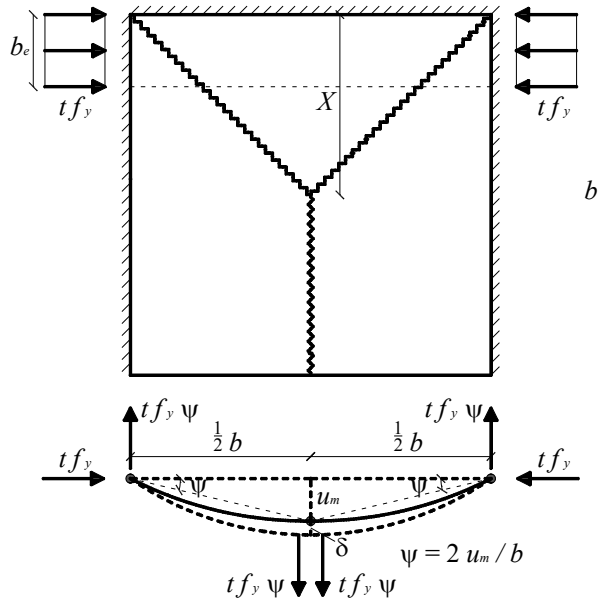


Figure 4.6: Failure mechanism for a square plate with one free edge

The work equations show that the effective width is determined by:

For  $b_e/b \leq X/b = 1/2$ :

$$\frac{f_y}{E} b_e^2 + \frac{t^2}{b} b_e - \frac{3}{2} t^2 = 0 \quad (4.9)$$

⇒

$$\frac{b_e}{b} = -\frac{1}{2} \lambda^{-2} + \sqrt{\frac{1}{4} \lambda^{-4} + \frac{3}{2} \lambda^{-2}} \quad (4.10)$$

For  $b_e/b \geq X/b = 1/2$ :

$$\left( \frac{f_y}{E} b + \frac{t^2}{b} \right) b_e = \frac{3}{2} t^2 + \frac{1}{4} \frac{f_y}{E} b^2 \quad (4.11)$$

⇒

$$\frac{b_e}{b} = \frac{\frac{1}{4} \lambda^2 + \frac{3}{2}}{\lambda^2 + 1} \quad (4.12)$$

In the above equations,  $\lambda$  is given by Equation (3.7),  $b$  is the total width,  $t$  the thickness,  $E$  Young's modulus and  $f_y$  is the yield stress.

Equations (4.10) and (4.12) are shown in Figure 4.7 together with the elastic buckling solution, Equation (3.8), and Winter's solution, Equation (4.7).

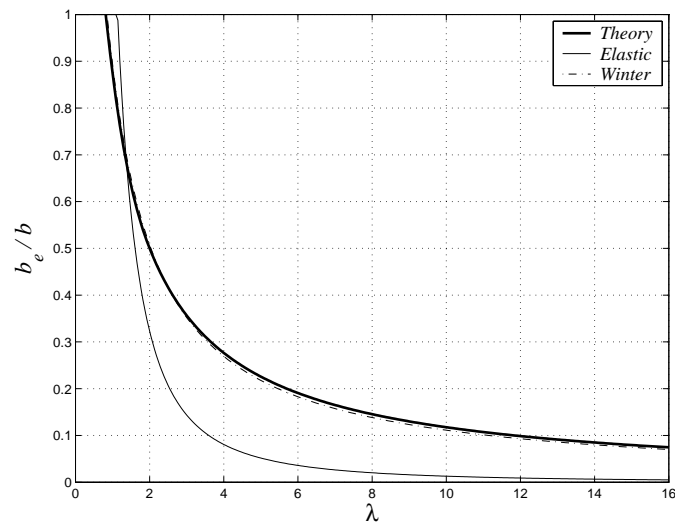


**Figure 4.7:**  $b_e/b$  as a function of  $\lambda$

Here, the buckling coefficient  $k = 1.43$  is applied, cf. (Timoshenko and Gere 1961), and Poisson's ratio is taken to be  $\nu = 0.30$ . Again, the theoretical solution gives almost the same result as Winter's semi-empirical solution. Unfortunately, no tests have been found in the literature to verify the theory. This however is not particularly important, since square plates with one free edge are seldom used in practice.

## 5 IMPERFECTIONS

Approximately imperfections may be taken into account by adding an initial deflection to the deflection used in the above calculations. Thus it is tacitly assumed that the imperfection has the same form as the deflected shape used before.

When considering rectangular plates supported along all edges, the deflection at maximum load is determined by, cf. Equation (3.3),

$$u_m = \frac{1}{4} \frac{f_y}{E} \frac{b^2}{t} + u_i \quad (5.1)$$

where  $u_i$  is the initial deflection,  $f_y$  the yield stress,  $E$  Young's modulus,  $b$  the total width and  $t$  is the thickness. Solving the work equation as shown in Section 3.1, leaves the result

$$\frac{b_e}{b} = \frac{-\lambda^{-2} + \sqrt{\lambda^{-4} + 4\lambda^{-2} \left( 4\lambda^{-2} \frac{u_i}{t} + 1 \right)}}{4\lambda^{-2} \frac{u_i}{t} + 1} \quad (5.2)$$

For an imperfection proportional to the thickness, the term,  $u_i/t$ , will be a constant. Another way of taking imperfections and other unknown parameters into account is simply to introduce an empirical coefficient,  $\mu$ , in the deflection formula. The deflection at maximum load may then be written

$$u_m = \mu \frac{1}{4} \frac{f_y}{E} \frac{b^2}{t} \quad (5.3)$$

The effective width is found to be

$$\frac{b_e}{b} = -\frac{1}{\mu} \lambda^{-2} + \sqrt{\frac{1}{\mu^2} \lambda^{-4} + 4 \frac{1}{\mu} \lambda^{-2}} \quad (5.4)$$

Imperfections may explain the large deviations in the tests by Sechler (Winter 1947), both from Winter's formula and the present theoretical estimate.

In Figure 3.12, it was shown that the tests by Sechler coincided closely with the theoretical estimate for small values of  $b_e/b$ , i.e. large values of  $\lambda$ , while for low values of  $\lambda$ , the deviation was large. For the tests by Sechler shown in Figure 3.12, the mean value is 1.202. By requiring the mean value 1.0 and by applying Equation (5.3) to find the imperfection coefficient,  $\mu = 1.52$  is found. The correlation between the tests and the theory, cf. Equation (5.4), with  $\mu = 1.52$  is shown in Figure 5.1. In this way, a smaller deviation is achieved for low values of  $\lambda$ , but the scatter is still large.

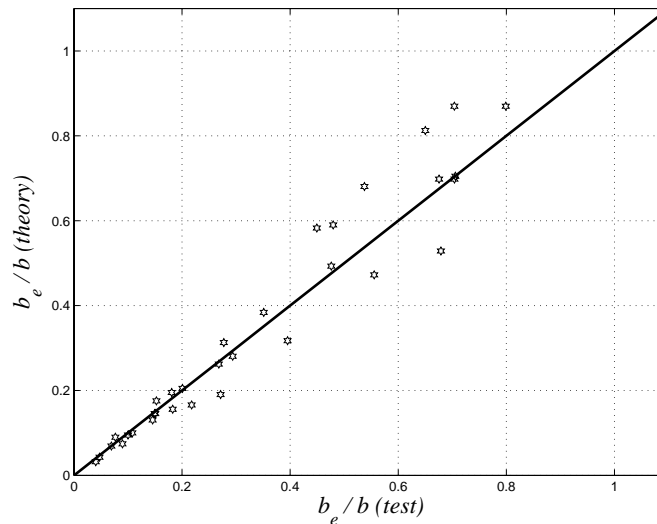


**Figure 5.1:** Theory versus tests for  $\mu = 1.52$

Unfortunately, the report by Sechler (1933) referred to by Winter has not yet been available to the author. From Winter's reference it is only possible to deduce the value of  $\lambda$ , while the thickness of the specimens remains unknown. By applying Equation (5.2) and require the mean value 1.0,  $u_i/t = 1.94$  is found. The correlation between the tests and the theory with  $u_i/t = 1.94$ , cf. Equation (5.2), is shown in Figure 5.2.

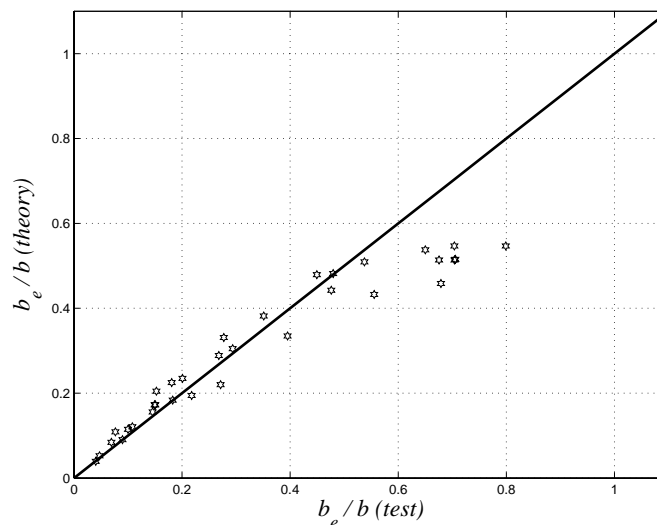


**Figure 5.2:** Theory versus tests for  $u_i/t = 1.94$

It appears that the effect is small for large values of  $\lambda$ , and large for low values of  $\lambda$ , which is precisely the requirement for removing the discrepancy. However, the effect on the result for low values of  $\lambda$  seems to be too great. Thus by applying Equation (3.12), the theory overestimates the load-carrying capacity for low values of  $\lambda$ , while the opposite is achieved by applying Equation (5.2). Hence it is not possible to verify Equation (5.2) by these tests.

Apart from initial imperfections, there may of course be other explanations for the large deviations found in the Sechler tests. In tests, it is very difficult to correctly establish the ideal support conditions. The supports require the four edges of the initial mid-plane of the plate to remain in the same plane at all times. A solution was

suggested by Schuman and Back (1930) for the case of single plate specimens. In their tests, the specimens were supported by V-grooves, which cause any initial curvature of the edges to increase, which may again cause failure at a lower load than otherwise expected. The effect will be relatively larger for the thicker specimens. Therefore problems related to V-grooves might also explain the deviations in the Sechler tests. However, this is quite hypothetical, since at the moment it is not known if this kind of support was even used in the tests.

## 6 OTHER APPLICATIONS OF THE THEORY

The simple theory developed above may be extended to apply to a large number of practically important cases that are not treated here.

Firstly, an external lateral load may be taken into account by simply adding the work done by the lateral load to the external work, calculated as above. Further, biaxial compressive loads may be treated in the same manner without difficulties. Stiffeners and the compression flange in plate girders may be calculated by formulae given above. Fixed supports may be treated by adding the contribution from the negative yield line at the fixed supports to the dissipation. However, the deflection at maximum load must also be changed, so that it corresponds to the fixed boundary conditions.

Finally, it is probably also possible to calculate in-plane bending loads. However, new mechanisms have to be invented in this case.

To further illustrate the case of fixed boundary conditions and lateral load, the square plate in Figure 3.5 may be considered again. If the two unloaded edges are assumed clamped, and the loaded edges still simply supported, the dissipation changes to, cf. Equation (3.10),

$$W_i = 8 m_p \left( \frac{3}{2} - \frac{b_s}{b} \right) \quad (6.1)$$

The external work is still given by Equation (3.9), i.e.

$$W_e = 8 t f_y u_m \frac{b_s^2}{b^2} \quad (6.2)$$

where the deflection at maximum load,  $u_m$ , must be estimated so it corresponds to the fixed boundary conditions.

Besides the uniaxial compression, if the plate is also subjected to a load,  $p$ , per unit area over the entire area of the plate, then the contribution to the external work from the lateral load is

$$W_e = \frac{1}{3} p b^2 \quad (6.3)$$

which is added to the contribution in Equation (6.2).

Equations (6.1) – (6.3) are all shown for a displacement increment,  $\delta$ , equal to unity.

## 7 CONCLUSION

It is shown that extremely simple estimates of the post-buckling strength of plates with in-plane loading may be obtained by using plastic solutions for the deflected shape. This shape must be known before the calculation can be carried out. It seems that useful estimates of the deflected shape may be found using simple formulae from beam theory and plate theory.

Initially, the calculation procedure is illustrated by simple solutions for columns. It seems that the theory is able to treat columns as well. However, the emphasis in this part is attached to plates, so columns are left for future work.

Solutions for plates are derived for the two practically important cases: Plates supported along all edges and plates with one free edge. In both cases, the theory is applied on both square and rectangular plates.

Furthermore, it is shown how imperfections may be taken into account. Finally, it is shortly explained how the theory may be extended to a large number of other practically important cases.

The results have been compared with the well-known formulae of Winter and with tests. The agreement in both cases is very good.

## 8 REFERENCES

- BAMBACH, M. R. and RASMUSSEN, K. J. R. (2004). Tests on Unstiffened Plate Elements under Combined Compression and Bending. *J. Struct. Eng. ASCE* **130**(10), 1602-1610.
- BRYAN, G. H. (1891). On the Stability of a Plane Plate under Thrusts in Its Own Plane, with Applications to the Buckling of the Sides of a Ship. *Proc. Lond. Math. Soc.* **22**.
- EUROPEAN COMMITTEE FOR STANDARDISATION (EC3 1993). *Eurocode 3: Design of Steel Structures – Part 1-1: General Rules and Rules for Buildings*. EN 1993-1-1: 1993. Brussels: CEN.
- EUROPEAN COMMITTEE FOR STANDARDISATION (EC3 2005). *Eurocode 3: Design of Steel Structures – Part 1-1: General Rules and Rules for Buildings*. EN 1993-1-1: 2005. Brussels: CEN.
- EUROPEAN COMMITTEE FOR STANDARDISATION (EC3 2006). *Eurocode 3: Design of Steel Structures – Part 1-5: Plated Structural Elements*. EN 1993-1-5: 2006. Brussels: CEN.
- HIRIYUR, B. K. J. and SCHAFER, B. W. (2004). Yield-Line Analysis of Cold-Formed Steel Members. *Submitted to International Journal of Steel Structures*, August 2004.
- JOHANSEN, K. W. (1943). *Brudlinieteorier*. Copenhagen: Gjellerup. An English translation is found in: JOHANSEN, K. W. (1962). *Yield Line Theories*. London: Cement and Concrete Association.
- KALYANARAMAN, V., WINTER, G. and PEKOZ, T. (1977). Unstiffened Compressed Elements. *J. Struct. Div. ASCE*, **103**(9), 1833-1848.
- KÁRMÁN, T. VON, SECHLER, E. E. and DONNELL, L. H. (1932). The Strength of Thin Plates in Compression. *Trans. ASME*, **54**, 53-57.
- MOXHAM, K. E. (1971). *Buckling Tests on Individual Welded Steel Plates in Compression*. Report CUED/C-Struct/TR.3. Cambridge: University of Cambridge.
- MURRAY, N. W. (1984). *Introduction to the Theory of Thin-Walled Structures*. Oxford: Clarendon Press, Oxford Science Publications.
- NIELSEN, M. P. (1998). *Limit Analysis and Concrete Plasticity* (2nd ed.). Boca Raton, Florida: CRC Press.
- SCHUMAN, L. and BACK, G. (1930). *Strength of Rectangular Flat Plates under Edge Compression*. Technical Report No. 356: National Advisory Committee for Aeronautics.
- SECHLER, E. E. (1933). *The Ultimate Strength of Thin Flat Sheet in Compression*. Publication No. 27. Pasadena: Guggenheim Aeronautics Laboratory, California Inst. of Technology.
- TIMOSHENKO, S. P. and GERE, J. M. (1961). *Theory of Elastic Stability* (2nd ed.). New York: McGraw-Hill Book Co., Inc.
- WINTER, G. (1947). Strength of Thin Steel Compression Flanges. *Trans. ASCE, Paper No. 2305*, **112**, 527-554.
- ZHAO, X. L. (2003). Yield Line Mechanism Analysis of Steel Members and Connections. *Structural Analysis and CAD, Prog. Struct. Engng. Mater.*, **5**, 252-262.

## 9 NOTATION

$a$	plate length
$b$	plate width
$b_e$	total effective width
$b_s$	width of effective strip
$f_y$	yield stress
$k$	elastic buckling coefficient
$m$	bending capacity of a yield line per unit length; fictitious moment
$m_b$	bending moment per unit length in a yield line
$m_p$	plastic yield moments per unit length
$n$	normal force per unit length
$n_p$	load-carrying capacity per unit length in pure compression or tension
$m_{px}, m_{py}$	plastic yield moment in the $x$ -direction and the $y$ -direction, respectively
$p$	lateral load per unit area
$t$	thickness
$u, u_A, u_B$	deflection; deflection at point $A$ and $B$ , respectively
$u_i$	deflection from imperfections
$u_m$	deflection at maximum load
$x, y$	coordinates in a Cartesian $x,y$ -system of coordinates
$A$	cross-sectional area
$C$	empirical coefficient
$E$	Young's modulus
$L$	length
$M$	total moment
$M_p$	plastic yield moment
$N$	normal force
$N_{cr}$	critical buckling load
$N_p$	load-carrying capacity in pure compression or tension
$W_e, W_i$	external work and dissipation, respectively
$X, Y$	free optimisation parameters
$\alpha$	parameter (shape of curvature function); imperfection factor
$\delta$	displacement increment
$\varepsilon_y$	yield strain
$\kappa, \kappa_{xy}$	curvature and torsional curvature, respectively
$\lambda$	non-dimensional parameter
$\lambda_r$	non-dimensional slenderness ratio according to EC3
$\mu$	empirical coefficient
$\nu$	Poisson's ratio
$\sigma$	normal stress
$\sigma_e$	edge stress
$\psi$	relative deflection increment
$\Delta$	difference
$\Phi$	EC3 parameter for calculation of columns

---

# **PART IV**

---

## **PATCH LOADING ON PLATE GIRDERS** **- A Simplified Theoretical Approach**



# PATCH LOADING ON PLATE GIRDERS

## - A Simplified Theoretical Approach

### 1 INTRODUCTION

When designing a plate girder according to the plastic tension field method, cf. PART II, it is assumed that transverse web stiffeners are added where concentrated loads act. However, this is not always possible to fulfil in practice, as the plate girder may, for instance, be subjected to wheel loads, loads from purlins and roller loads during construction. It is therefore necessary to check the unstiffened web, under the edge compressive loading, to ensure no localised failure will occur. In this part, a simplified method based on the theory of plasticity is presented.

The type of loading under consideration is illustrated in Figure 1.1, where a part of a plate girder is subjected to a uniform load along the length,  $c$ , on top of the flange. The loaded length,  $c$ , may vary between being very small or extended along the entire length of the web panel,  $b$ . This kind of loading on plate girders is popularly known as *patch loading*.

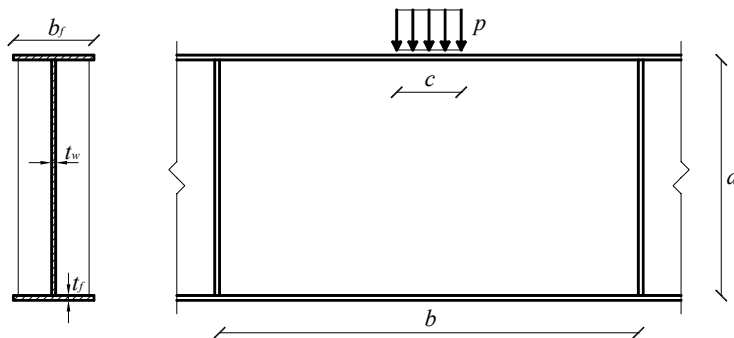


Figure 1.1: Plate girder subjected to patch loading

Patch loading on plate girders has been investigated by many researchers over the past fifty years. Theoretical investigators have concentrated on two main aspects of the problem. First, rigorous analytical and numerical solutions have been obtained for the elastic critical loads of web panels, with assumed idealised boundary conditions, e.g. (Zetlin 1955). These kinds of solutions show little or no correlation with experimental failure loads. This is due to the post-buckle reserve of strength possessed by restrained thin panels and interaction between the web and the flanges cf. (Roberts 1983). However, elastic critical loads may still have significance in design for the serviceability limit-state.

Second, simple empirical and semi-empirical methods for predicting the failure load have been proposed by several authors, differing only slightly in form. Some of these semi-empirical formulae are summarised in the following section.

Due to the complex material and geometrically non-linear nature of the problem, it has never been possible to derive a fully consistent theory. The present method is derived on the basis of the theory of plasticity without any empirical modification, but some assumptions that are difficult to justify are made in order to keep the theory as simple as possible, and to allow application of the theory in practical design projects. The general assumptions are described in Chapter 2. In Chapters 3 and 4, the theory is derived in cases where the patch load is the only load applied on the girder.

If the compression flange in a plate girder is subjected to a large normal force, and if the stiffness of the web plate is small, the normal force may lead to vertical buckling of the compression flange in the plane of the web. This phenomenon is popularly termed *flange induced buckling*, and is touched upon in Chapter 5.

In Chapter 6 it is shown how one would take the uniaxial tension stresses in the web into account. These stresses occur in the web when the girder is designed according to the plastic tension field method.

### 1.1 Other Methods

At the beginning of the last century, Sommerfield (1906), Timoshenko (1910) and Timoshenko and Gere (1961) were the first to obtain approximate solutions for the elastic critical load of a plate subjected to equal and opposite concentrated forces applied in the midpoint of the two sides. Khan and Walker (1972) obtained solutions for the same problem, but with the load distributed along a finite length,  $c$ . Zetlin (1955) provided a more detailed study of the problem using energy methods. White and Cottingham (1962) obtained solutions for clamped boundaries. The elastic solutions will not be treated here. A detailed summary of the elastic solutions is found in (Roberts 1983).

Granholm (1976) carried out a number of tests, and based on these tests he proposed that the ultimate load-carrying capacity may be predicted using the following simple formula:

$$P_u = 9000 t_w^2 \quad (1.1)$$

where the web thickness,  $t_w$ , is in millimetres and  $P_u$  is in Newton.

Bergfelt (1979) investigated a simple model based on the analogy of a beam on an elastic foundation, the flange being the beam and the web being the elastic foundation. The difficulty with this approach was in determining the equivalent spring stiffness of the web. Bergfelt also recognised the unsatisfactory nature of Equation (1.1) being dimensionally dependent, and proposed the alternative empirical formula

$$P_u = 4.5 \cdot 10^{-2} E t_w^2 \quad (1.2)$$

where  $E$  is Young's modulus in mega Pascal.

Several researchers have conducted tests to investigate the complex problem, e.g. Bergfelt and Hovik (1968, 1970); Bergfelt (1979); Skaloud and Novak (1975); Drdacky and Novotny (1977); Roberts and Rockey (1979) and Roberts (1983). The majority of the available test data has been summarised by Roberts and Rockey (1979). The above-mentioned tests are also used to verify the present theory, see Sections 3.3 and 4.3 respectively.

Each of the test series was followed by a new empirical formula, proposed by the respective author. Some of the authors have proposed several formulae. Only the proposal by Roberts and Rockey (1979) will be dealt with further here. They developed a semi-empirical method based partly on the upper-bound theorem of the theory of plasticity. The failure mechanism is shown in Figure 1.2. Here four plastic hinges form in the loaded flange accompanied by yield lines in the web. An estimate of the deflection of the flange just prior to collapse was made using elastic theory. By deriving the work equation, the length,  $\beta$ , was found by optimisation. The length,  $\alpha$ , must be determined empirically, and in the latest version of the method, cf. (Roberts 1983), it was simply taken that  $\alpha = 25 t_w$ ,  $t_w$  still being the web thickness.

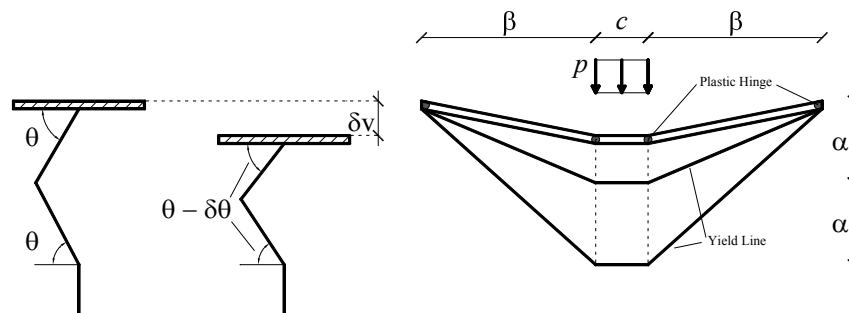


Figure 1.2: Failure mechanism according to Roberts and Rockey

Finally, the following two formulae were proposed:

$$P_u = 0.5 t_w^2 \sqrt{E f_{yw} \frac{t_f}{t_w} \left( 1 + \frac{3c}{d} \left( \frac{t_w}{t_f} \right)^{1.5} \right)} \quad (1.3)$$

$$P_u = 2 \sqrt{b_f t_f^2 f_{yf} f_{yw} t_w + f_{yw} t_w c} \quad (1.4)$$

Here,  $t$  is the thickness,  $b$  the width,  $f_y$  the yield stress with indexes  $f$  for flange and  $w$  for web.  $E$  is Young's modulus,  $d$  the girder depth and  $c$  is the length of the patch load.

Equation (1.3) is derived from the failure mechanism in Figure 1.2. This kind of failure is popularly termed *web crippling*, and the formula is adopted in EC3 (1993). The formula has been changed completely in the newest edition of EC3 (2006). The new formula leads to a very cumbersome calculation procedure. A description of the new EC3 rules may be found in (Johansson et al. 2001).

Equation (1.4) is based on failure by initiation of yielding in the web.

## 2 ASSUMPTIONS

The semi-empirical formula proposed by Robert and Rockey (1979), cf. Equation (1.3), is not satisfactory from the author's point of view. Firstly, the failure mechanism, cf. Figure 1.2, is not fully geometrically possible. The mechanism may be made geometrically possible if extra yield lines are added, cf. the dashed lines shown in the figure. Second, the work equation is derived in an uncertain way, especially with regards to the determination of the out-of-plane deflection of the web. However, the most important factor is that the method assumes that all failures induced by patch loading tend to be very localised, only involving a very small part of the web plate. This is certainly not always observed in tests. In several of the experiments found in the literature, the whole web plate seems to buckle, and the web crippling phenomenon tends to occur after the maximum load is reached. This is illustrated in Figure 2.1, where the contour lines of the web plate for specimen A21, Bergfelt's tests (Bergfelt 1979), are shown before maximum load (64 kN), at maximum load (84 kN), and after maximum load (82 kN). The figure also shows the lateral web deflection in the section under the loading point.

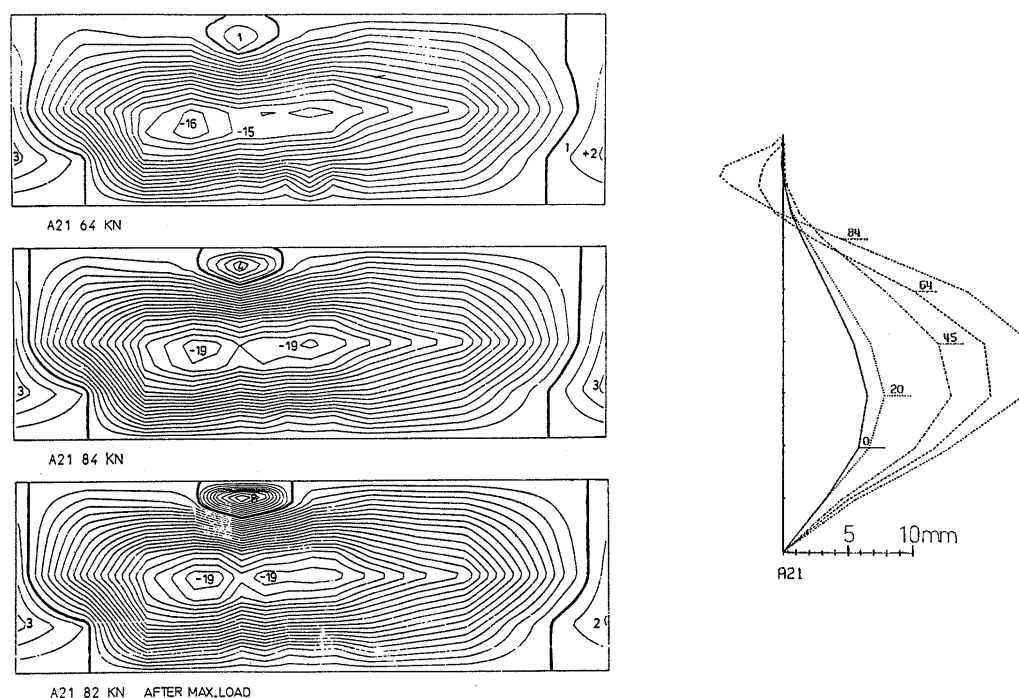


**Figure 2.1:** Contour lines and lateral deflection of the web plate for specimen A21<sup>1</sup>

In Figure 2.1, it is seen that the whole web plate is active. At maximum load, the deflection of the midpoint of the plate reaches -19 mm, and near the patch load +4 mm. After the maximum load is reached, the deflection near the patch load becomes twice as large, but the deflection in the middle of the web plate stays the same.

In the present theory, it is therefore assumed that the whole web panel is active. When the buckling mechanism develops, a redistribution of the stresses occurs. It is assumed that the true stress field is simplified using an effective area subjected to the yield

<sup>1</sup> The figure is taken from (Bergfelt 1979).

stress of the web material. This is the same approach as applied in PART III. Thus the stresses in the web concentrate in strips near the transverse web stiffeners. The post-buckling strength is calculated using the same assumptions as described in Chapter 2 in PART III.

Near the flange, the stresses in the web are assumed to be uniformly distributed. In order to transform the concentrated stresses in the strips to uniform stresses near the flange, an internal beam is imagined. This internal beam consists of the flange and the top part of the web plate.

The web plate, the internal beam and the flange are considered separately. The post-buckling strength of the web is given by the stresses in the strips. Thereafter, the stresses are uniformly distributed under the flange and utilised in the flange mechanism as an upwards, uniform reaction.

As a conservative assumption, all boundaries are considered to be simply supported, i.e. the boundaries at the connections between web and stiffeners and between web and flange, respectively.

### 3 PLATE GIRDERS WITH SQUARE WEB PANELS

First, the simplest case is treated, where the loaded web panel of the girder is square, see Figure 3.1.

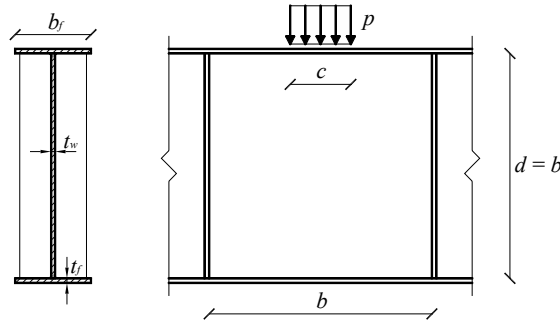


Figure 3.1: Plate girder with a square web panel

#### 3.1 The Web Mechanism

The post-buckling strength of the web is determined by calculating the effective width,  $b_e$ , done by applying the failure mechanism shown in Figure 3.2. The two strips with width,  $b_s$ , are subjected to a uniform load equal to the yield stress of the web,  $f_{yw}$ , multiplied by the thickness,  $t_w$ . Note that  $b_e = 2 b_s$ .

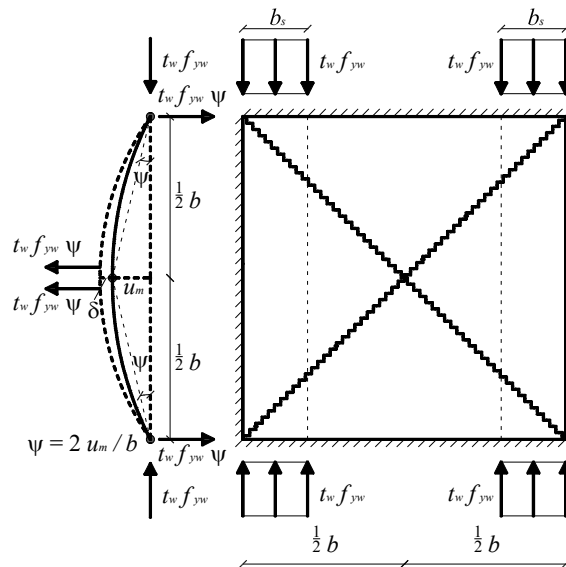


Figure 3.2: Simply supported square plate subjected to uniaxial compression along strips of width  $b_s$

The solution for a square plate simply supported along all edges is, cf. Equation (3.12) in PART III,

$$\frac{b_e}{b} = -\lambda^{-2} + \sqrt{\lambda^{-4} + 4\lambda^{-2}} \quad (3.1)$$

Here  $b_e/b \leq 1$  is required, and  $\lambda$  is given by

$$\lambda = \frac{b}{t_w} \sqrt{\frac{f_{yw}}{E}} \quad (3.2)$$

The force sustained by the web equals  $b_e f_{yw} t_w$ , and is utilised in the flange mechanism as an upwards, uniform load,  $n$ , see Section 3.2. Hence the internal beam, consisting of the compression flange and a part of the web plate,  $x$ , see Figure 3.3, must be able to transfer the uniform load,  $n$ , to the two reactions,  $\frac{1}{2} b_e f_{yw} t_w$ . It is assumed that the internal beam is simply supported. In reality the supports will act as fixed supports in the presence of adjacent web panels. Here, simple supports are applied in general as a conservative assumption.

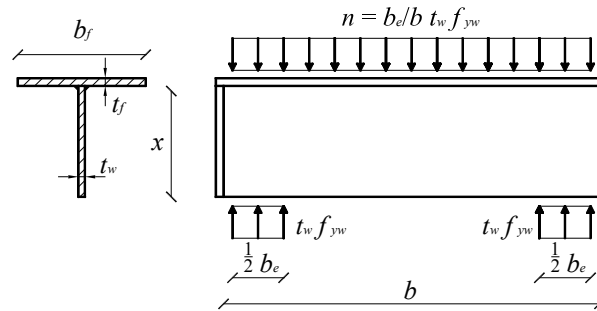


**Figure 3.3:** Internal beam simply supported by two strips

In order to keep the theory as simple as possible, the compressive stresses in the beam are assumed concentrated in the compression flange, and the tensile stresses are assumed uniformly distributed along the part,  $x$ , of the web plate. The plastic yield moment of the internal beam,  $M_p$ , then equals:

$$M_p = \frac{1}{2} x^2 t_w f_{yw} \quad (3.3)$$

Equilibrium implies that, cf. Figure 3.3,

$$\frac{1}{8} n b^2 \left(1 - \frac{b_e}{b}\right) = \frac{1}{2} x^2 t_w f_{yw} \quad (3.4)$$

Solving for  $x$  renders:

$$x = \frac{1}{2} \sqrt{b_e b - b_e^2} \quad (3.5)$$

If the strength of the flange is small, there might be stresses in the flange larger than the yield stress of the flange,  $f_{yf}$ . Hence a part of the compression must be carried by the web or  $x$ , and thereby,  $b_e$  must be reduced. In the latter case:

$$x_f = \frac{b_f t_f f_{yf}}{t_w f_{yw}} \quad (3.6)$$

Here,  $t$  is thickness,  $b$  the width,  $f_y$  the yield stress with indexes  $f$  for flange and  $w$  for web

Requiring  $x$  equal to  $x_f$ , and solving for  $b_e$ , leads to

$$b_e = \frac{1}{2}b - \frac{1}{2}\sqrt{b^2 - 16x_f^2} \quad (3.7)$$

If the flange is thin, buckling of the flange might also be a problem, hence the width,  $b_f$ , in Equation (3.6) must be replaced by the effective width of the flange determined by Equation (4.6) in PART III.

If the plastic yield moment of the internal beam is calculated by including a part of the web in the compression zone, the value of  $x$  will only differ slightly from the value determined by applying Equation (3.3).

### 3.2 The Flange Mechanism

In the failure mechanism for the flange of the girder, it is assumed that four plastic hinges will form. The patch load,  $p$ , acts on the flange along the length,  $c$ . At the two ends of this length, *inner plastic hinges* will develop. At a distance,  $\beta$ , away from the load, *outer plastic hinges* will develop in both ends, see Figure 3.4.

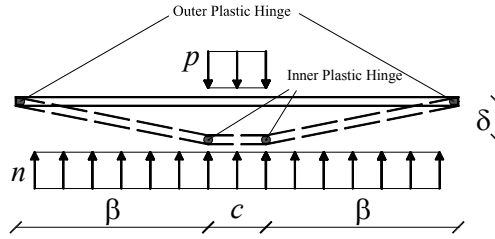


Figure 3.4: Flange mechanism with four plastic yield hinges

Equating the external work and the dissipation for a displacement increment  $\delta = 1$ , the work equation is

$$c p - n(c + \beta) = 4 \frac{M_{pf}}{\beta} \quad (3.8)$$

where  $n$  is the upwards, uniform load corresponding to the post-buckling strength of the web, and  $M_{pf}$  is the plastic yield moment of the flange given by

$$M_{pf} = \frac{1}{4} t_f^2 b_f f_{yf} \quad (3.9)$$

where  $t_f$ ,  $b_f$  and  $f_{yf}$  are the thickness, width and yield stress of the flange, respectively. The ultimate load-carrying capacity,  $P_u$ , is then determined as

$$P_u = c p = t_f^2 f_{yf} \frac{b_f}{\beta} + n(c + \beta) \quad (3.10)$$

If the uniformly distributed load,  $n$ , is constant and independent of the length,  $\beta$ , minimising  $P_u$  with regard to  $\beta$  gives

$$\beta = \sqrt{\frac{b_f t_f^2 f_{yf}}{n}} \quad (3.11)$$

Inserting Equation (3.11) into Equation (3.10), and utilising  $n = t_w f_{yw}$ , the same result as that of Roberts, based on failure by initiation of yielding in the web, is found, cf. Equation (1.4).

However, when the post-buckling strength of the web plate is determined by Equation (3.1),  $n$  will depend on  $\beta$ , i.e.

$$n = \frac{t_w f_{yw} b_e}{c + 2\beta} \quad (3.12)$$

Inserting this into Equation (3.10) leads to

$$P_u = t_f^2 f_{yf} \frac{b_f}{\beta} + t_w f_{yw} b_e \frac{c + \beta}{c + 2\beta} \quad (3.13)$$

Minimising  $P_u$  with regard to  $\beta$  shows that a minimum for  $P_u$  is found for  $\beta \rightarrow \infty$ , hence the two outer plastic hinges will always form at the nearest web stiffeners, i.e.

$$\beta = \frac{1}{2}(b - c) \quad (3.14)$$

By inserting  $\beta$  according to Equation (3.14) into Equation (3.13), the load-carrying capacity is found to be

$$P_u = 2t_f^2 f_{yf} \frac{b_f}{b - c} + \frac{1}{2}t_w f_{yw} \frac{b_e}{b}(b + c) \quad (3.15)$$

To sum up the notations,  $b$  is the web panel width (distance between two adjacent stiffeners),  $c$  the patch load length,  $b_e$  the calculated effective width of the web plate, by Equation (3.1) or Equation (3.7),  $t_f$  and  $t_w$  the flange and web thickness, respectively,  $b_f$  the flange width, and finally  $f_{yf}$  and  $f_{yw}$  are the yield stress of the flange and web material, respectively.

For a mechanism where only one inner plastic hinge develops in the midpoint of the length,  $c$ , the load-carrying capacity is given by

$$P_u = 2t_f^2 f_{yf} b_f \frac{b + c}{b^2} + \frac{1}{2}t_w f_{yw} \frac{b_e}{b}(b + c) \quad (3.16)$$

Whether one or two inner hinges will form in the flange depend mainly on the stiffness of the flange and a possible loading plate. For large stiffnesses, one inner hinge will form, otherwise two inner hinges will form.

In all the tests presented in Sections 3.3 and 4.3, the length,  $c$ , along which the load is transferred, is relatively small, thus there is only a minor influence on the load-carrying capacity regardless of whether one or two inner hinges form.

### 3.3 Comparison with Experimental Results

The experimental results used to verify the theories for plate girders with square web panels are all carried out on short specimens of the form shown in Figure 3.5. In all tests,  $b$  is equal to  $d$ .

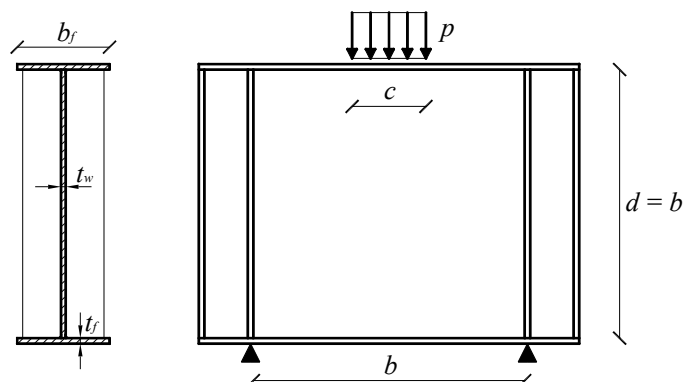


Figure 3.5: Typical short span girder

	Girder	No. of test	$b$ [mm]	$d$ [mm]	$t_w$ [mm]	$b_f$ [mm]	$t_f$ [mm]	$c$ [mm]	$f_{yw}$ [N/mm <sup>2</sup> ]	$f_{yf}$ [N/mm <sup>2</sup> ]
Skaloud & Novak	TG1	3	1000	1000	2.50	160	5.50	100	298	342
	TG2	2	1000	1000	2.50	200	10.09	100	299	253
	TG3	1	1000	1000	2.50	200	16.24	100	251	266
	TG4	1	1000	1000	2.50	200	20.17	100	254	231
	TG5	2	1000	1000	2.50	250	30.50	100	289	261
Drdaeky & Novotny	TTG1	1	300	300	3.97	49.4	10.00	30	285	269
	TTG2	1	300	300	4.00	50.5	9.90	30	270	258
	TTG3	1	300	300	4.01	49.4	15.90	30	281	265
	TTG4	1	450	450	3.97	49.3	10.00	45	257	267
	TTG6	1	450	450	3.96	49.6	15.80	45	249	265
	TTG7	1	600	600	3.57	50.5	10.00	60	257	274
	TTG8	1	600	600	3.63	49.5	10.10	60	282	279
	TTG9	1	600	600	3.67	49.0	16.00	60	306	282
	TTG1'	1	300	300	3.97	49.4	10.00	45	285	269
	TTG2'	1	300	300	4.00	50.5	9.90	60	270	258
	TTG3'	1	300	300	4.01	49.4	15.90	30	281	265
	TTG4'	1	450	450	3.97	49.3	10.00	60	257	267
	TTG6'	1	450	450	3.96	49.6	15.80	45	249	265
	TTG7'	1	600	600	3.57	50.5	10.00	30	257	274
	TTG8'	1	600	600	3.63	49.5	10.10	45	282	279
TTG9'	1	600	600	3.67	49.0	16.00	60	306	282	
Bergfelt	R1	1	800	800	2.05	300	15.50	40	266	295
	R3	1	800	800	2.00	120	5.07	40	266	285
	B8	1	800	800	2.07	120	5.03	40	285	290
	B41	1	400	400	2.07	120	5.03	40	285	290
	B83	1	800	800	2.90	250	12.35	40	328	298
Roberts	E10-1/1	1	500	500	9.95	150	10.05	<sup>1)</sup> 21.1	222	240
	E10-2/1	1	500	500	9.95	150	10.05	100	247	250

1)  $c = 2 t_f$  is applied.

Table 3.1: Dimensions and material properties for the test specimens with square web panels

In Table 3.1, the dimensions and the yield stresses of the flange and web material respectively, are summarised. TG1 – TG5 are conducted by Skaloud and Novak (1975), TTG1 – TTG9' by Drdacky and Novotny (1977), and R1 – B83 are conducted by Bergfelt (1979). When no specific values for the yield stresses of the material used in the girders have been quoted by the researchers, they have been inferred from similar specimens for which yield stresses have been quoted, cf. (Roberts and Rockey 1979), where these tests also are summarised.

The specimens in these experiments have relatively thin web plates, i.e.  $t_w = 2.00 - 4.01$  mm. Specimens E10-1/1 and E10-2/1 were tested by Roberts (1983), and both had a web plate thickness of  $t_w = 9.95$  mm. For E10-1/1, the patch load length  $c = 0$  is stated, but in the calculations,  $c = 2 t_f$  is used, where  $t_f$  is the flange thickness, assuming that the knife-edge load on the top of the flange will spread out under an angle of  $45^\circ$  through the flange.

Table 3.2 shows the predicted load-carrying capacity,  $P_u$ , determined by Equation (3.15), together with the load-carrying capacity,  $P_{exp}$ , obtained by the experiments.  $\lambda$  and  $b_e/b$  are determined by Equations (3.2) and (3.1) respectively. The value of  $x$  is given by the smaller value found from Equations (3.5) and (3.6). The effective width,  $b_e$ , is determined by either Equation (3.1) multiplied by the total width,  $b$ , or by Equation (3.7), depending on whether the value  $x$  or  $x_f$  are valid. The upwards, uniform load,  $n$ , applied on the flange, is given by Equation (3.12), where  $c + 2 \beta = b$ .

	Girder	$\lambda$ [ ]	$b_e/b$ [ ]	$x$ [mm]	$x/d$ [ ]	$b_e$ [mm]	$n$ [N/mm]	$P_u$ [kN]	$P_{exp}$ [kN]	$P_u/P_{exp}$ [ ]
Skaloud & Novak	TG1	15.07	0.128	167	0.17	128	95.7	56.29	51.50	1.093
	TG2	15.09	0.128	167	0.17	128	95.8	64.15	63.76	1.006
	TG3	13.83	0.140	173	0.17	139	87.5	79.32	68.67	1.155
	TG4	13.91	0.139	173	0.17	139	88.1	90.21	88.29	1.022
	TG5	14.84	0.130	168	0.17	130	94.2	186.67	179.00	1.043
Drdacky & Novotny	TTG1	2.78	0.601	73	0.24	180	679.9	122.02	130.00	0.939
	TTG2	2.69	0.618	73	0.24	185	667.6	119.62	147.50	0.811
	TTG3	2.74	0.609	73	0.24	183	686.7	137.82	169.50	0.813
	TTG4	3.97	0.445	112	0.25	200	453.8	118.81	120.00	0.990
	TTG6	3.91	0.450	112	0.25	202	443.7	126.02	150.00	0.840
	TTG7	5.88	0.313	139	0.23	187	286.7	99.73	140.00	0.712
	TTG8	6.06	0.304	<sup>2)</sup> 136	0.23	175	297.8	103.51	148.00	0.699
	TTG9	6.24	0.296	137	0.23	177	332.2	122.73	150.00	0.818
	TTG1'	2.78	0.601	73	0.24	180	679.9	127.70	150.00	0.851
	TTG2'	2.69	0.618	73	0.24	185	667.6	130.81	146.00	0.896
	TTG3'	2.74	0.609	73	0.24	183	686.7	137.82	150.00	0.919
	TTG4'	3.97	0.445	112	0.25	200	453.8	122.47	136.00	0.900
	TTG6'	3.91	0.450	112	0.25	202	443.7	126.02	160.00	0.788
	TTG7'	5.88	0.313	139	0.23	187	286.7	95.16	119.00	0.800
TTG8'	6.06	0.304	<sup>2)</sup> 136	0.23	175	297.8	101.13	138.00	0.733	
TTG9'	6.24	0.296	137	0.23	177	332.2	122.73	146.00	0.841	
Bergfelt	R1	13.89	0.139	138	0.17	111	75.7	87.77	84.50	1.039
	R3	14.24	0.136	137	0.17	109	72.2	32.62	38.00	0.858
	B8	14.24	0.136	137	0.17	109	80.0	35.92	48.00	0.748
	B41	7.12	0.262	88	0.22	105	154.5	38.88	53.00	0.734
	B83	10.90	0.176	152	0.19	140	166.7	99.91	121.00	0.826
Roberts	E10-1/1	1.63	0.906	73	0.15	453	2000.2	535.31	716.00	0.748
	E10-2/1	1.72	0.872	84	0.17	436	2142.2	661.61	787.00	0.841

2) Yielding in the flange occurs, so  $x_f$  is applied.

**Table 3.2:** Calculated data for the test specimens with square web panels

The theory seems to correlate well with the experimental results, but it slightly underestimates the load-carrying capacity, except in the tests by Skaloud and Novak, see Figures 3.6 and 3.7. The mean value of  $P_u/P_{exp}$  for all the tests is 0.874 and the standard deviation is 12.2 %. For the separate test series, the following results are obtained:

- Skaloud & Novak, TG1 – TG5: Mean 1.064, standard deviation 6.1 %.
- Drdacky & Novotny, TTG1 – TTG9: Mean 0.834, standard deviation 8.1 %.
- Bergfelt, R1 – B83: Mean 0.841, standard deviation 12.2 %.
- Roberts, E10-1/1 & -2/1: Mean 0.794, standard deviation 6.6 %.

The experiments conducted by Roberts (1983) had the aim of verifying his method for girders with a thick web plate, where yielding of the web is governing instead of buckling. From Table 3.2 it is seen that this is actually incorrect, as the value  $b_e/b$  does not exceed unity for both specimens, so buckling of the web will occur before yielding according to the present theory.

From Table 3.2 it is also seen that the ratio,  $x/d$ , at maximum reaches 1/4, hence it is only a relatively small part of the web plate that is included in the internal beam.

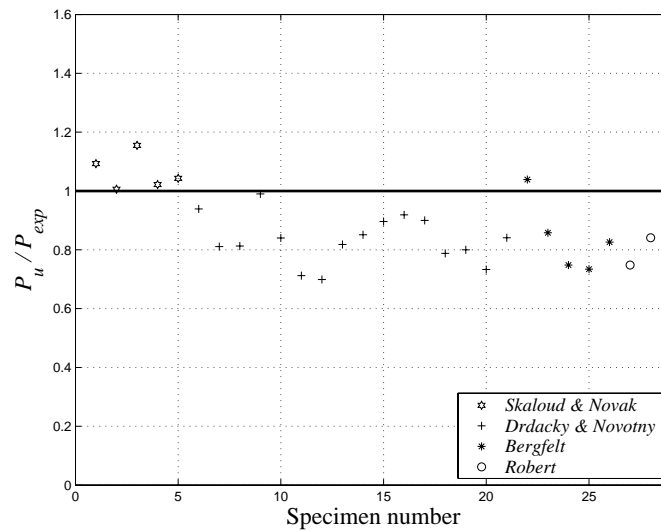


Figure 3.6: Comparison of theory and experimental results

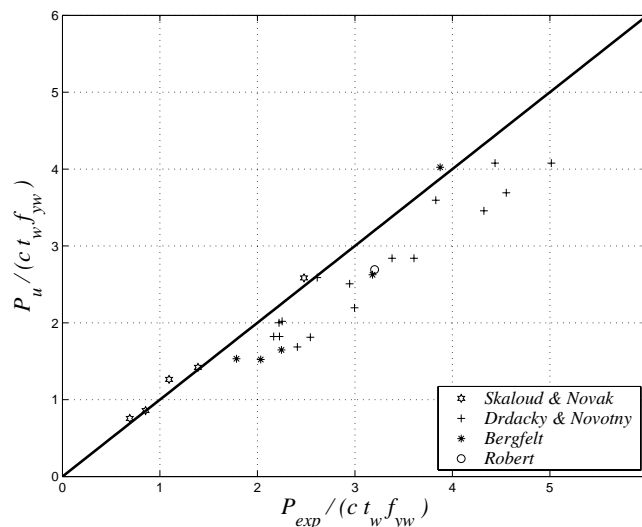


Figure 3.7: Comparison of theory and experimental results

## 4 PLATE GIRDERS WITH RECTANGULAR WEB PANELS

In a rectangular web panel, the distance between the stiffeners,  $b$ , is either smaller or larger than the depth of the girder,  $d$ .

The post-buckling strength of a web plate with  $b < d$  may be calculated as described in Section 3.2 in PART III, where a square yield line pattern with the side lengths equal to  $b$  is applied, see Figure 4.1. The effective width,  $b_e$ , is then given by Equation (3.1) and the load-carrying capacity,  $P_u$ , may be determined by Equation (3.15).

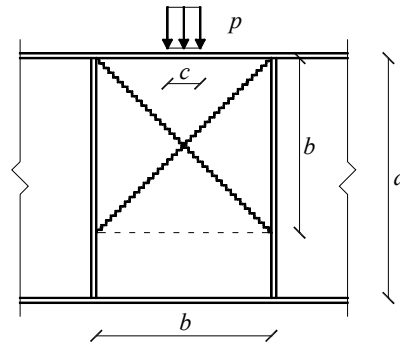


Figure 4.1: Failure mechanism for a web plate with  $b < d$

### 4.1 The Web Mechanism for Rectangular Panels

The post-buckling strength of a web plate with  $b > d$  may be determined by considering the yield line pattern shown in Figure 4.2. The plate is subjected to a load per unit length equal to the yield stress of the web,  $f_{yw}$ , multiplied by the thickness,  $t_w$ , along two strips of width  $b_s$ . The failure mechanism has the free parameter,  $X$ . The work equation must be derived separately for the two cases,  $b_s < X$  and  $b_s > X$ , respectively.

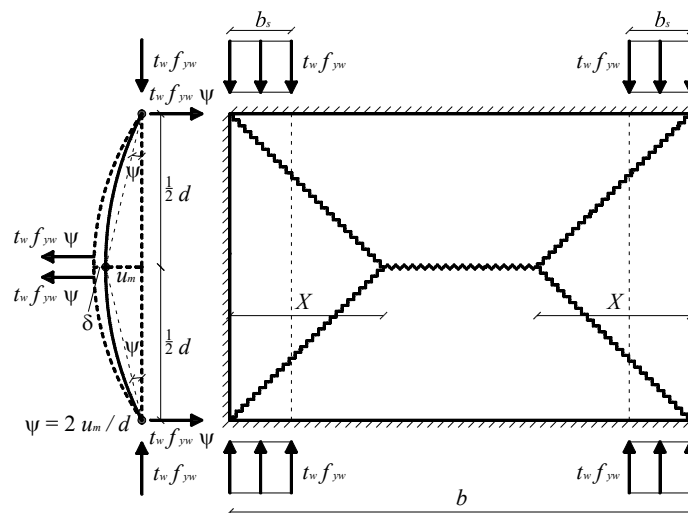


Figure 4.2: Failure mechanism for a web plate with  $b > d$  and  $b_s < X$

In the case  $b_s < X$ , the external work for  $\delta = 1$  is given by

$$W_e = 4 t_w f_{yw} \frac{u_m}{d} b_s^2 \quad (4.1)$$

and the dissipation

$$W_i = 4 m_p \left( \frac{b}{d} - 2 \frac{b_s}{d} + \frac{1}{2} \frac{d}{X} \right) \quad (4.2)$$

where  $m_p$  is the plastic yield moment per unit length given by

$$m_p = \frac{1}{4} t_w^2 f_{yw} \quad (4.3)$$

In the above equations,  $t_w$  is the web thickness,  $f_{yw}$  the yield stress of the web,  $d$  the girder depth, and  $b$  is the width of the web panel, i.e. distance between two adjacent stiffeners. The deflection corresponding to maximum load,  $u_m$ , is determined by assuming the yield strain ( $\varepsilon_y = f_{yw}/E$ ) to be reached in both faces of the web plate. Then

$$u_m = \frac{1}{8} \frac{2 \varepsilon_y}{t_w} d^2 = \frac{1}{4} \frac{f_{yw}}{E} \frac{d^2}{t_w} \quad (4.4)$$

Equalising the external work and the dissipation, the width of each strip,  $b_s$ , for  $b_s < X$  is found to be determined by

$$\frac{f_{yw}}{E} b_s^2 + 2 \frac{t_w^2 X}{d^2} b_s - t_w^2 \left( \frac{b X}{d^2} + \frac{1}{2} \right) = 0 \quad (4.5)$$

In the case  $b_s > X$ , the external work for  $\delta = 1$  is given by

$$W_e = 4 t_w f_{yw} \frac{u_m}{d} (2 b_s - X) \quad (4.6)$$

and the dissipation, which is identical to Equation (4.2), is

$$W_i = 4 m_p \left( \frac{b}{d} - 2 \frac{b_s}{d} + \frac{1}{2} \frac{d}{X} \right) \quad (4.7)$$

Equalising the external work and the dissipation, the width of each strip,  $b_s$ , for  $b_s > X$  is found to be determined by

$$\left( 2 \frac{f_{yw}}{E} d + 2 \frac{t_w^2}{d^2} \right) b_s = \frac{f_{yw}}{E} d X + t_w^2 \left( \frac{b}{d} + \frac{1}{2} \frac{d}{X} \right) \quad (4.8)$$

In Section 3.1 in PART III, it was shown that inclined yield lines under an angle of  $45^\circ$  are normally a good choice, noting that minimising  $b_s$  with regard to  $X$  will not lead to any useful result. Hence, an angle of  $45^\circ$  is also chosen here, i.e.  $X = \frac{1}{2} d$ .

Denoting the effective width  $b_e = 2 b_s$ , the effective width for  $b_s < X$  ( $\Rightarrow b_e < d$ ) is given by

$$\frac{b_e}{b} = -\lambda^{-2} \frac{d}{b} + \sqrt{\lambda^{-4} \left(\frac{d}{b}\right)^2 + 2\lambda^{-2} \left(\frac{d^2}{b^2} + \frac{d}{b}\right)} \quad (4.9)$$

and for  $b_s > X (\Rightarrow b_e > d)$

$$\frac{b_e}{b} = \frac{\frac{1}{2}\lambda^2 \frac{d}{b} + \frac{d}{b} + 1}{\lambda^2 + 1} \quad (4.10)$$

In both Equations (4.9) and (4.10),  $b_e/b \leq 1$  is required. Furthermore, the non-dimensional parameter,  $\lambda$ ,

$$\lambda = \frac{d}{t_w} \sqrt{\frac{f_{yw}}{E}} \quad (4.11)$$

has been introduced.

The parameter,  $b_e/b$ , through Equations (4.9) and (4.10) as a function of  $\lambda$  is shown for different values of  $b/d$  in Figure 4.3. In Figure 4.4, the ratio,  $b_e/d$ , as a function of  $\lambda$  is shown for different values of  $b/d$ . For the two cases treated above, the ratio,  $b_e/d$ , may be written as:

For  $b_e/d \leq 1$ :

$$\frac{b_e}{d} = -\lambda^{-2} + \sqrt{\lambda^{-4} + 2\lambda^{-2} \left(\frac{b}{d} + 1\right)} \quad (4.12)$$

For  $b_e/d \geq 1$ :

$$\frac{b_e}{d} = \frac{\frac{1}{2}\lambda^2 + \frac{b}{d} + 1}{\lambda^2 + 1} \quad (4.13)$$

By inserting  $b_e/d = 1$  in either Equation (4.12) or (4.13), it is found that the two curves, for any value of  $b/d$ , in both Figure 4.3 and Figure 4.4, intersect for

$$\lambda = \sqrt{2 \frac{b}{d}} \quad (4.14)$$

Since,  $b_e \leq b$  is required, a cut-off at  $b_e/b = 1$ , as shown in Figure 4.3, must be done for all curves. In Figure 4.4, it is shown that each curve has a cut-off for  $b_e/d$  equal to the value of  $b/d$  corresponding to the actual curve. By inserting  $b_e = b$  into, for instance, Equation (4.13), it is verified that the cut-off, in both Figure 4.3 and Figure 4.4, takes place for

$$\lambda = \left(\frac{b}{d} - \frac{1}{2}\right)^{-1/2} \quad (4.15)$$

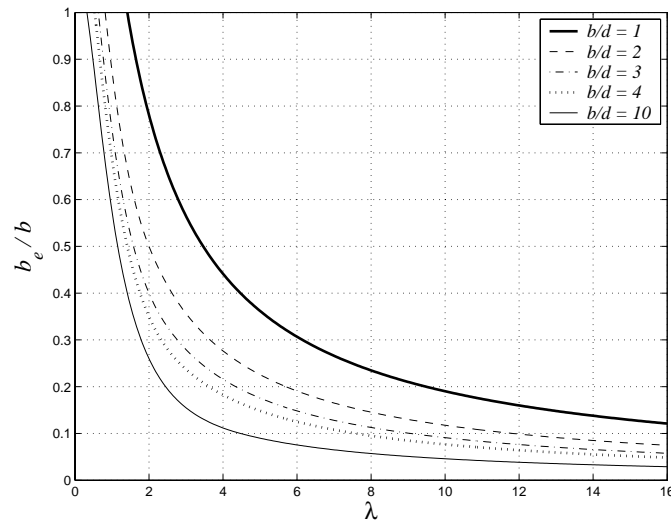


Figure 4.3:  $b_e/b$  as a function of  $\lambda$  for different values of  $b/d$

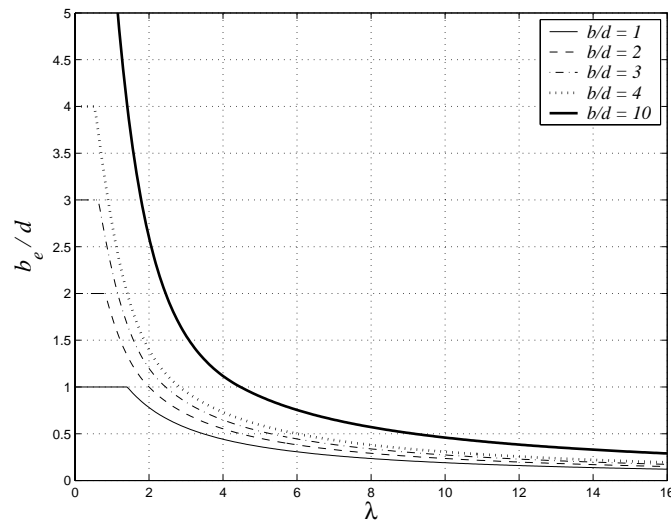


Figure 4.4:  $b_e/d$  as a function of  $\lambda$  for different values of  $b/d$

## 4.2 Load-Carrying Capacity

The flange mechanism for a plate girder with a rectangular web panel is identical to that presented for a plate girder with a square web panel, cf. Section 3.2. Hence the load-carrying capacity as a function of  $\beta$  of a plate girder with a rectangular web panel is given by, cf. Equation (3.13),

$$P_u = t_f^2 f_{yf} \frac{b_f}{\beta} + t_w f_{yw} b_e \frac{c + \beta}{c + 2\beta} \quad (4.16)$$

The only difference is that  $b_e$  here is either determined by Equation (4.9) or Equation (4.10). As previously, minimising  $P_u$  with regard to  $\beta$  will show that the minimum is found when  $\beta$  is as large as possible, i.e. the outer hinges will develop in the flange at the nearest stiffeners, independent of the length-to-depth ratio,  $b/d$ . Hence the load-carrying capacity is given by, cf. Equation (3.15),

$$P_u = 2t_f^2 f_{yf} \frac{b_f}{b-c} + \frac{1}{2}t_w f_{yw} \frac{b_e}{b}(b+c) \quad (4.17)$$

Here,  $b$  is the web panel width (distance between two adjacent stiffeners),  $c$  the patch load length,  $b_e$  the calculated effective width of the web plate, and  $b_f$  is the flange width. Furthermore,  $t$  is thickness and  $f_y$  is the yield stress with indexes  $f$  for flange and  $w$  for web.

The internal beam, cf. Figure 3.3, must also in this case be able to sustain the uniform load,  $n$ . The part of the web plate,  $x$ , in the internal beam, is determined either by Equation (3.5) or Equation (3.6).

If the ratio,  $b/d$ , is large, then the value of  $\beta$  also becomes large. This is not always observed in tests. Some tests have shown that the flange mechanism is very local, especially for specimens with low flange stiffness. Regardless, the theory correlates well with the test results presented in Section 4.3. This might be due to the fact that the minimum for  $P_u$  is flat, which is illustrated in Figure 4.5. Here,  $P_u$  as a function of  $\beta$ , cf. Equation (4.16), is shown for the long girder B14 from the tests by Bergfelt and Hovik (1968, 1970), which are described in the following section. For this specimen,  $c = 180$  mm and  $b/d = 2400/400$ . The permissible maximum value of  $\beta$  for this specimen is then  $\beta = 1110$  mm, cf. Equation (3.14). For this  $\beta$ -value, the minimum for  $P_u$  is found to be  $P_u = 62.7$  kN. If for instance  $\beta = 500$  mm is applied, then  $P_u$  will only become 10 % larger.

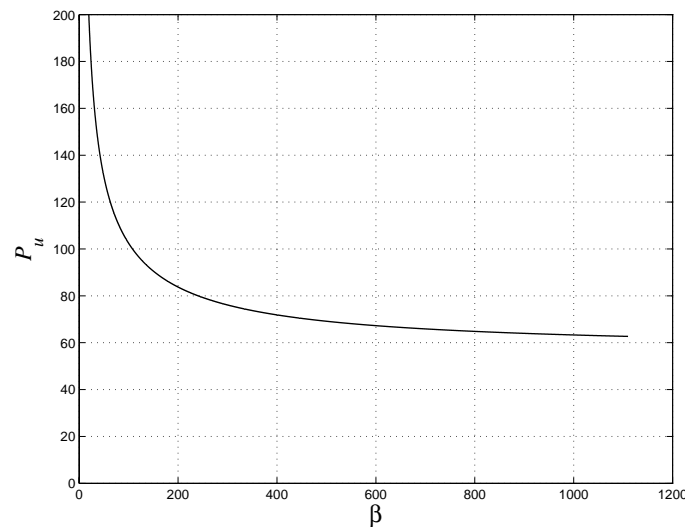
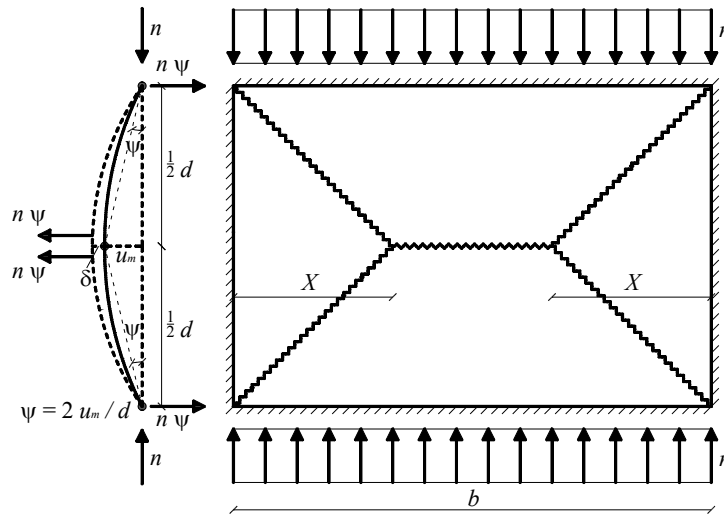


Figure 4.5:  $P_u$  as a function of  $\beta$  for specimen B14

Also, if the ratio,  $b/d$ , is large, it is not so obvious that the web stresses will be concentrated near the transverse stiffeners, if these are placed far away from the load. For the web mechanism in Figure 4.6, where the web is subjected to a load,  $n$ , per unit length along the entire width,  $n$  will be given by

$$\frac{n}{t_w f_{yw}} = -\frac{1}{2}\lambda^2 \left(1 - \frac{1}{2} \frac{d}{b}\right) + \sqrt{\frac{1}{4}\lambda^4 \left(1 - \frac{1}{2} \frac{d}{b}\right)^2 + \frac{d}{b} + 1} \quad (4.18)$$

Here the value of  $X$  for the web mechanism,  $X = \frac{1}{2} d$ , is applied, and  $\lambda$  is given by Equation (4.11). The left-hand side of Equation (4.18) as a function of  $\lambda$  is shown for different values of  $b/d$  in Figure 4.7. It is seen that when  $b/d$  is increased, the curve moves towards the curve corresponding to  $b/d = \infty$ .



**Figure 4.6:** Failure mechanism for a web plate with  $b > d$ , subjected to a load,  $n$ , per unit length along the entire width,  $b$

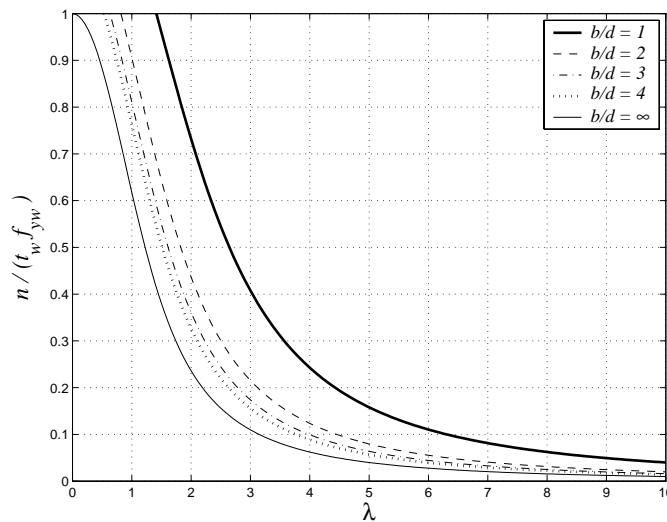


**Figure 4.7:**  $n/(t_w f_{yw})$  as a function of  $\lambda$  for different values of  $b/d$

Applying this value of  $n$  on the flange mechanism, cf. Equation (3.10), with  $\beta$  taken from Equation (3.14), the theory gives far too low values of  $P_u$  compared to the values from the tests. For  $b/d \rightarrow \infty$ , Equation (4.18) renders the same result as the column solution, cf. Equation (2.15) in PART III for  $\mu = 1.0$ . The column solution is almost identical to the elastic solution. According to Roberts (1983), elastic solutions give far too low results compared to patch loading tests in general.

### 4.3 Comparison with Experimental Results

No experimental results have been found in the literature for plate girders with  $b < d$ . The experimental results used to verify the theory for plate girder with  $b > d$  are all, except the tests B1-B10, carried out on short specimens of the form shown in Figure 3.5, but with  $b > d$ .

Tests B1-B10 were done on girders of length 9800 mm, with a constant bottom flange and with a top flange varying, as shown in Figure 4.8, which also shows the patch loading.

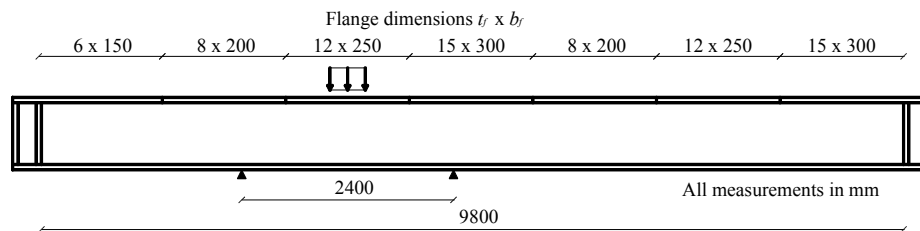


**Figure 4.8:** Details of test specimens B1-B10

In Table 4.1, the dimensions and the yield stresses of the flange and web material respectively, are summarised. The tests TG6 – TG15 were done by Skaloud and Novak (1975), B1 – B20 by Bergfelt and Hovik (1968, 1970), A11 – B43 by Bergfelt (1979), and B2-3 – B2-20 were done by Roberts (1983).

The specimens in these experiments all have relatively thin web plates, i.e.  $t_w = 2.00 - 3.40$  mm. The ratio,  $b/d$ , varies from 1.2 – 8.0. For the tests conducted by Bergfelt and Hovik (1968, 1970), the patch length  $c = 0$  for the odd specimen numbers, i.e. B1, B3, etc. Again,  $c = 2 t_f$ , where  $t_f$  is the flange thickness, is used in the calculations assuming that the knife-edge load on the top of the flange spreads out under an angle of  $45^\circ$  through the flange.

Table 4.2 shows the predicted load-carrying capacity,  $P_u$ , determined by Equation (4.17), together with the load-carrying capacity,  $P_{exp}$ , obtained by the experiments. The ratio,  $b_e/b$ , is determined by Equation (4.9) or (4.10), where  $\lambda$  is given by Equation (4.11). The value of  $x$  is the smaller value from Equations (3.5) and (3.6). The effective width,  $b_e$ , is determined by either Equation (4.9), (4.10) or (3.7), depending on which of the values  $x$  or  $x_f$  are valid. The upwards, uniform load,  $n$ , applied on the flange, is given by Equation (3.12).

The theory seems to correlate very well with the experimental results, see Figures 4.9 and 4.10. The mean value of  $P_u/P_{exp}$  for all tests is 0.992 and the standard deviation is 11.7 %. For the individual test series, the following results are obtained:

- Skaloud & Novak, TG6 – TG15: Mean 0.925, standard deviation 10.8 %.
- Bergfelt & Hovik, B1 – B20: Mean 1.001, standard deviation 10.2 %.
- Bergfelt, A11 – B43: Mean 0.987, standard deviation 12.0 %.
- Roberts & Rockey, B2-3 – B2-20: Mean 1.120, standard deviation 12.0 %.

From Table 4.2 it appears that the ratio,  $x/d \approx 1.00$ , is reached for the very long specimens, i.e.  $b/d \geq 8.0$ . Hence, the full depth of the web plate is utilised in the internal beam. Since the internal beam is calculated as simply supported, even ratios up to  $x/d \approx 1.40$  might be acceptable when the internal beam is calculated as simply

supported instead of having fixed supports. When  $x/d$  is large, the internal beam stress field should, strictly speaking, be taken into account when performing the yield line analysis of the web. This has not yet been done. A tensile stress field in the web is beneficial regarding the effects of change of geometry ( $N \psi$ -terms), but along the  $b_e$ -strips the yield condition is violated (vertical compression in the  $b_e$ -strips with superimposed horizontal tension).

	Girder	No. of test	$b$ [mm]	$d$ [mm]	$t_w$ [mm]	$b_f$ [mm]	$t_f$ [mm]	$c$ [mm]	$f_{yw}$ [N/mm <sup>2</sup> ]	$f_{yf}$ [N/mm <sup>2</sup> ]
Skaloud & Novak	TG6	2	2000	1000	3.00	160	6.29	100	290	294
	TG7	1	2000	1000	3.00	200	10.00	100	297	253
	TG8	1	2000	1000	3.00	200	16.55	100	308	266
	TG9	1	2000	1000	3.00	200	19.78	100	300	231
	TG10	2	2000	1000	3.00	250	30.00	100	299	261
	TG11	2	2000	1000	3.00	160	6.29	200	290	294
	TG12	1	2000	1000	3.00	200	10.00	200	297	253
	TG13	1	2000	1000	3.00	200	16.55	200	308	266
	TG14	1	2000	1000	3.00	200	19.78	200	300	231
	TG15	2	2000	1000	3.00	250	30.00	200	299	261
Bergfelt & Hovik	B2	1	2400	700	3.26	150	6.10	100	326	347
	B4	1	2400	700	3.26	200	8.50	100	326	235
	B6	2	2400	700	3.26	250	10.10	100	326	243
	B8	1	2400	700	3.26	250	11.90	100	326	232
	B10	2	2400	700	3.26	300	15.30	100	326	305
	B12	1	2400	300	2.00	100	6.00	180	294	294
	B14	1	2400	400	2.00	100	8.00	180	294	294
	B16	1	2400	500	2.00	100	10.00	180	294	294
	B18	1	2900	600	2.00	100	12.00	180	294	294
	B20	1	3500	700	2.00	100	15.00	180	294	294
	B1	2	2400	700	3.26	150	6.10	<sup>1)</sup> 12.2	326	347
	B3	2	2400	700	3.26	200	8.50	<sup>1)</sup> 17.0	326	235
	B5	2	2400	700	3.26	250	10.10	<sup>1)</sup> 20.2	326	243
	B7	2	2400	700	3.26	250	11.90	<sup>1)</sup> 23.8	326	232
	B9	3	2400	700	3.26	300	15.30	<sup>1)</sup> 30.6	326	305
	B11	1	2400	300	2.00	100	6.00	<sup>1)</sup> 12.0	294	294
	B13	1	2400	400	2.00	100	8.00	<sup>1)</sup> 16.0	294	294
	B15	1	2400	500	2.00	100	10.00	<sup>1)</sup> 20.0	294	294
	B17	1	2900	600	2.00	100	12.00	<sup>1)</sup> 24.0	294	294
	B19	1	3500	700	2.00	100	15.00	<sup>1)</sup> 30.0	294	294
Bergfelt	A11	1	2500	800	2.12	300	15.40	40	300	295
	A21	1	2500	800	3.03	250	12.05	40	245	265
	A31	1	2200	680	2.08	120	5.05	40	354	290
	B4	1	800	400	2.07	120	5.03	40	285	290
	B3	1	800	300	2.07	120	5.03	40	285	290
	B43	1	800	400	2.90	250	12.35	40	328	298
Roberts	B2-3	1	600	500	2.12	150	3.05	50	224	221
	B2-7	1	600	500	2.12	150	6.75	50	224	279
	B2-12	1	600	500	2.12	150	11.75	50	224	305
	B2-20	1	600	500	2.12	150	20.06	50	224	305

1)  $c = 2 t_f$  is applied.

**Table 4.1:** Dimensions and material properties for test specimens with rectangular web panels

The solution by Roberts (1983) is based on the same experiments as presented in Sections 3.3 and 4.3. He determined Equations (1.3) and (1.4) empirically so that they provide a lower-bound for the available tests. Hence by comparing Roberts' solution to the experiments as in Figures 3.6 and 4.9, all tests will be below the line corresponding to  $P_u/P_{exp}$  equal to one. Furthermore, the mean value of  $P_u/P_{exp}$  for all tests is 0.699 and the standard deviation is 15.8 %.

	Girder	$\lambda$ [ ]	$b_e/b$ [ ]	$x$ [mm]	$x/d$ [ ]	$b_e$ [mm]	$n$ [N/mm]	$P_u$ [kN]	$P_{exp}$ [kN]	$P_u/P_{exp}$ [ ]
Skaloud & Novak	TG6	12.39	0.096	294	0.29	191	83.2	89.35	81.90	1.091
	TG7	12.54	0.095	293	0.29	189	84.3	93.80	98.10	0.956
	TG8	12.77	0.093	290	0.29	186	85.9	105.49	117.72	0.896
	TG9	12.60	0.094	292	0.29	188	84.7	107.96	125.57	0.860
	TG10	12.54	0.094	292	0.29	189	84.6	150.60	147.15	1.023
	TG11	12.39	0.096	294	0.29	191	83.2	93.62	93.19	1.005
	TG12	12.54	0.095	293	0.29	189	84.3	98.31	117.72	0.835
	TG13	12.77	0.093	290	0.29	186	85.9	110.64	132.43	0.835
	TG14	12.60	0.094	292	0.29	188	84.7	113.26	152.05	0.745
	TG15	12.54	0.094	292	0.29	189	84.6	158.26	157.94	1.002
Bergfelt & Hovik	B2	8.46	0.099	<sup>2)</sup> 299	0.43	159	70.6	89.88	105.95	0.848
	B4	8.46	0.099	358	0.51	237	104.8	133.95	121.64	1.101
	B6	8.45	0.099	358	0.51	237	104.6	136.17	132.93	1.024
	B8	8.46	0.099	358	0.51	237	104.8	138.14	139.30	0.992
	B10	8.46	0.099	358	0.51	237	104.8	149.62	156.47	0.956
	B12	5.61	0.091	<sup>2)</sup> 300	1.00	161	39.4	51.76	65.73	0.788
	B14	7.48	0.080	326	0.82	193	47.3	62.69	59.84	1.048
	B16	9.35	0.074	313	0.63	176	43.2	58.41	55.92	1.045
	B18	11.23	0.061	348	0.58	178	36.1	58.65	61.80	0.949
	B20	13.10	0.052	388	0.55	181	30.4	59.98	56.90	1.054
	B1	8.46	0.099	<sup>2)</sup> 299	0.43	159	70.6	96.72	95.16	0.911
	B3	8.46	0.099	358	0.51	237	104.8	129.50	105.46	1.228
	B5	8.45	0.099	358	0.51	237	104.6	132.02	120.66	1.094
	B7	8.46	0.099	358	0.51	237	104.8	133.92	126.06	1.062
	B9	8.46	0.099	358	0.51	237	104.8	145.44	151.36	0.961
	B11	5.61	0.091	<sup>2)</sup> 300	1.00	161	39.4	48.39	57.88	0.836
	B13	7.48	0.080	326	0.82	193	47.3	58.69	54.44	1.078
	B15	9.35	0.074	313	0.63	176	43.2	54.77	54.94	0.997
	B17	11.23	0.061	348	0.58	178	36.1	55.67	54.44	1.023
B19	13.10	0.052	388	0.55	181	30.4	57.52	55.92	1.029	
Bergfelt	A11	14.26	0.063	303	0.38	157	40.0	67.86	64.00	1.060
	A21	9.02	0.098	372	0.46	245	72.8	100.27	84.00	1.194
	A31	13.42	0.065	<sup>2)</sup> 239	0.35	109	38.7	44.21	47.10	0.885
	B4	7.12	0.163	148	0.37	130	95.8	42.57	48.00	0.887
	B3	5.34	0.178	153	0.51	142	104.7	46.30	49.00	0.945
	B43	5.45	0.209	162	0.41	167	198.3	113.19	119.00	0.951
Roberts	B2-3	7.70	0.213	123	0.25	128	101.3	34.04	34.08	0.999
	B2-7	7.70	0.213	123	0.25	128	101.3	39.89	37.92	1.051
	B2-12	7.70	0.213	123	0.25	128	101.3	55.89	44.16	1.266
	B2-20	7.70	0.213	123	0.25	128	101.3	99.87	84.48	1.182

2) Yielding in the flange occurs, so  $x_f$  is applied.

**Table 4.2:** Calculated data for the test specimens with rectangular web panels

# PATCH LOADING ON PLATE GIRDERS

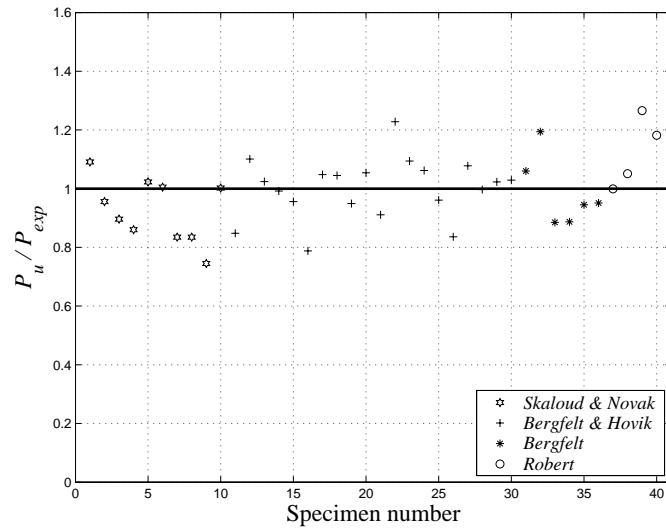


**Figure 4.9:** Comparison of theory and experimental results

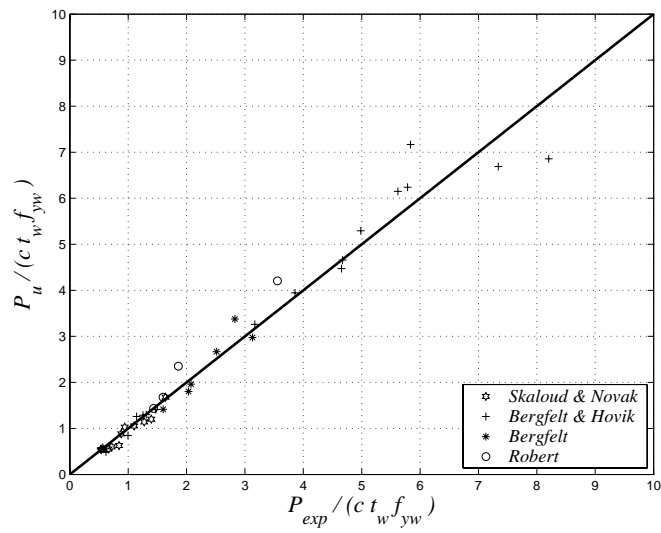


**Figure 4.10:** Comparison of theory and experimental results

## 5 FLANGE INDUCED BUCKLING

If the flange of a plate girder is subjected to a large normal force, and if the stiffness of the web plate is small, the normal force in the flange may lead to buckling of the compression flange. This phenomenon is called *flange induced buckling*.

According to EC3 (2006), flange induced buckling is prevented if the following criterion is met:

$$\frac{d}{t_w} \leq k \frac{E}{f_{yf}} \sqrt{\frac{A_w}{A_{fc}}} \quad (5.1)$$

where  $d$  is the girder depth,  $t_w$  the web thickness,  $E$  Young's modulus,  $f_{yf}$  the yield stress of the flange,  $A_w$  the cross-sectional area of the web, and  $A_{fc}$  is the effective cross-sectional area of the compression flange.

The value of the factor,  $k$ , should be taken as follows:

- plastic rotation utilised  $k = 0.30$
- plastic moment resistance utilised  $k = 0.40$
- elastic moment resistance utilised  $k = 0.55$

Equation (5.1) was originally derived by Basler and Thürlimann (1961). They assumed that the curvature of the flange causes the web to be acted upon by transverse uniform normal stresses,  $\sigma$ ,

$$\sigma = \frac{A_{fc} \sigma_f}{\rho t_w} \quad (5.2)$$

where  $\sigma_f$  is the stress in the flange and  $\rho$  is the radius of curvature assumed to be

$$\rho = \frac{d}{2} \frac{1}{1.5 \varepsilon_y} = \frac{1}{3} \frac{E}{f_{yf}} d \quad (5.3)$$

Here,  $\varepsilon_y = f_{yf}/E$  is the yield strain. The other notations are as in Equation (5.1).

The factor 1.5 is supposed to take into account the influence of residual stresses. The possibility of web buckling due to  $\sigma$  is then checked by using a transverse strip acting as a Euler column, with the effective length equal to the web depth, i.e.

$$\sigma_{cr} = \frac{\pi^2 E}{12(1-\nu^2)} \left( \frac{t_w}{d} \right)^2 \quad (5.4)$$

When considering flange failure,  $\sigma$  is taken to be equal to  $\sigma_{cr}$ , thus Equation (5.1) is found to be valid with  $k = 0.55$  if Poisson's ratio  $\nu = 0.30$  is applied.

So far in the present theory, the effect of normal forces in the compression flange has been disregarded. In fact, flange induced buckling does not seem to have any significant influence on the load-carrying capacity of the test girders in Sections 3.3 and 4.3. This might be due to the fact that the normal forces in the compression flange have been relatively small.

In the present theory, the compression flange is considered to be part of the internal beam, cf. Section 3.1. Hence the compressive stresses in the flange are equilibrated by the tensile stresses in the part of the web plate,  $x$ , included in the internal beam. Therefore there will be no resulting compression force to induce vertical buckling of the flange in the present theory. Regardless, the normal force in the flange may easily be taken into consideration, which is illustrated in the following.

Consider the failure mechanism for the flange in Figure 5.1, where the flange is subjected to a constant normal force,  $N$ . Change of geometry is taken into account by adding the two transverse forces,  $N \psi$ .

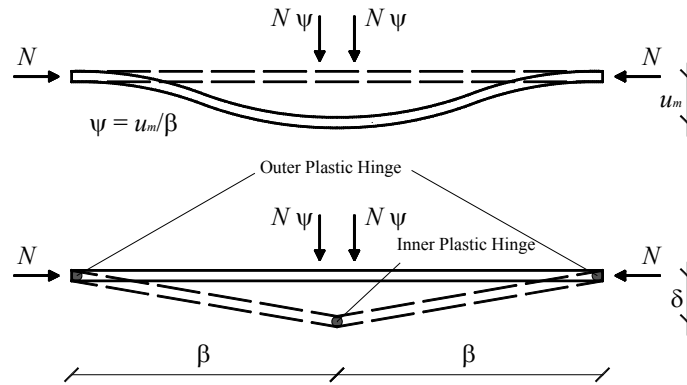


Figure 5.1: Flange mechanism for flange induced buckling

The external work for  $\delta = 1$  is

$$W_e = 2 N \psi = 2 N \frac{u_m}{\beta} \quad (5.5)$$

and the dissipation

$$W_i = 4 \frac{M_{pf}}{\beta} \left( 1 - \left( \frac{N}{N_p} \right)^2 \right) \quad (5.6)$$

where  $\beta$  is the length given in Figure 5.1,  $u_m$  the deflection at maximum load, and the plastic yield moment,  $M_{pf}$ , is given by Equation (3.9).  $N_p$  is the load-carrying capacity in pure compression or tension, equal to

$$N_p = b_f t_f f_{yf} \quad (5.7)$$

where  $b$  is the width,  $t$  the thickness,  $f_y$  the yield stress, and index  $f$  refers to the flange. Note that if  $N = N_p$ , the dissipation renders  $W_i = 0$ .

If the girder is also subjected to a patch load, the contribution from Equation (5.5) is added to the work equation on the left-hand side of Equation (3.8), and the dissipation on the right-hand side is given by Equation (5.6). Thus, with  $c$  being the patch load length and  $n$  the upwards, uniform reaction on the flange,

$$c p - n(c + \beta) + 2 N \frac{u_m}{\beta} = 4 \frac{M_{pf}}{\beta} \left( 1 - \left( \frac{N}{N_p} \right)^2 \right) \quad (5.8)$$

When estimating the deflection at maximum load,  $u_m$ , compatibility with the web must be taken into account. The maximum transverse deflection of the web,  $u_{m,web}$ , is given by Equation (4.4). Thus the following approximate formula, where  $d$  is the girder depth,

$$u_m = 2 \frac{u_{m,web}^2}{d} \quad (5.9)$$

may be used to estimate the  $u_m$ -value to be inserted in Equation (5.8).

It may be shown that the effect of compression normal forces in the flanges are small as long as one is dealing with first order deflections. Thus the flanges may be calculated as supported rigidly by the web. Of course transverse deflections of the flanges must be taken into account when analysing flange buckling in the regions between web supports and stiffener supports.

## 6 THE EFFECT OF UNIAXIAL TENSION STRESSES IN THE WEB

When a plate girder is designed according to the plastic tension field method, cf. PART II, uniaxial tension stresses equal to the yield stress of the web material exist in the web plate. These tension stresses must be taken into consideration when the plate girder is subjected to a patch load. The methodology for doing this is illustrated in the following. First the simplest case is illustrated, where the web panel is square and the uniaxial tension stresses act under an angle of  $45^\circ$ .

### 6.1 Square Web Panels with Uniaxial Tension at $45^\circ$

In this case the same failure mechanism as described in Section 3.1 is applied. The only difference is that the plate, besides the uniaxial compression stresses in the two strips of width  $b_s$ , is also subjected to uniaxial tension in the whole plate from the diagonal tension field, see Figure 6.1. The plate is also subjected to horizontal uniaxial tension along the part of the web plate,  $x$  or  $x_f$ , included in the internal beam calculation. In Table 3.2 it is shown that the ratio,  $x/d$ , is always relatively small, i.e.  $x/d \leq 1/4$  ( $d$  being the girder depth) for plate girders with a square web panel. Therefore, these tension stresses are neglected in the following calculations, since they only have a minor influence on the load-carrying capacity.

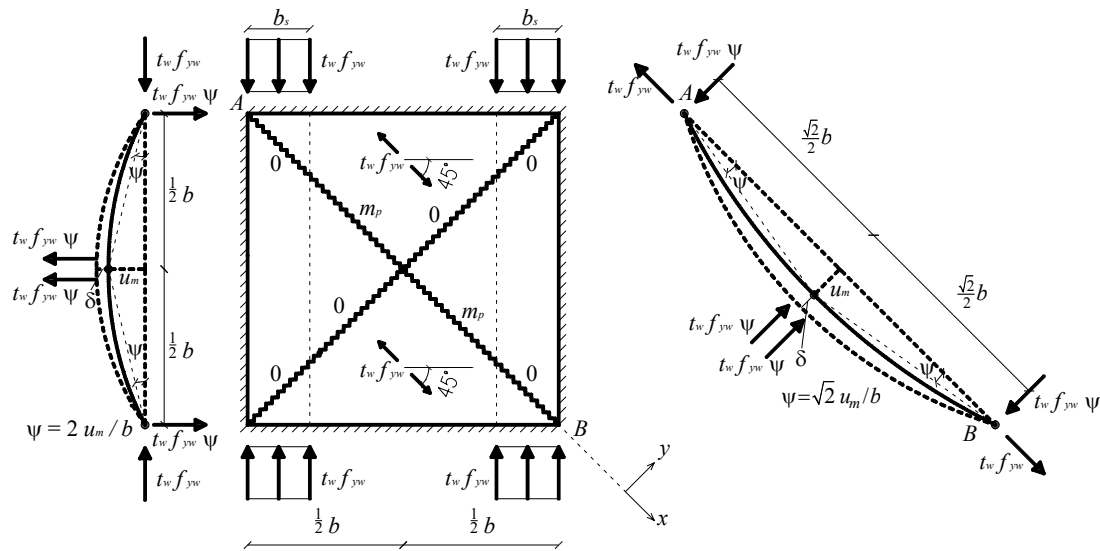


Figure 6.1: Failure mechanism for a square web plate with uniaxial tension stresses at  $45^\circ$

In the two strips, the stress condition is then a combination of uniaxial compression and uniaxial tension in different directions. When calculating the dissipation in the yield lines in the strips, the plastic yield moment of the yield lines should be reduced according to the resulting stresses in the strips. Referring to the Cartesian  $x,y$ -system of coordinates in Figure 6.1, the stresses from the uniaxial compression may be expressed as

$$\sigma_x = -\frac{1}{2} f_{yw} \quad \sigma_y = -\frac{1}{2} f_{yw} \quad \tau_{xy} = \frac{1}{2} f_{yw} \quad (6.1)$$

where  $f_{yw}$  is the yield stress of the web material.

The stresses from the uniaxial tension may be expressed as

$$\sigma_x = f_{yw} \quad \sigma_y = 0 \quad \tau_{xy} = 0 \quad (6.2)$$

By superimposing the stresses, the resulting stresses are found to be

$$\sigma_x = \frac{1}{2} f_{yw} \quad \sigma_y = -\frac{1}{2} f_{yw} \quad \tau_{xy} = \frac{1}{2} f_{yw} \quad (6.3)$$

In Figure 6.2, the three stress conditions are illustrated by applying Mohr's circle. It is seen that the resulting stresses will give shear stresses that are too high, i.e.  $\tau_{\max}$  larger than  $1/\sqrt{3} f_{yw}$  (assuming von Mises' yield criterion). Hence, as a simple and conservative assumption, the yield lines in the strips are considered to be fully utilised, i.e.  $m_p = 0$ .

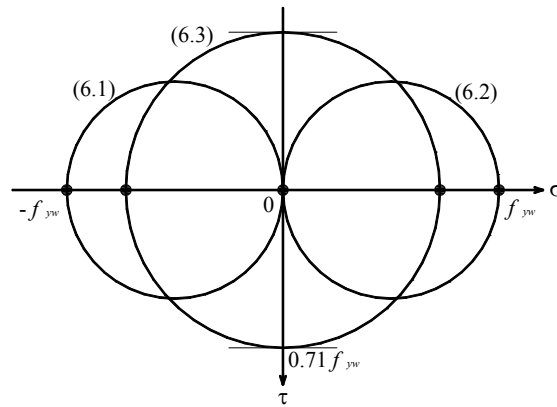


**Figure 6.2:** Mohr's circle for the stress conditions in the strips of width  $b_s$

The yield lines perpendicular to the uniaxial tension stresses will also be fully utilised, hence only the yield line between the two strips parallel to the uniaxial tension stresses will contribute to the dissipation.

The external work for  $\delta = 1$  is given by

$$W_e = 4 t_w f_{yw} u_m \left( 2 \frac{b_s^2}{b^2} - \frac{1}{2} \right) \quad (6.4)$$

and the dissipation is

$$W_i = 4 m_p \left( 1 - 2 \frac{b_s}{b} \right) \quad (6.5)$$

Here,  $t_w$  is the web thickness,  $f_{yw}$  the yield stress of the web material,  $u_m$  the deflection at maximum load,  $b$  the width of the web panel and  $b_s$  is the width of the effective strips.

It is seen that  $W_e = 0$  for  $b_s = \frac{1}{2} b$  and that  $W_e$  will always be negative for  $b_s < \frac{1}{2} b$ . Hence, the work done by the uniaxial tension stresses will always neutralise the work done by the uniaxial compression stresses. It is also seen that  $W_i = 0$  for  $b_s = \frac{1}{2} b$  and that  $W_i$  will always be negative for  $b_s < \frac{1}{2} b$ . By equalising the external work and the

dissipation, it is found that  $b_e = 2 b_s = b$ , hence buckling of the web plate due to the patch loading will not occur.

The restraining effect from the web plate, utilised in the flange mechanism, will then be equal to  $t_w f_{yw}$ . When the plastic tension field method is applied to design the girder, the vertical component of the uniaxial tension stresses must be transferred to the nearest stiffeners by the flange. This vertical component is carried by the flange, which for  $\beta = 45^\circ$  means that in the flange mechanism, a downwards uniform load equal to  $\frac{1}{2} t_w f_{yw}$  has to be carried, cf. Equations (2.2) and (2.7) in PART II. The resulting upwards, uniform load,  $n$ , applied on the flange is then given by, cf. Equation (3.12),

$$n = \frac{1}{2} \frac{t_w f_{yw} b}{c + 2\beta} \quad (6.6)$$

By inserting Equation (6.6) into Equation (3.10), it is again found that by minimising  $P_u$  with regard to  $\beta$ ,  $\beta$  is given by Equation (3.14). The load-carrying capacity may then written as

$$P_u = 2t_f^2 f_{yf} \frac{b_f}{b-c} + \frac{1}{4} t_w f_{yw} (b+c) \quad (6.7)$$

Here,  $b$  is the web panel width (distance between two adjacent stiffeners),  $c$  the patch load length and  $b_f$  is the flange width. Furthermore,  $t$  is thickness and  $f_y$  is the yield stress with indexes  $f$  for flange and  $w$  for web.

## 6.2 Rectangular Web Panels with Uniaxial Tension at $45^\circ$

From Table 4.2, it appears that the ratio,  $x/d$ , may become large especially if the length-to-depth ratio,  $b/d$ , is large, but when applying the plastic tension field method to design a plate girder, the web plate will always be close to fully utilised, so the stiffeners will always be relatively closely spaced. Hence, ratios  $b/d > 2.0$  will not be common. Therefore, the tension stresses in the part of the web plate,  $x$  or  $x_f$ , of the internal beam, cf. Section 3.1, are also neglected in this case.

The load-carrying capacity of plate girders with  $b < d$  is also given by Equation (6.7), following the same reasoning as illustrated in Figure 4.1. The failure mechanism for plate girders with  $b > d$  is similar to that described in Section 4.1. Again, the only difference is that the web plate, besides the uniaxial compression stresses in the two strips of width  $b_s$ , is also subjected to uniaxial tension stresses in the whole plate, see Figure 6.3.

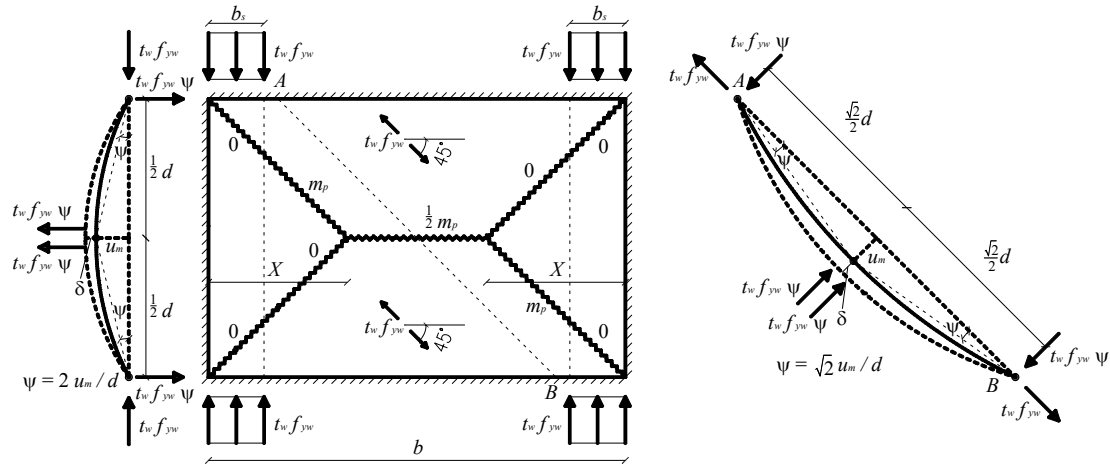


**Figure 6.3:** Failure mechanism for a rectangular web plate with uniaxial tension stresses at  $45^\circ$

As in Section 6.1, the plastic yield moments of the yield lines in the strips are assumed equal to zero. In the horizontal yield line, the plastic yield moment is reduced to  $\frac{1}{2} m_p$ , due to the uniaxial tension stresses under an angle of  $45^\circ$ , cf. Equation (2.3) in PART III.

The work equation must be derived separately for the two cases,  $b_s < X$  and  $b_s > X$ , respectively. As in Section 4.1, it is assumed that  $X = \frac{1}{2} d$  ( $d$  being the girder depth). In the case  $b_s < \frac{1}{2} d$ , the external work when  $\delta = 1$  is

$$W_e = 4 t_w f_{yw} u_m \left( 2 \frac{b_s^2}{d^2} - \frac{1}{2} \frac{b}{d} \right) \quad (6.8)$$

and the dissipation

$$W_i = 4 m_p \left( \frac{1}{2} \frac{b}{d} - 2 \frac{b_s}{d} + \frac{1}{2} \right) \quad (6.9)$$

For  $b_s < \frac{1}{2} d$  it is seen that  $W_e$  is always negative, so this case is never valid. In the case  $b_s > \frac{1}{2} d$ , the external work for  $\delta = 1$  is given by

$$W_e = 4 t_w f_{yw} u_m \left( 3 \frac{b_s}{d} - \frac{1}{2} \frac{b}{d} - 1 \right) \quad (6.10)$$

and the dissipation

$$W_i = 2 m_p \left( \frac{b}{d} - 2 \frac{b_s}{d} \right) \quad (6.11)$$

Equalising the external work and the dissipation, the width of each strip,  $b_s$ , is found to be determined by

$$\left( 3 \frac{f_{yw}}{E} d + \frac{t_w^2}{d^2} \right) b_s = \frac{f_{yw}}{E} \left( \frac{1}{2} d b + d^2 \right) + \frac{1}{2} t_w^2 \frac{b}{d} \quad (6.12)$$

Denoting as before the effective width  $b_e = 2 b_s$ , the width is given by

$$\frac{b_e}{b} = \frac{\lambda^2 \left( 2 \frac{d}{b} + 1 \right) + 1}{3\lambda^2 + 1} \quad (6.13)$$

In Equation (6.13),  $b_e/b \leq 1$  is required, and the non-dimensional parameter,  $\lambda$ , is given by Equation (4.11).

The left-hand side,  $b_e/b$ , of Equation (6.13) as a function of  $\lambda$  is shown for different values of  $b/d$  in Figure 6.4. In Figure 6.5, the ratio,  $b_e/d$ , as a function of  $\lambda$  is shown for different values of  $b/d$ . The ratio,  $b_e/d$ , may be written as:

$$\frac{b_e}{d} = \frac{\lambda^2 \left( \frac{b}{d} + 2 \right) + \frac{b}{d}}{3\lambda^2 + 1} \quad (6.14)$$

In Figure 6.4 it is seen that the curves move towards a constant value for  $\lambda \rightarrow \infty$ , which from Equation (6.13) is found to be

$$\frac{b_e}{b} = \frac{2}{3} \frac{d}{b} + \frac{1}{3} \quad (6.15)$$

The curves in Figure 6.5 move towards a constant value for  $\lambda \rightarrow \infty$ , which by Equation (6.14) is found to be

$$\frac{b_e}{d} = \frac{1}{3} \frac{b}{d} + \frac{2}{3} \quad (6.16)$$

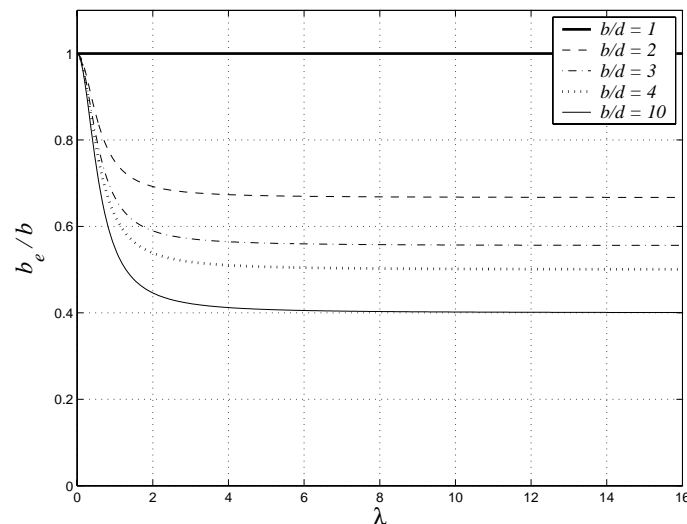


**Figure 6.4:**  $b_e/b$  as a function of  $\lambda$  for different values of  $b/d$

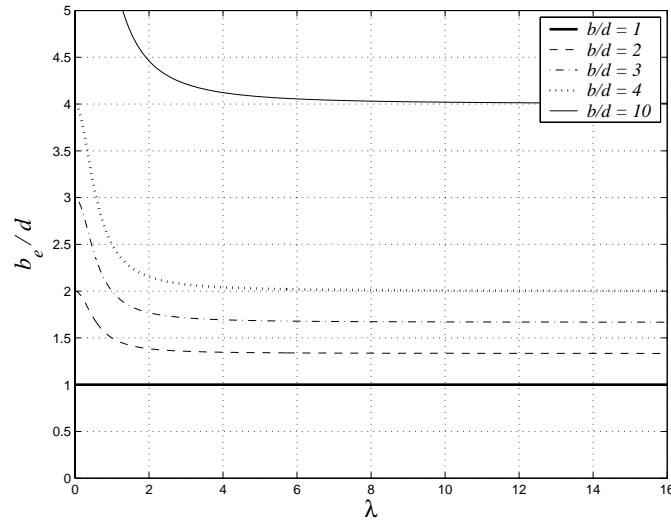


Figure 6.5:  $b_e/d$  as a function of  $\lambda$  for different values of  $b/d$

The vertical component of the uniaxial tension stresses has to be carried by the flange, hence in the flange mechanism, a downwards, uniform load equal to  $\frac{1}{2} t_w f_{yw}$ , cf. Equations (2.2) and (2.7) in PART II, is taken into account. For the value of  $\beta$  determined by Equation (3.14), the resulting upwards, uniform load,  $n$ , applied on the flange is then given by, cf. Equation (3.12),

$$n = t_w f_{yw} \left( \frac{b_e}{b} - \frac{1}{2} \right) \quad (6.17)$$

By inserting Equation (6.17) into Equation (3.10), the load-carrying capacity is found to be

$$P_u = 2t_f^2 f_{yf} \frac{b_f}{b-c} + \frac{1}{2} t_w f_{yw} \left( \frac{b_e}{b} - \frac{1}{2} \right) (b+c) \quad (6.18)$$

To sum up the notations,  $b$  is the web panel width (distance between two adjacent stiffeners),  $c$  the patch load length,  $b_e$  the calculated effective width of the web plate, by Equation (6.13), and  $b_f$  is the flange width. Furthermore,  $t$  is thickness and  $f_y$  is the yield stress with indexes  $f$  for flange and  $w$  for web.

### 6.3 Web Panels with Uniaxial Tension in an Arbitrary Direction

Steel plate girders subjected to patch loading and with uniaxial tensile stresses in the web panel under an angle different from  $45^\circ$  may be treated as described in Sections 6.1 and 6.2. However in general, the solutions are cumbersome and they will not be shown in detail here. Only a brief description follows.

The same failure mechanisms are assumed, cf. Figures 6.1 and 6.3. The plastic yield moment of the yield lines in the two effective strips are considered to be fully utilised, i.e.  $m_p = 0$ . The bending moments in the other yield lines must be reduced according to the direction of the uniaxial tension stresses, cf. Equation (2.3) in PART III. Thereafter, the relative deflection increment,  $\psi$ , must be determined in order to take the effect from change of geometry into consideration. Then the calculations may follow the procedure as described in Sections 6.1 and 6.3.

## 7 CONCLUSION

A simplified theory for calculating the load-carrying capacity of steel plate girders subjected to patch loading has been developed. The theory is simplified due mainly to the assumption that the whole web panel under the patch load will always be active. The post-buckling strength of the web panel is determined by the effective width approach. The stresses in these effective widths will be uniformly distributed under the flange and utilised in a flange mechanism, which is calculated separately.

The solutions are derived separately for girders with a square web panel and for those with a rectangular web panel.

Both solutions are compared with experimental results, and the theories correlate well with these tests, especially the girders with rectangular web panels.

Furthermore, it is shown how to calculate the load-carrying capacity of girders subjected to patch loading and designed according to the plastic tension field method, where uniaxial stresses equal to the yield stress occur.

Finally, the topic of flange induced buckling is touched upon, and it is shown that the theory is also able to deal with this phenomenon.

## 8 REFERENCES

- BASLER, K. and THÜRLIMANN, B. (1961). Strength of Plate Girders in Bending. *Proc. ASCE, J. Struct. Div.* **ST 7**, 153-181.
- BERGFELT, A. (1979). *Patch Loading on a Slender Web*. Int. skr. S79:1. Göteborg: Chalmers University of Technology, Inst. for konst., Stål-och Träbyggnad.
- BERGFELT, A. and HOVIK, J. (1968). Thin Walled Deep Plate Girders under Static Loads. *Proc. 8th Congr. IABSE*, New York, 465-478.
- BERGFELT, A. and HOVIK, J. (1970). *Shear Failure and Local Web Crippling in Thin Walled Plate Girders under Concentrated Loads*. Int. skr. S70:11b. Göteborg: Chalmers University of Technology, Inst. for konst., Stål-och Träbyggnad.
- DRDACKY, M. and NOVOTNY, R. (1977). *Partial Edge Load Carrying Capacity Tests on Thick Plate Girder Webs*. No. 5. Prague: Acta Tech.
- EUROPEAN COMMITTEE FOR STANDARDISATION (EC3 1993). *Eurocode 3: Design of Steel Structures – Part 1-1: General Rules and Rules for Buildings*. EN 1993-1-1: 1993. Brussels: CEN.
- EUROPEAN COMMITTEE FOR STANDARDISATION (EC3 2006). *Eurocode 3: Design of Steel Structures – Part 1-5: Plated Structural Elements*. EN 1993-1-5: 2006. Brussels: CEN.
- GRANHOLM, C. A. (1976). *Light Girders. Girders with Slender Flanges and Web*. Int. skr. S76:14. Göteborg: Chalmers University of Technology, Inst. for konst., Stål-och Träbyggnad.
- JOHANSSON, B., MAQUOI, R. and SEDLACEK, G. (2001). New Design Rules for Plated Structures in Eurocode 3. *Journal of Constructional Steel Research*, **57**, 279-311.
- KHAN, M. Z. and WALKER, A. C. (1972). Buckling of Plates Subjected to Localised Edge Loading. *Structural Engineer*, **50(6)**, 225-232.
- ROBERTS, T. M. (1983). Patch Loading on Plate Girders. In: R. Narayanan (Ed.), *Plated Structures: Stability and Strength* (Chapter 3 pp. 77-102). Essex: Applied Science Publishers Ltd.
- ROBERTS, T. M. and ROCKEY, K. C. (1977). A Mechanism Solution for Predicting the Collapse Loads of Slender Plate Girders when Subjected to in-Plane Patch Loading. *Proc. Instn. Civ. Engrs, Part 2*, **67**, 155-175.
- SKALOUD, M. and NOVAK, P. (1975). Post-Buckled Behaviour of Webs under Partial Edge Loading, *Acad. Sci. Rep.* **85(3)**. Prague.
- SOMMERFIELD, A. Z. (1906). *Z. Math. Phys.*, **54(113)**.
- TIMOSHENKO, S. P. (1910). *Z. Math. Phys.*, **58(357)**.
- TIMOSHENKO, S. P. and GERE, J. M. (1961). *Theory of Elastic Stability* (2nd ed.). New York: McGraw-Hill Book Co., Inc.
- WHITE, R. M. and COTTINGHAM, W. (1962). Stability of Plates under Partial Edge Loadings. *Proc. ASCE*, **88**, 67-86.
- ZETLIN, L. (1955). Elastic Instability of Flat Plates Subjected to Partial Edge Loads. *Proc. ASCE*, **81**, Paper 795, 1-24.

## 9 NOTATION

$b$	width of web panel
$b_e$	total effective width
$b_f$	flange width
$b_s$	width of effective strip
$c$	length of patch load
$d$	girder depth, i.e. depth of the web plate
$f_y$	yield stress
$f_{yf}, f_{yw}$	flange yield stress and web yield stress, respectively
$k$	factor
$m_p$	plastic yield moment per unit length
$n$	load per unit length; upwards, uniform reaction on flange mechanism
$p$	patch load per unit length
$t_f$	flange thickness
$t_w$	web thickness
$u_m$	deflection at maximum load
$u_{m,web}$	deflection at maximum load for web plate
$x, y$	coordinates in a Cartesian $x,y$ -system of coordinates
$x$	web plate depth included in the internal beam
$x_f$	web plate depth included in the internal beam from flange yielding
$A_w$	cross-sectional area of the web
$A_{fc}$	effective cross-sectional area of the compression flange
$E$	Young's modulus
$M_p$	plastic yield moment of internal beam
$M_{pf}$	plastic yield moment of flange
$N$	normal force
$N_p$	normal force, load-carrying capacity in pure compression or tension
$P_{exp}$	force, experimental load-carrying capacity
$P_u$	force, ultimate load-carrying capacity
$W_e$	external work
$W_i$	dissipation
$X$	free optimisation parameter
$\alpha$	length
$\beta$	length
$\delta$	displacement increment
$\delta_v$	vertical displacement increment
$\epsilon_y$	yield strain
$\lambda$	non-dimensional parameter
$\nu$	Poisson's ratio
$\theta$	angle
$\rho$	radius of curvature
$\sigma_{cr}$	elastic critical buckling stress
$\sigma_f$	flange normal stress
$\sigma_x, \sigma_y$	normal stress in the $x$ -direction and $y$ -direction, respectively
$\tau_{max}$	maximum shear stress
$\tau_{xy}$	shear stress in the $xy$ -plane
$\psi$	relative deflection increment

---

## **CONCLUSION & REFERENCES**

---



## CONCLUSION

Simple hand-calculation methods, which may be used to treat important practical design problems, are developed. The derived solutions concern statically loaded fillet welds, plate girders in shear, thin plates in compression and patch loading on plate girders, respectively.

Initially, yield conditions are determined for symmetric fillet welds and single fillet welds, respectively. If inclined uniaxial stress through the welds cannot be established, the load-carrying capacity must be reduced.

The yield conditions are compared to tests where emphasis is attached to the determination of the yield load instead of the failure load. There is a very good agreement with the tests. The best agreement is obtained with tests where the specimens have been cut out of a steel plate; hence the welds are only marked by the geometry. In this way, the number of unknown parameters is reduced.

Furthermore, a calculation method, i.e. the plastic tension field method for steel plate girders with transverse web stiffeners subjected to shear, is presented. The method differs from other theories by incorporating the strength of the transverse stiffeners and by the assumption that the tensile bands may pass the transverse stiffeners.

The load-carrying capacity of a given steel plate girder may be predicted by applying both the lower-bound and the upper-bound theorem. As a design method, the lower-bound theorem is the easiest to apply. By introducing circular fan solutions, almost any load case may be treated.

The theory is compared to both old and new plate girder experiments. The theory coincides closely with these tests, except for girder specimens without intermediate web stiffeners.

Additionally, it is shown that extremely simple estimates of the post-buckling strength of plates with in-plane loading may be obtained by using plastic solutions for the deflected shape. This shape must be known before the calculation can be carried out. It seems that useful estimates of the deflected shape may be found using simple formulae from beam and plate theory.

The results are compared with the well-known Winter's formulae and with tests. The agreement is very good in both cases.

Finally, a simplified theory for calculating the load-carrying capacity of steel plate girders subjected to patch loading is developed. The theory is simplified due mainly to the assumption that the whole web panel under the patch load will always be active. The post-buckling strength of the web panel is determined by the effective width approach. The stresses in these effective widths will be uniformly distributed under the flange and utilised in a flange mechanism, which is calculated separately.

The solutions are derived separately for girders with a square web panel and for those with a rectangular web panel.

Both solutions are compared with experimental results, and the theories correlate well with these tests, especially for girders with rectangular web panels.

It is also shown how one may calculate the load-carrying capacity of girders subjected to patch loading and designed according to the plastic tension field method, where uniaxial stresses equal to the yield stress occur.

## CONCLUSION

The topic of flange induced buckling is also touched upon, and it is shown that the theory is also able to deal with this phenomenon.

## RECOMMENDATIONS FOR FUTURE WORK

The load-carrying capacity of fillet welds under static loading is probably to a sufficient degree covered by the derived equations. However, it would be relevant to check the assumption of rigid-plastic materials. This might be possible by applying fracture mechanics to investigate the yield capacity of some common welded connections.

The described experiments relating to plate girders in shear have shown that the post-buckling strength of girders without intermediate web stiffeners is considerably larger than predicted by the theory. Hence, further investigations of this phenomenon are recommended, for instance through more experiments where the design of the web stiffeners, under the subjected loads, is varied. Alternatively, one might vary the stiffness of the end panels. Furthermore, the upper-bound solution may need to be modified, for instance by considering a failure mechanism with plastic yield hinges in the stiffeners under the subjected loads.

Deriving the solutions by applying a yield condition such as von Mises', without compressive strength, possibly may give a slightly larger load-carrying capacity. It would be of interest to see how much a more complicated yield condition would increase the load-carrying capacity.

Furthermore, the upper-bound solution for thick web plates should be extended, taking into account intermediate web stiffeners.

The design method applying circular fans is currently only able to treat plate girders with constant depth. It would be of interest to extend the method to treat plate girders with variable depth.

The post-buckling theory for thin plates in compression should be investigated further, as it may be able to deal with several other important cases, e.g. fixed boundaries, biaxial loading, lateral loading, etc.

Considering the theory of plate girders subjected to patch loading, it would be useful to carry out further tests, where the loaded flange is also subjected to a large compressive normal force, in order to investigate the flange induced buckling phenomenon more closely.

## REFERENCES

- BAKER, J. F., HORNE, M. R. and HEYMAN, J. (1956). *The Steel Skeleton – Volume II: Plastic Design and Behaviour*. Cambridge: Cambridge University Press.
- BAMBACH, M. R. and RASMUSSEN, K. J. R. (2004). Tests on Unstiffened Plate Elements under Combined Compression and Bending. *J. Struct. Eng. ASCE* **130**(10), 1602-1610.
- BASLER, K. (1961). Strength of Plate Girders in Shear. *Proc. ASCE, J. Struct. Div.* **ST 7**, **87**(2), 151-180.
- BASLER, K. and THÜRLIMANN, B. (1961). Strength of Plate Girders in Bending. *Proc. ASCE, J. Struct. Div.* **ST 7**, 153-181.
- BASLER, K., YEN, B., MUELLER and THÜRLIMANN, B. (1960). Web Buckling Tests on Welded Plate Girders. *Welding Research Council, Bulletin No. 64*.
- BERGFELT, A. (1973). Plate Girders with Slender Web-Survey and a Modified Calculation Method. *Report No. 11 2.2*. Oslo: Nordiske forskningsdager for stålkonstruksjoner.
- BERGFELT, A. (1979). *Patch Loading on a Slender Web*. Int. skr. S79:1. Göteborg: Chalmers University of Technology, Inst. for konst., Stål-och Träbyggnad.
- BERGFELT, A. and HOVIK, J. (1968). Thin Walled Deep Plate Girders under Static Loads. *Proc. 8th Congr. IABSE*, New York, 465-478.
- BERGFELT, A. and HOVIK, J. (1970). *Shear Failure and Local Web Crippling in Thin Walled Plate Girders under Concentrated Loads*. Int. skr. S70:11b. Göteborg: Chalmers University of Technology, Inst. for konst., Stål-och Träbyggnad.
- BONNERUP, B and JENSEN, B. C. (2003). *Stålkonstruktioner efter DS 412* (1. udg.). København: Ingeniøren/Bøger.
- BRYAN, G. H. (1891). On the Stability of a Plane Plate under Thrusts in Its Own Plane, with Applications to the Buckling of the Sides of a Ship. *Proc. Lond. Math. Soc.* **22**.
- BUTLER, L. J. and KULAK, G. L. (1971). Strength of Fillet Welds as a Function of Direction of Load. *Welding Journal Supplement*, **36**(5), 231-234.
- CALLADINE, C. R. (1973). A Plastic Theory for Collapse of Plate Girders under Combined Shearing Force and Bending Moment. *The Structural Engineer*, **51**(4), 147-154.
- CLARK, P. J. (1972). Basis of Design for Fillet-Welded Joints Under Static Loading. *Proceedings, Conference on Welding Product Design*. Vol. 2. Welding Institute, Abington U.K., 85-96.
- COOPER, P. B., LEW, H. S. and YEN, B. (1964). Welded Constructional Alloy Steel Plate Girders. *Proc. ASCE, J. Struct. Div.* **ST 1**, **90**, 1-36.
- D'APICE, M. M., FIELDING, D. J. and COOPER, P. B. (1966). Static Tests on Longitudinally Stiffened Plate Girders. *Welding Research Council, Bulletin No. 117*.
- DANSK STANDARD (1999). *DS 412: Norm for stålkonstruktioner* (3. udg.). København: Dansk Standard.
- DRDACKY, M. and NOVOTNY, R. (1977). *Partial Edge Load Carrying Capacity Tests on Thick Plate Girder Webs*. No. 5. Prague: Acta Tech.
- DRUCKER, D. C., GREENBERG, H. J. and PRAGER, W. (1952). Extended Limit Design Theorems for Continuous Media. *Q. Appl. Math.* **10**, 157-165.
- DUBAS, P. (1974). *Zur Erschöpfungslast schubbeanspruchter Stehbleche*. Karlsruhe: Professor Steinhardt Festschrift.
- DUBAS, P. and GEHRI, E. (1986). *Behaviour and Design of Steel Plated Structures: Applied Statics and Steel Structures*. Zürich: ECCS, ETH-Hönggerberg.
- EB VAN DER, W. J. (1952). The Testing of End Fillet Welds. *Vorbereich 4. Kongress Int. Ver. für Brückenbau und Hockbau*, 459-474.

## REFERENCES

- EUROPEAN COMMITTEE FOR STANDARDISATION (EC3 1993). *Eurocode 3: Design of Steel Structures – Part 1-1: General Rules and Rules for Buildings*. EN 1993-1-1: 1993. Brussels: CEN.
- EUROPEAN COMMITTEE FOR STANDARDISATION (EN 2001). *Metallic Materials – Tensile Testing – Part 1: Method of Test at Ambient Temperature*. EN 10002-1. Brussels: CEN.
- EUROPEAN COMMITTEE FOR STANDARDISATION (EC2 2004). *Eurocode 2: Design of Concrete Structures – Part 1-1: General Rules and Rules for Buildings*. EN 1992-1-1: 2004. Brussels: CEN.
- EUROPEAN COMMITTEE FOR STANDARDISATION (EC3 2005). *Eurocode 3: Design of Steel Structures – Part 1-1: General Rules and Rules for Buildings*. EN 1993-1-1: 2005. Brussels: CEN.
- EUROPEAN COMMITTEE FOR STANDARDISATION (EC3 2006). *Eurocode 3: Design of Steel Structures – Part 1-5: Plated Structural Elements*. EN 1993-1-5: 2006. Brussels: CEN.
- EUROPEAN COMMITTEE FOR STANDARDISATION (EC3 2005). *Eurocode 3: Design of Steel Structures – Part 1-8: Design of Joints*. EN 1993-1-8: 2005. Brussels: CEN.
- EUROPEAN CONVENTION FOR STRUCTURAL STEELWORK (ECCS 1989). *Background Documentation to Eurocode 3-1-1*. Chapter 6, Document 6.05.
- FUJII, T., FUKOMOTO, Y., NISHINO, F. and OKUMURA, T. (1971). Research Works on Ultimate Strength of Plate Girders and Japanese Provisions on Plate Girder Design. *IABSE Colloquium*, 21-48.
- GALAMBOS, T. V. (1988). *Guide to Stability Design: Criteria for Metal Structures* (4th ed.). New York: John Wiley & Sons, Inc.
- GATH, J. (1997). *Stålkonstruktioner: Beregning af svejsesamlinger i fågangspåvirkede stålkonstruktioner*. Lyngby: BYG•DTU, Danmarks Tekniske Universitet.
- GAYLORD, E. H. (1963). Discussion of K. Basler 'Strength of Plate Girders in Shear'. *Trans. ASCE*, **128**, Part II, pp. 712.
- GRANHOLM, C. A. (1976). *Light Girders. Girders with Slender Flanges and Web*. Int. skr. S76:14. Göteborg: Chalmers University of Technology, Inst. for konst., Stål-och Träbyggnad.
- GRIFFITH, A. A. (1921). The Phenomena of Rupture and Flow in Solids. *Phil. Trans. Roy. Soc. London*, Vol. A **221**, 163-197.
- GRIFFITH, A. A. (1924). The Theory of Ructure. *Proc. 1st Conf. Appl. Mech. Delft*.
- GVOZDEV, A. A. (1938). *Opredelenie velichiny razrushayushchei nagruzki dlya staticheskoi neopredelimoj sistem, preterpevayushchikh plasticheskie deformatsii*. Moscow/Leningrad: Akademia Nauk SSSR. An English translation is found in: GVOZDEV, A. A. (1960). The Determination of the Value of the Collapse Load for Statically Indeterminate Systems undergoing Plastic Deformation. *Int. J. Mech. Sci.* **1**, 322-333.
- HANSEN, T. (2004). *Plasticitetsteori for svejsesømme: Nedreværdiløsninger for statisk last*. R-144. Lyngby: BYG•DTU, Danmarks Tekniske Universitet.
- HANSEN, T. (2005). Plasticity Theory of Fillet Welds: Lower-Bound Solutions for Static Loading. *Proc. 4th European Conf. on Steel and Composite Structures. EUROSTEEL 2005, Vol. C, Maastricht, 8-10 June 2005 (pp. 4.10-99 - 4.10-106)*. Aachen: Druck und Verlagshaus Mainz GmbH Aachen.
- HANSEN, T. and NIELSEN M. P. (2005). The Diagonal Compression Field Method using Circular Fans. *Bygningsstatistiske Meddelelser*, **76(4)**, 95-124.
- HANSEN, T. and NIELSEN, M. P. (2005). The Plastic Tension Field Method. *Innovation & Sustainability of Structures: Proc. Intern. Symp. on Innovation & Sustainability of Structures in Civ. Eng. ISSS'2005, Vol. 1, Nanjing, 20-22 November 2005 (pp. 607-618)*. Nanjing: Southeast University Press.
- HANSEN, T. and NIELSEN, M. P. (2006). Effective Width Equations According to the Theory of Plasticity. *Progress in Steel, Composite and Aluminium Structures: Proc. XI<sup>th</sup> Intern. Conf. on Metal Structures. ICMS 2006, Rzeszów, 21-23 June 2006 (pp. 154)*. London: Taylor & Francis Group.
- HERZOG, M. (1974). Die Traglast unversteifter und versteifter, dünnwandigen Blechträger unter reinem Schub und Schub mit Biegung nach Versuchen. *Der Bauingenieur*, **49**, 382-389.

- HIRIYUR, B. K. J. and SCHAFER, B. W. (2004). Yield-Line Analysis of Cold-Formed Steel Members. *Submitted to International Journal of Steel Structures*, August 2004.
- HÖGLUND, T. (1973). *Design of Thin Plate I-Girders in Shear and Bending with Special Reference to Buckling*. No. 94. Stockholm: Kungl. Tekniska Högskolan, Inst. for bygnadsstatik.
- HÖGLUND, T. (1995). *Strength of Steel and Aluminium Plate Girders: Shear Buckling and Overall Web Buckling of Plane and Trapezoidal Webs – Comparison with Tests*. Tech. Report No. 4. Stockholm: Royal Institute of Technology, Department of Structural Engineering.
- INGERSLEV, Å. (1923). The Strength of Rectangular Slabs. *J. Inst. Struct. Eng.* **1**(1), 3-14.
- IRWIN, G. R. (1948). Fracture Dynamics. *Fracturing of Metals, American Soc. for Metals, Cleveland*, 147-166.
- JENSEN, C. D. (1934). Combined Stresses in Fillet Welds. *Journal of the American Welding Society*, **13**, pp 17-21.
- JENSEN, AA. P. (1991). *Svejsesømmes styrke*. Lyngby: Danmarks Ingeniørakademi.
- JOHANSEN, K. W. (1943). *Brudlinieteorier*. Copenhagen: Gjellerup. An English translation is found in: JOHANSEN, K. W. (1962). *Yield Line Theories*. London: Cement and Concrete Association.
- JOHANSSON, B., MAQUOI, R. and SEDLACEK, G. (2001). New Design Rules for Plated Structures in Eurocode 3. *Journal of Constructional Steel Research*, **57**, 279-311.
- KALYANARAMAN, V., WINTER, G. and PEKOZ, T. (1977). Unstiffened Compressed Elements. *J. Struct. Div. ASCE*, **103**(9), 1833-1848.
- KÁRMÁN, T. VON, SECHLER, E.E. and DONNELL, L.H. (1932). The Strength of Thin Plates in Compression. *Trans. ASME* **54**, 53-57.
- KHAN, M. Z. and WALKER, A. C. (1972). Buckling of Plates Subjected to Localised Edge Loading. *Structural Engineer*, **50**(6), 225-232.
- KIST, N. C. (1936). Berechnung der Schweissnähte unter Berücksichtigung konstanter Gestaltänderungsenergie. *Vorbereich 2. Kongress Int. Ver. für Brückenbau und Hochbau*.
- KOMATSU, S. (1971). Ultimate Strength of Stiffened Plate Girders Subjected to Shear. *IABSE Colloquium*, 49-65.
- LEW, H. S., NATARAJAN, M. and TOPRAC, A. A. (1969). Static Tests on Hybrid Plate Girders. *Welding Research Council, Supplement Vol. 75*, pp. 86.
- LIGTENBERG, F. K. and VAN MELLE, F. (1964). Onderzoek naar de Vervorming van statisch belaste hoekklasse. *Heron*, **12**(1).
- LONGBOTTON, E. and HEYMAN, J. (1956). Experimental Verification of the Strength of Plate Girders Designed in Accordance with the Revised British Standard 153: Tests on Full-Size and on Model Plate Girders. *Inst. Civ. Engrs. Proc.*, **5**, 462-486.
- LUNDGREN, H. (1949). *Cylindrical Shells*. Copenhagen: The Danish Technical Press, the Institution of Danish Civil Engineers.
- LYSE, I. and GODFREY, H. J. (1935). Investigation of Web Buckling in Steel Beams. *Trans. ASCE*, **100**, 675-695.
- MARSH, C. (1985). Strength of Aluminum Fillet Welds. *Welding Journal, Welding Research Supplement*, 335-338.
- MIAZGA, G. S. and KENNEDY, D. L. J. (1989). Behaviour of Fillet Welds as a Function of the Angle Loading. *Canadian Journal of Civil Engineering*, **6**, 583-599.
- MOXHAM, K. E. (1971). *Buckling Tests on Individual Welded Steel Plates in Compression*. Report CUED/C-Struct/TR.3. Cambridge: University of Cambridge.
- MURRAY, N. W. (1984). *Introduction to the Theory of Thin-Walled Structures*. Oxford: Clarendon Press, Oxford Science Publications.
- NIELSEN, M. P. (1998). *Limit Analysis and Concrete Plasticity* (2nd ed.). Boca Raton, Florida: CRC Press.

## REFERENCES

- NIELSEN, M. P. and CHRISTENSEN S. B. (1982). Post-Buckling Strength of Steel Plate Girders Subjected to Shear. *Bygningsstatistiske Meddelelser*, **53**(3), 95-124.
- NIELSEN, M. P. and PILEGAARD HANSEN, L. (1971). *AM 1.1. Stålkonstruktioner: Materialer og samlinger*. Aalborg: Danmarks Ingeniørakademi.
- NIELSEN, M. P., PILEGAARD HANSEN, L. and RATHKJEN, A. (2000). *Mekanik 2.2 del 2: Rumlige spændings- og deformationstilstande*. Aalborg/ København: Institut for Bærende Konstruktioner og Materialer, Danmarks Tekniske Universitet.
- NISHINO, F. and OKUMURA, T. (1968). Experimental Investigation of Strength of Plate Girders in Shear. *IABSE, Proc. 8th Congr, Final Report*, 451-463.
- OROWAN, E. (1948). Fracture and Strength of Solids. *Reports on Progress in Physics, Vol. XII*, 185.
- OSTAPENKO, A. and CHERN, C. (1971). Ultimate Strength of Longitudinal Stiffened Plate Girders under Combined Loads. *IABSE Colloquium*, 301-313.
- PARIS, P. C., GOMEZ, R. E. and ANDERSON, W. E. (1961). A Rational Analytic Theory of Fracture. *The Trends in Engineering*, **13**(1), 9-14.
- PORTER, D. M., ROCKEY, K. C. and EVANS, H. R. (1975). The Collapse Behavior of Plate Girders Loaded in Shear. *The Structural Engineer*, **53**(8), 313-325.
- ROBERTS, T. M. (1983). Patch Loading on Plate Girders. In: R. Narayanan (Ed.), *Plated Structures: Stability and Strength* (Chapter 3 pp. 77-102). Essex: Applied Science Publishers Ltd.
- ROBERTS, T. M. and ROCKEY, K. C. (1977). A Mechanism Solution for Predicting the Collapse Loads of Slender Plate Girders when Subjected to in-Plane Patch Loading. *Proc. Instn. Civ. Engrs, Part 2*, **67**, 155-175.
- ROCKEY, K. C. and SKALOUD, M. (1971). The Ultimate Behavior of Plate Girders Loaded in Shear. *IABSE Colloquium*, 1-19.
- SAKAI, F., DOI, K., NISHINO, F. and OKUMURA, T. (1966). *Failure Tests of Plate Girders using Large Sized Models*. Tokyo: Dept. of Civ. Eng., University of Tokyo.
- SCHUMAN, L. and BACK, G. (1930). *Strength of Rectangular Flat Plates under Edge Compression*. Technical Report No. 356: National Advisory Committee for Aeronautics.
- SECHLER, E. E. (1933). *The Ultimate Strength of Thin Flat Sheet in Compression*. Publication No. 27. Pasadena: Guggenheim Aeronautics Laboratory, California Inst. of Technology.
- SELBERG, A. (1963). *Stålkonstruksjoner*. Trondheim: Tapir Forlag.
- SKALOUD, M. (1971). Ultimate Load and Failure Mechanism of Thin Webs in Shear. *IABSE Colloquium*, 115-127.
- SKALOUD, M. and NOVAK, P. (1975). Post-Buckled Behaviour of Webs under Partial Edge Loading, *Acad. Sci. Rep.* **85**(3). Prague.
- SOMMERFIELD, A. Z. (1906). *Z. Math. Phys.*, **54**(113).
- SWANNELL, P. (1981). Rational Design of Weld Groups. *Journal of Structural Division. ASCE*, **107**(ST5), 789-802.
- SWANNELL, P. and SKEWES, I. C. (1978). The Design of Welded Brackets Loaded in Plane: (General Theoretical ultimate load techniques and experimental program). *Australian Welding Research Association Report P6-1-78. Australian Welding Research*, **7**, 55-70.
- TIMOSHENKO, S. P. (1910). *Z. Math. Phys.*, **58**(357).
- TIMOSHENKO, S. P. and GERE, J. M. (1961). *Theory of Elastic Stability* (2nd ed.). New York: McGraw-Hill Book Co., Inc.
- TOLDERLUND, M. (2000). Plasticitetsteori for ståldragere: Diagonaltrækmetoden (M.Sc. Thesis). Lyngby: BYG•DTU, Danmarks Tekniske Universitet.
- WAGNER, H. (1929). Ebene Blechwandträger mit sehr dünnen Stegblech. *Z. für Flugtechnik und Motorluftschiffahrt*, **20**, 200-207, 227-233, 279-284, 306-314.

- WHITE, R. M. and COTTINGHAM, W. (1962). Stability of Plates under Partial Edge Loadings. *Proc. ASCE*, **88**, 67-86.
- WINTER, G. (1947). Strength of Thin Steel Compression Flanges. *Trans. ASCE, Paper No. 2305*, **112**, 527-554.
- WITTEVEEN, J. and VAN DOUWEN, A. A. (1966). Voorstel tot Wijziging van de I.S.O.-formule voor lasberekeningen in een op de vloeihypothese van Huber-Hencky aansluitende formule. *Overdruk uit Lastechniek*, **32e** (6), Uitgevers Wyt-Rotterdam.
- ZETLIN, L. (1955). Elastic Instability of Flat Plates Subjected to Partial Edge Loads. *Proc. ASCE*, **81**, Paper 795, 1-24.
- ZHAO, X. L. (2003). Yield Line Mechanism Analysis of Steel Members and Connections. *Structural Analysis and CAD, Prog. Struct. Engng. Mater.*, **5**, 252-262.
- ØSKAN, A. and BAK, C. (2006). Diagonaltrækmetode for ståldragere (M.Sc. Thesis). Lyngby: BYG•DTU, Danmarks Tekniske Universitet.



---

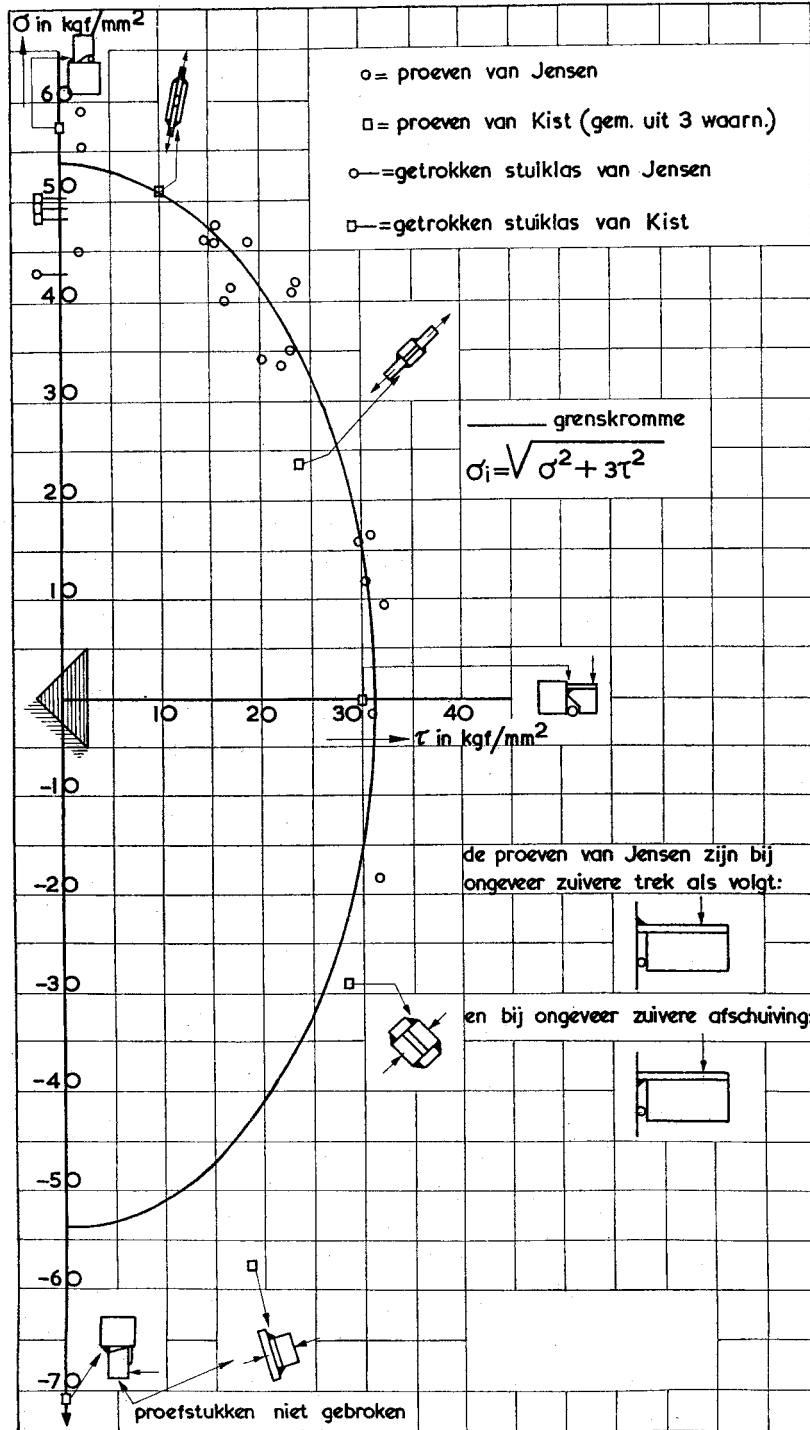
# APPENDICES

---



APPENDIX A

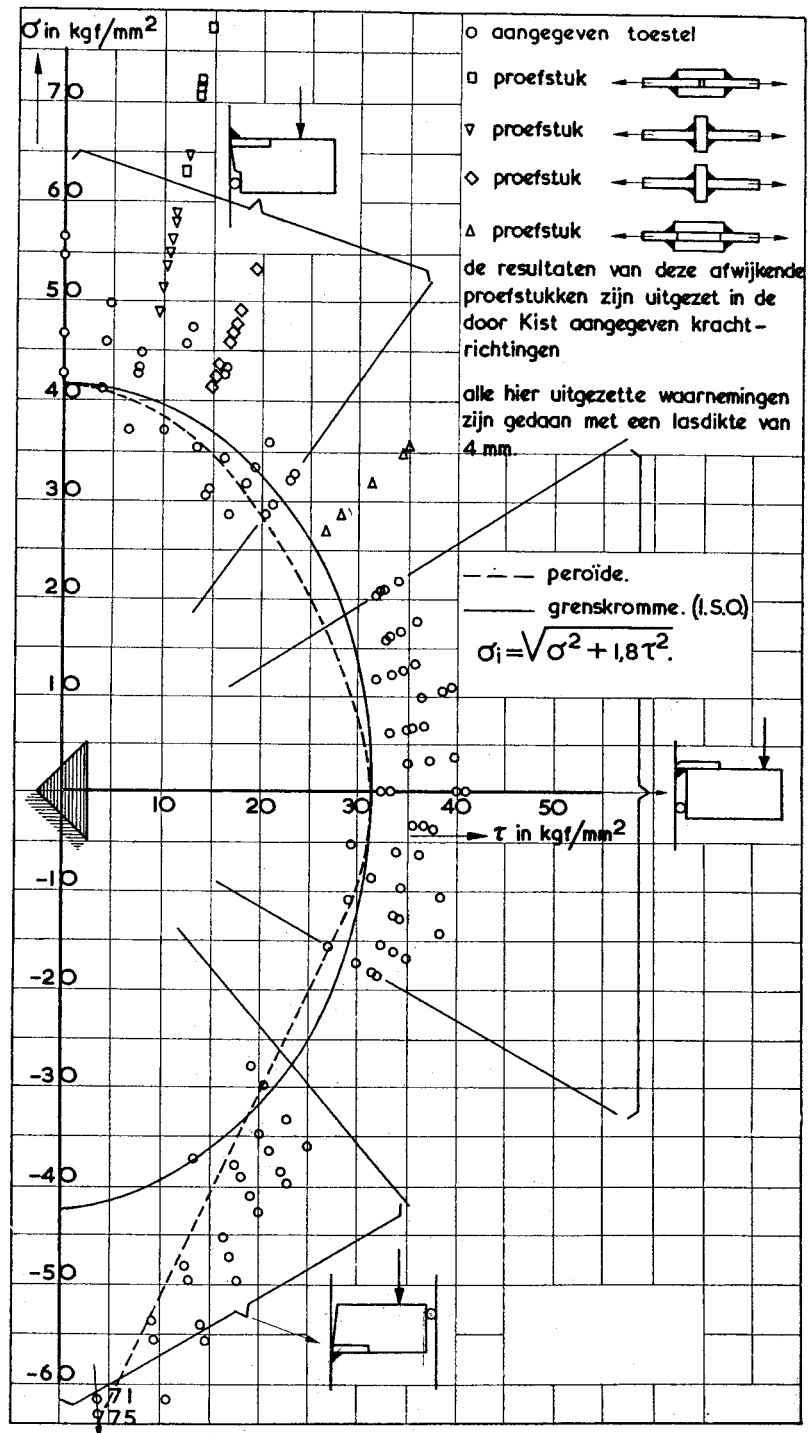
Test specimens and experimental results by Jensen (1934) and Kist (1936).



The figure is taken from (Witteveen and van Douwen 1966).

## APPENDIX B

Test specimens and experimental results by van der Eb (1952).

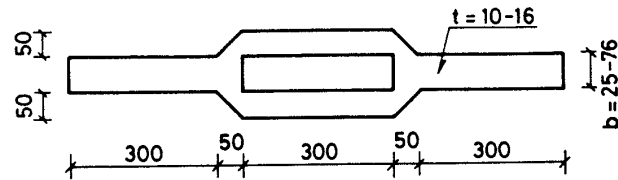


The figure is taken from (Witteveen and van Douwen 1966).

## APPENDIX C

## Tests with load case N.

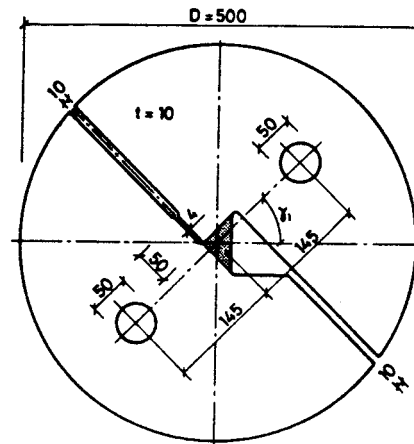
Experiments by Jensen (1991).



No.	Dimension			$f_y$ [MPa]	$N_y$ [kN]			$N_y / aL f_y$	$f_u$ [MPa]	$N_u$ [kN]	$N_u / aL f_y$
	$a$ [mm]	$L(t)$ [mm]	$b$ [mm]		Test	Lower	Upper				
1	36.8	9.5	46.3	275.0	113.1	111.0	126.9	1.176	414.0	183.1	1.265
2	36.5	9.4	45.9	273.0	113.1	108.2	123.6	1.207	412.0	175.1	1.239
3	36.6	9.4	46.1	277.0	115.9	110.0	125.8	1.216	422.0	179.8	1.238
4	36.7	9.4	46.3	274.0	112.1	109.1	124.8	1.186	413.0	181.1	1.271
5	36.7	16.3	55.7	247.5	169.1	171.0	195.4	1.142	414.0	374.8	1.513
6	37.1	16.4	56.4	246.0	169.1	172.8	197.5	1.130	411.5	378.0	1.510
7	36.2	16.3	56.0	256.0	175.8	174.4	199.4	1.164	411.5	369.0	1.520
8	36.4	15.3	56.1	248.0	156.8	159.5	182.3	1.135	413.0	368.5	1.602
9	36.7	16.2	66.1	244.0	168.2	167.5	191.5	1.159	417.7	403.0	1.623
10	36.6	16.3	66.2	250.0	166.3	172.2	196.8	1.115	415.0	-	-
11	36.4	16.3	65.9	247.0	167.2	169.2	193.4	1.141	410.0	-	-
12	36.2	16.3	66.3	241.5	177.7	164.5	188.1	1.247	417.7	402.5	1.633
13	36.1	12.3	76.9	284.0	157.7	145.6	166.4	1.251	417.7	264.5	1.426
14	36.7	12.4	76.1	286.5	152.0	150.6	172.1	1.166	439.5	405.0	2.025
15	36.4	12.4	76.3	288.5	146.3	150.4	171.9	1.124	417.7	-	-
16	36.8	12.3	76.5	285.0	150.1	149.0	170.3	1.164	436.5	405.0	2.050
Average:								1.170			1.532

**Test series S02.**

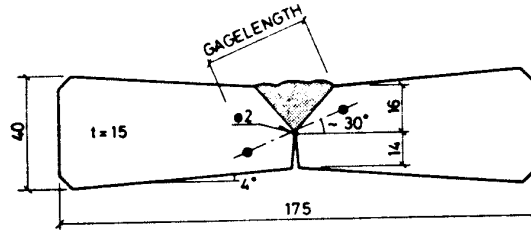
Experiments by Jensen (1991).



No.	$\gamma_1$ [°]	$P_y$ [kN]	$P_u$ [kN]	Throat area [mm <sup>2</sup> ]	$f_y$ [MPa]	$P_u / P_y$	$P_y / aL f_y$	$\sigma_{eff} / f_y$
01	90	80	131.0	336	251.5	1.64	0.94	1.056
02	80	70	131.5	336	251.5	1.88	0.82	1.042
03	70	60	126.5	336	251.5	2.11	0.70	1.089
04	60	55	119.5	339	251.5	2.17	0.65	1.049
05	50	48	110.0	343	251.5	2.29	0.56	1.087
06	40	45	101.5	338	251.5	2.11	0.53	1.047
07	20	40	92.0	336	251.5	2.30	0.47	1.060
08	0	40	91.5	339	251.5	2.29	0.48	1.066
09	10	38	85.0	350	225.0	2.24	0.48	1.026
10	30	40	96.0	347	225.0	2.40	0.51	1.017
12	65	54	112.0	350	225.0	2.07	0.69	1.053
13	75	65	128.0	350	225.0	1.97	0.83	0.989
14	85	75	135.0	347	225.0	1.80	0.96	0.961
<i>Average:</i>								1.042

**Test series 323.14 and 323.18.**

Experiments by Jensen (1991).



**323.14**

No.	aw / an	$\gamma_1$ [°]	$f_y$ [MPa]	L [mm]	Throat			$P_y$ [kN]	Theory $\sigma_{eff} / f_y$
					a [mm]	$a(1+\delta)$ [mm]	$\delta$		
2	an	45	427	14.4	15.1	16.7	0.11	47.5	1.253
3	-	0	-	14.7	15.4	16.7	0.08	44.0	1.186
4	-	90	-	14.2	13.5	14.5	0.07	71.5	1.225
5	-	60	-	14.6	14.2	15.9	0.12	61.3	1.095
6	-	75	-	14.3	13.7	14.8	0.08	68.0	1.103
7	-	30	-	14.4	14.5	15.6	0.08	51.0	0.984
1	aw	60	394	14.5	15.4	17.4	0.13	68.5	0.982
2	-	45	-	14.6	15.1	17.3	0.15	59.5	0.969
3	-	30	-	14.9	14.1	16.1	0.14	55.0	0.894
4	-	90	-	15.0	15.2	17.2	0.13	93.0	1.092
5	-	15	-	14.7	14.6	16.6	0.14	55.5	0.863
6	-	0	-	14.5	15.8	17.4	0.10	54.5	0.911
Average:									1.046

aw: as welded  
an: annealed

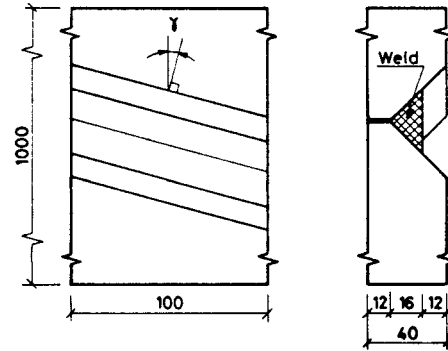
**323.18**

No.	aw / an	$\gamma_1$ [°]	$f_y$ [MPa]	L [mm]	Throat			$P_y$ [kN]	Theory $\sigma_{eff} / f_y$
					a [mm]	$a(1+\delta)$ [mm]	$\delta$		
1	aw	0	394	14.9	16.5	18.7	0.13	54.3	1.008
2	-	30	-	14.9	16.5	17.2	0.04	59.0	0.890
3	-	45	-	14.9	16.5	17.8	0.08	67.0	0.901
4	-	60	-	14.8	16.4	18.2	0.11	76.7	0.937
8	-	75	-	15.0	15.7	17.3	0.10	84.2	0.990
6	-	90	-	14.8	15.5	17.3	0.12	92.2	1.098
11	an	0	427	14.9	14.0	16.3	0.16	44.7	1.156
12	-	30	-	15.3	14.8	16.5	0.11	52.6	1.063
13	-	45	-	14.8	13.6	15.0	0.10	55.5	0.983
17	-	60	-	15.0	15.2	16.6	0.09	54.5	1.318
18	-	75	-	14.9	15.0	15.8	0.05	68.0	1.223
19	-	90	-	15.2	15.2	15.7	0.03	81.0	1.254
Average:									1.068

aw: as welded  
an: annealed

**Test series 323.23.**

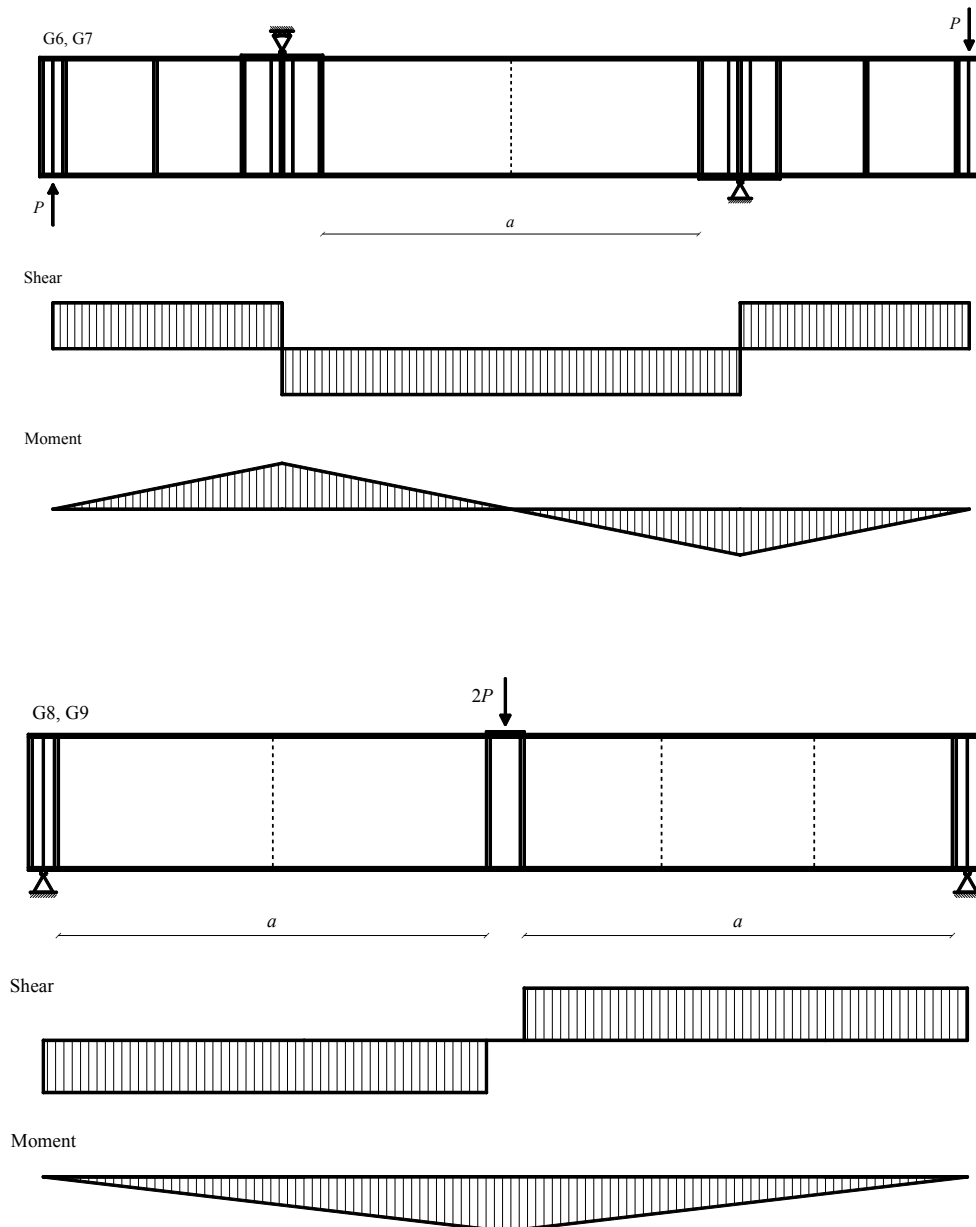
Experiments by Jensen (1991).



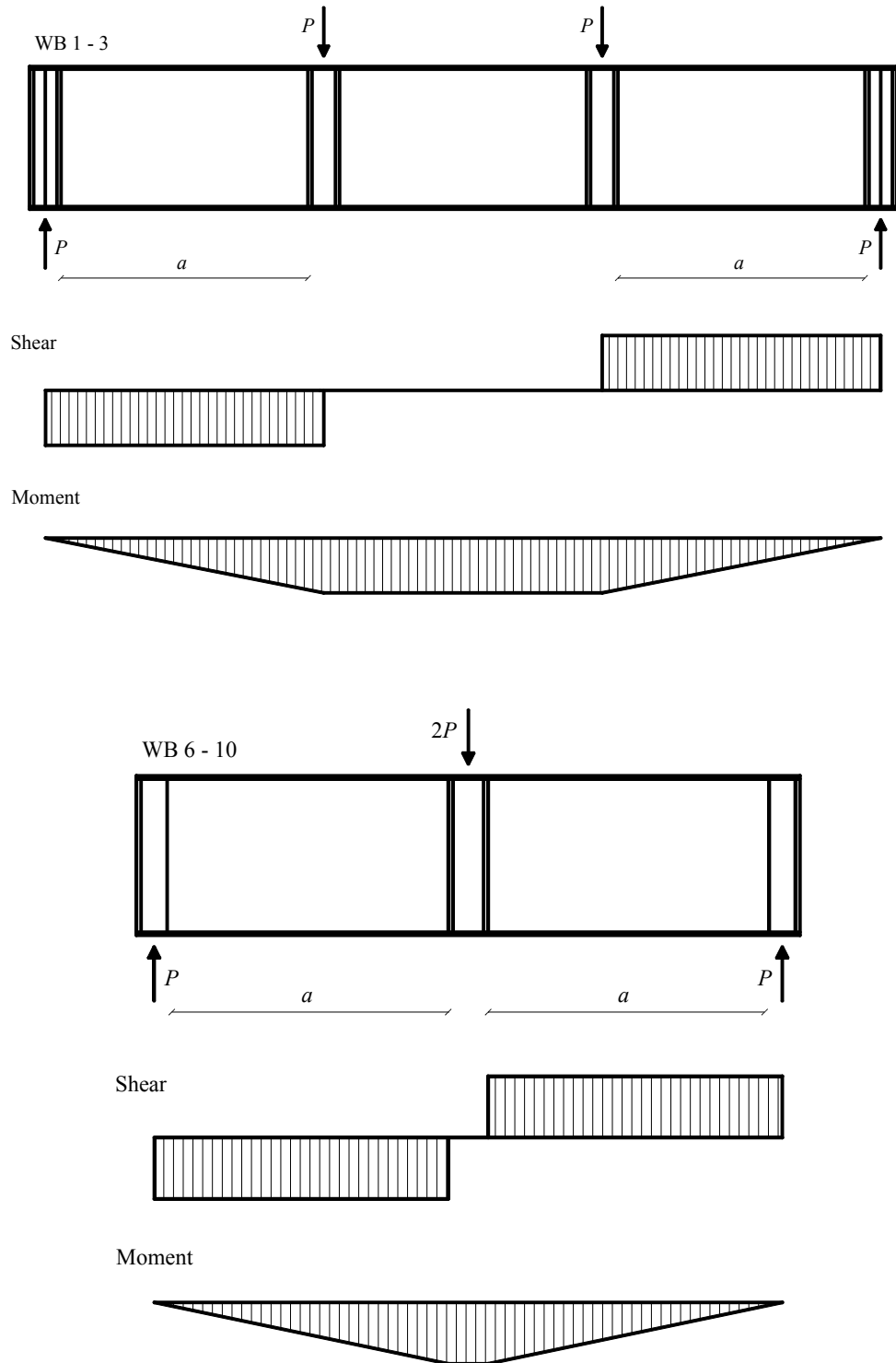
Group	$a$ [mm]	$\gamma$ [°]	$f_y$ [MPa]	$L$ [mm]	$P_y$ [kN]	Theory $\sigma_{eff} / f_y$
A	16.7	0	427	98.8	738	0.955
	17.9	15	-	103.5	778	0.955
	16.7	30	-	115.5	728	0.924
	16.8	45	-	141.4	677	1.059
B	15.2	0	427	99.5	735	0.879
	16.2	15	-	102.5	671	0.992
	14.8	30	-	114.3	628	0.939
	16.0	45	-	137.3	695	0.954
<i>Average:</i>						0.957

## APPENDIX D

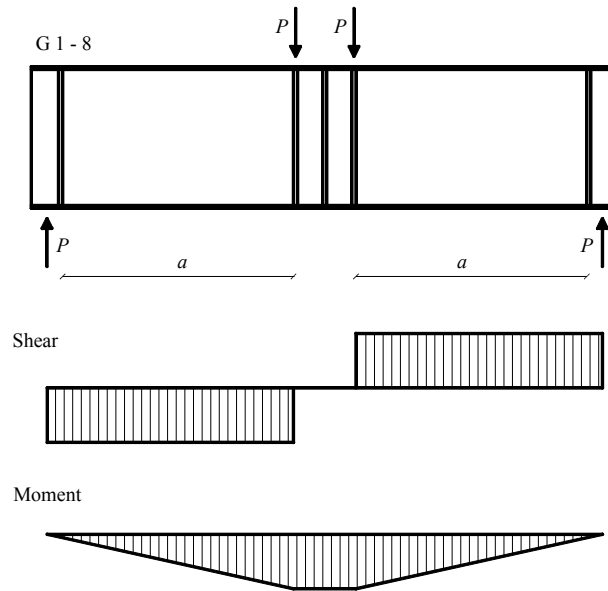
Experiments by Basler et al. (1961).



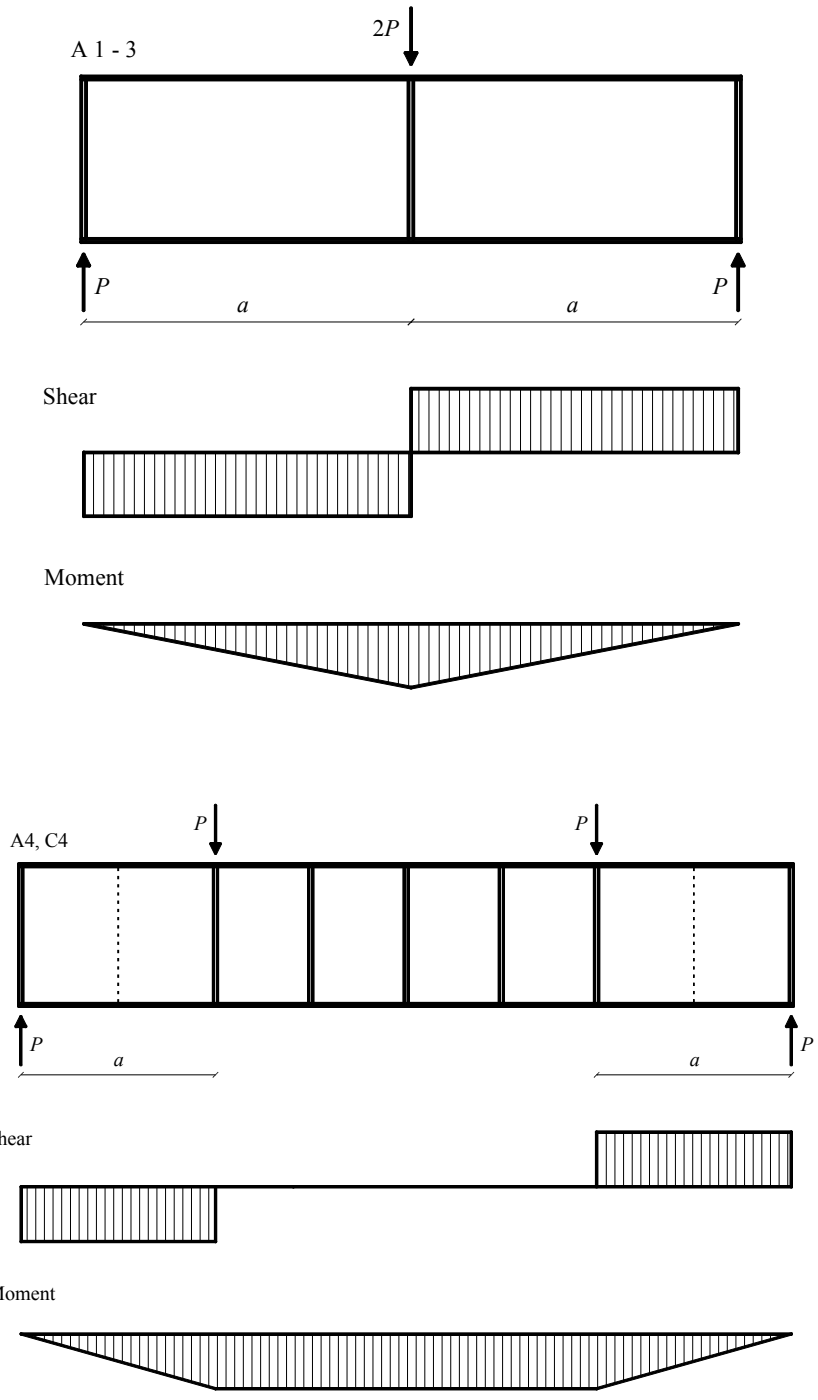
Experiments by Lyse and Godfrey (1935).



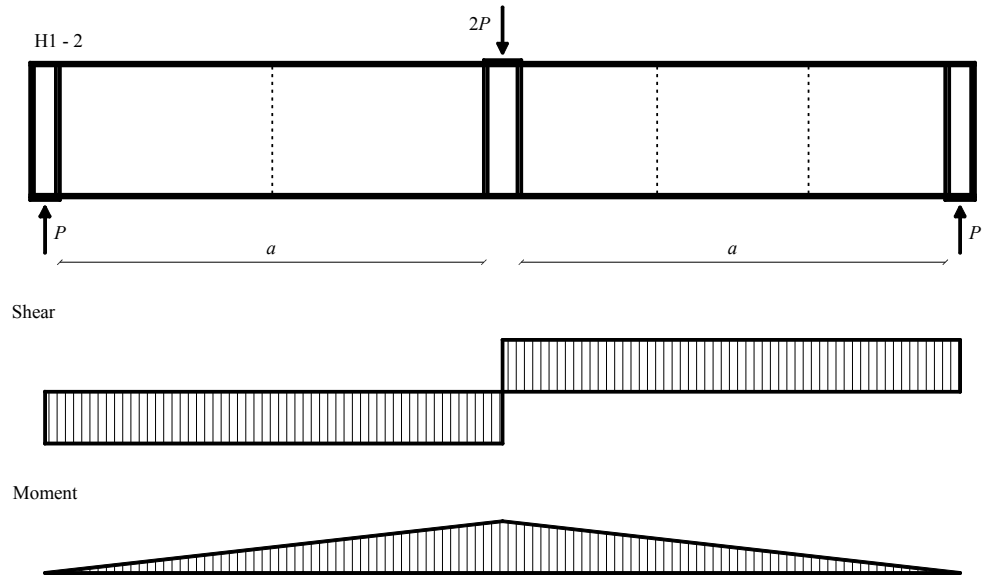
Experiments by Nishino and Okumura (1968).



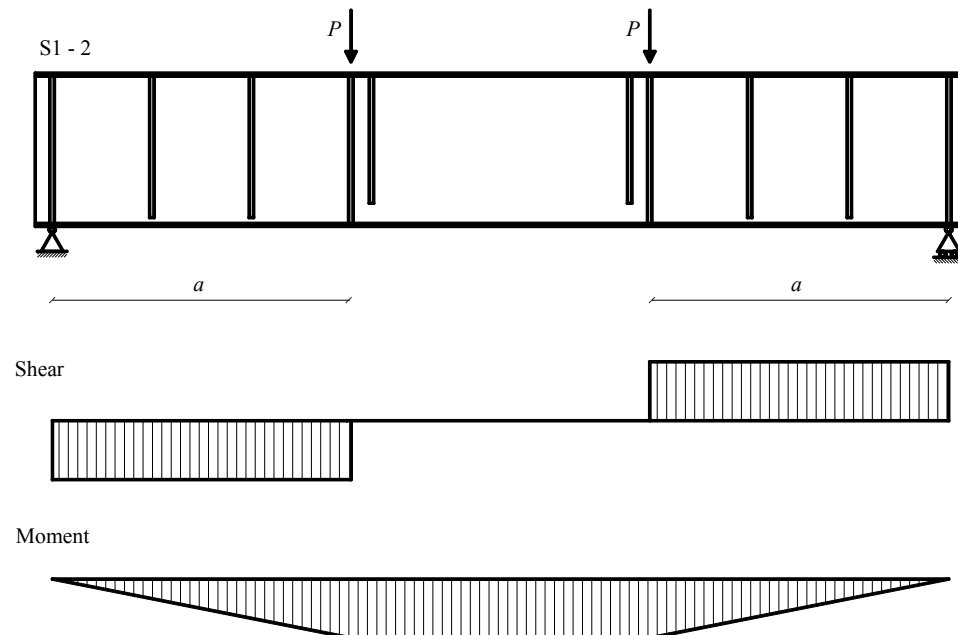
Experiments by Longbottom and Heyman (1956).



Experiments by Cooper et al. (1964).



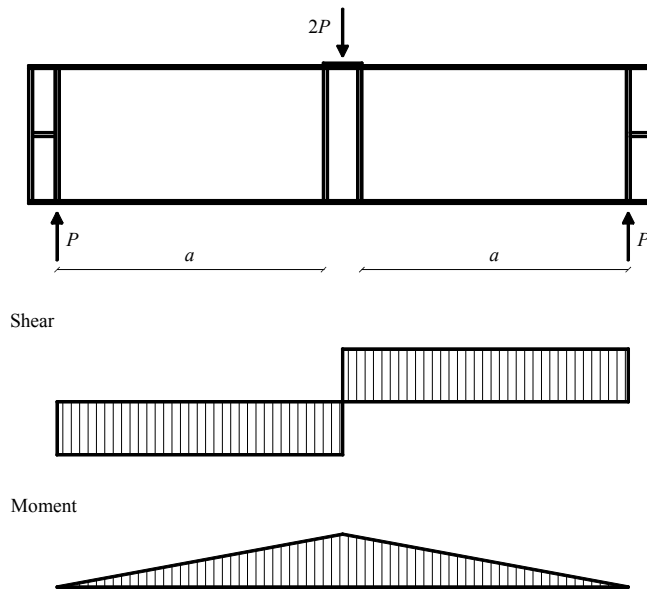
Experiments by Lew et al. (1969).



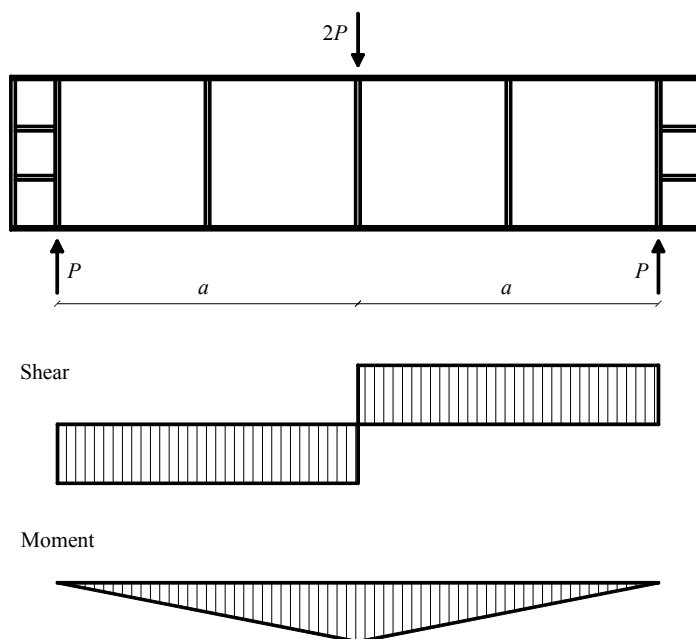
APPENDIX D

Experiments by Skaloud (1971), Sakai et al. (1966), d'Apice et al. (1966) and Rockey and Skaloud (1971).

TG1 – 5	Skaloud (1971)
G1 – 7, 9	Sakai (1966)
LST1	d'Apice et al. (1966)
TG1 – 5, 9, 10, 13	Rockey and Skaloud (1971)



TG14 – 20                      Rockey and Skaloud (1971)



	Girder	$L$ [in]	$d$ [in]	$t_w$ [in]	$f_{yw}$ [ksi]	$b_f$ [in]	$t_f$ [in]	$f_{yf}$ [ksi]	$A_s$ [in <sup>2</sup> ]	$f_{ys}$ [ksi]	$P_{epx}$ [kips]
Basler et al.	G6T1	150	50	0.193	36.7	12.13	0.778	37.9	1.0	43	116
	G6T2	150	50	0.193	36.7	12.13	0.778	37.9	1.0	43	150
	G6T3	150	50	0.193	36.7	12.13	0.778	37.9	1.0	43	177
	G7T1	150	50	0.196	36.7	12.19	0.768	37.6	1.0	43	140
	G7T2	150	50	0.196	36.7	12.19	0.768	37.6	1.0	43	145
	G8T1	150	50	0.197	38.2	12.00	0.750	41.3	1.0	43	85
	G8T2	150	50	0.197	38.2	12.00	0.750	41.3	1.0	43	100
	G8T3	150	50	0.197	38.2	12.00	0.750	41.3	1.0	43	117
	G9T1	150	50	0.131	44.5	12.00	0.750	41.8	1.0	43	48
	G9T2	150	50	0.131	44.5	12.00	0.750	41.8	1.0	43	75
Lyse & Godfrey	WB-1	41.9	13.97	0.25	43.3	6.5	1.5	43.5	-	-	109
	WB-2	42.0	14.00	0.25	47.8	6.5	1.5	43.5	-	-	128
	WB-3	48.0	16.00	0.25	49.6	6.5	1.5	43.5	-	-	139
	WB-6	52.6	17.55	0.25	33.1	6.5	1.5	43.5	-	-	96
	WB-7	46.0	15.33	0.25	33.7	6.5	1.5	43.5	-	-	95
	WB-8	47.0	15.65	0.25	29.7	6.5	1.5	43.5	-	-	100
	WB-9	37.5	12.49	0.25	30.3	6.5	1.5	43.5	-	-	92
	WB-10	37.4	12.45	0.25	30.3	6.5	1.5	43.5	-	-	94
Longbottom & Heymann	C4	20.00	13.50	0.056	16.7	1.625	0.25	18.6	0.042	16.7	4.15
	A1	6.78	5.25	0.056	16.7	1.000	0.25	18.6	-	-	2.88
	A2	10.75	5.25	0.056	16.7	1.000	0.25	18.6	-	-	2.43
	A3	22.50	5.25	0.056	16.7	1.000	0.25	18.6	-	-	1.49
	A4	10.00	4.75	0.056	16.7	1.325	0.25	18.6	-	-	2.60
Lew et al.	S1	36	36	0.189	40.8	8.02	0.522	105	0.563	36	115.8
	S2	36	36	0.189	40.8	7.99	0.528	105	0.563	36	108.1
Cooper et al.	H1-T1	150	50	0.393	108.1	18.06	0.980	106.4	1.875	108.1	630.0
	H1-T2	150	50	0.393	108.1	18.06	0.980	106.4	1.875	108.1	769.0
	H2-T1	150	50	0.390	110.2	18.06	2.012	107.2	1.875	110.2	917.0
	H2-T2	150	50	0.390	110.2	18.06	2.012	107.2	1.875	110.2	112.5

	Girder	$L$ [mm]	$d$ [mm]	$t_w$ [mm]	$f_{yw}$ [MPa]	$b_f$ [mm]	$t_f$ [mm]	$f_{yf}$ [MPa]	$A_s$ [mm <sup>2</sup> ]	$f_{ys}$ [MPa]	$P_{epx}$ [kN]
Nishino & Okumura	G1	1450	543	9.1	380	301	22.4	440	-	-	1105
	G2	1450	543	9.1	380	220	22.4	440	-	-	1040
	G3	1900	722	9.4	380	302	22.2	440	-	-	1245
	G4	1900	720	9.2	380	243	22.1	440	-	-	1145
	G5	2360	899	9.0	380	291	22.3	440	-	-	1235
	G6	2360	900	8.9	380	212	22.3	440	-	-	1090
	G7	2850	1080	9.1	380	282	22.4	440	-	-	1270
	G8	2850	1080	8.9	380	221	22.2	440	-	-	1120

APPENDIX D

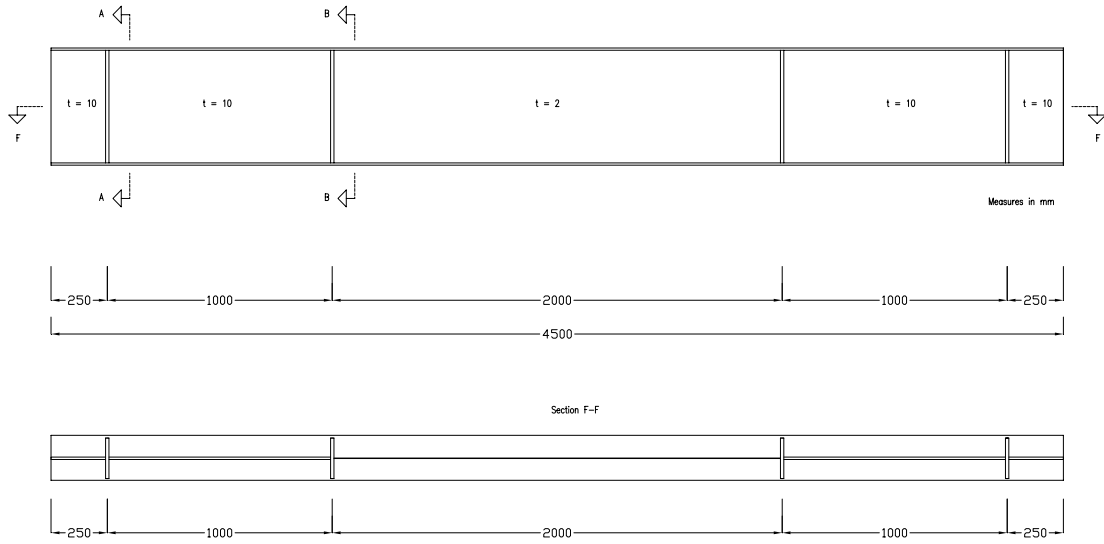
	Girder	$L$ [cm]	$d$ [cm]	$t_w$ [cm]	$f_{yw}$ [t/cm <sup>2</sup> ]	$b_f$ [cm]	$t_f$ [cm]	$f_{yf}$ [t/cm <sup>2</sup> ]	$A_s$ [cm <sup>2</sup> ]	$f_{ys}$ [t/cm <sup>2</sup> ]	$P_{exp}$ [ton]
Skaloud	TG1	100	100	0.25	2.037	16.0	0.517	2.86	-	-	15.45
	TG1'	100	100	0.25	2.037	16.0	0.517	2.86	-	-	11.85
	TG2	100	100	0.25	2.037	20.0	1.010	2.86	-	-	16.30
	TG2'	100	100	0.25	2.037	20.0	1.010	2.86	-	-	14.15
	TG3	100	100	0.25	2.037	20.0	1.646	2.86	-	-	19.40
	TG3'	100	100	0.25	2.037	20.0	1.646	2.86	-	-	19.35
	TG4	100	100	0.25	2.037	20.0	2.016	2.86	-	-	22.30
	TG4'	100	100	0.25	2.037	20.0	2.016	2.86	-	-	21.10
	TG5	100	100	0.25	2.037	25.0	2.971	2.86	-	-	31.45
	TG5'	100	100	0.25	2.037	25.0	2.971	2.86	-	-	30.60

	Girder	$L$ [mm]	$d$ [mm]	$t_w$ [mm]	$f_{yw}$ [kg/mm <sup>2</sup> ]	$b_f$ [mm]	$t_f$ [mm]	$f_{yf}$ [kg/mm <sup>2</sup> ]	$A_s$ [mm <sup>2</sup> ]	$f_{ys}$ [kg/mm <sup>2</sup> ]	$P_{exp}$ [ton]
Sakai et al.	G1	1150	440	8	44	160	30	42	-	-	82
	G2	1150	440	8	44	200	30	42	-	-	84
	G3	1407	560	8	44	160	30	42	-	-	99
	G4	2000	560	8	44	250	30	42	-	-	97
	G5	1500	560	8	44	250	30	42	-	-	107
	G6	687	560	8	44	250	30	42	-	-	120
	G7	1500	560	8	44	250	30	42	-	-	107
	G8	1500	560	8	44	250	30	42	-	-	107
	G9	2000	720	8	44	250	30	42	-	-	118

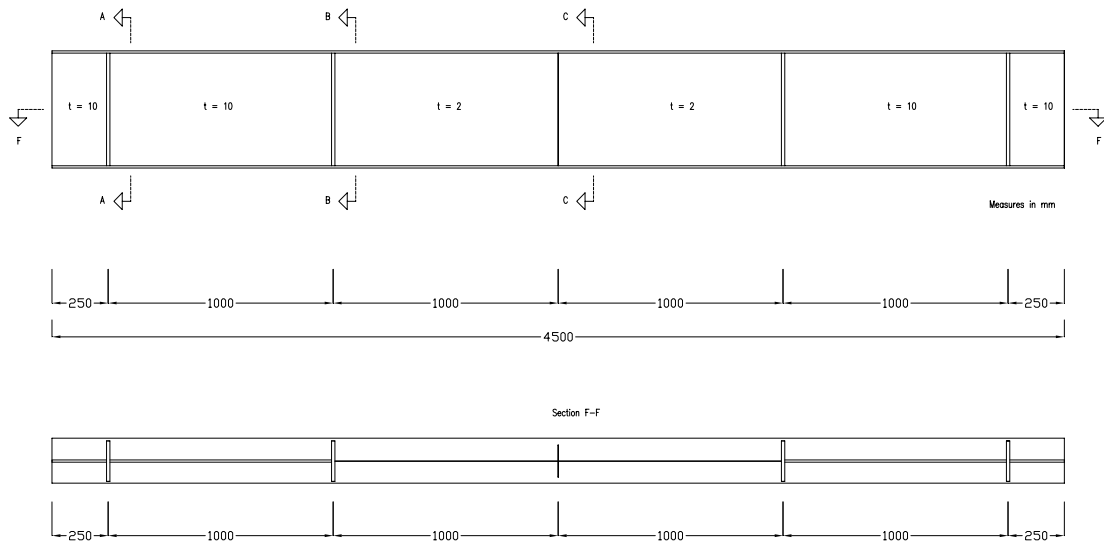
	Girder	$L$ [in]	$d$ [in]	$t_w$ [in]	$f_{yw}$ [t/in <sup>2</sup> ]	$b_f$ [in]	$t_f$ [in]	$f_{yf}$ [t/in <sup>2</sup> ]	$A_s$ [in <sup>2</sup> ]	$f_{ys}$ [t/in <sup>2</sup> ]	$P_{exp}$ [ton]
d'Apice	LST1	150	50	0.195	46.8	14.10	1.498	30.4	2.25	30.5	[kips] 182
Rockey & Skaloud	TG1	24	24	0.107	15.95	4.0	0.188	15.95	-	-	11.30
	TG1'	24	24	0.107	15.95	4.0	0.188	15.95	-	-	12.00
	TG2	24	24	0.107	15.95	4.0	0.250	15.95	-	-	12.60
	TG2'	24	24	0.107	15.95	4.0	0.250	15.95	-	-	11.75
	TG3	24	24	0.108	15.95	4.0	0.500	15.95	-	-	14.25
	TG3'	24	24	0.108	15.95	4.0	0.500	15.95	-	-	13.50
	TG4	24	24	0.107	15.95	4.0	0.650	15.95	-	-	15.90
	TG4'	24	24	0.107	15.95	4.0	0.650	15.95	-	-	15.15
	TG13	24	24	0.103	18.30	4.0	1.000	18.30	-	-	20.85
	TG5	36	24	0.103	18.30	8.0	0.375	18.30	-	-	11.70
	TG5'	36	24	0.103	18.30	8.0	0.375	18.30	-	-	13.00
	TG14	24	12	0.038	14.36	3.0	0.123	14.36	0.075	20.0	2.55
	TG15	24	12	0.038	14.36	3.0	0.197	14.36	0.075	20.0	2.95
	TG16	24	12	0.038	14.36	4.0	0.254	14.36	0.075	20.0	3.12
	TG17	24	12	0.038	14.36	4.0	0.367	20.18	0.075	20.0	3.90
	TG18	24	12	0.038	14.36	4.0	0.510	19.70	0.075	20.0	5.00
	TG19	24	12	0.038	14.36	4.0	0.611	17.35	0.075	20.0	5.45
	TG20	24	12	0.080	14.81	4.0	0.128	19.90	0.075	20.0	5.10
	TG9	48	24	0.104	18.3	8.0	0.388	18.30	-	-	12.30
	TG9'	48	24	0.104	18.3	8.0	0.388	18.30	-	-	12.03
TG10	48	24	0.104	18.3	8.0	0.625	18.30	-	-	12.85	

## APPENDIX E

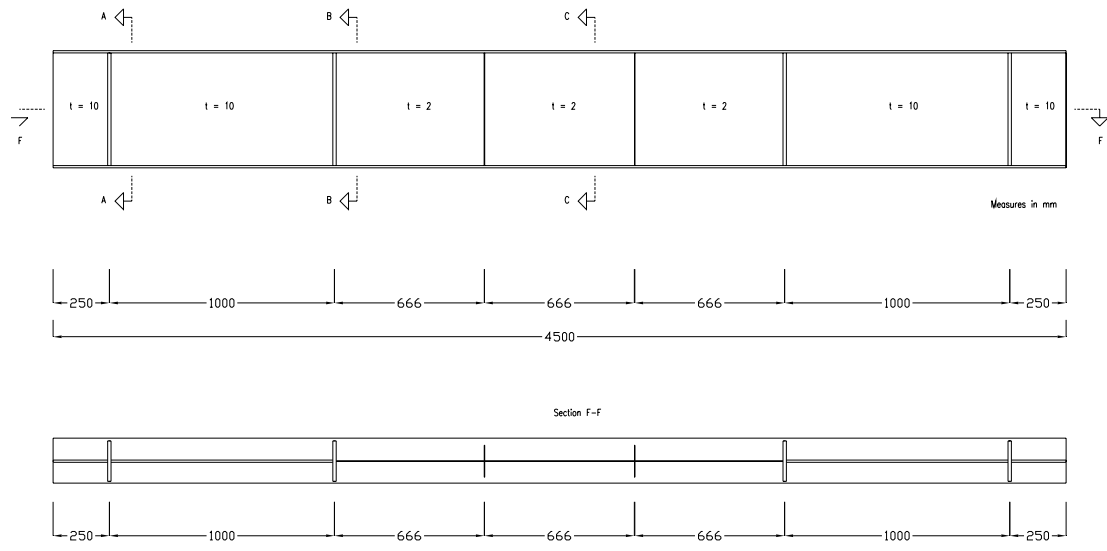
### Girder Specimen G1



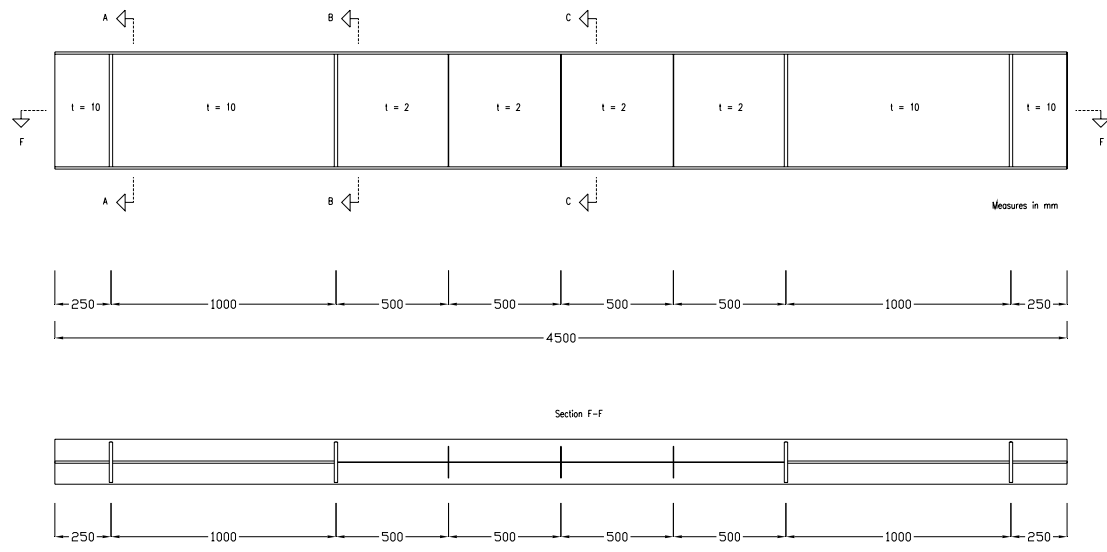
### Girder Specimen G2



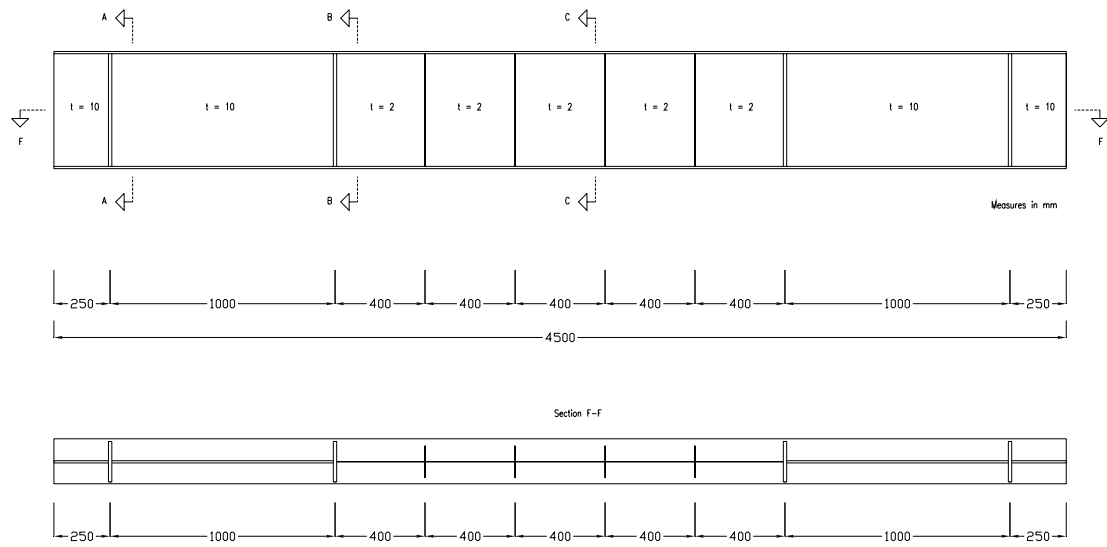
**Girder Specimen G3**



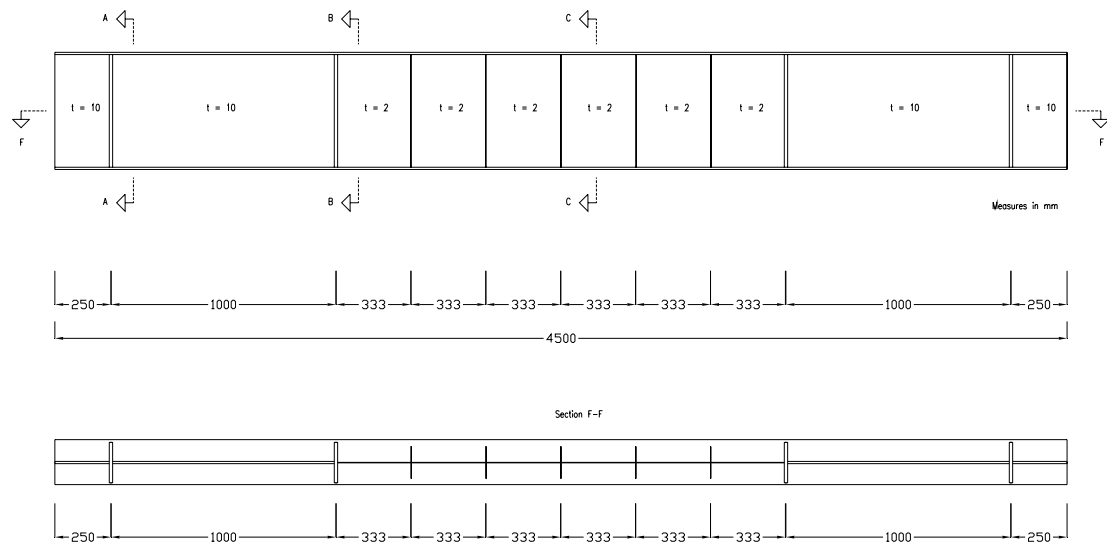
**Girder Specimen G4**



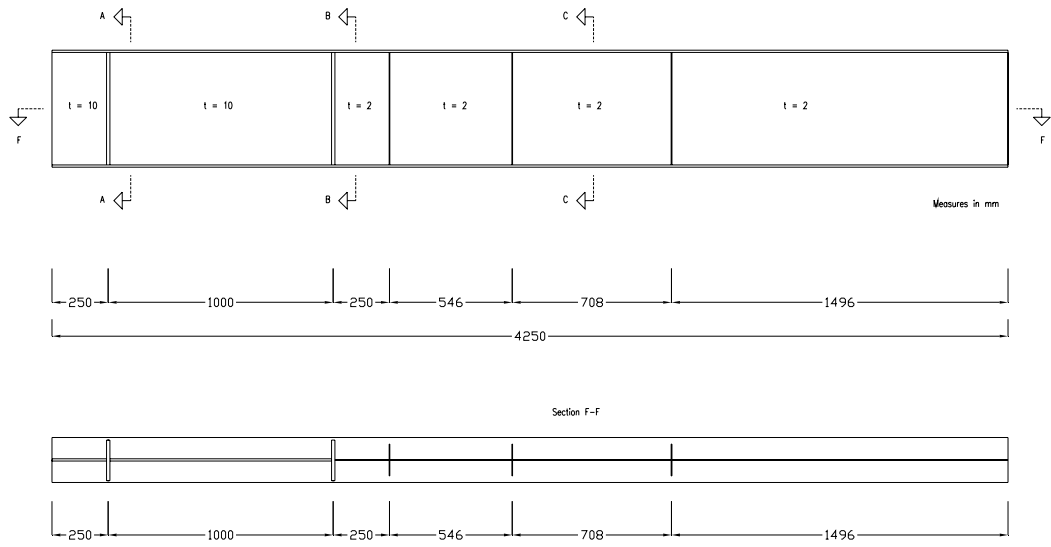
**Girder Specimen G5**



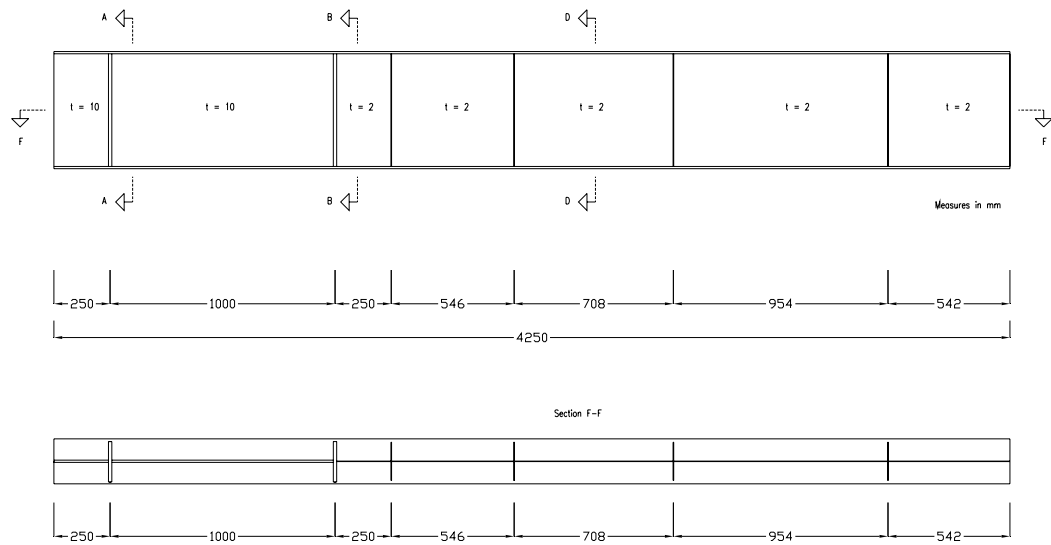
**Girder Specimen G6**



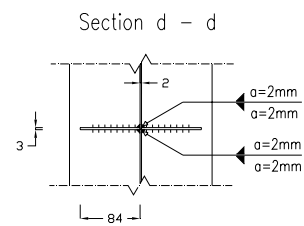
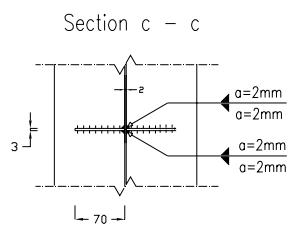
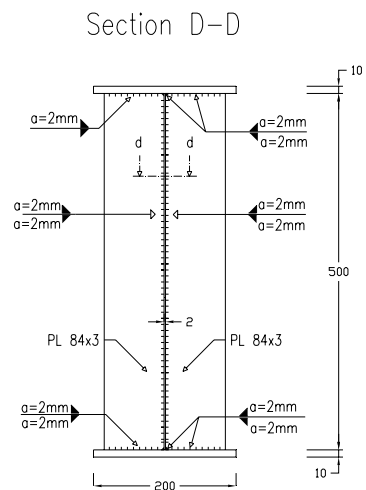
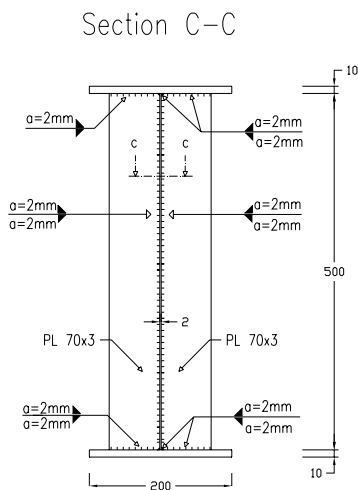
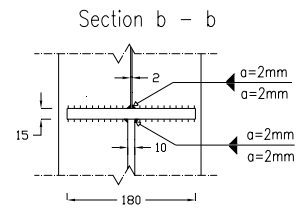
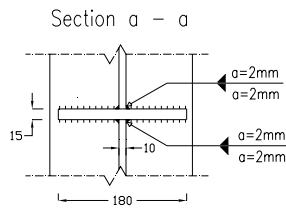
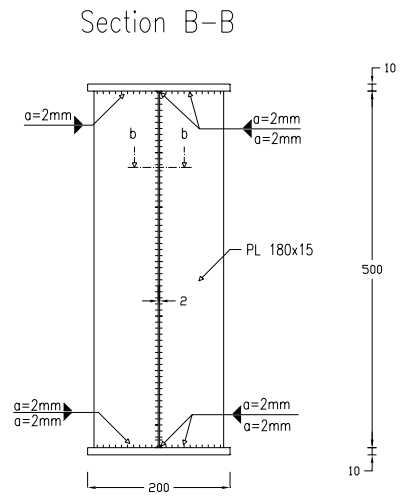
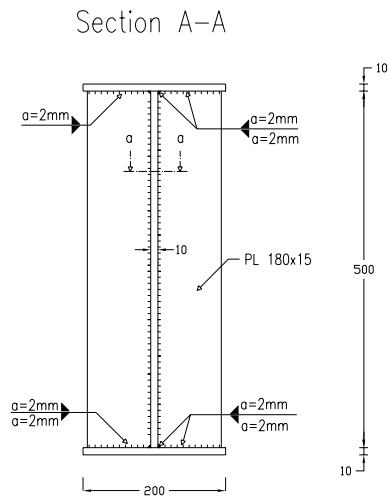
**Girder Specimen G7**



**Girder Specimen G8**

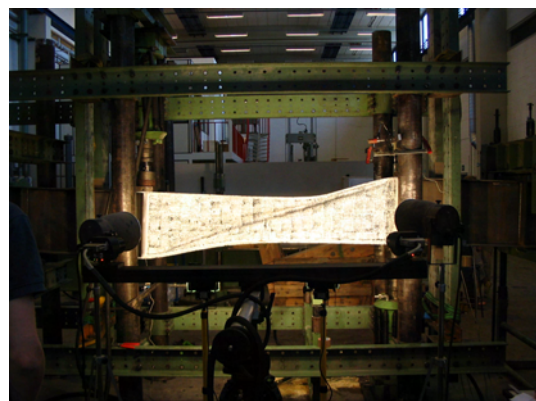
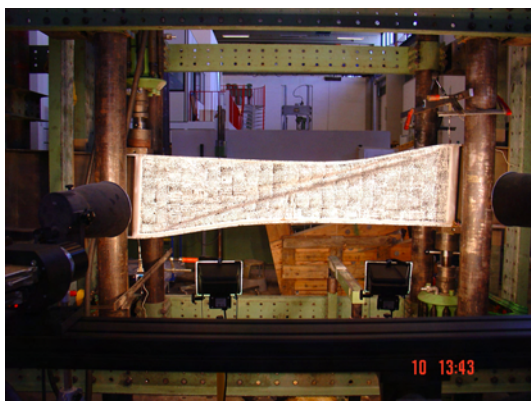
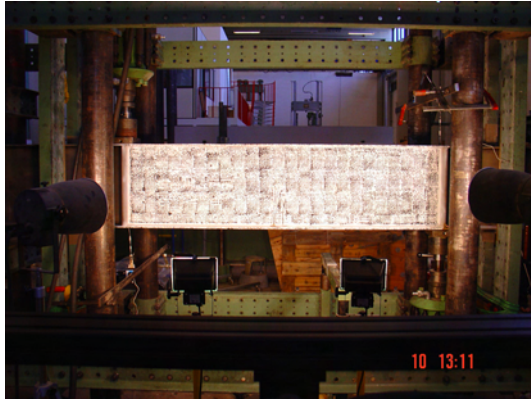


**Cross-Sections**



## APPENDIX F

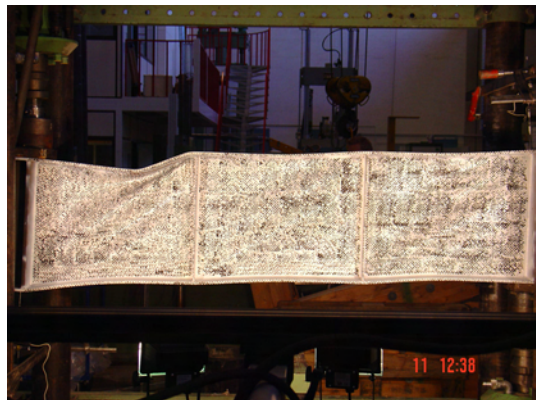
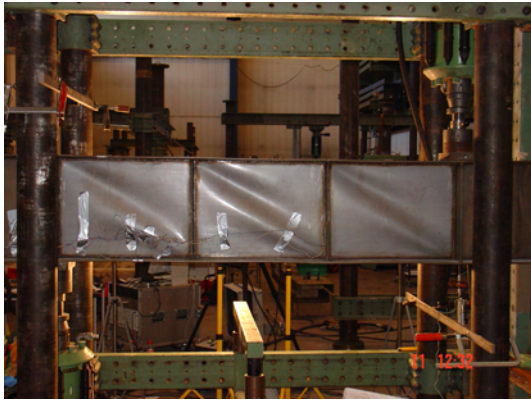
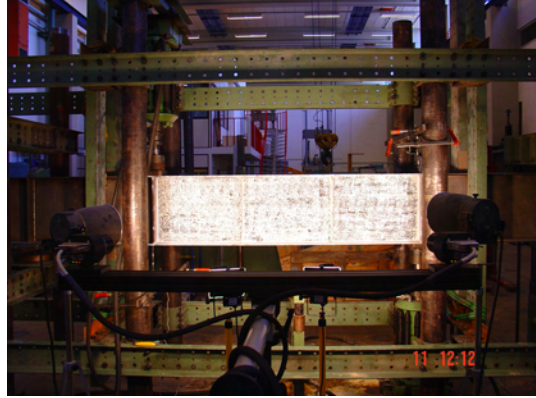
### Photos of Girder G1



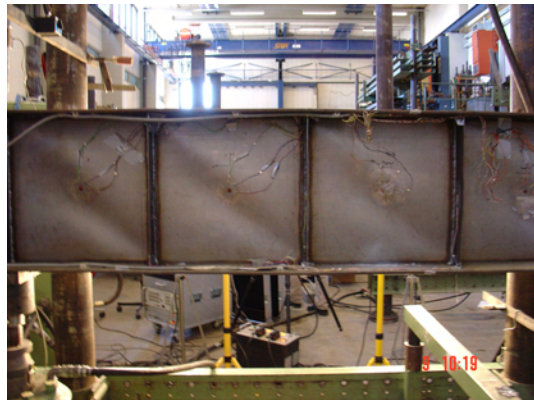
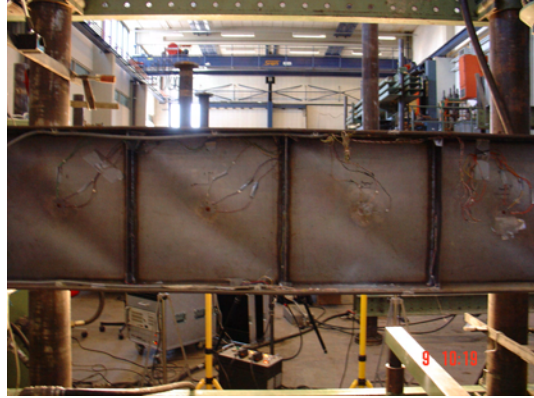
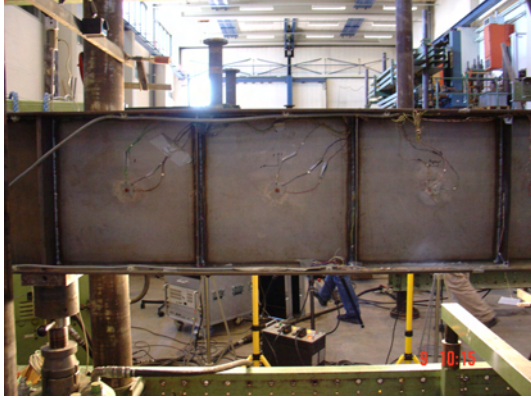
Photos of Girder G2



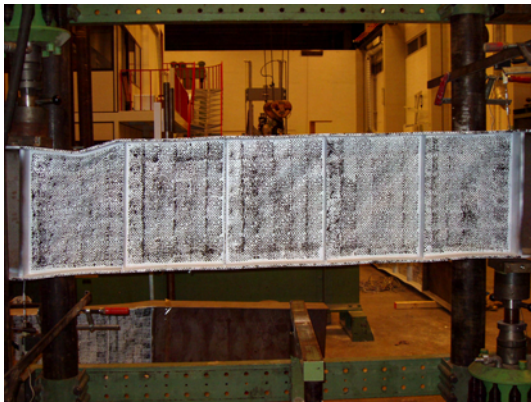
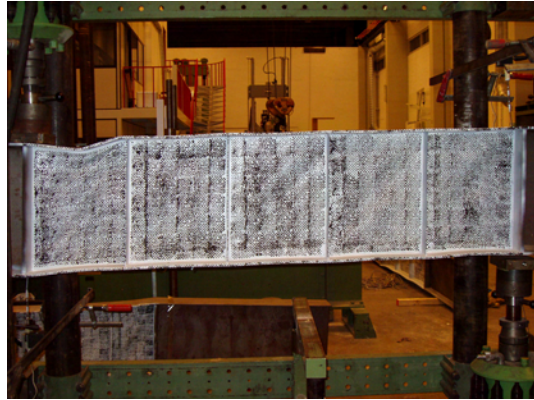
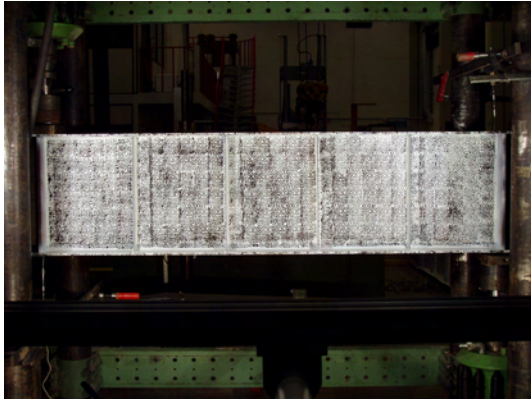
**Photos of Girder G3**



Photos of Girder G4



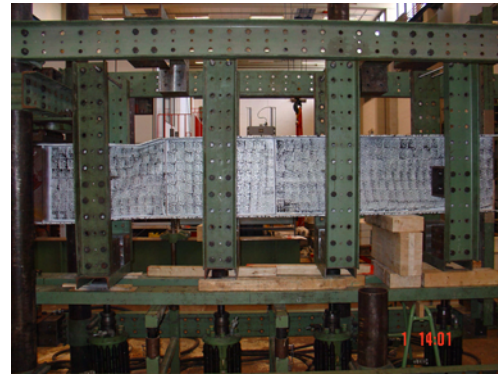
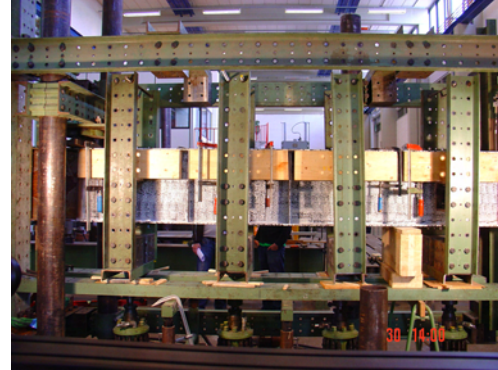
**Photos of Girder G5**



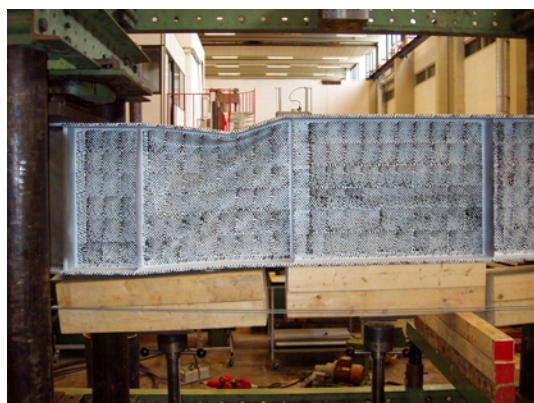
**Photos of Girder G6**



**Photos of Girder G7**

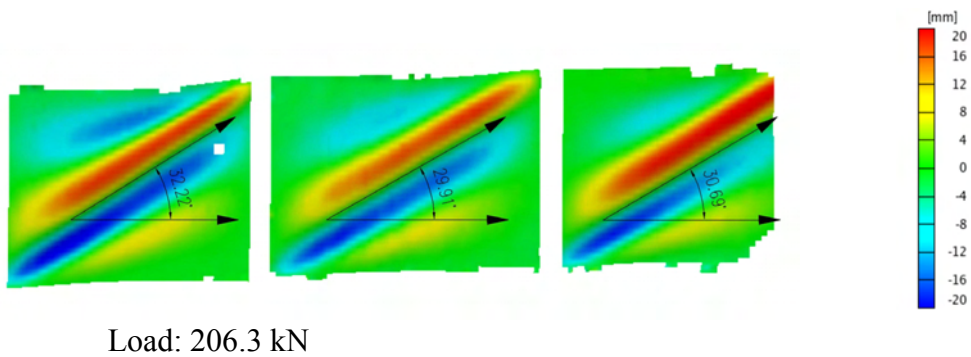
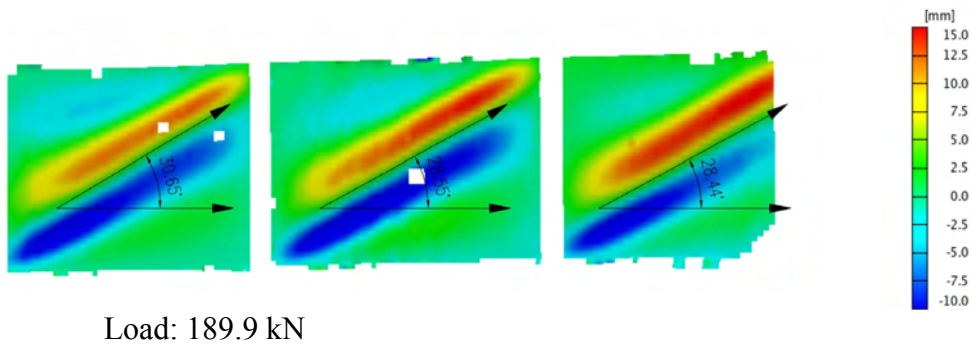
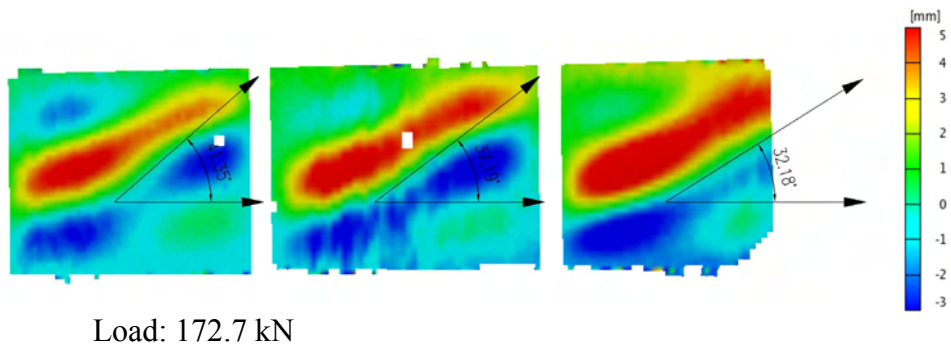
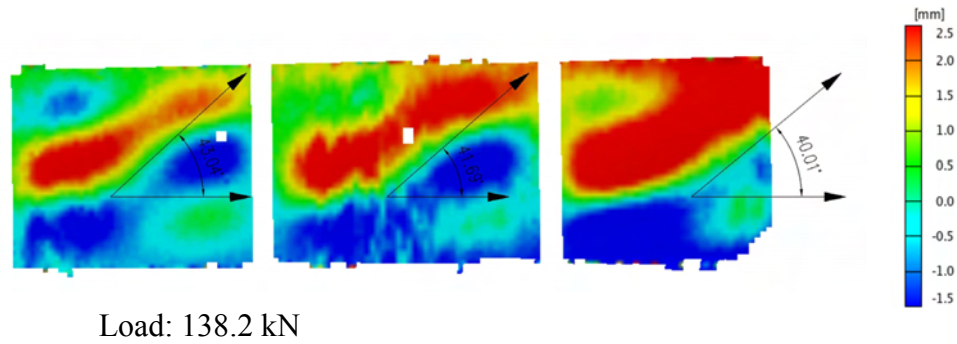


Photos of Girder G8

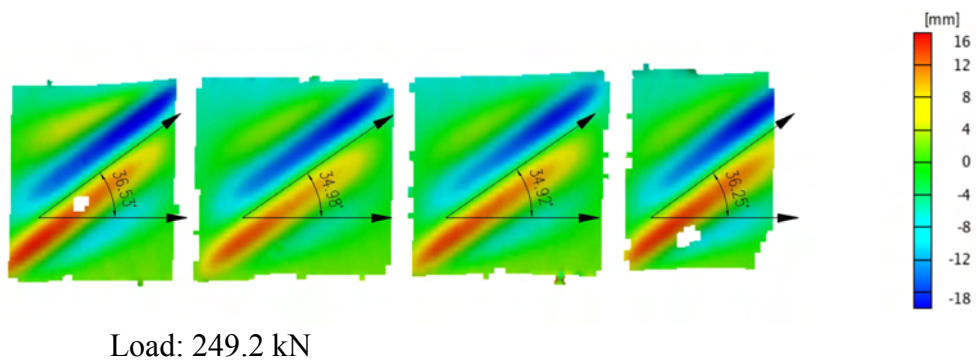
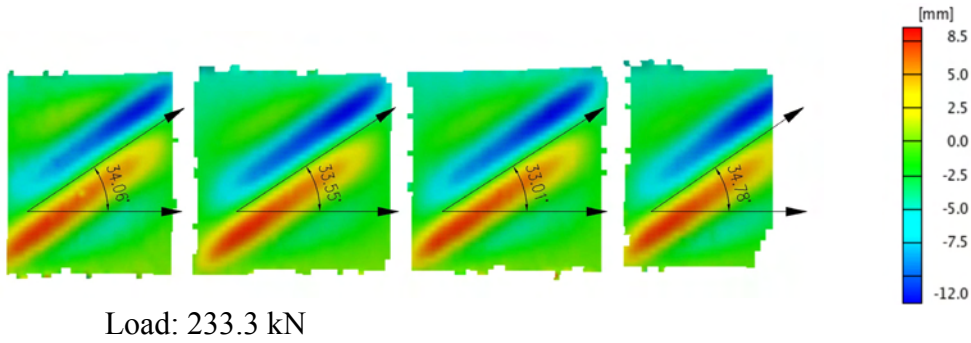
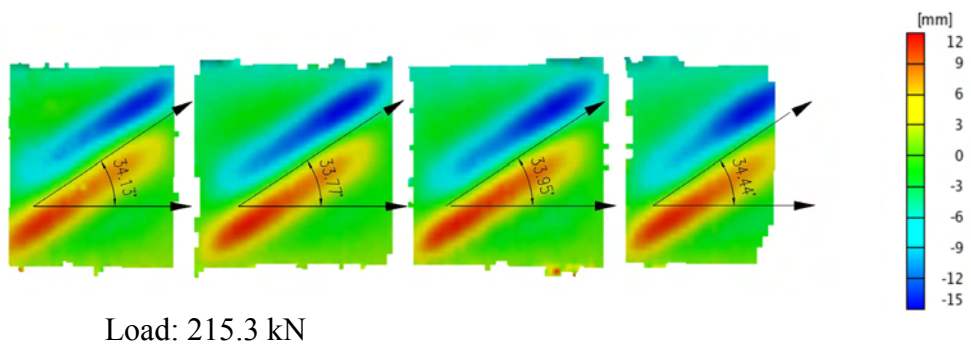
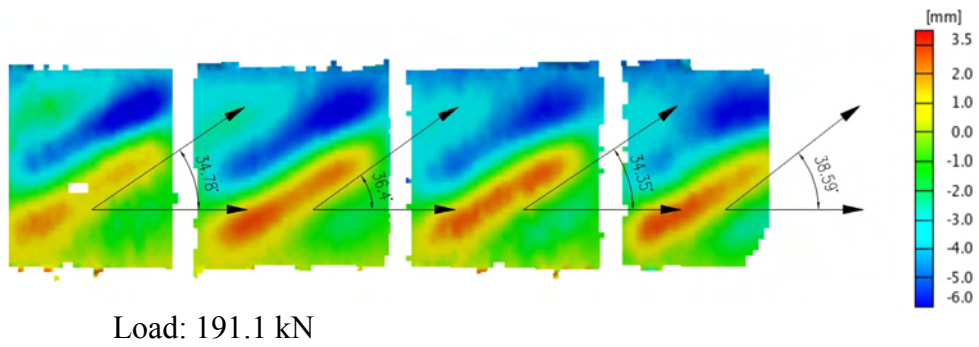


## APPENDIX G

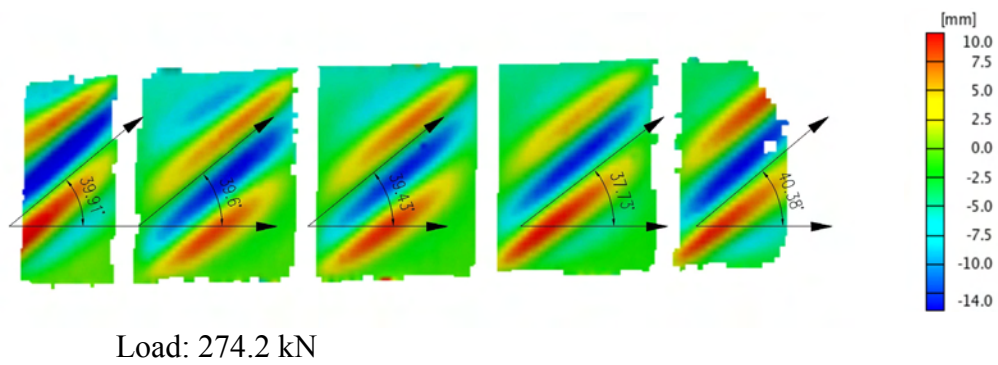
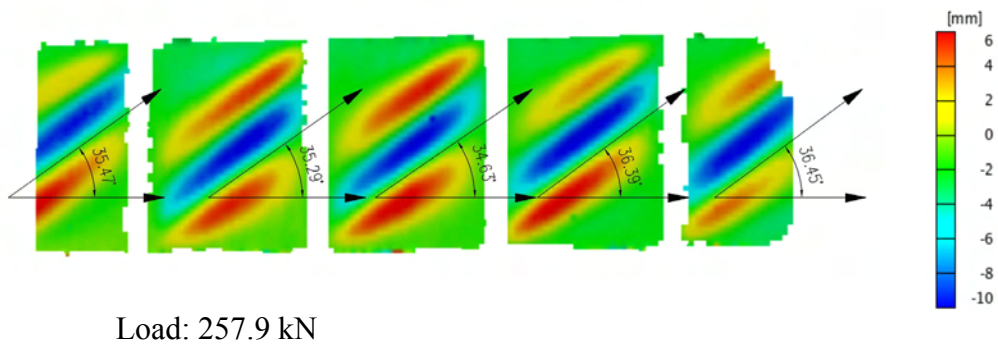
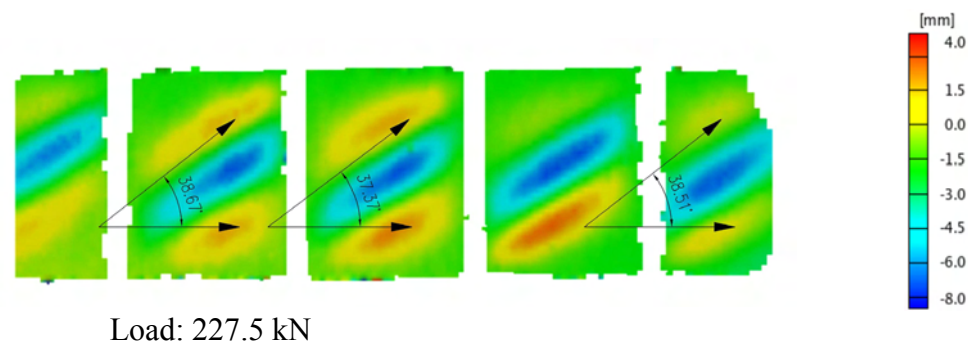
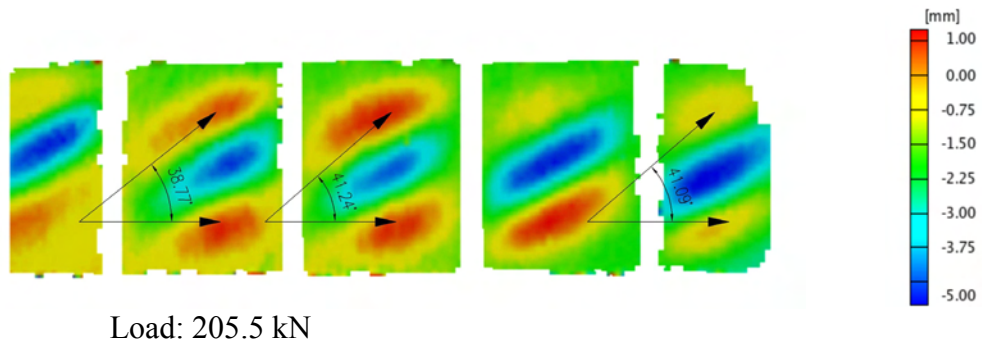
### Deformation plots from Aramis – Girder G3



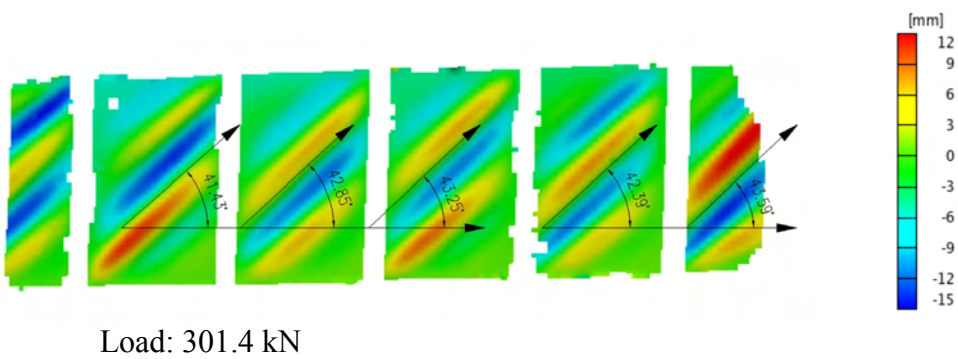
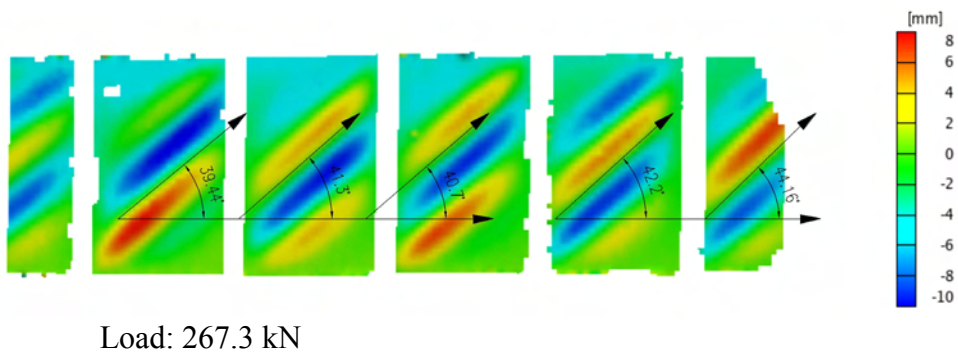
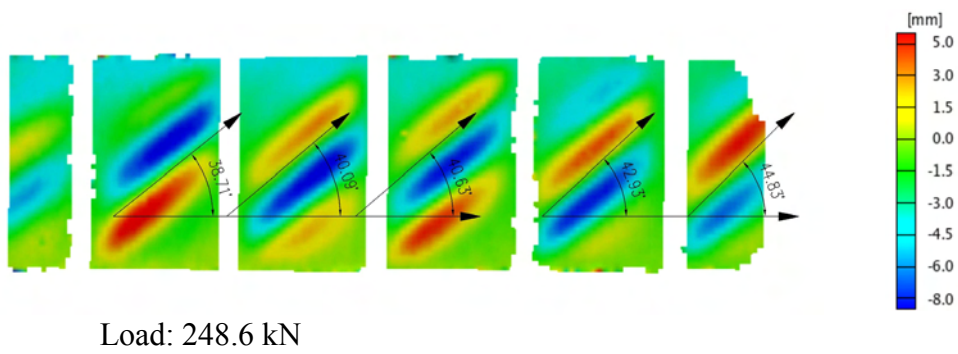
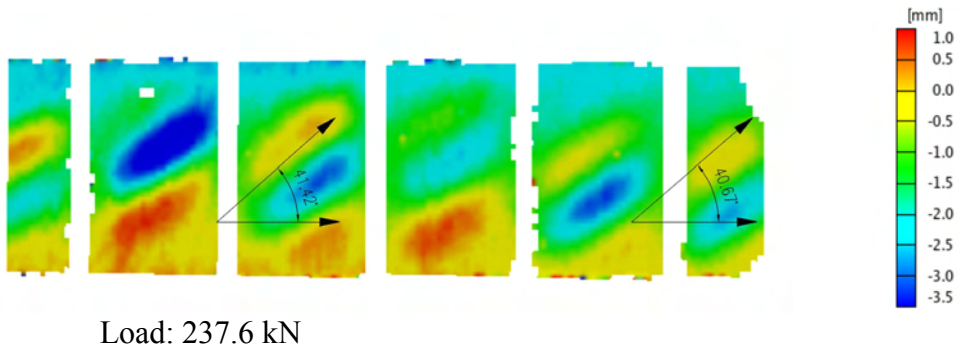
Deformation plots from Aramis – Girder G4



Deformation plots from Aramis – Girder G5

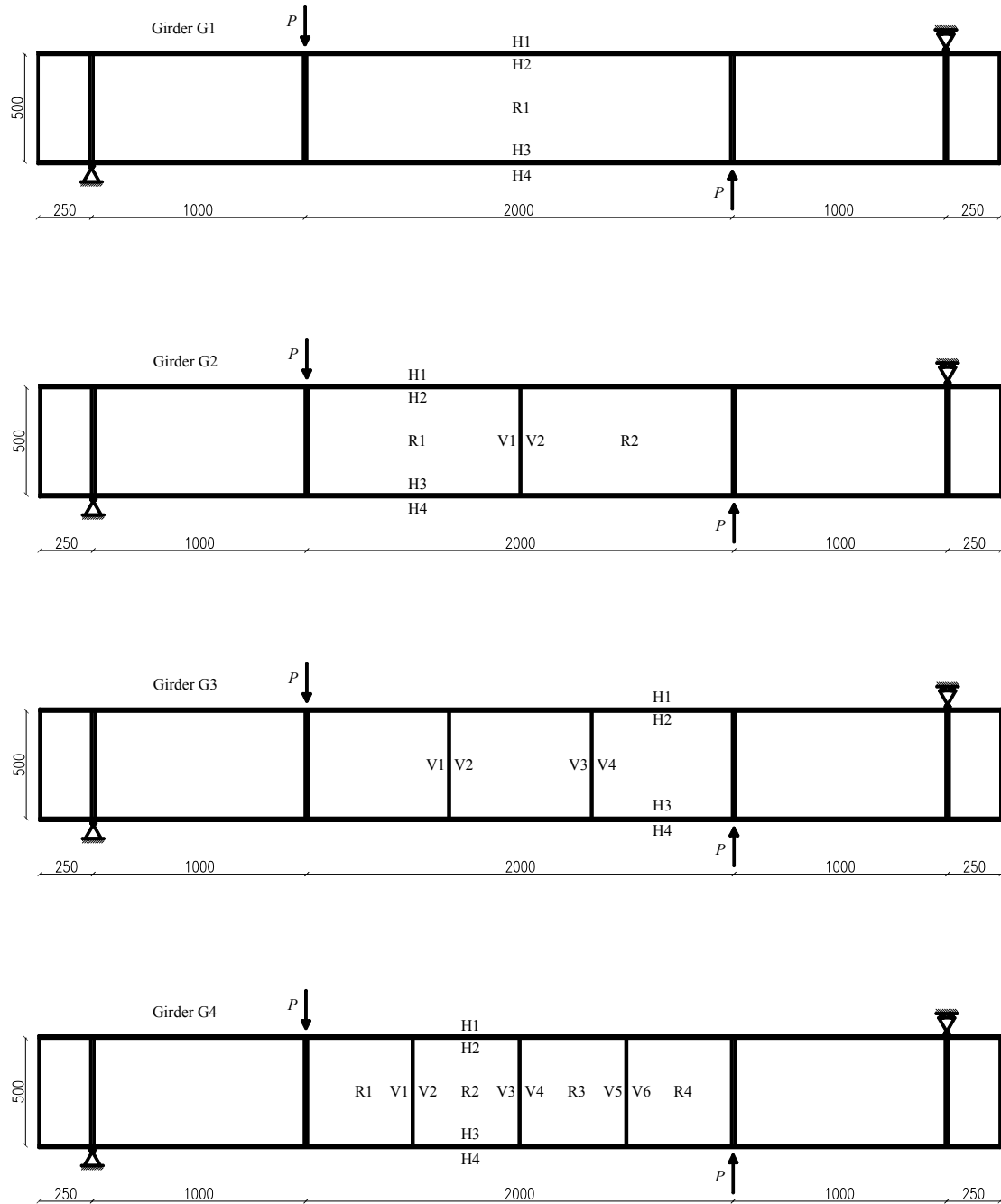


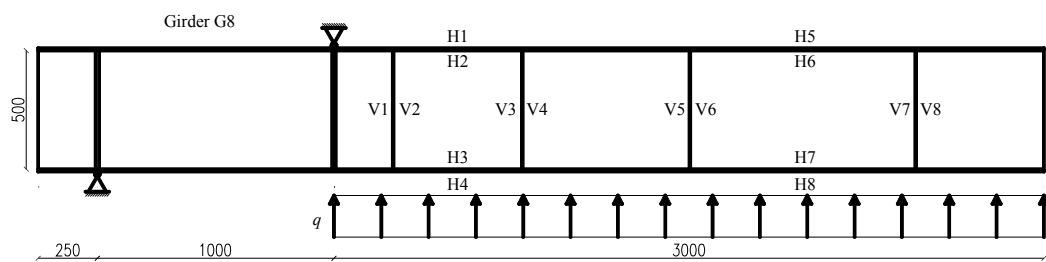
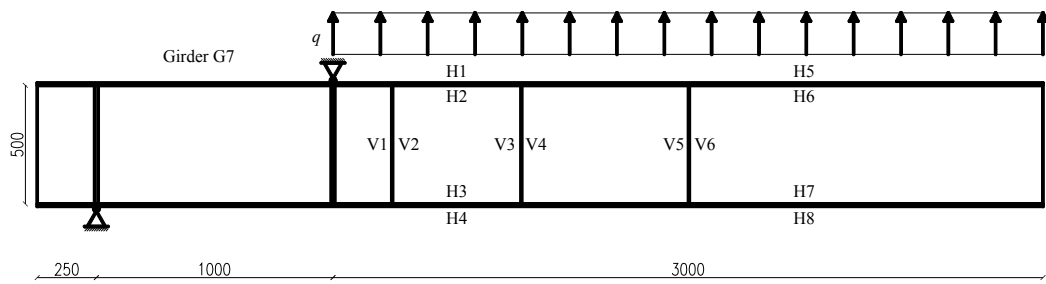
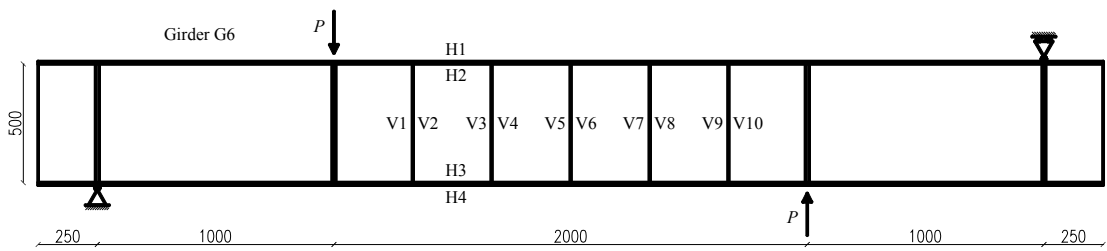
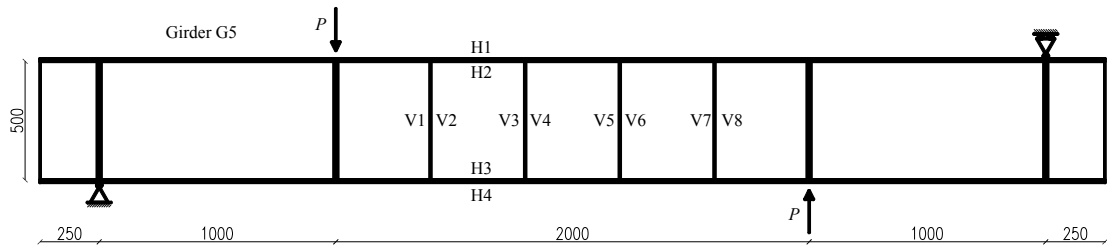
Deformation plots from Aramis – Girder G6



## APPENDIX H

### Location of Strain Gauges on Girder Specimens





## APPENDIX I

## Plates in Compression Supported Along All Edges.

Experiments by Sechler<sup>1</sup> (1933).Test series *Sechler*.

No.	$\lambda$	$C$	$b_e/b$		Theory / Test
			Test	Theory	
1	50.00	2.01	0.040	0.040	0.984
2	37.45	1.77	0.047	0.053	1.113
3	21.41	1.92	0.090	0.091	1.018
4	23.09	1.60	0.069	0.085	1.223
5	17.64	1.35	0.077	0.110	1.437
6	16.67	1.67	0.100	0.117	1.165
7	15.80	1.71	0.108	0.123	1.135
8	12.00	1.75	0.146	0.160	1.098
9	10.72	1.60	0.149	0.178	1.193
10	10.72	1.61	0.151	0.178	1.183
11	10.00	1.83	0.183	0.190	1.041
12	9.37	2.04	0.218	0.202	0.929
13	8.11	2.20	0.271	0.232	0.855
14	8.83	1.34	0.153	0.214	1.403
15	7.89	1.43	0.181	0.238	1.316
16	7.50	1.51	0.201	0.249	1.242
17	5.77	1.55	0.268	0.318	1.186
18	5.36	1.57	0.294	0.340	1.158
19	4.69	1.85	0.395	0.384	0.970
20	4.76	1.32	0.277	0.378	1.364
21	3.80	1.33	0.351	0.462	1.316
22	3.00	1.67	0.556	0.565	1.017
23	2.86	1.36	0.476	0.588	1.236
24	2.63	1.79	0.679	0.629	0.927
25	2.34	1.05	0.449	0.691	1.536
26	2.31	1.11	0.480	0.699	1.458
27	1.94	1.04	0.537	0.800	1.489
28	1.88	1.27	0.676	0.820	1.213
29	1.88	1.32	0.704	0.820	1.164
30	1.85	1.31	0.706	0.827	1.172
31	1.54	1.00	0.650	0.944	1.453
32	1.40	0.99	0.704	1.000	1.421
33	1.40	1.12	0.799	1.000	1.252
<i>Average:</i>					1.202

<sup>1</sup> The results are taken from (Winter 1947)

Experiments by Winter (1947).

Test series *U-beams*.

No.	$\lambda$	$C$	$b_e/b$		$Theory / Test$
			<i>Test</i>	<i>Theory</i>	
1	6.00	2.32	0.387	0.307	0.793
2	5.08	2.05	0.404	0.357	0.883
3	4.69	1.25	0.267	0.384	1.435
4	4.48	1.47	0.328	0.400	1.220
5	4.55	1.65	0.364	0.394	1.084
6	4.69	1.71	0.364	0.384	1.054
7	4.00	1.83	0.457	0.441	0.967
8	3.41	1.53	0.450	0.507	1.127
9	3.41	1.33	0.391	0.507	1.296
10	3.23	1.49	0.463	0.531	1.148
11	2.73	1.77	0.650	0.611	0.940
12	2.24	1.69	0.756	0.726	0.946
13	3.85	1.36	0.354	0.457	1.292
14	3.85	1.76	0.458	0.457	0.998
15	3.16	1.31	0.414	0.541	1.307
16	3.13	1.25	0.401	0.546	1.361
17	3.00	1.20	0.400	0.565	1.412
18	2.67	1.19	0.444	0.621	1.399
19	3.06	1.97	0.645	0.555	0.861
20	2.27	1.95	0.857	0.707	0.826
21	2.07	1.51	0.728	0.761	1.045
22	2.04	1.60	0.784	0.769	0.981
23	1.99	1.57	0.792	0.785	0.991
24	1.95	1.52	0.780	0.796	1.021
25	1.84	1.47	0.797	0.831	1.043
26	1.51	1.29	0.858	0.958	1.116
<i>Average:</i>					1.098

APPENDIX I

Experiments by Winter (1947).

Test series *I-beams*.

No.	$b/t$ [ ]	$f_y$ [psi]	$\lambda$ [ ]	$b_e$ [in]	$b_e/b$		Theory / Test
					Test	Theory	
I-1	14.3	35700	0.49	14.1 t	0.986	1.000	1.014
I-2	16.3	33100	0.54	16.5 t	1.012	1.000	0.988
I-3	16.4	33100	0.54	16.6 t	1.012	1.000	0.988
I-4	19.2	35100	0.65	19.2 t	1.000	1.000	1.000
I-5	22.9	33100	0.75	21.8 t	0.952	1.000	1.050
I-6	23.6	36200	0.81	23.4 t	0.992	1.000	1.009
I-7	24.0	35100	0.81	22.6 t	0.942	1.000	1.062
I-8	28.9	30200	0.91	27.4 t	0.948	1.000	1.055
I-9	32.0	36200	1.10	31.7 t	0.991	1.000	1.009
I-10	38.3	30200	1.21	37.2 t	0.971	1.000	1.030
I-11	42.6	37300	1.49	39.6 t	0.930	0.965	1.038
I-12	45.0	30300	1.42	40.8 t	0.907	0.998	1.100
I-13	56.0	37300	1.96	48.8 t	0.871	0.793	0.910
Average:							1.019

Experiments by Moxham (1971).

Test series *Welded*.

Ref.	$b/t$ [ ]	$t$ [in]	$a/b$ [ ]	$f_y$ [tsi]	$\lambda$ [ ]	$P$ [ton]	$P/(b t f_y)$		Theory / Test
							Test	Theory	
11a	55.5	0.126	4.0	15.1	1.86	11.4	0.857	0.823	0.961
11b	55.5	0.126	4.0	15.1	1.86	11.3	0.849	0.823	0.969
11a	55.5	0.126	4.0	15.1	1.86	11.7	0.879	0.823	0.936
11b	55.5	0.126	4.0	15.1	1.86	11.3	0.849	0.823	0.969
11a	55.5	0.126	4.0	15.1	1.86	12.5	0.940	0.823	0.879
11b	55.5	0.126	4.0	15.1	1.86	12.4	0.932	0.823	0.883
12a	63.5	0.126	4.0	15.1	2.13	9.3	0.611	0.744	1.217
12b	63.5	0.126	4.0	15.1	2.13	9.8	0.644	0.744	1.155
12a	63.5	0.126	4.0	15.1	2.13	10.7	0.703	0.744	1.058
12b	63.5	0.126	4.0	15.1	2.13	11.1	0.729	0.744	1.020
13a	71.4	0.126	4.0	15.1	2.40	9.5	0.555	0.678	1.222
13b	71.4	0.126	4.0	15.1	2.40	9.3	0.543	0.678	1.248
13a	71.4	0.126	4.0	15.1	2.40	9.9	0.578	0.678	1.173
13b	71.4	0.126	4.0	15.1	2.40	10.4	0.608	0.678	1.116
14a	79.5	0.126	4.0	15.1	2.67	9.7	0.509	0.622	1.222
14b	79.5	0.126	4.0	15.1	2.67	9.5	0.498	0.622	1.248
14a	79.5	0.126	4.0	15.1	2.67	10.0	0.525	0.622	1.186
14b	79.5	0.126	4.0	15.1	2.67	9.5	0.498	0.622	1.248
14a	79.5	0.126	4.0	15.1	2.67	9.9	0.519	0.622	1.198
14b	79.5	0.126	4.0	15.1	2.67	9.6	0.504	0.622	1.235
14a	79.5	0.126	4.0	15.1	2.67	10.5	0.551	0.622	1.129
14b	79.5	0.126	4.0	15.1	2.67	10.5	0.551	0.622	1.129
14a	79.5	0.126	4.0	15.1	2.67	11.7	0.614	0.622	1.013
14b	79.5	0.126	4.0	15.1	2.67	10.5	0.551	0.622	1.129
14a	79.5	0.126	4.0	15.1	2.67	12.1	0.635	0.622	0.980
14b	79.5	0.126	4.0	15.1	2.67	12.0	0.630	0.622	0.988
Average:									1.097

Experiments by Moxham (1971).

Test series *Unwelded*.

Ref.	$b/t$ [ ]	$t$ [in]	$a/b$ [ ]	$f_y$ [tsi]	$\lambda$ [ ]	$P$ [ton]	$P / (b t f_y)$		Theory / Test
							Test	Theory	
7a	36.5	0.126	4.0	15.1	1.23	8.9	1.017	1.000	0.983
7b	36.5	0.126	4.0	15.1	1.23	9.0	1.029	1.000	0.972
8a	40.5	0.126	4.0	15.1	1.36	9.3	0.958	1.000	1.044
8b	40.5	0.126	4.0	15.1	1.36	9.9	1.020	1.000	0.981
9a	43.6	0.126	4.0	15.1	1.46	10.6	1.014	0.977	0.964
9b	43.6	0.126	4.0	15.1	1.46	10.6	1.014	0.977	0.964
10a	47.5	0.126	4.0	15.1	1.60	11.8	1.036	0.921	0.889
10b	47.5	0.126	4.0	15.1	1.60	11.6	1.019	0.921	0.904
11a	55.5	0.126	4.0	15.1	1.86	13.1	0.985	0.823	0.836
11b	55.5	0.126	4.0	15.1	1.86	13.1	0.985	0.823	0.836
12a	63.5	0.126	4.0	15.1	2.13	12.9	0.847	0.744	0.878
12b	63.5	0.126	4.0	15.1	2.13	12.8	0.841	0.744	0.884
13a	71.4	0.126	4.0	15.1	2.40	12.7	0.742	0.678	0.914
13b	71.4	0.126	4.0	15.1	2.40	12.6	0.736	0.678	0.921
14a	79.5	0.126	4.0	15.1	2.67	12.5	0.656	0.622	0.948
14b	79.5	0.126	4.0	15.1	2.67	12.1	0.635	0.622	0.980
Average:									0.931

Test series *Short*.

Ref.	$b/t$ [ ]	$t$ [in]	$a/b$ [ ]	$f_y$ [tsi]	$\lambda$ [ ]	$P$ [ton]	$P / (b t f_y)$		Theory / Test
							Test	Theory	
-	55.5	0.126	0.875	15.1	1.85	10.9	0.827	0.757	0.916
-	55.5	0.126	0.875	15.1	1.85	11.6	0.880	0.757	0.861
-	64.0	0.126	0.875	15.1	2.15	10.7	0.697	0.675	0.967
-	64.0	0.126	0.875	15.1	2.15	11.5	0.750	0.675	0.900
-	80.0	0.126	0.875	15.1	2.69	10.6	0.553	0.564	1.020
-	80.0	0.126	0.875	15.1	2.69	10.7	0.558	0.564	1.011
Average:									0.946

## APPENDIX J

### Plates in Compression with One Free Edge.

Experiments by Bambach and Rasmussen (2004).

Test series *Plates*.

No.	$b$ [mm]	$t$ [mm]	$E$ [MPa]	$f_y$ [MPa]	$\lambda$ [ ]	$P$ [kN]	$P / (b t f_y)$		Theory / Test
							Test	Theory	
60 (1)	61.2	4.77	202000	272.2	0.471	78.8	0.992	1.000	1.008
60 (2)	60.6	4.77	202000	272.2	0.466	82.4	1.047	1.000	0.955
60 (w1)	61.0	4.77	202000	272.2	0.469	80.2	1.013	1.000	0.988
60 (w2)	60.5	4.77	202000	272.2	0.466	73.2	0.932	1.000	1.073
80 (1)	80.0	4.75	199000	317.2	0.672	95.1	0.789	0.811	1.028
80 (2)	79.9	4.75	199000	317.2	0.672	103.0	0.856	0.812	0.949
80 (w1)	79.9	4.75	199000	317.2	0.672	97.3	0.808	0.812	1.004
80 (w2)	79.7	4.75	199000	317.2	0.670	103.5	0.862	0.813	0.943
100 (1)	100.4	4.77	202000	272.2	0.773	114.2	0.876	0.729	0.833
100 (2)	100.3	4.77	202000	272.2	0.772	94.3	0.724	0.730	1.008
100 (w1)	100.4	4.77	202000	272.2	0.773	97.5	0.748	0.729	0.975
100 (w2)	100.3	4.77	202000	272.2	0.772	88.5	0.680	0.730	1.074
125 (1)	125.6	4.77	202000	272.2	0.967	94.8	0.581	0.610	1.049
125 (2)	125.8	4.77	202000	272.2	0.968	94.3	0.577	0.609	1.055
125 (w1)	125.5	4.77	202000	272.2	0.966	85.5	0.525	0.610	1.163
125 (w2)	125.3	4.77	202000	272.2	0.964	100.7	0.619	0.611	0.987
175 (1)	175.2	4.77	202000	272.2	1.348	123.3	0.542	0.460	0.849
175 (2)	175.0	4.77	202000	272.2	1.347	127.0	0.559	0.461	0.824
175 (w1)	175.4	4.77	202000	272.2	1.350	113.4	0.498	0.460	0.923
175 (w2)	175.2	4.77	202000	272.2	1.348	111.3	0.489	0.460	0.941
Average:									0.981

Experiments by Kalyanaraman et al. (1977).

Test series *Stub-column*.

No.	$b/t$ [in]	$k$ [ ]	$E$ [ksi]	$f_y$ [ksi]	$\lambda$ [ ]	$\sigma_{cr}$ [ksi]	$b_e/b$		Theory / Test
							Test	Theory	
SC-I 1	57.63	1.040	29503	31.59	1.886	8.35	0.555	0.341	0.614
SC-I 2	57.71	0.964	29510	30.73	1.862	7.72	0.565	0.345	0.611
SC-II 1	51.52	0.949	29523	25.68	1.519	9.54	0.613	0.414	0.676
SC-II 2	50.08	0.912	29484	30.26	1.604	9.69	0.574	0.395	0.688
SC-III 1	42.93	0.948	29511	31.29	1.398	13.72	0.610	0.446	0.731
SC-III 2	42.95	0.955	29515	31.11	1.394	13.81	0.622	0.447	0.718
SC-IV 1	35.25	0.985	29506	31.29	1.148	21.14	0.743	0.528	0.711
SC-IV 2	34.98	0.986	29493	30.50	1.125	21.48	0.725	0.538	0.741
SC-V 1	29.74	0.876	29492	33.18	0.998	26.40	0.787	0.594	0.755
SC-V 2	29.76	0.848	29490	31.05	0.966	25.52	0.721	0.610	0.847
UD-1	16.20	0.700	29502	41.90	0.611	71.12	1.100	0.870	0.791
UD-2	20.55	0.787	29501	41.90	0.774	49.69	0.973	0.728	0.748
UD-3	24.86	0.825	29507	41.90	0.937	35.60	0.890	0.626	0.703
UD-4	29.17	0.858	29516	41.90	1.099	29.90	0.782	0.548	0.701
Average:									0.717

Experiments by Kalyanaraman et al. (1977).

Test series *Beams*.

No.	$b/t$ [in]	$k$ [ ]	$E$ [ksi]	$f_y$ [ksi]	$\lambda$ [ ]	$\sigma_{cr}$ [ksi]	$b_e/b$		<i>Theory</i> / <i>Test</i>
							<i>Test</i>	<i>Theory</i>	
B-1	60.5	0.961	29457	51.0	2.517	6.99	0.419	0.262	0.625
B-2	53.1	0.920	29908	53.8	2.252	8.82	0.466	0.290	0.623
B-3	44.5	0.832	29556	53.8	1.899	11.21	0.500	0.339	0.679
B-4	36.9	0.791	29559	51.0	1.533	15.52	0.514	0.411	0.800
B-5	29.8	0.798	28984	51.3	1.254	23.54	0.555	0.490	0.883
B-6	23.7	0.584	29477	51.3	0.989	27.70	0.595	0.599	1.006
UP-9	26.0	0.747	29567	42.0	0.980	29.53	0.739	0.603	0.816
UP-10	32.1	0.666	29546	36.0	1.120	17.26	0.622	0.539	0.867
UP-11	38.0	0.804	29430	36.0	1.329	14.81	0.609	0.466	0.765
UP-12	42.8	0.560	29352	36.0	1.499	8.11	0.500	0.419	0.839
<i>Average:</i>									0.790

Experiments by Winter (1947).

Test series *I-beams*.

No.	$b/t$ [ ]	$f_y$ [psi]	$\sigma$ [psi]	$\lambda$ [ ]	$b_e/b$		<i>Theory</i> / <i>Test</i>
					<i>Test</i>	<i>Theory</i>	
I-S-2	9.3	35400	34600	0.317	0.977	1.000	1.023
I-S-3	10.1	49400	35800	0.407	0.725	1.000	1.380
I-B-3	10.1	37300	30200	0.353	0.810	1.000	1.235
I-B-4	17.5	36800	40300	0.608	1.095	0.873	0.797
I-S-6	18.5	35400	31800	0.631	0.898	0.850	0.946
I-S-7	19.0	34500	26100	0.639	0.757	0.842	1.112
I-S-8	19.1	49400	38800	0.769	0.785	0.732	0.932
I-B-5	20.3	37300	29400	0.710	0.788	0.778	0.987
I-B-6	20.8	34000	29200	0.695	0.859	0.791	0.921
I-B-7	21.6	32600	28800	0.707	0.883	0.781	0.884
I-S-9	21.6	34000	25500	0.722	0.750	0.769	1.025
I-B-8	25.2	38700	30000	0.898	0.775	0.647	0.835
I-S-10	27.1	34500	22900	0.912	0.664	0.639	0.963
I-S-11	27.8	34000	23900	0.929	0.703	0.630	0.896
I-S-12	27.8	34500	29200	0.936	0.846	0.626	0.740
I-S-13	28.3	49400	29200	1.140	0.591	0.532	0.899
I-B-9	28.9	29200	26200	0.895	0.897	0.649	0.724
I-B-10	29.9	32600	24600	0.978	0.755	0.604	0.800
I-B-11	30.6	34900	25700	1.036	0.736	0.576	0.782
I-B-12	31.2	37300	28300	1.092	0.759	0.551	0.727
I-B-14	33.1	34000	23000	1.106	0.676	0.545	0.806
<i>Average:</i>							0.925



Report no R-146  
ISSN 1601-2717  
ISBN 87-7877-218-4